

# **Inorganic carbon dynamics at the land-ocean interface**

**Ruth Matthews**

Submitted for the degree of Doctor of Philosophy

University of East Anglia

School of Environmental Sciences

December 2022

This copy of the thesis has been supplied on condition that anyone who consults it is understood to recognise that its copyright rests with the author and that use of any information derived there-from must be in accordance with current UK Copyright Law. In addition, any quotation or extract must include full attribution.

## Abstract

Recent studies have recognised the importance of estuaries in the context of land-ocean carbon cycling, but large uncertainties around estuarine CO<sub>2</sub> outgassing estimates remain. Furthermore, there is debate about the relative contribution of different factors to estuarine dissolved inorganic carbon (C<sub>T</sub>) and total alkalinity (A<sub>T</sub>) concentrations.

This thesis contributes measurements of C<sub>T</sub> and A<sub>T</sub> in 16 UK estuaries, covering range of sizes, weather regimes and geologies. Estuarine C<sub>T</sub> and A<sub>T</sub> concentrations are found to vary from 0 – 5000 μmol kg<sup>-1</sup> at the freshwater inflow. Between-estuary differences are controlled by catchment lithology; chalk bedrock weathering drives the highest freshwater C<sub>T</sub> and A<sub>T</sub> concentrations, moderate freshwater C<sub>T</sub> and A<sub>T</sub> concentrations are driven by limestone weathering, and estuaries draining non-carbonate bedded catchments have low freshwater C<sub>T</sub> and A<sub>T</sub> concentrations. Mixing is the dominant control on estuarine carbonate chemistry along the salinity gradient.

Given that estuarine C<sub>T</sub> and A<sub>T</sub> dynamics are controlled ultimately by their riverine concentrations, a range of geochemical tracer variables were measured in four rivers and end member mixing models are constrained to determine the quantitative contribution of different bedrock types to river flow. Chalk and limestone bedrock weathering have measurably different geochemical signatures. Secondary geological data are well-described by the models, so future UK studies may avoid this complex analysis entirely.

The partial pressure (pCO<sub>2</sub>) and water-to-air fluxes of CO<sub>2</sub> (FCO<sub>2</sub>) are calculated. pCO<sub>2</sub> is related to temperature and organic carbon concentration, suggesting that outgassing is driven by river-derived organic carbon degradation. UK-wide estuarine outgassing is estimated, using FCO<sub>2</sub> interpolation and upscaling, to be equivalent to approximately ¼ of the current UK fossil fuel emission.

This study presents the first full examination of the factors that drive carbonate chemistry between estuaries, which was only made possible because of the uniquely large number of estuaries sampled.

## **Access Condition and Agreement**

Each deposit in UEA Digital Repository is protected by copyright and other intellectual property rights, and duplication or sale of all or part of any of the Data Collections is not permitted, except that material may be duplicated by you for your research use or for educational purposes in electronic or print form. You must obtain permission from the copyright holder, usually the author, for any other use. Exceptions only apply where a deposit may be explicitly provided under a stated licence, such as a Creative Commons licence or Open Government licence.

Electronic or print copies may not be offered, whether for sale or otherwise to anyone, unless explicitly stated under a Creative Commons or Open Government license. Unauthorised reproduction, editing or reformatting for resale purposes is explicitly prohibited (except where approved by the copyright holder themselves) and UEA reserves the right to take immediate 'take down' action on behalf of the copyright and/or rights holder if this Access condition of the UEA Digital Repository is breached. Any material in this database has been supplied on the understanding that it is copyright material and that no quotation from the material may be published without proper acknowledgement.

## **Table of Contents**

<b>i. List of Tables</b>	<b>6</b>
<b>ii. List of Figures</b>	<b>7</b>
<b>iii. Acknowledgements</b>	<b>9</b>
<b>Introduction</b>	<b>10</b>
<b>1.1 Climate change and the inorganic carbon cycle</b>	<b>11</b>
<b>1.2 Rivers as sources of atmospheric CO<sub>2</sub></b>	<b>16</b>
<b>1.3 Inner estuaries as sources of atmospheric CO<sub>2</sub></b>	<b>19</b>
<b>1.4 Carbonate chemistry</b>	<b>23</b>
<b>1.5 Thesis aims</b>	<b>28</b>
<b>Generic Methods</b>	<b>30</b>
<b>2.1 Sampling context: LOCATE</b>	<b>31</b>
<b>2.2 Sampling</b>	<b>32</b>
<b>2.3 Laboratory analysis of C<sub>T</sub> and A<sub>T</sub></b>	<b>33</b>
<b>2.4 C<sub>T</sub> calculation</b>	<b>36</b>
<b>2.5 A<sub>T</sub> calculation</b>	<b>37</b>
<b>2.6 Organic alkalinity experiment</b>	<b>37</b>
<b>2.7 General remarks</b>	<b>38</b>
<b>Drivers of dissolved inorganic carbon and alkalinity in the inner estuaries of the UK</b>	<b>40</b>
<b>3.1 Introduction</b>	<b>41</b>
<b>3.1.1 Research Questions</b>	<b>44</b>
<b>3.2 Chapter-specific Methods</b>	<b>44</b>
<b>3.2.1 Sampling</b>	<b>44</b>
<b>3.2.2 Additional Data</b>	<b>47</b>
<b>3.2.3 Data analysis</b>	<b>52</b>
<b>3.3 Results and Discussion</b>	<b>53</b>
<b>3.3.1 - Group 1: High freshwater C<sub>T</sub> and A<sub>T</sub> concentration group</b>	<b>58</b>
<b>3.3.2 Group 2: Low freshwater C<sub>T</sub> and A<sub>T</sub> concentration group</b>	<b>70</b>
<b>3.3.3 - Group 3: Estuaries with positive and negative C<sub>T</sub> and A<sub>T</sub> gradients</b>	<b>75</b>
<b>3.4 – Conclusions</b>	<b>79</b>

<b><i>Contribution of catchment lithology to the variation in freshwater <math>C_T</math> and <math>A_T</math> concentrations in UK rivers</i></b>	<b>81</b>
<b><i>4.1 Introduction</i></b>	<b>82</b>
4.1.1 Summary of relevant findings so far .....	83
<b><i>4.2 Methods</i></b>	<b>85</b>
4.2.1 COVID-19 impacts.....	85
4.2.2 Sampling .....	86
4.2.3 Laboratory analysis .....	88
4.2.4 End member mixing model .....	89
4.2.5 End member data.....	89
<b><i>4.3 Results and Discussion</i></b>	<b>94</b>
<b><i>4.4 Conclusions</i></b>	<b>105</b>
<b><i>Propagating inorganic carbon and alkalinity measurements in a diverse range of UK estuaries through to annual <math>CO_2</math> outgassing</i></b>	<b>107</b>
<b><i>5.1 Introduction</i></b>	<b>108</b>
5.1.1 Research Questions .....	110
<b><i>5.2 Methods</i></b>	<b>110</b>
5.2.1 Sampling + Measurements.....	110
5.2.2 $pCO_2$ calculation .....	110
5.2.3 Statistical Analysis .....	111
5.2.4 Water-to-air $CO_2$ flux ( $FCO_2$ ) calculation .....	112
5.2.5 Temporal interpolation .....	115
5.2.7 Uncertainty analysis – $CO_2$ flux .....	118
5.2.8 Spatial Interpolation & overall outgassing estimate.....	119
<b><i>5.3 Results and Discussion</i></b>	<b>120</b>
5.3.1 $pCO_2$ water .....	120
5.3.2 $CO_2$ flux.....	125
<b><i>5.4 Conclusions</i></b>	<b>133</b>
<b><i>Synthesis and Future Work</i></b>	<b>134</b>
<b><i>6.1 Thesis overview</i></b>	<b>135</b>
6.1.1 What factors define the carbonate chemistry of rivers and estuaries, and what are their relative importance?.....	135
6.1.2 How much $CO_2$ is emitted from estuaries into the atmosphere, and what drives that emission? .....	137
<b><i>6.2 Key findings</i></b>	<b>138</b>
6.2.1 Chapter 3: Drivers of dissolved inorganic carbon and alkalinity in the inner estuaries of the UK.....	138
6.2.2 Chapter 4: Contribution of catchment lithology to the variation in freshwater $C_T$ and $A_T$ concentrations in UK rivers. ....	139
6.2.3 Chapter 5: Propagating inorganic carbon and alkalinity measurements in a diverse range of UK estuaries through to annual estimated $CO_2$ outgassing..	141

<b>6.3 General discussion and future directions</b> .....	<b>142</b>
<b>6.3.1 Riverine inorganic carbon</b> .....	<b>143</b>
<b>6.3.2 Riverine organic carbon</b> .....	<b>144</b>
<b>6.3.3 Estuarine organic carbon</b> .....	<b>145</b>
<b>6.3.4 Future directions</b> .....	<b>145</b>
<b>6.4 Concluding Remarks</b> .....	<b>148</b>
<b>Appendix</b> .....	<b>149</b>
<b>List of Abbreviations/Terms</b> .....	<b>185</b>
<b>Reference list</b> .....	<b>187</b>

**i. List of Tables**

Table	Description	Page
1.1	Contemporary estimates of global inland water carbon budgeting terms.	17
2.1	Definition of seasons according to the months of the year as used in this thesis.	31
2.2	Detail on where samples and data used in this thesis have been sourced from.	39
3.1	Key catchment metrics for LOCATE estuaries	57
4.1	Salinities of samples collected in 2020 - 2021 in each river / estuary.	87
4.2	End member compositions of rainwater and pristine stream water influenced by carbonate, silicate and calcite bedrock.	93
4.3	Percentages of river flow originating from rainwater, carbonate and silicate bedrock in the Clyde, Forth and Tyne	101
4.4	Percentages of river flow originating from rainwater, calcite and carbonate in the Great Ouse	102
5.1	Number of ERA5 grid points used per estuary	112
5.2	Linear mixed effects model results predicting pCO <sub>2</sub>	122
5.3	Mean CO <sub>2</sub> flux values for 3 major salinity brackets in each estuary	127
A4.1	Certified and measured values of SUERC calibration standards	179
A4.2	Measured $\delta^{13}\text{C}_{\text{DIC}}$ data collected for Chapter 4 but not used	179-181

## ii. List of Figures

Figure	Description	Page
1.1	Summary schematic of the present anthropogenic perturbation to the global carbon cycle, sourced from the Global Carbon Budget 2022	12
1.2	The present and pre-industrial contributions of different processes and forms of storage within the LOAC to the global carbon cycle, sourced from Regnier et al. (2022)	15
1.3	Schematic sourced from Abril and Borges (2005) of the key elements of a theoretical, northern hemisphere, funnel-shaped estuary.	21
1.4	Schematic of the impact of different biogeochemical processes on $C_T$ and $A_T$ , sourced from Humphreys et al. (2018)	26
3.1	Map of estuaries sampled by LOCATE.	46
3.2	UK map of BGS bedrock data as categorised in this study.	48
3.3	Maps showing the catchment and NRFA gauging station locations for each estuary, relative to the sampling locations.	50
3.4	Intersection of (CEH/NRFA) catchment area and (BGS) bedrock classifications for the Thames.	51
3.5	River discharge data for each estuary from April 2017 - May 2018.	52
3.6	Variations in $C_T$ and $A_T$ for all LOCATE samples in 2017 – 18 from UK estuaries with salinity.	56
3.7	Map showing the catchment and NRFA gauging station locations for the Trent river, the 11 'Humber rivers', and the Hull, Ancholme and Graveney tributaries, relative to the sampling locations	60
3.8	Variations in $C_T$ and $A_T$ concentrations with salinity in Group 1 estuaries with individual regression lines.	61
3.9	Variations in $C_T$ and $A_T$ concentrations with salinity in Group 1 estuaries with overall regression lines.	62
3.10	Variation in $A_T$ concentration with nitrate concentration in Group 1 estuaries.	64
3.11	Mixing lines of $C_T$ and $A_T$ in Group 1 estuaries.	66
3.12	Residual $C_T$ and $A_T$ concentrations for Group 1 estuaries as shown in Fig. 3.9 according to temperature.	67
3.13	Residual $C_T$ and $A_T$ concentrations as a function of river discharge in Group 2 estuaries.	69
3.14	Variations in $C_T$ and $A_T$ concentrations with salinity in Group 2 estuaries with individual regression lines.	71
3.15	Mixing lines of $C_T$ and $A_T$ in Group 2 estuaries.	73

3.16	Residual $C_T$ and $A_T$ concentrations as a function of river discharge in Group 2 estuaries.	74
3.17	Variations in $C_T$ and $A_T$ concentrations with salinity in Group 3 estuaries with individual regression lines.	76
3.18	Mixing lines of $C_T$ and $A_T$ in Group 3 estuaries.	77
3.19	Residual $C_T$ and $A_T$ concentrations as a function of river discharge in Group 3 estuaries.	78
4.1	2017-18 $C_T$ and $A_T$ measurements from the four estuaries to be sampled in Chapter 4.	84
4.2	Estimated and measured Sr concentration.	92
4.3	$C_T$ concentrations in the four estuaries sampled.	94
4.4	$A_T$ concentrations in the four estuaries sampled.	95
4.5	Mixing diagrams for first end member mixing model.	96
4.6	Mixing diagrams for second end member mixing model.	97
4.7	A comparison of the percentage of flow calculated using Ca and Mg for the two mixing models.	99
4.8	Percentage of river flow from carbonate bedrock as a function of geological variables.	104
5.1	Map showing the location of Mace Head atmospheric observatory.	113
5.2	PCHIP interpolation of Mace Head $xCO_2$ measurements.	113
5.3	Scatterplot of hourly estimated $CO_2$ flux overlain with wind speed.	116
5.4	Differences between $FCO_2$ calculated at the sampling time and the seasonal $FCO_2$ estimate.	117
5.5	$pCO_2$ variations with salinity	121
5.6	Relationship between NPOC and $pCO_2$ concentration	123
5.7	$CO_2$ flux across the salinity gradient in all LOCATE estuaries	126
5.8	Seasonal $CO_2$ flux values in four example estuaries, showing the difference between the sampling date, all dates in the season, and the mean seasonal estimate	129
5.9	Proportional significance of constituents of $pCO_2$ uncertainty	130
5.10	Example of $CO_2$ flux interpolation for the Mersey estuary	131
A1	Contributions of input parameters to uncertainty in $pCO_2$	150
A2	Seasonal flux interpolations across estuarine surface areas	151-173
A3	Figure 1 – Map of LOCATE sampling locations; Figure 2 – seasonal $C_T$ and $A_T$ salinity gradients in four estuaries; Figure 3 – hypothesis schematic showing expected changes in isotopic composition	176-177
A6	Fig. 3.8 replicated using Mg calculations	184
A7	pH variation with salinity in LOCATE estuaries	184

### iii. Acknowledgements

This work was made possible by funding from NERC (industrial CASE PhD Studentship NE/R007632/1), Cefas Seedcorn (T205422), by the collection of samples as part of the LOCATE programme (N E/N018087/1), and by laboratory analysis completed as a result of a NEIF grant-in-kind (2238.0320).

There are so many people I would like to thank for their invaluable help, mostly during my PhD, but also for inspiring me to pursue it in the first place.

Firstly, to my supervisors, Dorothee, Naomi, Matthew, Silke and Richard. I am so grateful for your guidance and encouragement, for the opportunities you offered, and for the helpful criticism. It's been a rollercoaster ride, but you've all been so valuable in keeping the cart on the in-places slightly dodgy tracks. Dorothee, I feel very fortunate to have had you as a primary supervisor, particularly during the COVID-19 pandemic. You kept all of us going with your enthusiasm, one-to-one walks and picnics. Thank you so much.

I'm also so grateful to our 'girls', the lovely VINDTAs (I'm saying nice things, for their next customers' benefit!), for letting me put them through their paces, sure. But mostly, for the trials and tribulations. In those moments, friendships blossomed. Gareth, you teaching me to emotionally connect with inanimate objects was one of the best things that has ever happened to me. Elise, crying about Laurel and Lucy, and laughing through our PhDs has been the best. I miss us sharing an office with all my heart, and you are my joint favourite office mate (Mol does give good cuddles).

To my friends that have kept me going (a special mention to Vicky, Jade, Sarah and Joanna), mainly with cake, I will always be so grateful for your kindness, for listening to my rants and for sharing your own, but mainly for the cake. To my family, for going out of your way to give me every opportunity you possibly could. Want to learn 4 musical instruments? Sure. Swimming lessons? No problem. Trip to the eye hospital? Of course. Knowing you have always had, and will always have my back, is so precious to me. And to Ed, thank you for supporting me always and for being my joint number one fan with our furry daughter. Love you.

Finally, I would like to take a moment to thank one particular secondary school teacher; let's call him Mr. Smith. I came into Environmental Sciences through the Physical Geography route. I hated Geography as a teen, until the day I joined Mr Smith's class. Often Mr Smith would make factual errors in what he taught, to the great delight of the class, but his sheer enthusiasm for learning about our planet has stuck with me to this day and is probably the single biggest reason I chose this path. Mr Smith will almost certainly never read this, but to him I am eternally grateful.

**Chapter 1**  
**Introduction**

## 1.1 Climate change and the inorganic carbon cycle

*“... it’s easy to forget that ultimately the emergency climate comes down to a single number, the concentration of carbon in our atmosphere. The measure that greatly determines global temperature and the changes in that one number is the clearest way to chart our own story, for it defines our relationship with our world.”*

- *David Attenborough, Statement at COP26 opening ceremony, 1<sup>st</sup> November 2021*

Climate change is one of the key issues defining a generation. Earth’s climate is changing beyond recognition: global surface air temperatures, upper ocean temperatures, and precipitation are increasing, glaciers are retreating, while ocean pH and oxygen concentrations are decreasing, and sea levels are rising, to name but a few significant and measurable changes since 1850 (IPCC, 2021). The unprecedented increase in atmospheric carbon dioxide (CO<sub>2</sub>) mole fraction since preindustrial times is widely accepted to be a major cause of recent and projected changes to Earth’s climate (IPCC, 2014, 2021). As the climate of our planet continues to evolve in response to anthropogenic greenhouse gas emissions, and as the international message of commitment to limiting future climatic changes continues to gain momentum, the need for accurately evaluating the mole fraction of CO<sub>2</sub> in our atmosphere (and indeed in other environmental inventories, such as land and ocean) has never been greater, as so eloquently pointed out in the preceding quotation (Attenborough, 2021).

An international inter-disciplinary research effort is dedicated to resolving the gaps in our understanding of carbon cycle, by improving our understanding of the numerous feedback loops that work to regulate our climate. Without a full understanding of the various CO<sub>2</sub> sources (processes that act to release CO<sub>2</sub> to the atmosphere) and sinks (processes that act to take up atmospheric CO<sub>2</sub>), both in a baseline ‘natural’ state, and in their current functionality having been influenced by anthropogenic disturbance, accurate prediction of future changes is challenging. The forthcoming text details the reasons for these challenges, and some suggestions as what can be done to improve this understanding.

Carbon cycle research is aggregated in budgeting exercises. The Global Carbon Project (GCP, 2021) publishes an annual Global Carbon Budget, which provides a synthesis of the update to our understanding of the present-day magnitude of sources and sinks of CO<sub>2</sub>. Figure 1.1 provides their present assessment of the anthropogenic perturbation to the various sources, sinks, and storage mechanisms of CO<sub>2</sub> at a global scale (Friedlingstein et

al., 2022). The ‘Budget imbalance’ (Fig. 1.1), the difference between the net effect of these budget terms and measured CO<sub>2</sub> emissions, valued as -0.3 Pg C yr<sup>-1</sup>, implies either:

1. that there is an underestimated sink or overestimated source within their assessment;
2. that there is a net sink unaccounted for in the Global Carbon Budget; or
3. that the complex combination of uncertainties in the estimates result in an overall underestimation of the total combined carbon sink, or indeed an overestimation of the carbon source.

## The global carbon cycle

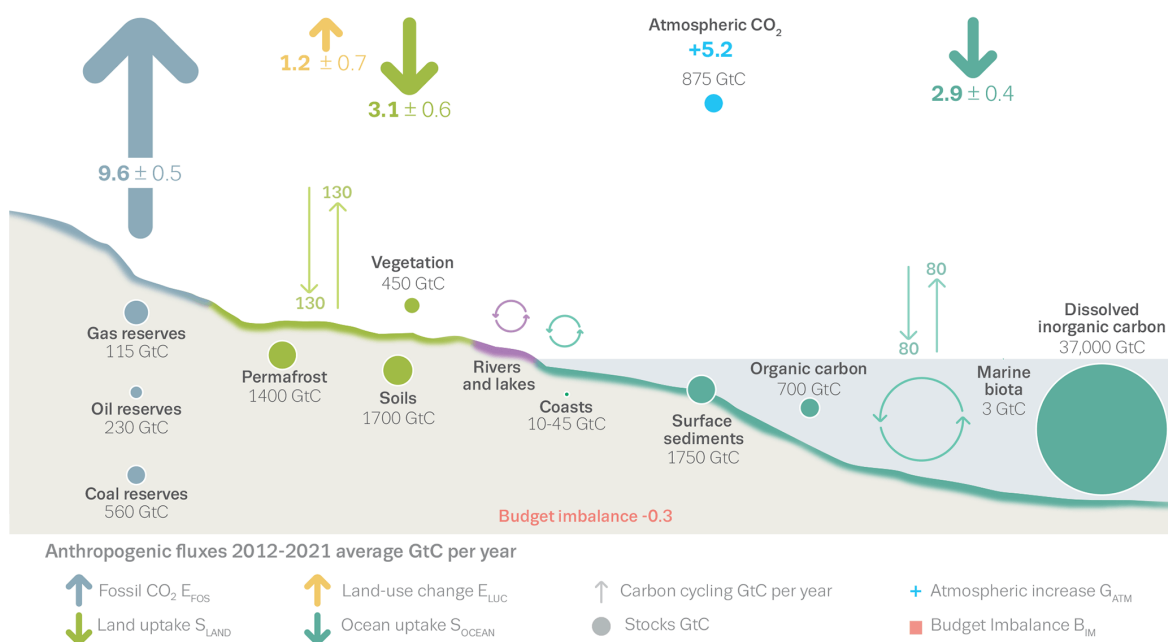


Figure 1.1 – A summary schematic of the present anthropogenic perturbation to the global carbon cycle, sourced from the Global Carbon Budget 2022 (from Friedlingstein et al., 2022). (N. B. Units of Gt and Pg (10<sup>15</sup> g) are equal units; Pg is used in the text of this chapter to be consistent with other studies)

The Global Carbon Budget identifies four processes that are not accounted for in their assessment:

1. Some anthropogenic CO<sub>2</sub> and methane (CH<sub>4</sub>) processes are not fully accounted for: cement production emissions, fossil fuel oxidation, CH<sub>4</sub> from oil production that is not immediately oxidised and anthropogenic emissions of CH<sub>4</sub> and carbon monoxide (CO) that are eventually oxidised to CO<sub>2</sub>;

2. CO<sub>2</sub> emissions from select industrial processes involving carbonates; emissions of fossil carbonates except from cement are not accounted for;
3. Reduction in land CO<sub>2</sub> sink from land use change since the preindustrial; and
4. The anthropogenic perturbation to the land-ocean aquatic continuum (LOAC) (Friedlingstein et al., 2022).

'LOAC' is a term used to aggregate the aquatic path across the interface between land and ocean, and includes rivers, estuaries, and coastal seas (Bauer et al., 2013; Regnier et al., 2013). Observational studies into the transport of carbon (C) through the LOAC have only been conducted in recent decades, so large uncertainties around the net carbon source / sink estimate for each constituent of the LOAC still exist. This, in addition to the intricate spatial resolution over which these transport processes occur, as well as strong heterogeneity between estuaries, means that the LOAC has, as of yet, only been included in biogeochemical models that cover the individual river – estuary - coast scale (e.g. Vanderborght et al., 2002; Hofmann et al., 2008; Regnier et al., 2013; Volta et al., 2016).

The LOAC transports organic and inorganic carbon from land to ocean. Some fraction of this transport will have existed prior to anthropogenic manipulation of the earth system; transport of terrestrial organic carbon and inorganic carbon from rock dissolution or respiration of terrestrially derived organic matter, by way of example, are not solely recent phenomena (Regnier et al., 2013, 2022). Several anthropogenic processes may have altered the lateral flux of carbon through the LOAC. Changes to precipitation and evapotranspiration alter the concentration of carbon within waters, as well as weathering rates, while direct anthropogenic disturbance of land use and nutrient inputs through agricultural activity and land use change alter the amount of carbon reaching the water (Bauer et al., 2013). Carbon inputs to the LOAC are expected to have increased, mainly due to anthropogenic perturbation of soil carbon export (Regnier et al., 2013). This has implications for both the land and ocean sink terms used in the Global Carbon Budget (Friedlingstein et al., 2022). The 'extra' anthropogenic carbon input to rivers is partly outgassed, and partly stored as sediment, with a small proportion (~10%) reaching the open ocean (Regnier et al., 2013).

Recent estimates for lateral carbon fluxes, which here includes inorganic and organic forms of carbon, have been limited by two key factors. Firstly, lacking data availability on the different forms of carbon processing and storage along the LOAC has historically led the LOAC being treated as a pipeline in budgeting exercises: a passive transporter of carbon from land to ocean, a treatment initially used by Sarmiento and Sundquist (1992) and still used in some recent estimates of carbon processing between land and ocean (Jacobson et al., 2007). Secondly, sparse measurement data inadequately represents the variability

between different LOAC systems. Different systems experience differences in climate, morphology, river discharge, bedrock composition, ecosystem characteristics and human pressures. The bias in LOAC systems sampled towards the northern hemisphere and towards large, macrotidal systems hinders our understanding of LOAC functioning at a larger scale.

The two recent estimates of lateral carbon transport from land to ocean that are most commonly cited in current literature, including in the recent IPCC AR6 Report (Canadell et al., 2021), are  $0.45 \pm 0.18 \text{ Pg C yr}^{-1}$  (Jacobson et al., 2007) and  $0.78 \pm 0.41 \text{ Pg C yr}^{-1}$  (Resplandy et al., 2018). The latter of these two estimates (Resplandy et al., 2018) was proposed as an improvement to the estimate provided by Jacobson et al. (2007), because it is closer in value to the total estimated ocean carbon sink, as calculated using empirical air-sea  $\text{CO}_2$  flux measurements, thus assuming a value to fill a gap in their total carbon budget (Resplandy et al., 2018). Neither estimate, therefore, accounts for the variety of different processing and storage mechanisms present within the LOAC.

Regnier et al. (2022) presents the first global LOAC carbon budget that attempts to account for the range of real-world sources and sinks found across the LOAC (Fig. 1.2), and they do so for both the present-day (with anthropogenic perturbation (Fig. 1.2 a) and for the pre-industrial LOAC (Fig. 1.2 b). The anthropogenic terms associated with outgassing in the riverine and estuarine portions of the LOAC (Fig. 1.2 a, circled terms in red text were determined based on bottom-up data-driven approaches. They have  $2 \sigma$  (2 standard deviations) uncertainty estimates equal to the flux estimates themselves. They are both denoted as 'low' confidence according to the IPCC classifications (Regnier et al., 2022). The inland waters outgassing term refers to rivers as well as lakes. The estuaries and tidal wetland term, whose negative sign indicates a net sink, includes outgassing from estuaries and  $\text{CO}_2$  uptake by tidal wetlands.

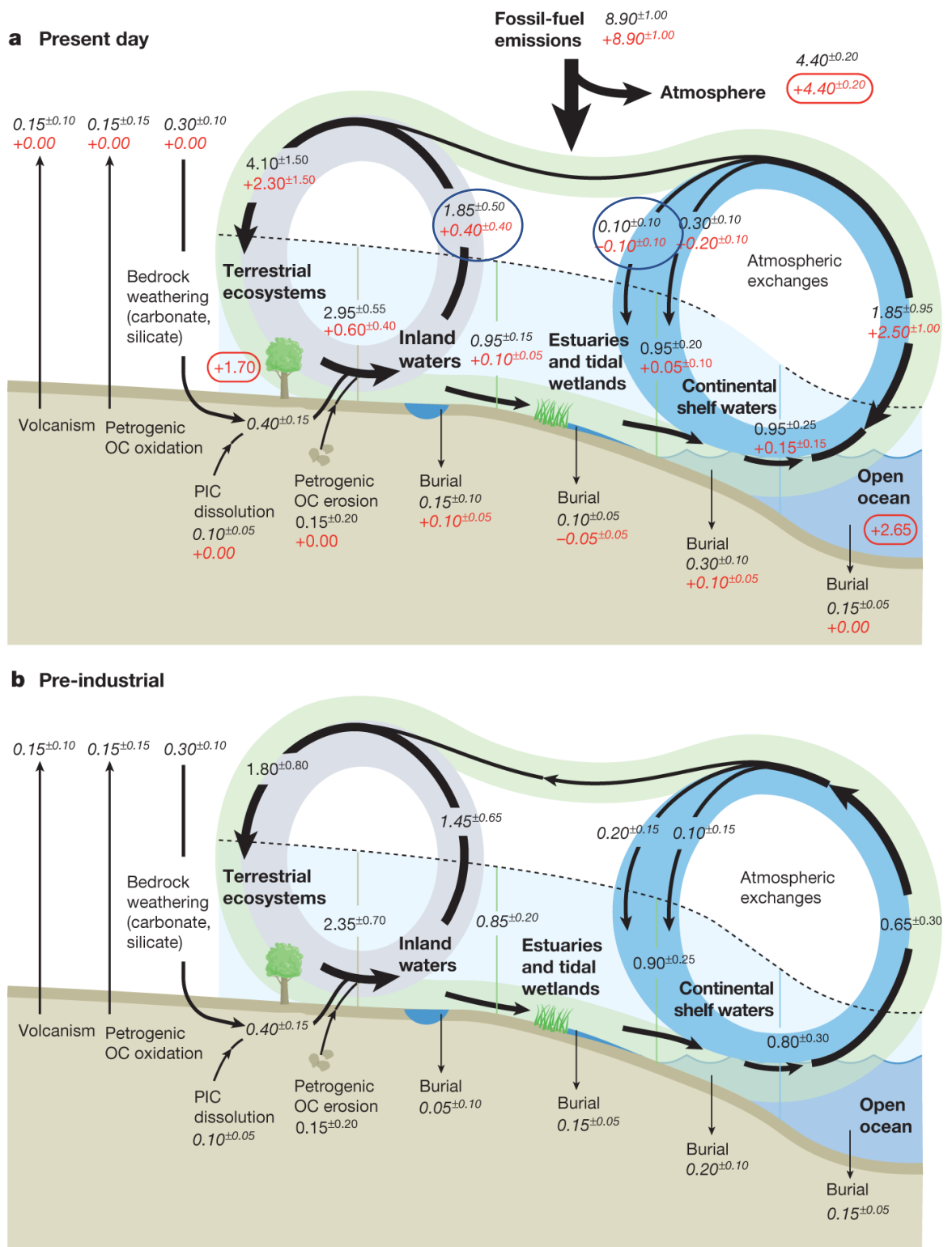


Figure 1.2 – The present (a) and pre-industrial (b) contributions of different processes and forms of storage within the LOAC to the global carbon cycle, sourced from Regnier et al. (2022). Values are given in Pg C yr<sup>-1</sup> and values given in red (a) represent the anthropogenic portion of each source, sink or transport term. The present-day values associated with riverine and estuarine outgassing are circled in blue. 2  $\sigma$  uncertainties are provided. PIC refers to particulate inorganic carbon and OC refers to organic carbon. N. B. The net term indicates uptake of carbon by estuaries and tidal wetlands. This term includes inorganic and organic carbon, and wetlands are a substantial carbon

*sink (0.18 Pg C yr<sup>-1</sup>), in excess of the in-stream outgassing (0.10 Pg C yr<sup>-1</sup>) which is the subject of this thesis (Regnier et al., 2022, supplementary information)*

Clearly, therefore, our understanding of riverine and estuarine CO<sub>2</sub> outgassing could be improved, and by improving these estimates we would benefit our wider understanding of CO<sub>2</sub> dynamics across the LOAC. The recent IPCC report presents an aim for future work to “Improve representation of the variability and trends in the transport of carbon through the land–ocean continuum, which has implications for partitioning the land and ocean CO<sub>2</sub> sinks” (Canadell et al., 2021, pg.769), work to improve understanding in this area of carbon cycle research could have far-reaching benefits across the climate science and policy communities.

## **1.2 Rivers as sources of atmospheric CO<sub>2</sub>**

As recently as the turn of this century, understanding of the carbon cycle essentially followed that there are three broad carbon reservoirs: land, ocean and geological reservoirs, which each exchange carbon with the atmosphere and to a limited extent with each other (Prentice et al., 2001). Rivers, lakes, and reservoirs, collectively known as inland waters, were historically thought to be minor contributors to global and regional carbon cycles because their surface area covered a comparatively small portion of the earth’s surface. Where budgets accounted for riverine carbon transport, they went no further than precisely that (e.g. Prentice et al., 2001): rivers were represented as passive pipes (Sarmiento and Sundquist, 1992) that solely transport carbon from its terrestrial source to the coastal ocean. Cole et al. (2007) put forward the first major budgeting exercise that accounted for the processes of CO<sub>2</sub> outgassing and carbon storage in sediments. Subsequent studies have developed upon this more representative view of the riverine contribution to carbon dynamics (Table 1.1 and references therein).

Riverine carbon processing can therefore be summarised as follows. Carbon is input laterally into freshwaters in organic and inorganic forms. Organic carbon in freshwater is sourced almost entirely from terrestrial ecosystems (Regnier et al., 2022). Soils contain a mixture of plant- and root-derived organic matter (Schmidt et al., 2011; Lehmann and Kleber, 2015) which reach the stream either as overland flow or through groundwater. Inorganic carbon inputs to freshwater are from bedrock weathering and from breakdown of organic matter. Both carbonate and silicate rock weathering release bicarbonate, which acts to increase inorganic carbon transport to freshwaters.

Table 1.1 – Contemporary estimates of global inland water carbon budgeting terms. Estimates are given in Pg C yr<sup>-1</sup>. Blank cells indicate that an estimate was not calculated for that term. Estimates of carbon outputs often do not sum to the input because photosynthesis is not included, and because where possible, only riverine outgassing rather than outgassing for all inland waters is shown. Where this was not possible it is indicated: (b).

a – bracketed term refers only to inorganic C. Unbracketed term refers to total C  
 b – includes lakes, reservoirs and wetlands as well as streams and rivers; inland waters  
 c – flux is from rivers into estuaries (because these studies account for estuarine processing separately)

Study	Terrestrial C input (Pg C yr <sup>-1</sup> )	C Storage in reservoirs / lakes / wetlands (Pg C yr <sup>-1</sup> )	CO <sub>2</sub> Outgassing (Pg C yr <sup>-1</sup> )	C transport into ocean (Pg C yr <sup>-1</sup> )
Cole et al. (2007)	1.9	0.23	0.23	0.71 (0.26 <sup>a</sup> )
Jacobson et al. (2007)				0.45
Tranvik et al. (2009)	2.9	0.6	1.4 <sup>b</sup>	0.9
Battin et al. (2009)	2.7	0.6	1.2 <sup>b</sup>	0.9
Aufdenkampe et al. (2011)			0.56	
Regnier et al. (2013)	2.5	0.6	1.1 <sup>b</sup>	1.0 <sup>c</sup>
Raymond et al. (2013)			1.8	
Lauerwald et al. (2015b)			0.65	
Sawakuchi et al., 2017)			2.48	
Drake et al. (2018)	5.1			
Resplandy et al. (2018)				0.78
Regnier et al., (2022)	2.95	0.15	1.85	0.95 <sup>c</sup>

A further source of both organic and inorganic carbon comes from rainwater itself. Airborne organic and inorganic carbon particles from a variety of sources including atmospheric dust, terrestrial plant emissions such as isoprene and through their combustion for example in wildfires, burning of fossil fuels, and industrial and agricultural emissions, act as condensation nuclei for water vapour (Pio et al., 2001; Riipinen et al., 2011; Simoneit and Elias, 2000; Snyder et al., 2009; Ward et al., 2017). This term is implicitly included in estimates of lateral terrestrial-derived inputs to rivers calculated through mass balance (Ward et al., 2017).

Estimates of the total (inorganic and organic) input of carbon into inland waters vary from 1.9 – 5.1 Pg C yr<sup>-1</sup> (Cole et al., 2007; Tranvik et al., 2009; Drake et al., 2018a; Regnier et al., 2022; Battin et al., 2009; Regnier et al., 2013). There is no particular trend to the estimates over the 15 years they span, but four of the six estimates are notably closer together in value, from 2.5 – 2.95 Pg C yr<sup>-1</sup> (Table 1.1; Battin et al., 2009; Regnier et al., 2013, 2022; Tranvik et al., 2009). Given that this term is usually calculated using a mass balance approach relative to measurable C fluxes further downstream (Regnier et al., 2022), in itself the large variability in this estimate gives some indication of the current understanding of LOAC carbon processing at a whole system level. The most recent of these studies finds that of the total lateral carbon input to inland waters, only approximately 13.6% is inorganic carbon with the remainder as organic carbon (Regnier et al., 2022).

Rivers are generally agreed to be net heterotrophic systems, whereby respiration exceeds photosynthesis overall (Raymond et al., 1997; Thorp and Delong, 2002; Wetzel, 2001). Allochthonous organic matter, transported from land into streams as described above, decomposes instream, releasing CO<sub>2</sub> (Battin et al., 2008). It is this *in situ* inorganic carbon production, rather than the inorganic carbon transported into freshwaters from chemical rock weathering, that is thought to sustain CO<sub>2</sub> supersaturation in river environments with respect to atmospheric CO<sub>2</sub> and thus drive CO<sub>2</sub> outgassing from rivers (Raymond et al., 2013). Again, estimates of CO<sub>2</sub> outgassing from rivers and inland waters are variable, with no clear trend in estimates over the last 15 years (Table 1.1 and references therein). The estimates of CO<sub>2</sub> outgassing are calculated by compiling direct measurements from inland waters and / or compiling other literature estimates which were themselves calculated using direct measurements, so the variability in the estimates has two main causes: different representation of processes or data, for example where estimates give studies more or less weight depending on their representation of lakes in particular (Regnier et al., 2013) and also differences in parameterisation of the water-to-air CO<sub>2</sub> flux calculation. The latter issue will be discussed in more detail in section 1.4. The estimates agree that rivers are net sources of CO<sub>2</sub> to the atmosphere.

Carbon burial in inland waters constitutes a relatively small carbon sink relative to the other terms (Battin et al., 2009; Cole et al., 2007; Regnier et al., 2022; Tranvik et al., 2009), and no riverine-specific estimates have been made to date. The most recent assessment of the riverine carbon cycle suggests that carbon burial only accounts for approximately 5% of the lateral influx of carbon to freshwaters, and, as such, is a relatively minor consideration here (Regnier et al., 2022).

The remaining carbon in the stream is transported into the next constituent unit of the LOAC: the estuary. The two studies which specifically report global transport flux of carbon from rivers into estuaries, rather than to the coastal ocean, show good agreement on estimated value (Regnier et al., 2013, 2022). In the 2022 LOAC budget (Regnier et al., 2022), the authors included 11 additional studies not available for their 2013 study. The similarity between the two estimates of lateral C transport from rivers to estuaries suggests that these additional studies show on average good agreement to those included in the earlier estimate (Regnier et al., 2022). Of the total carbon export from rivers to estuaries (or input to estuaries from rivers, depending on viewpoint) estimated in the most recent study to be  $0.95 \text{ Pg C yr}^{-1}$  (Regnier et al., 2022), inorganic carbon contributes  $0.37 - 0.45 \text{ Pg C yr}^{-1}$  globally (Kempe, 1979; Lacroix et al., 2020; Li et al., 2017; Middelburg et al., 2020).

Smaller scale empirical riverine studies suggest that the relative contribution of inorganic carbon to total dissolved carbon flux from rivers to estuaries may be higher than this in some locations. Carbon measurements in the 7 largest rivers of the UK (Thames, Severn, Trent, Tay, Tweed, Great Ouse and Yorkshire Ouse) taken in 2007 showed that on average 80% of their total dissolved carbon flux consisted of inorganic carbon (range: 57 – 91%; Jarvie et al., 2017). A study of carbon processing in the UK using measurements taken in 39 rivers across the UK in 2017 found that 69% of the total carbon export to estuaries was inorganic carbon (Tye et al., 2022b; Williamson et al., 2021). Therefore, inorganic carbon flux, consisting in some combination of bedrock-weathered material and respired organic matter, is an important, yet variable, carbon input to estuaries.

### **1.3 Inner estuaries as sources of atmospheric CO<sub>2</sub>**

There are a number of ways of defining the term, 'estuary'. The definition itself has been the subject of some debate over the last approximately 60 years (Potter et al., 2010). One of the earliest formal definitions of an estuary is "a semi-enclosed coastal body of water, which has free connection with the open sea, and within which seawater is measurably diluted with freshwater derived from land drainage" (Pritchard, 1967). This definition is still

commonly used today, but with a variety of updates and caveats depending on the location of the study. For example, the definition provided by Pritchard (1967) is less suitable for some southern hemisphere regions where sand banks at the estuarine mouth can periodically fully enclose the estuarine mouth, and where hypersalinity can result from evaporation in warm, dry climates (Potter et al., 2010). The updated definition provided by Potter *et al.* (2010) can be applied to all climates but will not be used here because it proves superfluous for classical Northern hemisphere estuaries, as will be the subject of this thesis, and therefore has not been used widely by carbonate chemistry studies in estuaries to date. For continuity and simplicity therefore, the Pritchard (1967) definition is used in this thesis.

Often studies separate the inner estuary from the estuarine plume. The inner estuary is bound by the limit of salinity or tidal influence at the upper limit, depending on the definition used. In this thesis the limit of salinity is used because the sampling locations were defined by salinity. The inner estuary is bound by the estuarine mouth at the seaward end, essentially by drawing a straight line between the opposing banks of the estuary at the coastline (Fig. 1.3; Abril and Borges, 2005). The estuarine plume is where the influence of estuarine outflow can be traced across the near-shore coastal waters. This can often be traced using salinity, which was first identified as a tracer when defining estuarine plumes (Ketchum, 1983). More recent studies have also used other biogeochemical tracer variables, such as temperature, chlorophyll *a*, inorganic nutrients, total alkalinity and coloured dissolved organic matter (Borges, 2005 and references therein). The results of this thesis (Chapters 3 – 5) use the generic term ‘estuary’ to refer essentially to inner estuaries, with results pertaining to the area bounded by the estuarine mouth, with the limitation here imposed by sampling locations, as well as, where applicable, secondary estuary boundary data being solely available with a cutoff at the estuarine mouth (JNCC, 2013). This definition does not include saltmarshes, seagrasses or other blue carbon habitats, which themselves act as carbon sinks (Regnier et al., 2022, supplementary information).

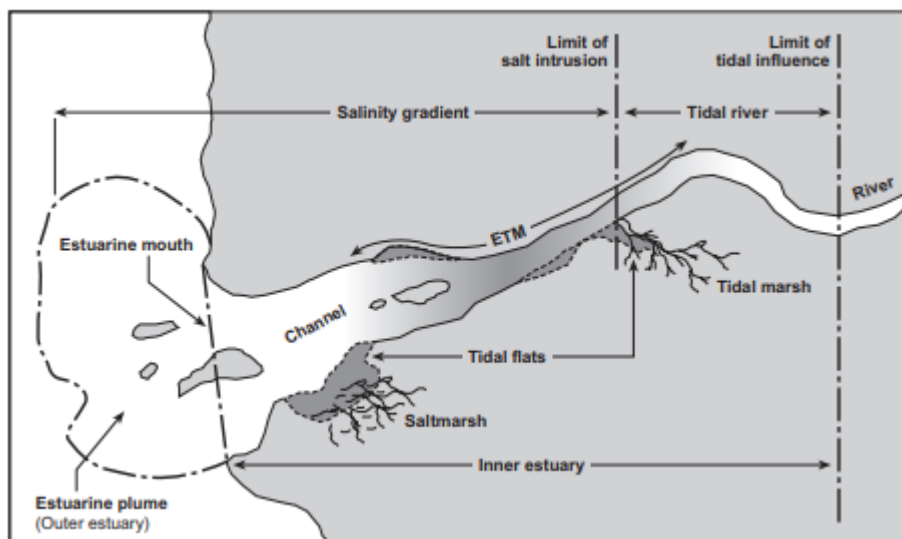


Figure 1.3 – Schematic taken from Abril and Borges (2005) of the boundaries between key elements of a theoretical, northern hemisphere, funnel-shaped estuary. ‘ETM’ is used to refer to the estuarine turbidity maximum, the localised area in an estuary which experiences high concentrations of suspended sediment (Geyer, 1993). The estuary definition used in this thesis refers to the area between the limit of salt intrusion and the linear boundary between the two banks at the estuarine mouth, as shown in this diagram.

Globally, lateral transport of carbon from estuaries into the coastal ocean is approximately equal to the riverine input of carbon at the estuarine inflow (Regnier et al., 2022). Whereas for the river-estuary lateral flux there are data available on the relative contribution of inorganic and organic carbon to the total lateral flux (Kempe, 1979; Lacroix et al., 2020; Li et al., 2017; Middelburg et al., 2020; Tye et al., 2022b; Williamson et al., 2021), the same is not the case for the estuarine lateral transport of carbon to the coastal ocean. However, estuaries are considered sites of intense organic carbon processing (e.g. Abril and Borges, 2005; Bakker et al., 2014);  $\text{CO}_2$  outgassing fluxes cannot be sustained by riverine inorganic carbon input alone, so organic carbon decomposition in estuaries must be sufficient to sustain measured outgassing fluxes (Borges et al., 2006). This  $\text{CO}_2$  outgassing is approximately balanced by carbon burial in wetlands and estuarine sediments (Regnier et al., 2022), but nevertheless constitutes an important indicator of the efficiency of estuaries at returning a portion of the land-derived carbon they receive to the atmosphere as  $\text{CO}_2$ .

Outgassing fluxes have been calculated from carbonate chemistry measurements in a range of estuaries and upscaled to represent the global estuarine  $\text{CO}_2$  emission. Global estimates range from  $0.09 - 0.6 \text{ Pg C yr}^{-1}$  (Abril and Borges, 2004; Bauer et al., 2013; Borges and Abril, 2012; Borges, 2005; Borges et al., 2005; Cai, 2011; Chen et al., 2013; Chen and Borges, 2009; Ciais et al., 2021; Cole et al., 2007; Laruelle et al., 2010, 2013;

Maher and Eyre, 2012; Regnier et al., 2013, 2022; Zscheischler et al., 2017), with the most recent estimates tending toward an outgassing flux of  $0.1 \text{ Pg C yr}^{-1}$  (Regnier et al., 2022).

This variety in global and regional estimates of  $\text{CO}_2$  outgassing fluxes from estuaries results from a number of factors. Firstly, estimates of the global surface area of estuaries are highly uncertain. The global estimate of estuarine surface area, of inner estuaries including blue carbon habitats (highly productive coastal ecosystems, including mangroves, seagrasses and saltmarshes) of  $1.75 \times 10^6 \text{ km}^2$  (Woodwell et al., 1973) is commonly used to upscale estuarine  $\text{CO}_2$  outgassing to a global scale. Woodwell et al. (1973) compiled data on U.S. coastline lengths, together with concurrent surface area estimates of both open water and 'marsh', which they use to describe blue carbon habitat types and assume that the ratios between coastline lengths and estuarine surface areas in the U.S. hold true for coastlines across the globe. They estimate that their surface area estimate may not be accurate to within  $\pm 50 \%$  (Woodwell et al., 1973). Their estuarine surface area value is likely to be overestimated, but provides a good first-order approximation for inner estuaries (Borges, 2005).

More recently, advances in Geographical Information Systems (GIS) have enabled an updated quantification; Laruelle et al. (2010) calculated the surface area of 138 estuaries to encompass the different estuary types proposed by Dürr et al. (2011), and estimated their relative contribution to the global estuarine surface area. Uncertainty remains, however; deriving even a single estuary's boundary data is complex, with the competing effects of tides, conservative mixing and outer estuaries, we must remain skeptical of estuarine surface area estimates. For example, the revised surface area estimate of  $1.067 \times 10^6 \text{ km}^2$  (Laruelle et al., 2010) following the estuarine typology presented by Dürr et al. (2011) includes inner estuaries only. This approach well suits the thesis presented here, but other studies must be cautious as to its application to their own data, particularly since the upper limit of the estuary is not well defined in these studies, only as 'bordered by rivers' (Dürr et al., 2011, pg. 442).

Secondly, the gas transfer velocity,  $k$ , value used in the calculation of gas flux is parameterised using wind speed for open ocean and shelf waters. However, variability in physicochemical conditions between and within estuaries, such as fetch (the surface area of water over which the wind blows) and surfactants (natural and/or anthropogenic compounds that can affect the physical properties of the surface microlayer of natural waters) (e.g. Jaeger et al., 2019), mean that using seawater parameterisations of gas transfer velocity to estimate  $\text{CO}_2$  flux from estuaries may not be appropriate (Abril and Borges, 2004; Raymond and Cole, 2001). This will be explored in more detail in section 1.4.

Furthermore, due to substantial spatial and seasonal heterogeneity, with no clear method of determining how representative the sampled estuaries are, global estimates of estuarine contribution to the carbon cycle are subject to large uncertainties (Abril and Borges, 2004). To date, there are few regions of the world where estuary sampling has occurred to gain insight into their contribution to atmospheric CO<sub>2</sub>. Those empirical studies which do exist have focused almost exclusively on large, macrotidal estuary systems, often on a single estuary (Howland et al., 2000; Hydes and Hartman, 2012; Joesoef et al., 2017; Oliveira et al., 2017; Raymond et al., 2000). The large spatial heterogeneity in estuarine systems prevents the accurate quantification of their contribution to the global carbon cycle (Abril and Borges, 2004). As a result, the scope of the literature to determine accurate estimates of global estuarine water-airCO<sub>2</sub> flux is limited.

Overall, one of the key sources of uncertainty when quantifying the contribution of estuaries to the global carbon cycle is insufficient spatial coverage of measurements. As a result, the study of a variety of estuaries, of different sizes and experiencing different biogeochemical background conditions is vital to the more accurate quantification of the estuarine CO<sub>2</sub> source.

This has implications for the study of both the present and the future of the carbon cycle. The large spatial heterogeneity in physical and environmental factors between estuaries means that as the atmospheric CO<sub>2</sub> mole fraction increases, consequences for the carbonate system in estuaries, and indeed downstream in outer estuaries and the coastal ocean may vary depending on local biogeochemical conditions (McGrath et al., 2019). For example, in the Eastern North Pacific, the coastal CO<sub>2</sub> sink is increasing (Wong et al., 2010), whereas in the North Sea, the coastal CO<sub>2</sub> sink is decreasing in magnitude (Thomas et al., 2007), with important implications for coastal ocean acidification. Without fully understanding the present state of the estuarine carbon source, we are not adequately equipped to predict future changes.

#### **1.4 Carbonate chemistry**

Understanding the dynamics of CO<sub>2</sub> in natural waters requires the characterisation of their carbonate chemistry. This section provides a brief explanation of some of the key concepts in aquatic carbonate chemistry that we must understand before making CO<sub>2</sub>-relevant measurements in waters across the LOAC.

There are four commonly measured variables with which the carbonate system in natural waters can be described: pH, partial pressure of CO<sub>2</sub> (pCO<sub>2</sub>), dissolved inorganic carbon (C<sub>T</sub>) and total alkalinity (A<sub>T</sub>). If two of these four variables are known, as well as the

temperature, salinity, pressure / depth and dissolved inorganic nutrients (phosphate and silicate) of a sample, it is possible to calculate the remaining two variables and thus characterise the entire carbonate system. Selection of the two variables to be measured should be based on their relevance to the study, although it is often also dictated by the availability of equipment. The selection of variables relevant to the research questions is critical, because although the calculation of the other two carbonate chemistry variables is possible from any two chosen, each variable pairing propagates a different degree of uncertainty into the other calculated variables (Millero, 1995; Orr et al., 2018).

Of these parameters, total alkalinity,  $A_T$ , is particularly important in estuaries because differences in riverine alkalinity delivery at the estuarine inflow have been identified as a factor affecting the vulnerability of estuaries and coastal oceans to acidification (Van Dam et al., 2018; Van Dam and Wang, 2019). Furthermore, in estuaries the minor components of alkalinity may be more important than in seawater, because they can be produced through anaerobic processes (Schiettecatte et al., 2006; Thomas et al., 2009).  $A_T$  is usually conservative with salinity but at the scale of estuaries and shelf seas, denitrification and manganese, iron and sulfate reductions are likely to occur under anoxic conditions, as well as  $\text{CaCO}_3$  (calcium carbonate) dissolution, all of which act to produce alkalinity (Chen and Wang, 1999; Thomas et al., 2009). The most widely-recognised definition of alkalinity is provided by Dickson (1981, pg. 611): “The total alkalinity of a natural water is thus defined as the number of moles of hydrogen ion equivalent to the excess of proton acceptors (bases formed from weak acids with a dissociation constant  $K \leq 10^{-4.5}$ , at 25°C and zero ionic strength) over proton donors (acids with  $K > 10^{-4.5}$ ) in one kilogram of sample.” (where  $K$  is a unitless constant, Eq. 1.1).

*Equation 1.1*

$$A_T = [\text{HCO}_3^-] + 2[\text{CO}_3^{2-}] + [\text{B(OH)}_4^-] + [\text{OH}^-] + [\text{HPO}_4^{2-}] + 2[\text{PO}_4^{3-}] + [\text{SiO(OH)}_3^-] + [\text{HS}^-] + 2[\text{S}^{2-}] + [\text{NH}_3] - [\text{H}^+] - [\text{HSO}_4^-] - [\text{HF}] - [\text{H}_3\text{PO}_4] \text{ (Dickson, 1981, pg. 612)}$$

Dissolved inorganic carbon,  $C_T$ , the sum of  $\text{CO}_2$ , bicarbonate ( $\text{HCO}_3^-$ ) and carbonate ( $\text{CO}_3^{2-}$ ) concentrations in solution (Eq. 1.2) is often paired with  $A_T$  measurements in carbonate chemistry studies for two key reasons, one based on rationale and one practical. Practically, for recent carbonate chemistry studies, this is because a common apparatus for carbonate chemistry measurements, the Versatile INstrument for the Determination of Total inorganic carbon and titration Alkalinity (VINDTA) (Mintrop et al., 2000) analyses seawater samples for  $C_T$  and  $A_T$  samples simultaneously. The rationale for measuring  $C_T$  in LOAC studies is twofold. Firstly, budgeting exercises including those discussed previously (e.g.

Friedlingstein et al., 2022; Regnier et al., 2022) commonly constrain fluxes of carbon, including  $C_T$  between the different parts of the LOAC and indeed the whole Earth system. Making  $C_T$  measurements across the LOAC therefore acts to constrain carbon budgeting exercises. Secondly, the combination of  $C_T$  and  $A_T$  is valuable, particularly in estuaries which span a large range of salinities.  $C_T$  and  $A_T$  both mix conservatively: as two hypothetical parcels of water mix in different ratios, all other factors held equal,  $C_T$  and  $A_T$  concentrations (in addition to salinity) can be calculated simply from that same ratio. Therefore, non-linear changes in  $C_T$  and  $A_T$  as salinity increases towards the seawater end member may be used to describe biogeochemical processes acting to change the carbonate chemistry of the water other than mixing.

*Equation 1.2*

$$C_T = [\text{CO}_2] + [\text{HCO}_3^-] + [\text{CO}_3^{2-}] \text{ (Zeebe and Wolf-Gladrow, 2001, pg. 3),}$$

where (Eq. 1.3):

*Equation 1.3*

$$[\text{CO}_2] = [\text{CO}_2(\text{aq})] + [\text{H}_2\text{CO}_3] \text{ (Zeebe and Wolf-Gladrow, 2001, pg. 2)}$$

A variety of such biogeochemical and physico-chemical processes exist. Figure 1.4 provides a visual representation of a number of these processes and the impact they have on  $C_T$ ,  $A_T$ , and how that links to  $p\text{CO}_2$  (Humphreys et al., 2018). Of particular relevance to estuarine carbonate chemistry are the sea-air  $\text{CO}_2$  flux (in our case, water-to-air  $\text{CO}_2$  flux),  $\text{CaCO}_3$  dissolution, and remineralisation (respiration / decomposition) terms. Estuaries are widely agreed to be net sources of  $\text{CO}_2$  to the atmosphere (Section 1.3 and references therein). This outgassing, or water-to-air  $\text{CO}_2$  flux, reduces the  $p\text{CO}_2$  and  $C_T$  but does not impact  $A_T$  concentration (Figure 1.4; Humphreys et al., 2018). Similarly, estuaries are net heterotrophic (Borges et al., 2006; Cai, 2011; Raymond et al., 2000), which acts to increase  $p\text{CO}_2$  and  $C_T$  but decrease  $A_T$  (Figure 1.4; Humphreys et al., 2018).

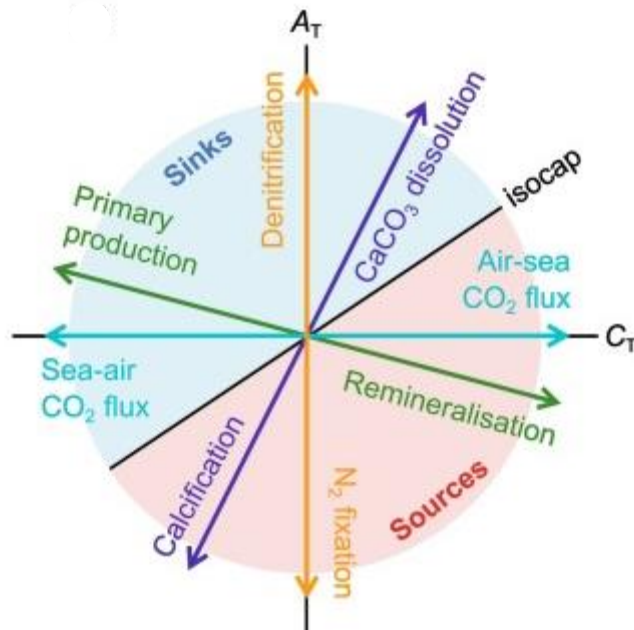


Figure 1.4 – schematic of the impact of different biogeochemical processes on  $C_T$  and  $A_T$  (x and y axes respectively), from Humphreys et al. (2018). Processes falling in the red ‘sources’ segment act to increase  $pCO_2$  and processes in the blue ‘sinks’ segment decrease  $pCO_2$  in the water. The black line, labelled ‘isocap’, is a theoretical horizon that indicates where the  $C_T$  and  $A_T$  changes balance each other out, with no net effect on  $pCO_2$ .

$CaCO_3$  production / dissolution in the marine context usually refers to biogenic calcite/aragonite as  $CaCO_3$ , but here is equally applicable to the contribution of calcium carbonate bedrock more likely to substantially influence riverine and estuarine  $C_T$  and  $A_T$  concentrations.  $CaCO_3$  dissolution acts to lower  $pCO_2$  while increasing both  $C_T$  and  $A_T$  concentrations (Figure 1.4; Humphreys et al., 2018). Higher-than-seawater  $C_T$  and  $A_T$  concentrations at low salinities in estuaries have been recently attributed to limestone bedrock dissolution (McGrath et al., 2016, 2019).

Water-to-air  $CO_2$  fluxes in estuaries are a key uncertainty in budgeting exercises (Section 1.3). However, calculating  $CO_2$  fluxes from rivers and estuaries to the atmosphere is challenging. In seawater,  $CO_2$  fluxes ( $FCO_2$ ) are often calculated from  $pCO_2$  values (Eq. 1.4), which in turn can be calculated from  $C_T$  and  $A_T$ .

Equation 1.4

$$FCO_2 = k(pCO_{2\ water} - pCO_{2\ air})$$

where  $k$ , the gas transfer velocity is expressed by an equation of the format:

Equation 1.5

$$k = n u^2 (Sc/660)^{-0.5}$$

where  $u$  refers to wind speed at a height of 10 m, the Schmidt number,  $Sc$ , is proportional to  $k$  at temperatures between 0 – 30 °C (Jähne et al., 1987; Wanninkhof, 1992), and  $n$  here denotes a proportionality constant between wind speed and  $k$ .

Equation 1.5 is for seawater; the value of  $Sc$  varies depending on the gas in question, here  $CO_2$ , temperature and salinity. The  $Sc$  of seawater at 20 °C is 660; in freshwater it is 600 (Wanninkhof, 1992). For intermediate salinities, the freshwater and seawater Schmidt numbers are calculated, from which  $Sc$  at the appropriate salinity can be calculated using the equation of the straight line between freshwater and seawater  $Sc$  values.

Difficulty arises when applying Equations 1.4 and 1.5 to freshwater and estuarine  $pCO_2$  data. At the start of this century, there were very few direct measurements of  $k$  in rivers and estuaries, which made assessing the applicability of gas transfer parameterisations of the form of Equation 1.4 to the estuarine/riverine problem impossible (Raymond and Cole, 2001). The value of  $k$  varies according to turbulent mixing in the surface boundary layer; in the open ocean and across bodies of water with large surface areas (e.g. large lakes) this turbulence is largely driven by wind stress, so wind speed is an appropriate variable by which to estimate  $k$  (e.g. Wanninkhof, 1992). In streams and shallow rivers, the surface layer turbulence is driven by the same factors, but also has a contribution from turbulence generated from friction as water passes over the riverbed (Raymond and Cole, 2001). A number of riverine parameterisations have been proposed (e.g. Alin et al., 2011; Lauerwald et al., 2015; Raymond et al., 2000), which use either wind speed and a measure of stream dimensions, or water current velocity.

Estuaries may be subject to either or both of these constraints. The theoretical primary controls on estuarine gas transfer velocities were put forward by Cerco (1989) as wind stress and water shear stress, meaning that estuarine  $k$  parameterisations should ideally include depth, tidal velocity and wind speed (Raymond and Cole, 2001). However, more recent studies have found that in practice,  $k$  parameterisations based solely on wind speed are sufficient in estuaries (Borges et al., 2004; Jiang et al., 2008). Ho et al. (2016) found that ocean-derived parameterisations of gas transfer velocity were significantly better predictors of gas transfer in an estuary study than estuarine-derived parameterisations. Similarly, the gas transfer velocity parameterisation of Ho et al. (2006) provide the best fit for a range of estuarine measurements (Jiang et al., 2008, Fig. 2) when compared to an estuarine-specific parameterisation (Raymond and Cole, 2001).

## 1.5 Thesis aims

This thesis aims to address some of the outstanding questions in estuarine and riverine carbon cycle research in the context of LOAC carbon processing and outgassing of CO<sub>2</sub>.

- i. What factors define the carbonate chemistry of rivers and estuaries, and what is their relative importance?*

In Chapter 3 (estuaries) and Chapter 4 (rivers), carbonate chemistry measurements from the natural aquatic environment are used to identify the key factors that drive differences in carbonate chemistry between catchments. Chapter 3 explores the processes identified in Section 1.4 that may contribute to changes in C<sub>T</sub> and A<sub>T</sub> concentrations in 16 estuaries around the UK. In particular, carbonate bedrock dissolution has been found to drive large differences between low salinity concentrations of C<sub>T</sub> and A<sub>T</sub> (Section 1.4), so Chapter 3 uses secondary data describing catchment geology to determine its effect on C<sub>T</sub> and A<sub>T</sub> concentrations. A smaller-scale riverine study (Chapter 4) using additional variables (solute concentrations and strontium isotopic signatures) considers the applicability of secondary bedrock data to this form of study and attempts to quantify the contribution of different bedrock types to river flow. Taken together, these works are an important contribution to understanding of carbonate chemistry dynamics across a broad range of calcium carbonate bedrock contributions, as the UK is uniquely placed to provide.

- ii. How much CO<sub>2</sub> is emitted from estuaries into the atmosphere, and what drives that emission?*

Building on data analysed in Chapter 3, pCO<sub>2</sub> and CO<sub>2</sub> fluxes are calculated from 14 estuaries around the UK (Chapter 5). pCO<sub>2</sub> is thought to be sustained primarily by organic carbon degradation in estuaries (Section 1.3) so a range of data collected as part of a wider sampling programme the samples in Chapters 3 and 5 came from (Section 2.1) are used to examine the contribution of factors related to organic carbon degradation to pCO<sub>2</sub>. Additionally, this chapter explores whether the same factors that defined C<sub>T</sub> and A<sub>T</sub> concentrations (Chapter 3), from which pCO<sub>2</sub> is calculated (Chapter 5), have an effect on pCO<sub>2</sub> and subsequently FCO<sub>2</sub>. Finally, the calculated fluxes to are used to calculate a bottom-up estimate of the UK estuarine outgassing flux. This is the first quantification of UK estuarine outgassing and adds important measurements to the still small global pool of

studies that have measured or calculated CO<sub>2</sub> fluxes from estuaries, thus contributing to understanding of inner estuaries as constituents of the carbon cycle.

Overall, the large number of variables measured as part of each chapter of this thesis enables the quantification of a variety of different contributors to carbonate chemistry. Furthermore, Chapters 3 and 5 of this thesis are unique in the estuarine carbonate chemistry field thus far, as a result of my inclusion in a UK-wide sampling programme (Section 2.1), in the number and variety of different estuaries included. Through more representative studies of these highly variable biogeochemical units, it will be possible to further refine our understanding of their contribution to the carbon cycle at a regional and global scale.

## **Chapter 2**

### **Generic Methods**

The methods specific to each chapter (3 – 5) are presented within each chapter. Here, methodology that was used across all of the chapters is detailed.

## 2.1 Sampling context: LOCATE

The samples that the results of Chapters 3 and 5 are based on were collected as part of the Land Ocean CARbon TransfEr (LOCATE) programme. The sampling will be described in those chapters (in particular, in section 3.2), but due to its importance to this thesis as a whole, here some context to the programme overall is provided.

LOCATE (NERC grant: NE/N018087/1) is a programme that has brought together researchers and resources from institutions across the UK. LOCATE was led by the National Oceanography Centre (PI: Prof. Richard Sanders), with key partner institutions: UK Centre for Ecology and Hydrology, British Geological Survey, Plymouth Marine Laboratory and the Universities of East Anglia, Lancaster, Durham, Hull and of the Highlands and Islands.

The programme aimed to sample 16 UK estuaries and many more rivers for a range of different variables. The variables measured were: temperature, salinity, conductivity, salinity, concentrations of ammonium, nitrate, phosphate, non-purgeable organic carbon, total dissolved carbon, total nitrogen, total phosphorus, dissolved organic matter fluorescence and absorbance, particulate organic carbon and nitrogen,  $^{13}\text{C}$  and  $^{15}\text{N}$ . These data, including the measurements as presented in Chapter 3 of this thesis, are published as Tye et al. (2022a).

Both the estuary and river sampling efforts spanned one year, with each river being sampled in one location on a monthly basis. The aim of the estuary sampling was to sample across the salinity gradient seasonally, from April 2017 – April 2018. Seasons are defined according to the months of the year as shown in Table 2.1, and this definition is used throughout the thesis.

*Table 2.1 – Definition of seasons according to the months of the year as used in this thesis.*

Season	Months
Winter	January, February, March
Spring	April, May, June
Summer	July, August, September
Autumn	October, November, December

Sampling of a salinity gradient was achieved by collecting samples at salinities of approximately: 0, 2, 5, 10, 15 and 20 - 25. It was not possible to sample this salinity range in two of the estuaries, due to physical obstacles to sampling. As a result, samples were collected in Spring only for the Tees and the Mersey estuaries, but in the remaining 14 estuaries, the full seasonal cycle was sampled.

A number of measures were taken to ensure consistency of approach in sampling and analysis: An identical set of sampling protocols was followed by each institution; sampling equipment was purchased centrally; all institutions conducted sampling within the same week; all samples for a given variable were sent to a single institution responsible for its analysis. Samples collected for  $C_T$  and  $A_T$  were analysed as part of this thesis.

## **2.2 Sampling**

All  $C_T$  and  $A_T$  samples, whether collected as part of the LOCATE sampling programme or specifically for this thesis, were collected following the Standard Operating Procedure for ocean carbonate chemistry sampling (Dickson et al., 2007). Unless specified otherwise in the methods section of a specific chapter, all samples were collected by drawing a bucket of water from over the side of a boat, or from the bank of the channel. Clean 250 ml borosilicate bottles were rinsed three times with sample, and then completely filled from the bucket by gently submerging them so as to not generate bubbles. A Pasteur pipette was used to remove 2.5 ml of sample to create a headspace of 1% by volume. 50  $\mu$ l of saturated mercuric chloride solution was added to each sample. A ground glass stopper was greased with Apiezon<sup>®</sup> L grease, inserted into the sampling bottle and rotated to firmly seal shut. Each lid was secured onto the bottle, either by wrapping electrical tape around the lid and bottle twice, or by wrapping an elastic band around the lid and bottle and securing the elastic with a cable tie. Bottles were stored in the dark until analysis, which occurred between 2 months and 1.5 years after collection.

Salinity was measured at each LOCATE sampling site by immersing a calibrated salinity probe into the bucket of water from which the samples were taken. Where the institution collecting the samples did not have access to a salinity probe, a salinity sample was taken in a 125 ml bottle sealed shut with electrical tape to prevent loss by evaporation. These samples were analysed by probe on return from the field. Participants were instructed to ensure they were happy with the calibration of their salinity meter. Salinity was measured at each sampling site in Chapter 4 by immersing a Castaway CTD (Sontek), which measures conductivity and reports calculated salinity according to the Practical Salinity Scale (Fofonoff and Millard Jr, 1983). The Castaway was calibrated by the manufacturer

and is built with six electrodes in the flow channel, as opposed to the two that are required, which improves measurement accuracy and provides resistance to calibration error (Sontek, 2012). A Castaway must be immersed at a depth of at least 20 cm, so at each sampling location in Chapter 4, the Castaway measurement was taken instream at as little depth as possible, immediately prior to bucket sampling. This introduces a source of uncertainty in the salinity values because the salinity measurement is not taken from sampling bucket or bottle itself. However, a salinity difference of 1 between the Castaway value and true salinity of the sample, which in itself would be highly unlikely at the freshwater end member, would yield an alkalinity difference of approximately  $3 \mu\text{mol kg}^{-1}$ , using the mean concentrations of  $C_T$ ,  $A_T$ , phosphate and silicate for the 2017-18 sampling campaign, and salinity values of 0.5 and 1.5 respectively. Relative to the differences expected between four of the most disparate systems in terms of their carbonate chemistry, this uncertainty is relatively small.

### **2.3 Laboratory analysis of $C_T$ and $A_T$**

The Versatile INstrument for the Determination of Total dissolved inorganic carbon and titration Alkalinity (VINDTA 3C, #4 and #7, Marianda, Germany) was developed by Marianda, originally to measure  $A_T$  in seawater. Its capability was later extended to simultaneously analyse  $C_T$ . The instrument performs the standard operating procedures to analyse  $C_T$  by coulometry and  $A_T$  by potentiometric open-cell titration (Dickson et al., 2007). Certified Reference Material (CRM) from Andrew Dickson (Dickson et al., 2003, batches 90, 97, 133 and 182) were used to calibrate  $C_T$  and  $A_T$  measurements, and in the absence of duplicate samples, to assess the precision of the instruments.

The analysis of  $C_T$  is achieved by measuring out a known volume of sample, in this case approximately 20 ml, which is acidified immediately with approximately 1.5 ml of 8.5% phosphoric acid (Dickson et al., 2007; Johnson et al., 1993). This converts all of the dissolved inorganic carbon in the sample to  $\text{CO}_2$ , which is carried by  $\text{CO}_2$ -free nitrogen into the coulometer cell (Johnson et al., 1993). The coulometer records the 'counts' of carbon dioxide received, and once the per-minute increase in counts has decreased to a level decided by the user, it stops. This method is designed for seawater samples but the method remains appropriate for samples of all salinities and  $C_T$  concentrations; the coulometer settles at different rates depending on the  $C_T$  concentration in the sample, and only settles once all of the  $C_T$  has been measured.

The VINDTA 3C analyses alkalinity by titrating a known volume of seawater, approximately 100 ml, with 0.1 M hydrochloric acid in 0.15 ml increments using a Metrohm Titrino, until a

total volume of 4.2 ml has been added. It records the temperature, volume of acid added, and electromotive force (EMF) for each acid addition. The titration curve produced is put into a computer program, of which there are several developed for the purpose, to calculate the alkalinity of the sample. This analysis is potentially problematic for non-seawater samples due to two factors: non-seawater salinity, and also a broad range of alkalinity.

For non-seawater salinity, the VINDTA 3C manual offers a potential solution. Between titrations, the alkalinity cell is flushed three times with 0.7 M NaCl (aq), to match the salinity of seawater (Mintrop, 2004). The VINDTA manufacturer suggests avoiding any problems involving salinity by changing the concentration of the NaCl solution to match the average salinity of the samples being analysed (Mintrop, 2004), and by extension, changing the salinity of the HCl titrant to match the average salinity of the samples.

The alkalinity problem was more substantial. Seawater  $A_T$  tends to fall within a relatively small range, from 2000 - 2500  $\mu\text{mol kg}^{-1}$  (as denoted in Dickson et al., 2007), whereas estuarine  $A_T$  can cover a very large range (e.g. McGrath et al., 2019). Software such as Calkulate (Humphreys and Matthews, 2022) used to calculate alkalinity relies on a specific pH range of the titration to have been adequately measured. If the usual volumes of acid are used on a low-alkalinity sample, the sample will acidify too quickly, meaning that there are insufficient data points within the required pH range with which the calculation can be completed. Conversely, a high-alkalinity sample will not reach the required pH range with the volume of acid usually dispensed.

The large range of  $A_T$  concentrations and salinities in the estuarine samples made it important to find a single method for applying the VINDTA 3C to estuarine samples, particularly because CRMs are available at seawater salinity and alkalinity. Changing the titration setup or the salinity of the acid and flushing liquid for certain subsets of samples is not an adequate solution when the reference material could not then be analysed. The standard electrode setup, with a Thermo Orion Ross pH electrode, a Metrohm reference Ag/Cl electrode and a titanium earthing rod, was insufficient for this task. Using this existing formation, it was necessary to change the 0.7 M NaCl used as the flushing solution and reference outer electrode solution to match the salinity of the samples, or else the difference in salinity between the sample and the deionised water caused the VINDTA software to crash. The large range in estuarine salinities would require frequent changing of the NaCl solution, which, aside from the impracticality, would mean that the reference electrode, whose purpose is to provide a constant reference for the pH electrode, is no longer providing constant conditions. It was therefore necessary to seek a more appropriate electrode system.

The Metrohm Ecotrode Plus combined pH electrode performs better than the usual VINDTA electrode system across a range of salinities, as it does not alter the EMF values, even when changing between seawater and freshwater, and it is not necessary to change the flushing / reference solution (G. Emmanuele & A. Dickson, *pers. comm.*, 9-11 January 2019). This electrode replaces the pH electrode, the reference electrode and the titanium earthing rod. The following cell setup is therefore recommended for the analysis of alkalinity at any salinity: a jacketed cell at 25°C with internal capacity sufficient to hold ~100 ml of sample, up to ~10 ml of HCl per  $A_T$  titration, and the following probes: a Metrohm Ecotrode Plus combined pH electrode; a sensor to determine whether the cell is full; a temperature probe and a Metrohm acid dispenser with diffusive tip.

This electrode setup was used to analyse alkalinity salinities and alkalinities. The total volume of acid,  $B$ , was calculated using the estimated  $A_T$  concentration (Radtke et al., 1998, pg. 18):

*Equation 2.1*

$$B = \frac{V_{\text{samp}} \times A_T}{C_a}$$

Where  $B$  is the volume of acid (ml) required to reach the bicarbonate endpoint,  $V_{\text{samp}}$  is the volume of sample (ml),  $A_T$  is the estimated sample alkalinity ( $\text{mol kg}^{-1}$ ), and  $C_a$  is the acid concentration ( $\text{mol kg}^{-1}$ ). Calculating the volume of acid added to reach the bicarbonate endpoint in seawater samples showed that the bicarbonate end point occurs approximately at the 16<sup>th</sup> of 29 acid additions using the standard seawater method. Therefore, the increment was calculated by dividing 'B' by 16, and the total volume of acid used was always at least double 'B', to ensure that the full titration curve is achieved. This means that there are a minimum of 32 titration points for each sample, so the measurement time is longer than for seawater measurements, but this is necessary in order to achieve accurate results.

Two key factors made the changes to the VINDTA 3C analysis method possible. Firstly, the above (Eq. 2.1) requires some prior knowledge of expected sample alkalinity, though this does not need to be exact. Conveniently, riverine alkalinity measurements were available from the concurrent LOCATE riverine study (Tye et al., 2022b) prior to analysis, so the approximate alkalinity of each sample could be calculated. The straight line equation between the average riverine  $A_T$  (Tye et al., 2022b) for a given estuary and generic seawater salinity /  $A_T$  concentrations (Hartman et al., 2019) was used to approximate  $A_T$  concentrations for the salinity of each sampling point in that estuary. Where similar data is not available, the user could analyse a single low salinity sample very slowly, with very small acid additions over a large total acid volume, calculate its alkalinity, and then similarly estimate the alkalinity of the other samples.

Secondly, and relatedly, this analysis was only possible because the UEA VINDTA software is uniquely customisable: the software was rewritten in Visual Basic some years ago, and so the user is able to change the volume of acid. The only additional input required was to code in a refill of the acid burette once it had dispensed its maximum volume of 4.2 ml, for high alkalinity samples.

For approximately 60 samples, there were initial 'teething' issues in the methodology presented here. Initially, the titanium earthing rod was kept in the titration cell when changing the electrode setup, and this caused unusual EMF behaviour in some titrations. Other titrations did not have similar 'jumps' in EMF; upon closer inspection the earthing rod was corroded, so in some titrations was effectively disconnected from the cell. For the samples with ill-formed EMF data, the remaining sample from the bottle collected at that site was kept for a repeat analysis. The volume of remaining sample was much smaller than the approximately 100 ml the titration cell holds, and it was not possible to use the existing titration cell for these smaller volume titrations because the sample did not reach far enough up the pH electrode. For these samples, an additional jacketed beaker was made, with approximate total internal volume of 60 ml. The alkalinity procedure was rerouted, using the customisable UEA VINDTA software, to use two fills of the  $C_T$  pipette, which holds approximately 20 ml, to dispense a total volume of approximately 40 ml for these titrations.

## 2.4 $C_T$ calculation

$C_T$  was calculated using Equation 2.2:

*Equation 2.2*

$$C_T = \frac{m(C_{T(tot)} - B_{(tot)} \times t)}{\rho}$$

Where  $C_{T(tot)}$  is the sample  $C_T$  measurement in total counts,  $B_{(tot)}$  is the background coulometer reading in counts taken across the minute following the measurement,  $t$  is the time in minutes of the measurement, and  $\rho$  is the sample density in  $\text{kg m}^{-3}$ .  $m$  is a constant, calculated for each coulometer cell, to convert between  $C_T$  in counts and  $C_T$  in  $\mu\text{mol kg}^{-1}$  (Eq. 2.3).

*Equation 2.3*

$$m = \frac{C_{T\text{ crm}} \times \rho_{\text{crm}}}{(C_{T(tot)} - B_{(tot)} \times t)}$$

where  $k$  is calculated for each CRM subsample and then the mean is calculated for all of the CRM subsamples measured with a given coulometry cell, and  $C_{T\text{ crm}}$  is the certified CRM  $C_T$  concentration.

## 2.5 $A_T$ calculation

I calculated  $A_T$  from titrations data using Calculate (Version 23.3; Humphreys and Matthews, 2022), which uses the least-squares solving method for alkalinity described by Dickson (1981), but with one alteration to the standard procedure. For seawater measurements, the salinity of the HCl titrant is approximately matched to sample salinity, so the salinity (and density) of the subsample does not change during the titration. Over a large salinity range, this is problematic; the  $A_T$  calculation requires HCl concentration to be precisely known. Known  $A_T$  concentrations of CRMs are used to back-calculate the acid concentration from CRM  $A_T$  titrations, but the CRMs are only available for seawater salinity. To match sample and acid salinity would mean calibrating several acids with a CRM, whose salinity, and crucially, density, would not match that of the HCl titrant. HCl salinity was therefore kept constant experimentally ( $S = 0$ ), but since Calculate assumes that HCl salinity matches the salinity of the sample, the calculation was adjusted to account for the difference in salinity between the sample and the titrant.

## 2.6 Organic alkalinity experiment

The contribution of organic alkalinity to  $A_T$  can be calculated by measuring three carbonate system parameters, one of which must be  $A_T$ . The two other variables are used to calculate  $A_T$  as defined by the inorganic carbonate system. The difference between the measured and calculated  $A_T$  values is attributed to organic alkalinity (e.g. Delaigue et al., 2020; Kim and Lee, 2009; Kuliński et al., 2014). Estuarine waters can experience measurable contributions of organic alkalinity (Cai et al., 1998), and this thesis both interprets  $A_T$  measurements and uses them to calculate other carbonate system variables, so calculating estuarine organic alkalinity would be a valuable exercise in understanding the magnitude of the uncertainty within the  $A_T$  measurements presented here.

The LOCATE programme organised several additional intensive sampling campaigns each in a single river / estuary system, including in the Tamar catchment in July 2019. Participants conducted their own experiments but, similarly to the 2017 - 18 sampling programme, temperature and salinity measurements and inorganic nutrient samples were taken at all

sites. The estuary was sampled across the salinity gradient, with salinities of approximately 0, 2, 5, 10, 15 and 20 – 25 as in 2017 – 18, on two occasions during July 2019 (09/07 and 16/07). For this thesis, estuary samples were taken as described above for  $C_T$  and  $A_T$ , and additionally for pH using the same sampling procedure, with the desired outcome of calculating  $A_T$  from  $C_T$  and pH measurements and comparing these data with  $A_T$  measurements to determine the contribution of organic alkalinity in this estuary. Samples for  $C_T / A_T$  and pH were taken in quintuplicate at each salinity. pH was measured within 3 days of sample collection using a spectrophotometer built in-house at PML and with an accuracy of 0.003 units (Kitidis, 2019, *pers. comm.*). The pH measurements were inconsistent between samples collected at the same site, by up to 0.5 units. A secondary pH measurement was taken from the excess  $C_T / A_T$  sample using a Metrohm Ecotrode. Again, these measurements were inconsistent. This led to the organic alkalinity experiment being abandoned because the inconsistency in the pH measurements key to the calculation of inorganic alkalinity concentration would yield high uncertainties in the calculation of organic alkalinity contribution.

## **2.7 General remarks**

Unless specified otherwise, all code was written in Python 3.8.

For clarity, Table 2.2 provides detail on who conducted data collection and data analysis that has contributed to this thesis.

Table 2.2 – Detail on where samples and data used in this thesis have been sourced from.

<b>Samples/Data</b>	<b>Collection</b>	<b>Analysis</b>	<b>Interpretation for this thesis</b>
C <sub>T</sub> and A <sub>T</sub> (2017-18)	LOCATE	Author	Author
C <sub>T</sub> and A <sub>T</sub> (2020-2021)	Author	Author	Author
Nutrients (2017-18)	LOCATE	PML	Author
Nutrients (2020-21)	Author	Author + UEA	Author
NPOC (2017-18)	LOCATE	CEH	Author
Salinity and temperature (2017-18)	LOCATE	N/A	Author
Salinity and temperature (2020-21)	Author	N/A	Author
Ca, Mg, Sr	Author	UEA	Author
DOC	Author	UEA	Author
$\Delta^{13}\text{C}_{\text{DIC}}$	Author	SUERC	N/A
$^{87}\text{Sr}/^{86}\text{Sr}$	Author	BGS	Author
Catchment geology	BGS	BGS	Author
xCO <sub>2</sub>	Mace Head Observatory	Mace Head Observatory	Author
2 m dewpoint temperature, 10 m eastward and northward wind speed components, surface pressure	European Centre for Medium-range Weather Forecasts	European Centre for Medium-range Weather Forecasts	Author
River discharge	NRFA/CEH	N/A	Author
Catchment boundaries	NRFA/CEH	NRFA/CEH	Author
Estuary boundaries	JNCC	JNCC	Author

## **Chapter 3**

### **Drivers of dissolved inorganic carbon and alkalinity in the inner estuaries of the UK**

### 3.1 Introduction

Estuaries are important components of the land-ocean interface: dynamic conduits of terrestrial-derived and riverine inorganic and organic, particulate and dissolved, carbon and nutrients into the coastal ocean. Of particular interest is the dissolved inorganic carbon system in coastal waters, in the wider context of the carbon cycle, ocean acidification and climate change research. Recent estimates of global estuarine CO<sub>2</sub> outgassing have large (Cai, 2011; Laruelle et al., 2010; Regnier et al., 2013) or unreported (Laruelle et al., 2013) uncertainties. Increasing temporal and spatial coverage of the carbonate chemistry data that inform these estimates improves our grasp of carbon cycle mechanics. Water-to-air CO<sub>2</sub> fluxes are calculated from pCO<sub>2</sub>, which itself is often calculated from C<sub>T</sub> and A<sub>T</sub> measurements (Humphreys et al., 2022; Lewis and Wallace, 1998), like those presented in this chapter.

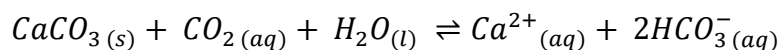
In addition to providing the building blocks to calculate carbon fluxes, C<sub>T</sub> and A<sub>T</sub> data offer direct insight into biogeochemical processes in estuaries. Estuaries are dynamic environments, with a range of processes affecting their carbonate chemistry in addition to water-air gas exchange, including mixing of freshwater and saltwater (e.g. Carstensen et al., 2018; Sims et al., 2022), primary production and remineralisation (e.g. Gattuso et al., 1998; Herrmann et al., 2015; Smith and Hollibaugh, 1993), and carbonate precipitation and dissolution (e.g. Abril et al., 2003; Cai et al., 2008; Shen et al., 2019 (in bottom waters)). For further detail on how these processes each affect each of C<sub>T</sub> and A<sub>T</sub> numerically, see Humphreys et al. (2018) and Section 1.4.

Furthermore, fluxes of C<sub>T</sub> and A<sub>T</sub> into the coastal ocean, and particularly their covariance, are important to quantify because of their potential contribution to coastal ocean acidification (Ghosh et al., 2021; Joesoef et al., 2017; Simpson et al., 2022). Therefore, understanding more fully the present-day and pre-industrial controls on estuarine carbon system dynamics, which in part is simply achieved through greater spatial and temporal coverage of measurements, improves our ability to predict future changes in the coastal zone and beyond.

While changes along an estuarine salinity gradient are thought to be due to mixing and in situ biogeochemical processes as detailed above, to a large extent estuarine concentrations of C<sub>T</sub> and A<sub>T</sub> are driven by riverine (and ultimately land-derived) inputs. The main source of river-derived inorganic carbon is through chemical weathering of carbonate and silicate bedrock (Cai, 2003; Cai et al., 2008; Joesoef et al., 2017; Regnier et al., 2013, 2022). Bedrock weathering has been understood to affect catchment water chemistry, particularly in riverine studies, for some years (Meybeck, 1987; White and Blum, 1995). Both carbonate and silicate weathering consume CO<sub>2</sub> in favour of bicarbonate (HCO<sub>3</sub><sup>-</sup>):

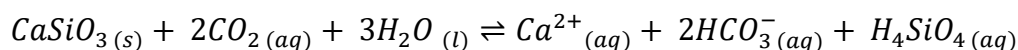
Carbonate weathering follows the equation:

*Equation 3.1*



Only one example of silicate weathering is presented here, since silicate is more compositionally diverse. Wollastonite weathering, is often used as to represent silicate weathering more generally:

*Equation 3.2*



(Garrels and Berner, 1983; Penman et al., 2020). Global estimated lateral fluxes from carbonate weathering (Ca-derived weathering flux, measured in mol-Ca million-yr<sup>-1</sup>) through rivers are approximately fourfold higher than silicate weathering fluxes (Berner et al., 1983).

Until relatively recently, weathering has not been explored in detail with regard to estuarine carbonate chemistry in estuarine environments. Estuaries are diverse environments and are well known to experience a range of different conditions. However, observational estuarine carbonate chemistry studies, including those that explore weathering by-products both as inputs and as contributors to water-air or lateral fluxes from estuaries, are often limited to a single, usually large estuary (Abril et al., 2003, 2004; Cai, 2003; Cai et al., 2004; Joesoef et al., 2017; Raymond and Cole, 2003; Simpson et al., 2022). This makes sense from a logistical perspective, being easier to sample a single large estuary in more detail than a range of smaller estuaries, and also from the perspective of transport flux to the world's coastal oceans. For example, Cai et al. (2008) use data from 25 of the world's largest rivers to extrapolate an estimated C<sub>T</sub> transport flux for the world's top 200 rivers by discharge, which account for 67% of global river discharge between them. But is this appropriate, given that there are relatively few sampled estuaries in the world? More recent studies suggest that smaller estuaries can vary substantially in their C<sub>T</sub> and A<sub>T</sub> concentrations (McGrath et al., 2016, 2019), which in turn impacts their delivery of alkalinity to the coastal ocean, and therefore may influence coastal ocean acidification (McGrath et al., 2019). Further spatial coverage of estuaries of all shapes and sizes across the globe is required to better determine these important impacts of estuarine carbon fluxes.

Weathering, particularly of carbonate bedrock, is thought to be a key source of estuarine C<sub>T</sub> and A<sub>T</sub> (Eq. 3.7). However, the majority of estuarine carbonate chemistry studies have historically reported C<sub>T</sub> and A<sub>T</sub> concentrations close to, or below, normal seawater concentrations, whereas estuaries draining carbonate catchments have C<sub>T</sub> and A<sub>T</sub>

concentrations much higher than seawater (McGrath et al., 2016, 2019). For example, the analysis of large lateral DIC fluxes in 25 of the world's major rivers by Cai et al. (2008), while representative of the global contribution of carbonate bedrock (16.8% (n=22) compared to estimates of its global contribution of 15.9% (Meybeck, 1987) and 13.4% (Amiotte Suchet et al., 2003), only includes two rivers with  $\text{HCO}_3^-$  concentrations ( $\text{HCO}_3^-$  is the main constituent of  $C_T$  in riverine and estuarine environments) higher than standard seawater  $C_T$  concentrations. Results presented here include catchments with higher contributions of carbonate bedrock and many with higher  $C_T$  concentrations than experienced by these larger rivers, so understanding the link between carbonate bedrock and  $C_T$  (and  $A_T$ ) delivery into the river or estuary at the individual estuary scale in this study may broaden understanding of carbonate bedrock-derived  $C_T$  and  $A_T$  at these larger scales.

A recent modelling study into the estuaries surrounding the North Sea by contrast used data from 6 estuaries, selected for location and data availability, of which three estuaries (Scheldt, Elbe, Thames) had higher  $C_T$  concentrations than seawater (Volta et al., 2016). Adding more representative data to these larger scale, regional and global studies will improve our ability to accurately model estuaries and their impact on the coastal ocean downstream. More recently, smaller-scale observational studies have indeed determined high  $C_T$  and  $A_T$  concentrations in estuaries in carbonate bedrock dominated catchments. McGrath et al. (2019) found  $C_T$  and  $A_T$  concentrations to be controlled dominantly by carbonate weathering in carbonate bedrock-rich Irish catchments, and McGrath et al. (2016) found the elevated concentrations of  $C_T$  and  $A_T$  to propagate into coastal waters, whereas non-calcareous catchments had lower  $C_T$  and  $A_T$  concentrations than those in shelf waters.

The UK is a uniquely appropriate environment for obtaining a representative sample of catchment bedrock types, as it is geologically diverse, with some of its catchments dominated by carbonate bedrock, in addition to the logistical possibility of sampling from a range of these. Despite this, there are a lack of carbonate chemistry measurements in UK estuaries to date. In fact, Volta et al. (2016) had to estimate dissolved inorganic carbon concentrations from Total Alkalinity for use as an estuarine biogeochemical model input because of inadequate data coverage in the Thames estuary meaning only one carbonate system variable was available. For a study whose aims included modelling  $\text{CO}_2$  outgassing, this is a substantial limitation. At the simplest, qualitative scale, alkalinity can be viewed as the capacity of water to contain  $C_T$  (Humphreys et al., 2018). By estimating  $C_T$  from  $A_T$  via a constant ratio, the user excludes any biogeochemical processing that has affected  $C_T$  and  $A_T$  in different ratios, including  $\text{CO}_2$  flux itself, carbonate weathering / precipitation and respiration / primary production.

$A_T$  is defined as the excess of proton acceptors over proton donors in moles, per kilogram of solution (Dickson, 1981), a definition which accounts for both inorganic and organic

contributors to alkalinity. Its chemical expression (Eq. 1.1; Dickson, 1981), however, includes the major inorganic components of alkalinity. Organic components of alkalinity are in practice measured during  $A_T$  titrations alongside their inorganic counterparts, particularly in water samples with high dissolved organic matter content (Kerr et al., 2021 and references therein), including in estuaries (Cai et al., 1998). This has been found to be problematic in the presence of organic molecules that contribute to  $A_T$ , both in the interpretation of  $A_T$  titration data (e.g. Kim and Lee, 2009; Sharp and Byrne, 2020), and in the subsequent calculation of other carbonate system parameters (Abril et al., 2015; Kerr et al., 2021; Kuliński et al., 2014; Sharp and Byrne, 2020). As discussed in Chapter 2.6, it was not possible to explore the quantitative impact of organic alkalinity in this work, but instead it is important to acknowledge that these results may be subject to this additional uncertainty.

It is clear that we are lacking a comprehensive understanding of carbonate chemistry in a representative sample of estuaries, and that this is due to insufficient data. In this study, we present  $C_T$  and  $A_T$  measurements for a range of UK estuaries seasonally in 2017-18, and explore differences between seasons and estuaries, particularly in relation to weathering upstream.

### **3.1.1 Research Questions**

1. How do  $C_T$  and  $A_T$  vary from river to sea, and why?
2. How different are freshwater end member  $C_T$  and  $A_T$  concentrations in a range of estuaries, why do those differences exist, and how do these differences affect  $C_T$  and  $A_T$  concentrations downstream?

## **3.2 Chapter-specific Methods**

### **3.2.1 Sampling**

The UK-based, NERC (Natural Environment Research Council)-funded LOCATE (Land Ocean Carbon Transfer) programme coordinated UK institutions to collect samples from 16 UK estuaries (Avon, Clwyd, Clyde, Conwy, Dart, Forth, Great Ouse, Halladale, Mersey, Tamar, Tay, Tees, Test, Thames, Trent and Tyne estuaries (Fig. 3.1)) once per season between April 2017 and April 2018 (Spring 2017, Summer 2017, Autumn 2017, Winter 2017/18, Spring 2018). The Severn Estuary, although draining one of the largest rivers in the UK, was not sampled as part of the estuary sampling programme because of the logistical challenge of sampling an estuary a long distance from any of the partner sampling

institutions by boat within the same week as all of the other estuaries were sampled on each occasion.

The samples collected were measured for a range of variables, including inorganic and organic carbon variables, nutrients, temperature and salinity. Here, analysis pertaining to the  $C_T$  and  $A_T$  samples is presented. To calculate  $C_T$  and  $A_T$  from laboratory measurements, water temperature, salinity, silicate, and phosphate measurements were used, which were measured as part of the wider LOCATE programme (Tye et al., 2022a).

Samples for  $C_T$  and  $A_T$  analysis were collected from a bucket according to the methods set out in Chapter 2 and according to the Standard Operating Procedure (Dickson et al., 2007). Samples were stored in the dark for 1 - 2 years until analysis in February - June 2019.

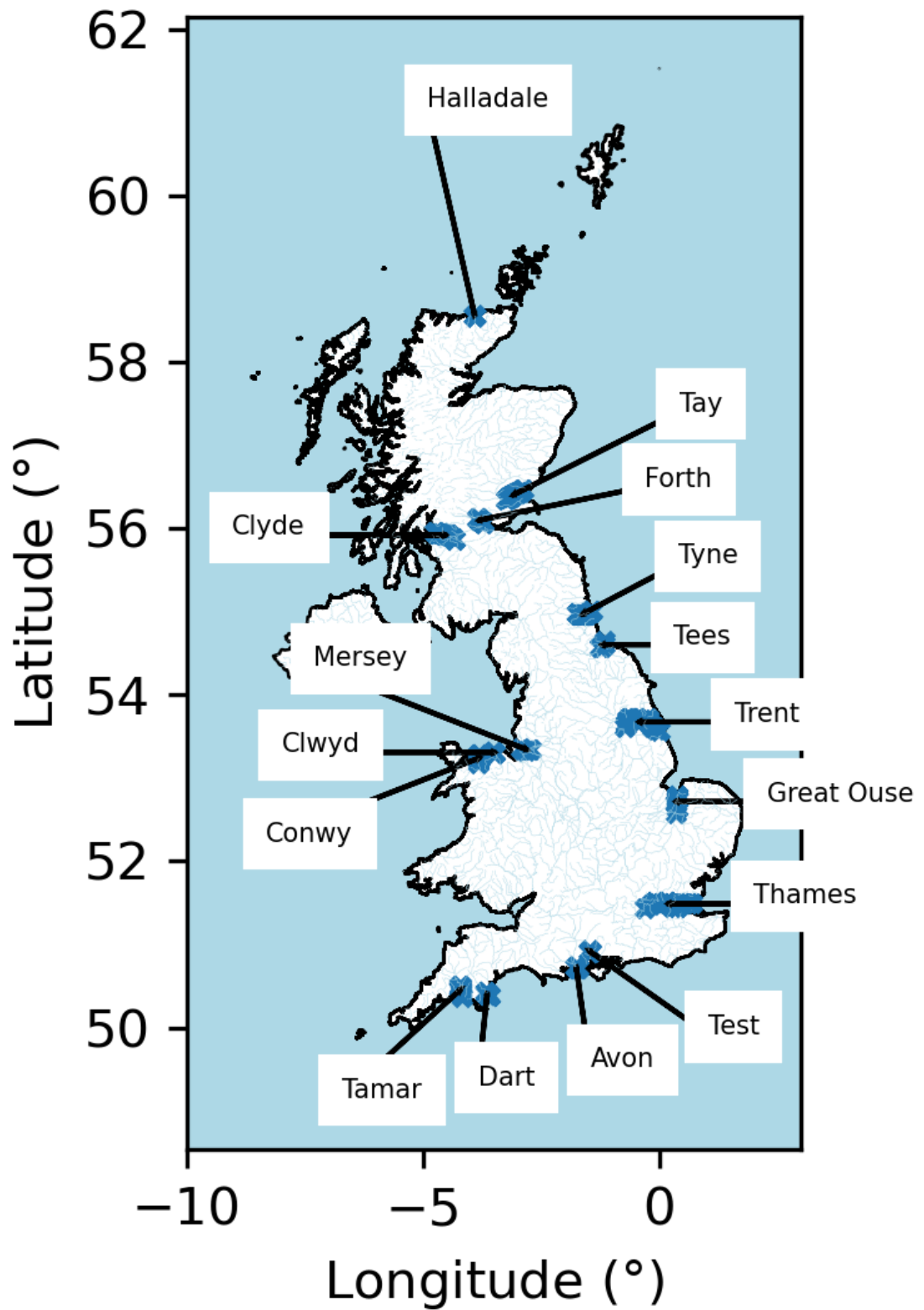


Figure 3.1 – Map of estuaries sampled by LOCATE. Blue scatter points correspond to the GPS coordinate of a sampling location (Tye et al., 2022), displayed with the UK boundary (GADM, 2022, (Version 4.1)) and all UK rivers (Defense Mapping Agency, 1992).

### 3.2.2 Additional Data

I used 1 : 625,000 Geology of Britain spatial data, specifically the bedrock .shp shapefile, to quantify and locate the areas of the UK with limestone and chalk bedrock (Fig. 3.2) (British Geological Survey (BGS), 2008). The BGS also produce more detailed geological maps (1:250000, 1:50000, 1:10000) but of these, only the 1:250000 map provides total coverage of the UK, and all three maps are only available under license, albeit with free sample maps of small spatial areas. Therefore, at this time, it was only possible to use the crudest form of geological data available. The shapefile contains a column ('RCS\_D') which describes the rock type of each unique bedrock area in the UK, which were sorted through using the keywords 'LIMESTONE' and 'CHALK' to create a new bedrock variable, which solely saved the limestone and chalk bedrock geometries. Note that there is a deliberately placed space at the beginning of the 'LIMESTONE' keyword string, to exclude metamorphosised limestone, labelled 'METALIMESTONE' and thus keep the carbonate variable sedimentary in nature. Metamorphosised limestone is likely also to deliver alkalinity and dissolved inorganic carbon to rivers, but at a different weathering rate to sedimentary limestone, so for simplicity it is not included. An additional keyword search was conducted of all cells specifically starting with 'LIMESTONE' so as not to exclude bedrock whose primary descriptor word was 'LIMESTONE'. Finally, a small number of data entries included the string 'LMST' in the 'RCS\_X' column of the BGS shapefile but are not described as 'LIMESTONE' in the 'RCS\_D' column, despite all 'RCS\_D' entries including the word 'LIMESTONE' also being described as 'LMST', so 'LMST' was also included as a search term.

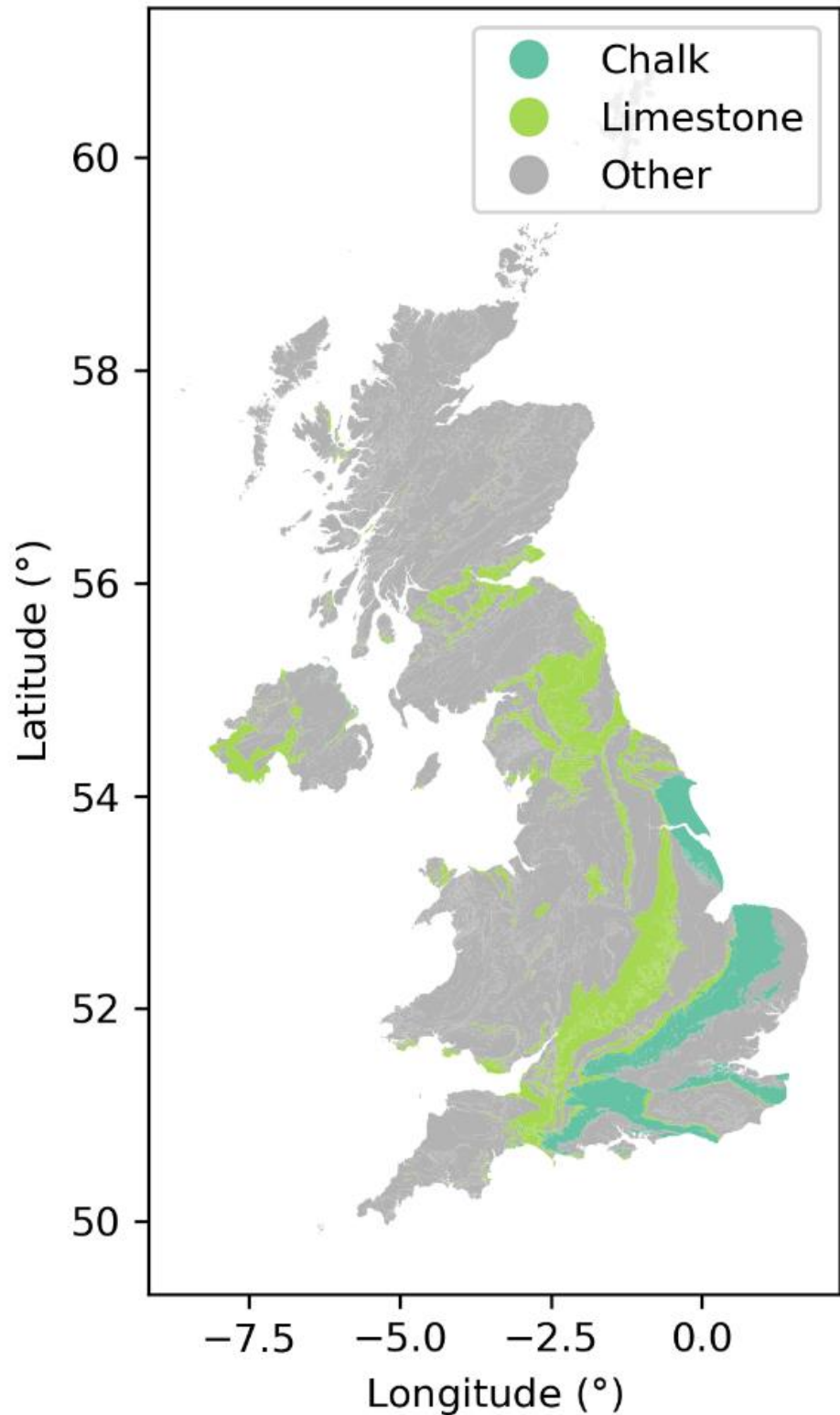


Figure 3.2 - UK map of BGS bedrock data as categorised in this study. The 'Chalk' and 'Limestone' variables are both included within the '% Carbonate' variable used within this study (British Geological Survey, 2008).

BGS geological data were used in conjunction with catchment boundary data from the National River Flow Archive (NRFA) run by the Centre for Ecology and Hydrology (CEH) to quantify the proportion of the surface area of each catchment that is underlain by limestone or chalk bedrock, a variable we hereon refer to as '% carbonate', in addition to the mean

bedrock age of each catchment. CEH catchment boundary shapefiles are freely available online, as a separate file for each gauging station (NRFA, 2017). Where a river catchment contained several gauging stations, the closest station to the estuary sampling sites was selected (Fig. 3.3), which is a consistent approach to the wider LOCATE programme (Tye et al., 2022) in addition to being the most representative station of estuarine sampling sites.

'% carbonate' was calculated for each estuary's catchment by calculating the area of each limestone or chalk bedrock that intersected with the CEH catchment boundary (e.g. Thames catchment, Fig. 3.4), as a proportion of the total area of that catchment, multiplied by 100 to convert into a percentage. Similarly, the mean bedrock age for each catchment was calculated by using taking the area-weighted mean age of bedrock geometries that intersect with a given catchment boundary.

Additionally, NRFA gauging station river discharge data is freely available for each catchment, providing a single daily estimate of river discharge for each estuary at a given point in time (NRFA, 2020). Discharge ( $\text{m}^3 \text{s}^{-1}$ ) is measured daily; on each sampling occasion, the sampling date of a given estuary was matched to the mean discharge rate for that date, for the corresponding NRFA gauging station (Fig. 3.5).

Discharge at the NRFA river gauging station may not adequately represent estuarine discharge at the sampling locations and indeed at the mineral weathering site; the lag between the occurrence of mineral dissolution and subsequent elevation of  $C_T$  and  $A_T$  concentrations downstream is not known, in particular. Nevertheless, the choice to use the river discharge data for the sampling date as provided (NRFA, 2020) was for two reasons. Firstly, here discharge is used to talk about the sampling occasion, rather than the season as a whole. This is because if discharge is a key factor in determining  $C_T$  and  $A_T$  concentrations, those concentrations were measured on a particular sampling date, and so choosing a different daily discharge rate may not represent the river discharge conditions that helped determine a given carbonate chemistry signature, in the same way that other predictor variables (e.g. temperature) use data for the sampling date, rather than the whole season.

Secondly, river discharge is measured some way upstream of estuarine sampling sites in many cases (Fig. 3.3), already adding a source of uncertainty. There is likely to be variation between catchments in flow dynamics and residence times but these data are not available at present. While it may take some time for river to travel to the sampling sites from the gauging station, we have no way of knowing on an individual estuary scale how long this period of time may be, nor how it changes with variation in discharge. Therefore, the daily discharge data as provided by CEH for the sampling date and time was used, because

arbitrarily selecting a date range or different date for discharge data would reduce confidence in the results.

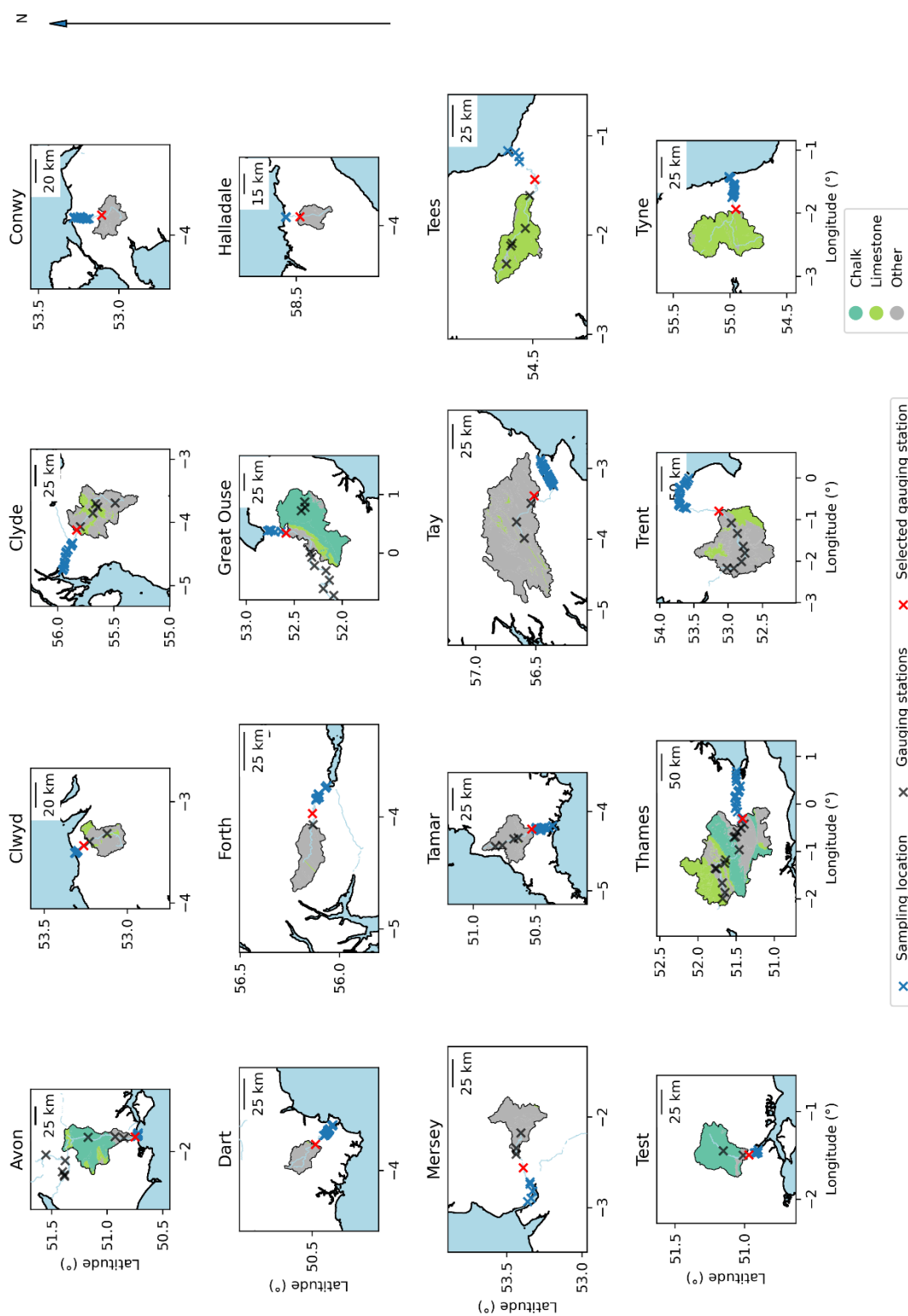


Figure 3.3 – Maps showing the catchment and NRFA gauging station locations for the river that flows into each estuary, relative to the sampling locations. Black lines indicate boundaries between land

and sea (GADM, 2022), as well as the catchment boundary data provided by the selected NRFA gauging station (NRFA, 2017). Light blue lines represent UK rivers and water bodies (Ordnance Survey, 2015). Catchment boundaries are filled with their lithology: chalk, limestone and other rock types (see legend in bottom right corner), as described above and as shown in more detail in Fig. 3.4 (British Geological Survey, 2008). Scatter points represent the locations of all NRFA gauging stations for a given river (black) and the NRFA gauging station used in this thesis (red) (NRFA, 2017), as well as sampling locations (blue) used in this and chapter and in Chapter 5 (Tye et al., 2022a). A degree of longitude is equivalent to ~71km at 50°N and ~59 km at 58°N and a degree of latitude is equivalent to ~111 at 53°N (calculated using geopandas distance function).

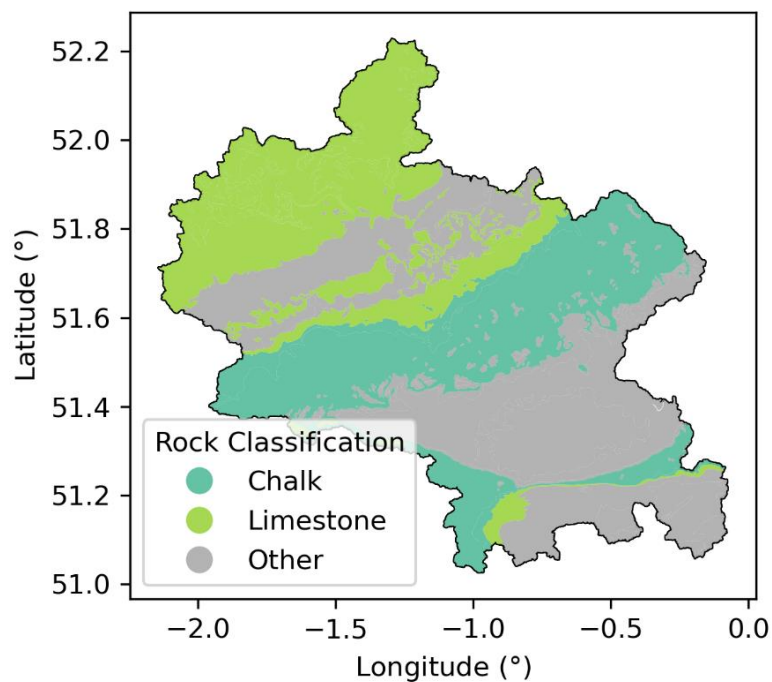


Figure 3.4 – Map of intersection between catchment area and bedrock classifications, using BGS bedrock data (British Geological Survey, 2008) and CEH/NRFA catchment boundary data (NRFA, 2017) for the Thames catchment.

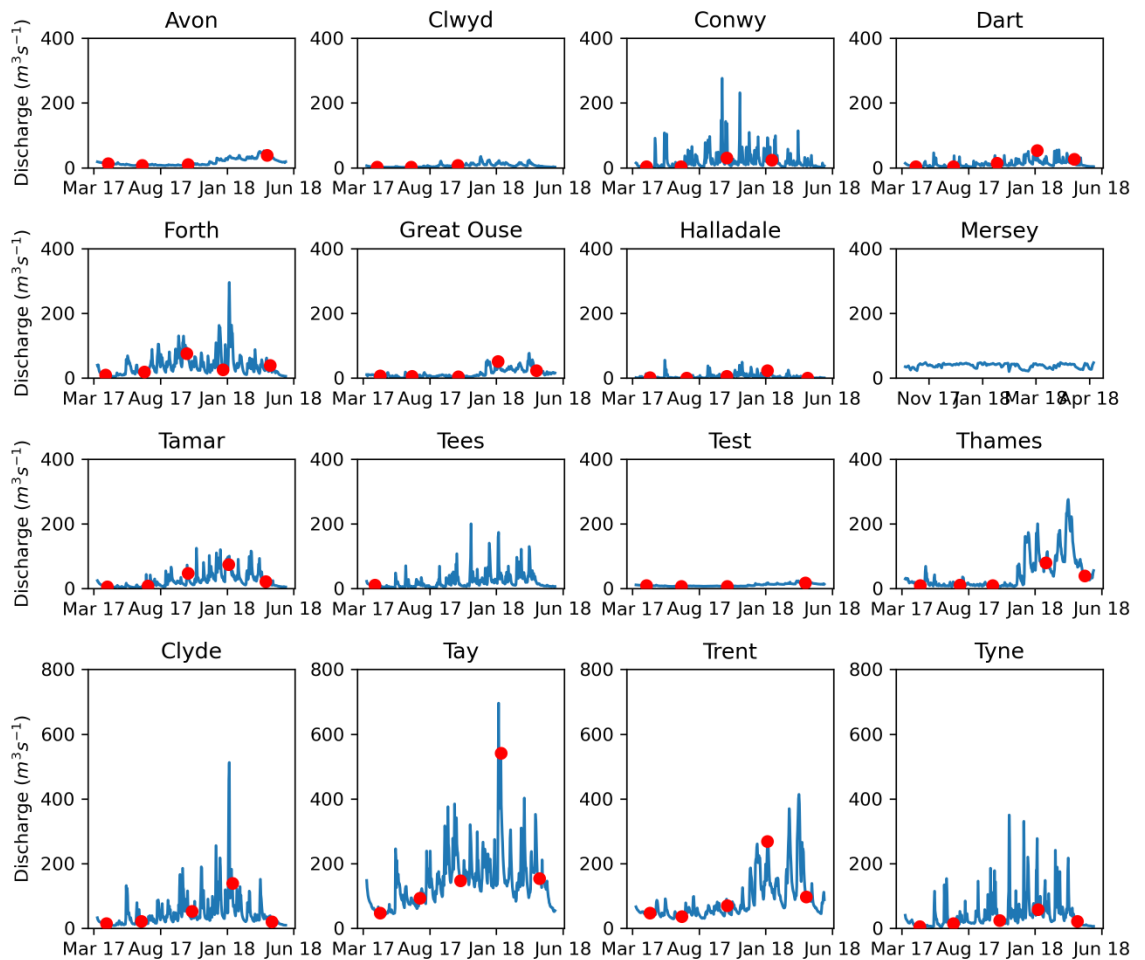


Figure 3.5 - River discharge data for each estuary from April 2017 - May 2018, the duration of the sampling campaign. Red points indicate the discharge on the sampling date, which is used henceforth to represent discharge on the sampling dates.

### 3.2.3 Data analysis

Data analysis was conducted in Python 3.8, using the following packages: numpy (Version 1.21.5, Harris et al., 2020), scipy (Version 1.7.3, Virtanen et al., 2020), calculate (Version 23.3, Humphreys and Matthews, 2022). pandas (Version 1.4.1) and pickle. Spatial data analysis was completed using geopandas (Version 0.9.0, Waskom, 2021). Graphs were made using matplotlib (Version 3.5.1, Hunter, 2007) and seaborn (Version 0.11.2).

Regression lines and their  $r^2$  values were calculated using the linregress function in scipy.stats (linear least-squares regression). Where data are labelled as 'residual' this was calculated by determining the regression line between either  $C_T$  or  $A_T$  and salinity for a specific estuary, giving a regression line equation of the form:

$$C_T = pSal \times m + c ,$$

where  $m$  and  $c$  refer to the gradient and y-intercept, respectively, and  $pSal$  represents salinity. The residual of each  $C_T$  or  $A_T$  datapoint is then calculated by subtracting the estimated concentration (Eq. 3.3) from the measured value.

### 3.3 Results and Discussion

The UK estuaries sampled experience a large range of  $C_T$  and  $A_T$  concentrations ( $\sim 0$  to  $> 5000 \mu\text{mol kg}^{-1}$ ) at low salinities (Fig. 3.6). These concentrations converge approximately linearly towards typical seawater  $C_T$  and  $A_T$  concentration ranges (Hartman et al., 2019) at the marine end member (Fig. 3.6). Per-estuary linear regression predict  $C_T$  ranging between  $1924 - 2606 \mu\text{mol kg}^{-1}$  and  $A_T$  ranging between  $2034 - 2683 \mu\text{mol kg}^{-1}$  at a salinity of 30. Differences in  $C_T$  and  $A_T$  concentrations between estuaries at low salinity are related to bedrock characteristics within a catchment (Fig. 3.6; Table 3.1). The approximately linear salinity-concentration relationships suggest that the dominant driver of change between  $C_T$  and  $A_T$  concentrations at low salinity in each estuary, and normal seawater concentrations at high salinity is mixing. Differences in freshwater  $C_T$  and  $A_T$  concentrations will be the specific focus of a later chapter, so in this chapter, particular attention is given to deviations from predominantly linear  $C_T$  and  $A_T$  salinity gradients.

For the most part, estuaries draining catchments with a high proportion of carbonate bedrock experience higher freshwater  $C_T$  and  $A_T$  concentrations than those with catchments containing smaller proportions of carbonate bedrock (Fig. 3.6). The four estuaries with the highest mean concentrations of  $C_T$  and  $A_T$  are the only four estuaries whose riverine catchments contain chalk bedrock according to the classification system provided by BGS (2008) (Table 3.1). Taken together, this suggests that estuaries draining chalk-bedded catchments experience high  $C_T$  and  $A_T$  concentrations, and estuaries draining catchments with near-zero carbonate bedrock contribution experience low  $C_T$  and  $A_T$  concentrations, with moderate  $C_T$  and  $A_T$  concentrations in estuaries with limestone-bedded (but crucially not chalk-bedded) catchments (Fig. 3.6, Table 3.1).

It is important to note that mean  $C_T$  and  $A_T$  concentrations at low salinity are not perfectly correlated with the percentage of a catchment underlain by either limestone or chalk where they are present (Table 3.1). There are a number of possible explanations for this imperfect relationship. Firstly, the complex range of processes that could affect different estuaries in different ways is not accounted for here. Differing concentrations of organic alkalinity may

impact  $A_T$  deviations from the relationship with carbonate bedrock, although this would not be reflected in  $C_T$  concentrations. Similarly, biological nitrate uptake and nitrification both cause an increase in  $A_T$ , though not in  $C_T$  (Zeebe and Wolf-Gladrow, 2001). However, the differences between estuaries are reflected in both  $C_T$  and  $A_T$  concentrations, so it is unlikely that these processes are the key differentiators of this pattern, although they may be part of a complex interplay of driving factors.

Secondly, this may be because using bedrock classification data may not be sufficiently representative of the chemical composition of rocks, overlying sediments, nor their weathering fluxes (Amiotte Suchet et al., 2003; Hagedorn and Cartwright, 2009, 2010), a phenomenon that will be explored further in Chapter 4. Concentration-salinity gradients may also be driven by a combination of sedimentary carbonate and trace carbonate present in other rocks. Indeed, Hartmann et al. (2014) found approximately half of the measured weathering flux originates from trace carbonate minerals in igneous rocks. This line of reasoning would be difficult to establish without extensive geological sampling and measurement, but the alternative explanation, that the true annual mean  $C_T$  and  $A_T$  concentrations per estuary are slightly different from those presented here, could be more simply established through a higher temporal sampling resolution. Here, a single sampling occasion is used to represent a season, or five sampling occasions to represent an entire year. By contrast, river gauging station measurements for inorganic nutrients are taken at approximately monthly resolution (Environment Agency, 2018), which for estuarine carbonate chemistry measurements would give a more reliable estimate of mean annual concentrations in addition to a full seasonal cycle.

An additional partial explanation is that the catchment boundaries for the selected gauging stations do not perfectly describe the area drained by a given estuary, in particular where the riverine catchment boundary is far removed from the estuarine sampling points (e.g. Trent estuary, Fig. 3.7). Finally, not all bedrock is equally accessible to freshwater flows. Carbonate bedrock only contributes to estuarine  $C_T$  and  $A_T$  concentrations where it intersects the flow of water delivered to the river, and subsequently to the estuary. Where the presence of carbonate bedrock does not result in elevated  $C_T$  and  $A_T$  concentrations, either because it is removed from the flow path locations or because it is buried under superficial deposits, it does not contribute to the delivery of  $C_T$  and  $A_T$  to estuarine environments. Specifically, the BGS geology map identifies superficial deposits at the same spatial resolution as bedrock geology. Additionally the BGS provides model output for a superficial thickness model. Identifying the presence and thickness of superficial deposits over chalk and limestone bedrock types would enable an understanding of whether the thickness of any deposits impacts the delivery of  $C_T$  and  $A_T$  to estuarine environments.

Interestingly, mean area-weighted catchment bedrock age is a better predictor of low-salinity  $C_T$  and  $A_T$  concentrations when compared to the percentage of carbonate bedrock in the catchment drained by an estuary (Fig. 3.6, Table 3.1). Catchment bedrock age and carbonate bedrock percentage are linked variables: chinks are among the youngest rocks, with sedimentary limestone also generally younger than other broad rock classifications. To some extent therefore, the two geological variables provide different ways of answering the same question. Catchment bedrock age and carbonate percentage both provide insight into the capacity of bedrock to be weathered. Here, the primarily focus is on carbonate bedrock percentage, because it is more closely linked to carbonate and silicate weathering (Equations 3.1 and 3.2) which are thought to ultimately provide the  $C_T$  and  $A_T$  to the estuary, and because the binary presence or absence of chalk and sedimentary limestone are closely linked to the salinity behaviour of  $C_T$  and  $A_T$  (Fig. 3.6, Table 3.1).

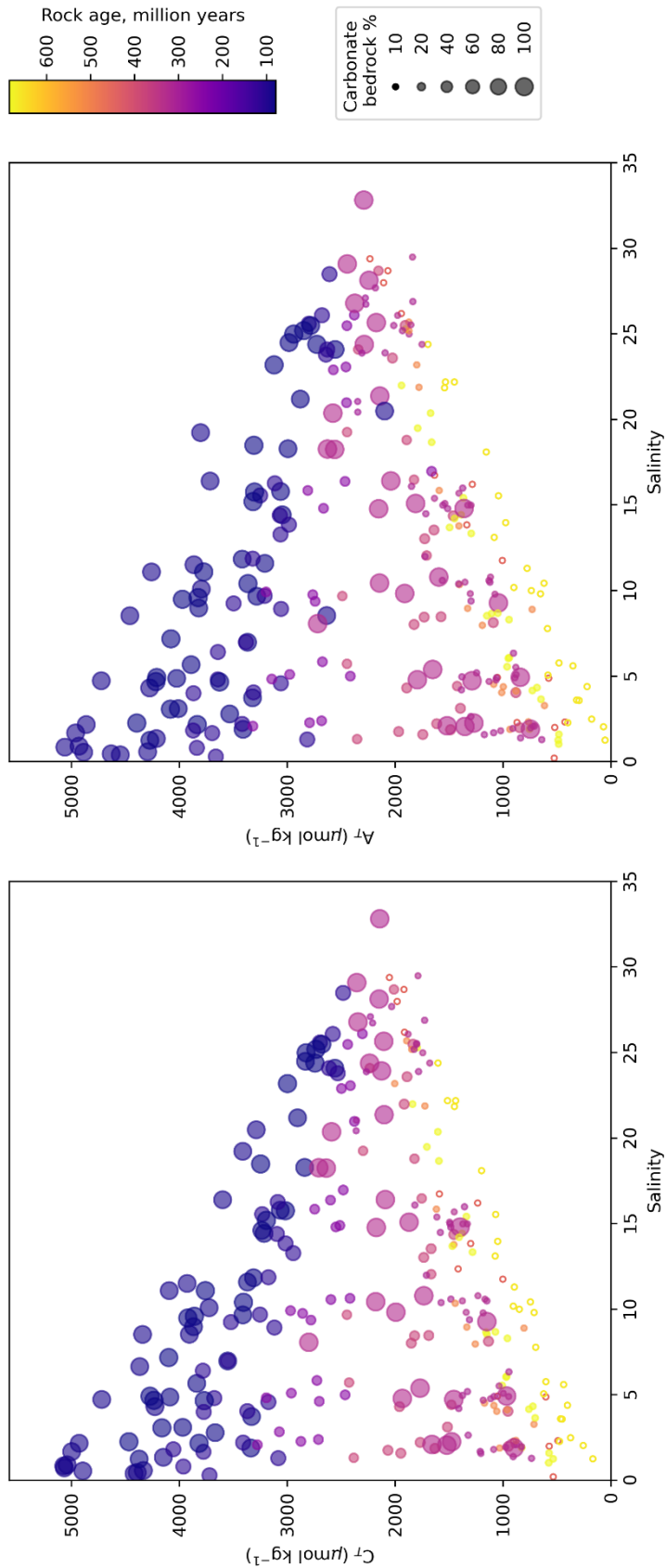


Figure 3.6 - Variations in a)  $C_T$  and b)  $A_T$  for all samples collected by LOCATE in 2017–18 from UK estuaries with salinity. Scatter points are on a continuous scale according to the percentage of the total catchment area with chalk and / or limestone bedrock. Where an estuary's catchment contains

precisely 0% carbonate bedrock, this is indicated with an open circle, to differentiate between these and other points with very small percentages of carbonate bedrock in their catchments. Scatter points are coloured according to the average (mean) age of rock within the catchment, in millions of years.

Table 3.1 - Key catchment metrics, also see Figure 3.6. Catchments are ordered from highest to lowest in terms of  $C_T$  and  $A_T$ , where 'Mean  $C_T$ ' and 'Mean  $A_T$ ' are the means of measured  $C_T$  and  $A_T$ , respectively, at salinity of < 5; 'Carbonate (%)' refers to the percentage of the total catchment area that is underlain by carbonate bedrock, including both chalk and limestone. Chalk (%) refers to the percentage of the total catchment with chalk bedrock. 'Mean bedrock age' refers to the mean age (in millions of years) of all bedrock within the catchment boundary, weighted to the proportion of each rock by surface area in the catchment.  $C_T$  and  $A_T$  concentrations are rounded to the nearest whole number. Carbonate, chalk and mean bedrock age are given to 1 d. p. The latter three metrics are calculated using data from BGS and CEH catchment boundary data (British Geological Survey, 2008; NRFA, 2017). The Mersey and Tees are excluded from the table because they were only sampled on one occasion at high salinity.

Estuary	Mean $C_T$ ( $\mu\text{mol kg}^{-1}$ )	Mean $A_T$ ( $\mu\text{mol kg}^{-1}$ )	Carbonate (inc. chalk) (%)	Chalk (%)	Mean bedrock age (Myr)
Great Ouse	4686	4735	86.2	76.2	90.4
Test	4119	4032	91.2	91.2	79.1
Avon	3797	3760	86.1	72.9	83.2
Thames	3603	3519	57.9	29.2	110
Trent	2970	2981	17.6	0	254
Clwyd	1929	1875	15.7	0	378
Clyde	1598	1472	18.9	0	374
Tyne	1414	1258	94.5	0	326
Dart	1154	1106	1.0	0	314
Tamar	986	897	0.1	0	327
Forth	983	897	1.1	0	510
Conwy	690	660	0	0	451
Tay	669	608	2.4	0	685
Halladale	370	217	0	0	661

Group 1

Group 3

Group 2

I sorted the estuaries into three groups by calculating the gradient of  $C_T$  with salinity, for which there were slightly more data points than  $A_T$  as fewer measurements failed, for each season in each estuary. The estuaries were grouped according to whether those seasonal gradients were all negative (group 1), all positive (group 2) or both positive and negative (group 3). For the purpose of this analysis, similarly to Table 3.1, the Tees and Mersey estuaries were excluded, as they were only sampled on one occasion, so it is not possible to assign them to a group.

### **3.3.1 - Group 1: High freshwater $C_T$ and $A_T$ concentration group**

#### **Estuaries (North to South): Trent, Great Ouse, Thames, Test, Avon**

All four estuaries with chalk bedrock present within their catchment (Great Ouse, Thames, Test and Avon) have freshwater concentrations of  $C_T$  and  $A_T$  that exceed typical seawater concentrations year-round. However, the exact proportion of the catchment underlain by chalk itself does not perfectly correlate with low-salinity  $C_T$  and  $A_T$  (Fig. 3.6, Table 3.1). The catchments drained by these estuaries are geologically the youngest subset. The concentrations of  $C_T$  and  $A_T$  decrease approximately linearly along the salinity gradient to typical seawater concentrations at seawater salinity, which implies that mixing is the dominant process determining  $C_T$  and  $A_T$  concentrations at a given salinity.

One additional estuary experiences a negative  $C_T$  and  $A_T$  salinity-concentration gradient year-round. The Trent estuary, although lower in  $C_T$  and  $A_T$  concentrations than the other estuaries in this group, experiences low-salinity  $C_T$  and  $A_T$  concentrations higher than typical seawater concentrations on all sampling occasions, but according to the bedrock classification technique described previously, its catchment does not contain chalk bedrock (British Geological Survey, 2008). Despite exhibiting similar behaviour to this chalk-rich group of estuaries, it seems to drain a catchment with more similar characteristics to Group 3 estuaries, with no chalk present but with non-chalk carbonate bedrock present (Table 3.1). The Trent catchment is also geologically older than the other estuaries in the Group 1, though younger than any of the non-Group 1 estuaries, but experiences  $C_T$  and  $A_T$  concentrations slightly higher than seawater at low salinity, decreasing to typical seawater concentrations at high salinity.

There are two potential explanations. Firstly, that there is an additional source of  $C_T$  and  $A_T$  to the River Trent at low salinity year-round, such as additional tributaries or groundwater influence further downstream than the gauging station, or anthropogenic inputs. Secondly, that the temporal variability of  $C_T$  and  $A_T$  in the Trent, and indeed in other estuaries, is not

adequately reflected by the temporally sparse sampling strategy. In practice, for the Trent Estuary, this may suggest that on a substantial proportion of the unsampled days and times throughout the year, low-salinity  $C_T$  and  $A_T$  concentrations were lower than typical seawater concentrations, but that the sampling occasions were too infrequent and few in number to reflect this.

On reflection, the former explanation seems more likely. The NRFA catchment boundary data denote the boundary that a river has drained prior to the gauging station (NRFA, 2017). The Humber is one of the largest estuaries in the UK and has several main tributaries including the Trent. The LOCATE sampling in majority took place in the main estuary, during the course of which several major tributaries join the channel (Fig. 3.7), but on some sampling occasions included the Trent river, so data from this gauging station was used both by the main LOCATE study (Tye et al., 2022a) and by this study. However, the Trent gauging station is approximately 80 km south of the main estuary, close to Newark-on-Trent. It is therefore likely that the percentage of carbonate in the entire area drained by the Trent estuary is higher than that described by the carbonate bedrock variable presented here. For example, including the River Ouse, the main contributor to discharge in the Humber (Uncles et al., 2006), in the calculation of carbonate bedrock as a proportion of total catchment area revises this figure to 23.4% from the Trent-only estimate of 17.6%, though no chalk is present. Perhaps more crucially, the presence of chalk bedrock draining into the Trent estuary (Fig. 3.7) supports the theory posed in this chapter that year-round negative salinity-concentration gradients of  $C_T$  and  $A_T$  are caused by chalk weathering.

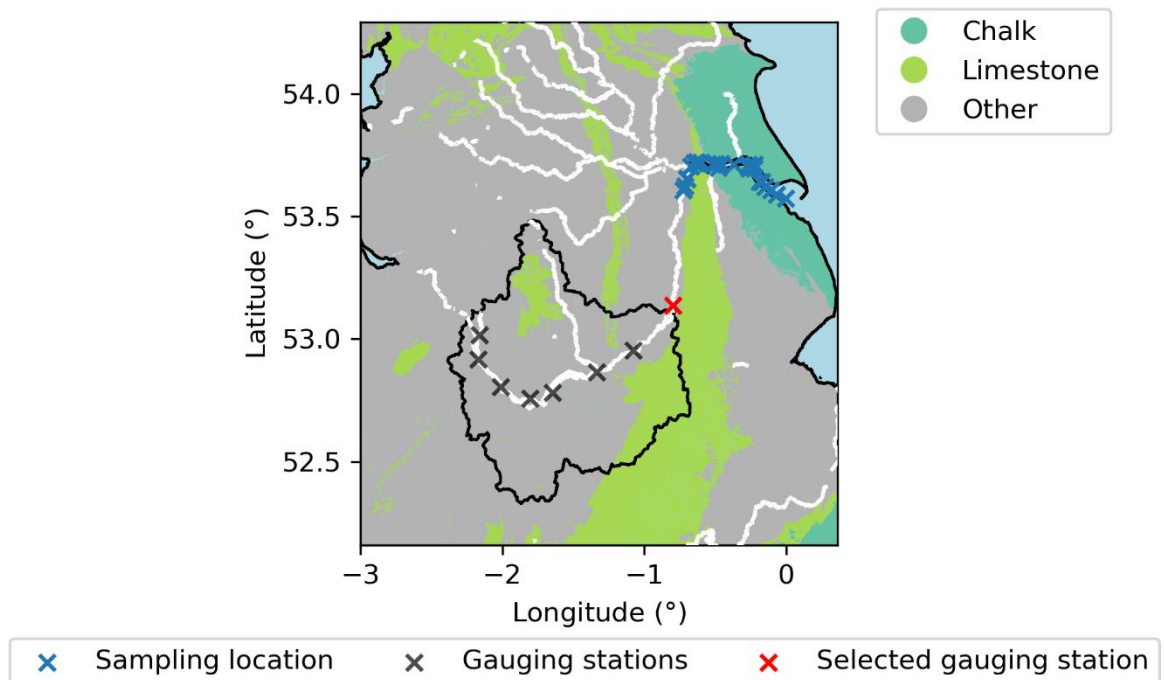


Figure 3.7 - Map showing the catchment and NRFA gauging station locations for the Trent river and estuary, as well as the 11 'Humber rivers' (Jarvie et al., 1997; Ordnance Survey, 2015), in addition to the Hull, Ancholme and Graveney tributaries, relative to the sampling locations. White lines indicate river locations (Ordnance Survey, 2015), black lines show the UK land boundary (GADM, 2022) and the Trent river catchment (British Geological Survey, 2008) and colours indicate lithology.

Mixing dominates the signature of  $C_T$  and  $A_T$  concentrations along the salinity gradient, with strong, predominantly linear relationships with salinity for all estuaries in Group 1 (Fig. 3.8). Estuaries in this group experience linear decreases in  $C_T$  and  $A_T$  concentrations from the freshwater inflow to the seawater end member. High  $r^2$  values for the concentration-salinity relationships for each sampling occasion indicate that this relationship is driven by mixing (Fig. 3.8), although care should be taken in interpreting these values given that they are each based on a small sample size (3 – 5 samples).

From hereon, where data are referred to as 'residual', the overall concentration gradient for that estuary for all seasons (Fig. 3.9) has been subtracted from each point (Section 3.2.3). The residual data can be interpreted as deviations from the average  $C_T$  or  $A_T$  concentration for that salinity across the sampling period. The overall gradient, rather than the gradient for each season, is used in this context for two reasons. Firstly, the seasonal gradients are each based on 3-5 samples, so uncertainty in any individual point may have a substantial impact on the seasonal gradient (e.g. Fig. 3.8, Great Ouse  $A_T$ , Summer 2017) whereas using the larger sample size for all seasons is more robust. Secondly, using the overall concentration gradient, rather than those nominally based on seasons enables the exploration of the factors that cause any seasonal changes. In this light, residual concentration changes that coincide with, for example, changes in temperature, provide

insight into the changes between seasons that may influence the estuarine carbonate chemistry.

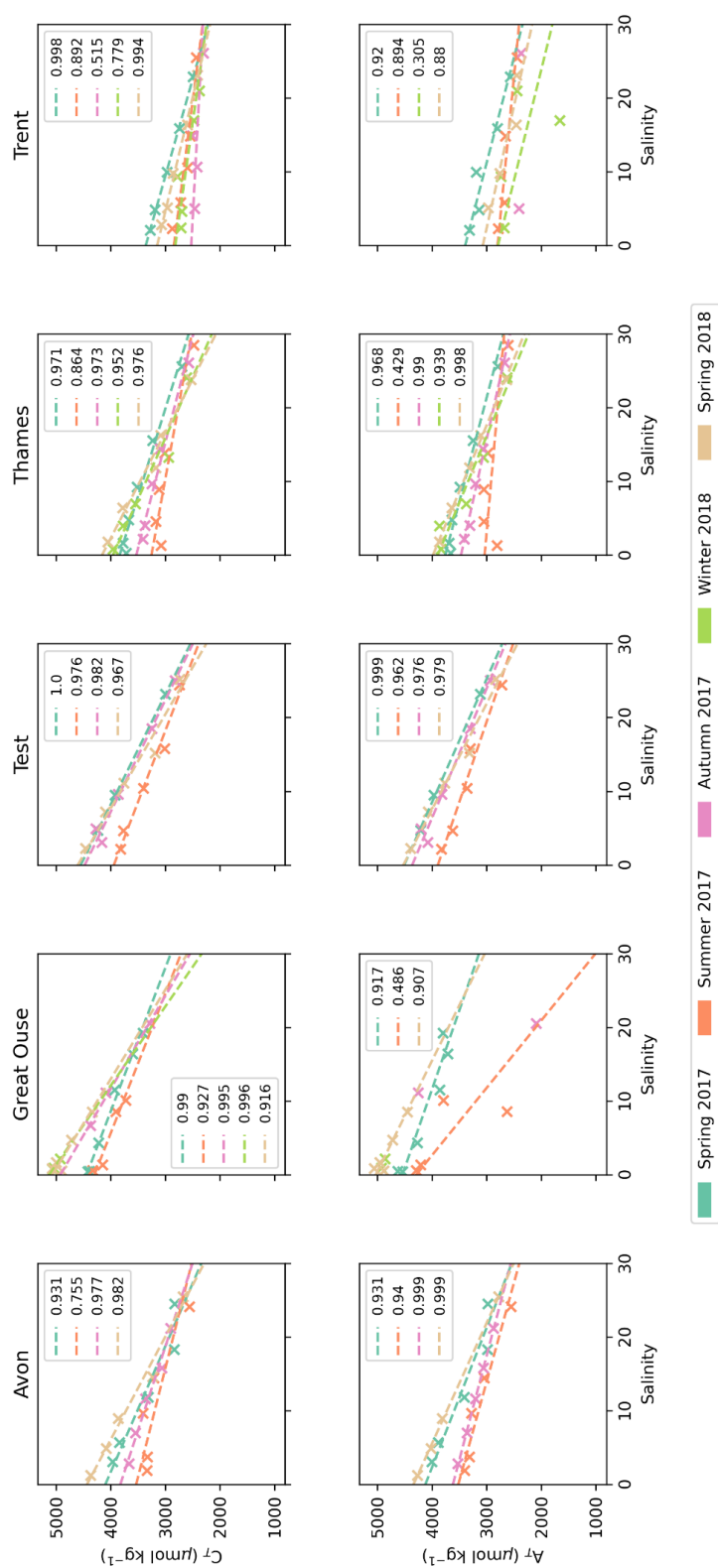


Figure 3.8 - Variations in  $C_T$  and  $A_T$  concentrations with salinity in each of the Group 1 estuaries coloured by season. Dashed lines show the linear least-squares regression of the scatter points for each season, and the coefficients of determination,  $r^2$ , are indicated in each subplot.

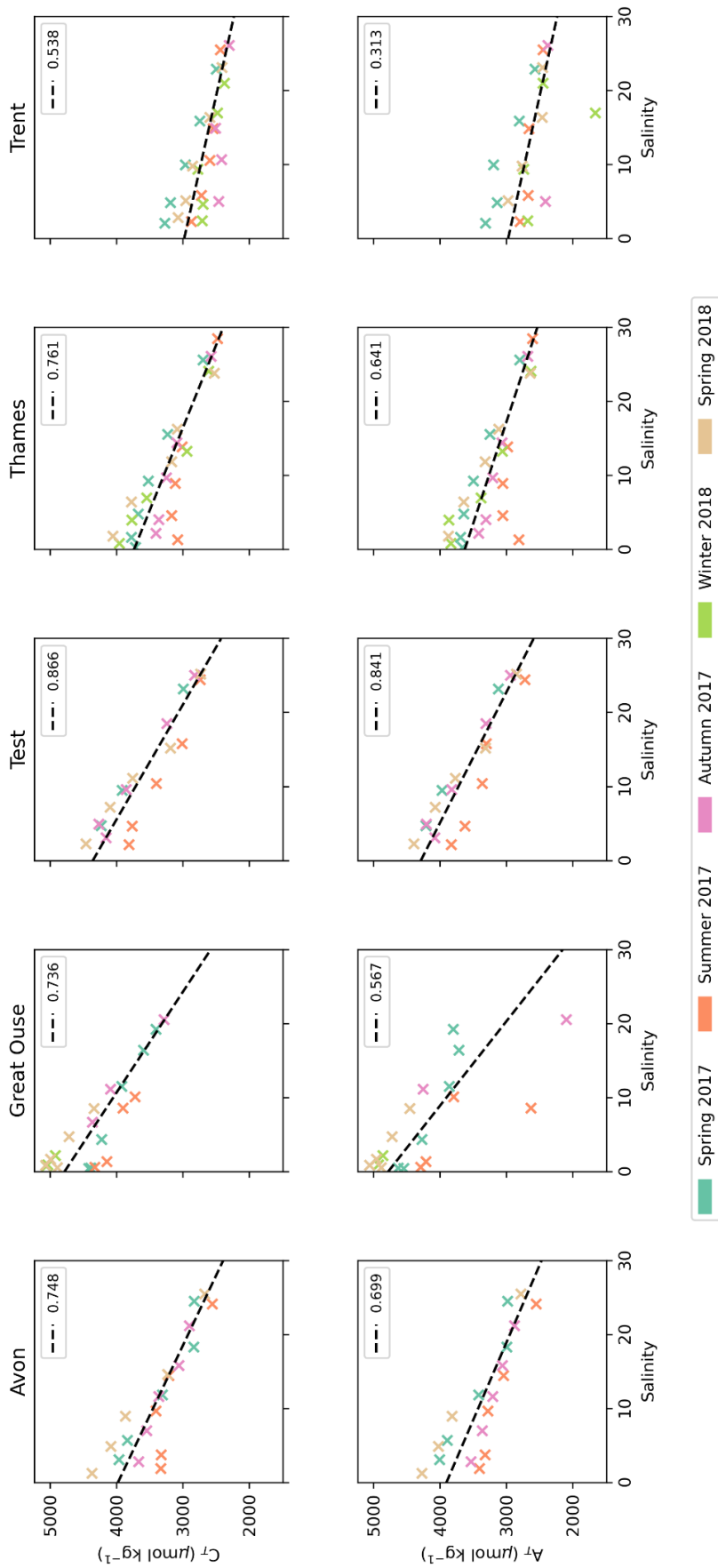


Figure 3.9 - Variations in  $C_T$  and  $A_T$  concentrations with salinity in each of the Group 1 estuaries coloured by season. Dashed lines show the linear least-squares regression of the scatter points, and the coefficient of determination,  $r^2$ , is indicated in each subplot.

However, the large gradients of  $C_T$  and  $A_T$  concentrations in this group of estuaries mask more subtle changes on each sampling occasion. Conservative mixing can be described using a straight line between the freshwater and saltwater end members in terms of salinity and either  $C_T$  or  $A_T$  on any given sampling occasion, known as a mixing line. Figure 3.10 shows deviations from the mixing line between the highest and lowest salinity data for each estuary and each season in Group 1. In practice, this acts as a first-order estimate of concentration changes excluding the process of mixing: if the points fall directly on the horizontal line, then  $C_T$  and  $A_T$  concentrations at a given salinity are determined by mixing (or some process or combination of processes that coincidentally affects  $C_T$  and  $A_T$  in the same ratio along the salinity gradient). If the points deviate from the horizontal line, then some other process occurs as well.

There are a number of likely candidates: primary production takes up 1 mole of  $C_T$  and releases 0.21 moles of  $A_T$  due to concurrent nutrient uptake for each mole of organic carbon formed, with the reverse true for remineralisation of organic matter; in situ  $\text{CaCO}_3$  precipitation takes up 1 mole of  $C_T$  and 2 moles of  $A_T$  for every mole of  $\text{CaCO}_3$  formed, with the reverse true for  $\text{CaCO}_3$  dissolution (Humphreys et al., 2018; Wolf-Gladrow et al., 2007); nitrate uptake releases 1 mole of  $A_T$  for every mole of  $\text{NO}_3$  taken up with no effect on  $C_T$ , and nitrification which takes up 2 moles of  $A_T$  for every mole of  $\text{NH}_3$  taken up with no effect on  $C_T$  (e.g. McGrath et al., 2016) (Section 1.4). For example, high nitrate concentrations were found at low salinities and often corresponded to high  $A_T$  (Fig. 3.10); in the growing season where nitrate is consumed during primary production this will be accompanied by an increase in  $A_T$  (e.g. McGrath et al., 2016).

It is not possible with the data available to quantify the relative contribution of all of these particular processes, but qualitatively, points above the line (Fig. 3.11) indicate an addition of  $C_T$  or  $A_T$ , which could indicate primary production or  $\text{CaCO}_3$  dissolution, and points below the horizontal line indicate that  $C_T$  and  $A_T$  are being used, through remineralisation of organic matter and / or  $\text{CaCO}_3$  precipitation (Section 1.4). However, the relatively sparse sampling strategy means that any 'jumps' in concentration could theoretically reflect an extremely localised process, but also could reflect a more gradual change that was not sampled.

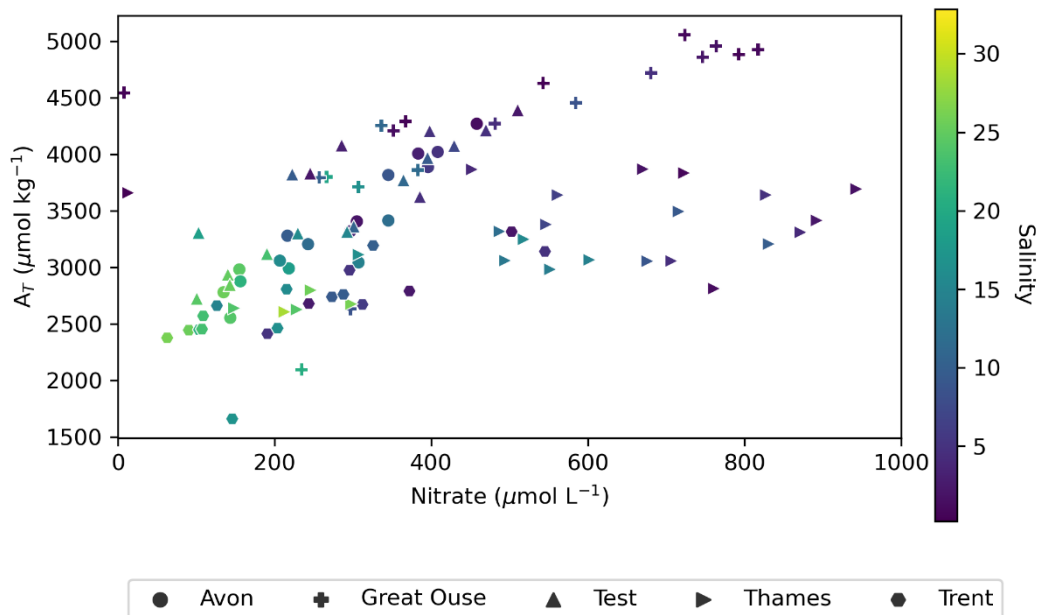


Figure 3.10 – Variation in  $A_T$  concentration with nitrate concentration in Group 1 estuaries, coloured by salinity.

I can therefore be confident that while mixing is the dominant driver of change in this group of estuaries (Fig. 3.8), there are other processes going on that act to influence  $C_T$  and  $A_T$  concentrations at a finer scale (Fig. 3.11). Since the variability in seawater  $C_T$  and  $A_T$  concentrations is much smaller than the variability at lower salinity (Fig. 3.8), the main determinant of  $C_T$  and  $A_T$  concentrations at a given salinity is their freshwater concentration. Within each estuary in this group, those freshwater concentrations vary by up to  $\sim 1000 \mu\text{mol kg}^{-1}$  between the sampling occasions (Fig. 3.8, 3.9). Figures 3.8 and 3.11 nominally refer to these sampling occasions as seasons, but it would be more valuable to consider what specifically changed across the sampling occasions to cause these differences, and whether that factor is (or factors are) seasonal in nature. Given that the high freshwater concentrations in this group relate to the presence of chalk bedrock in addition to carbonate bedrock more generally, it should follow that the cause of between-sampling occasion variability relates to carbonate (including chalk) weathering. Two variables could be possible contributors: temperature (measured as part of the LOCATE sampling campaign (Tye et al., 2022a)) and river discharge (collated for this chapter from NRFA gauging station data (NRFA, 2020)).

Group 1 estuaries generally experience high nitrate concentrations, particularly at low salinity (Fig. 3.10), and therefore low salinity  $A_T$  would be expected to increase in the growing season as nitrate is consumed during primary production. Where  $A_T$  is elevated relative to  $C_T$  during the spring and summer, this suggests that nitrate uptake is the differentiating factor, for example in the Thames in Summer 2017 and in the Test in Spring 2017 and 2018 (Fig. 3.11). As mentioned previously, increasing the sampling frequency to

monthly, as is common practice in the Environment Agency for nutrient analysis, would increase confidence that this is a true seasonal signal.

Weathering in general (e.g. White et al., 1999) and of carbonates in particular is related to temperature, with carbonate weathering rates highest at temperatures between 10 – 15 °C (Gaillardet et al., 2019). In this dataset, temperature was found to exert a small influence on the deviation of  $C_T$  and  $A_T$  concentrations from mean conditions across the year ( $r^2 = 0.176$  and  $0.111$  for  $C_T$  and  $A_T$  respectively, Fig. 3.12). That this influence is small could be because the temperature as measured on the day at the sampling sites does not adequately reflect the temperature during bedrock weathering. Low salinity sampling sites may be marginally more reflective of bedrock weathering conditions due to proximity, but there is no indication that low salinity temperatures relate better to  $C_T$  and  $A_T$  concentrations (Fig. 3.12). In the absence of an understanding of lag times from the time of bedrock weathering to the delivery of  $C_T$  and  $A_T$  to the estuary, and without knowing the precise location of the weathering source(s), it is not possible to refine this estimate further.

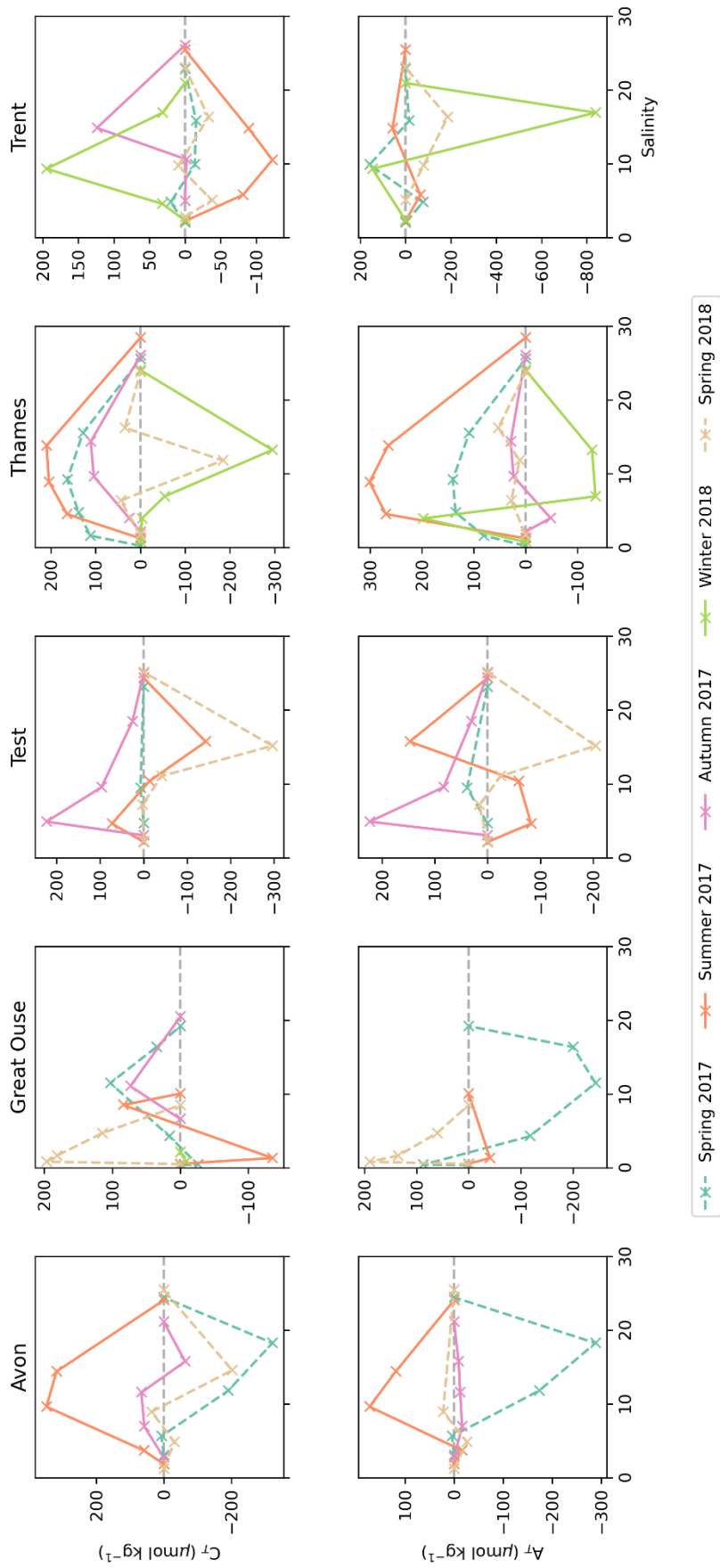


Figure 3.11 - Variations in  $C_T$  and  $A_T$  concentrations with salinity in each of the Group 1 estuaries coloured by season. Concentrations are here expressed as deviations from the seasonal mixing line for each sampling occasion. A positive value denotes a concentration higher than achieved by mixing

alone, and a negative value represents a  $C_T$  or  $A_T$  concentration lower than the achieved by mixing alone.

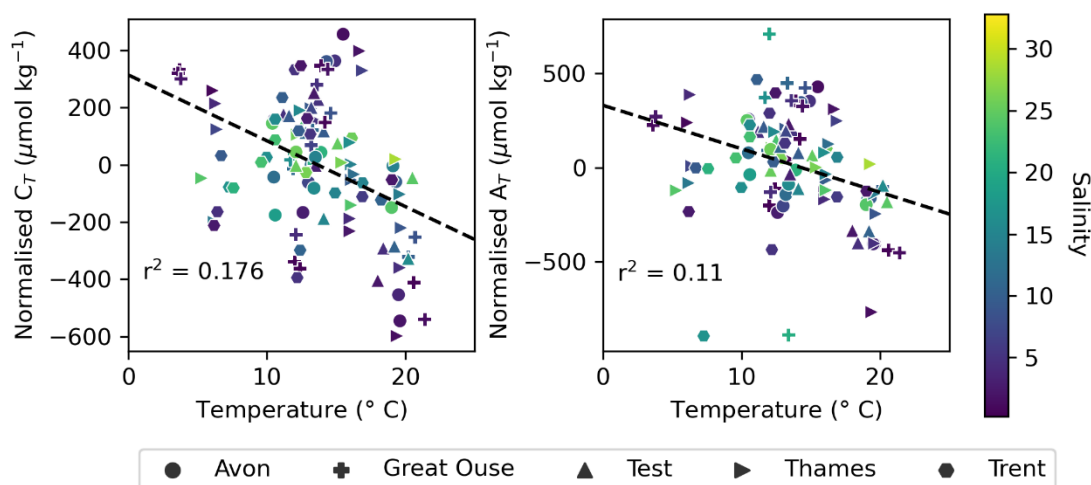


Figure 3.12 - Variations in residual  $C_T$  and  $A_T$  concentrations for Group 1 estuaries as shown in Fig. 3.9 according to temperature, coloured by salinity. The temperature-residual concentration regression line is shown in black with the coefficient of determination,  $r^2$ , indicated on each subplot.

River discharge has been widely studied in relation to riverine solute transport (e.g. Godsey et al., 2009; Maher, 2011). Commonly, rivers experience lower solute concentrations (inc.  $C_T$  and  $A_T$ ) at high discharge (e.g. Hill and Neal, 1997; Jarvie et al., 1997; Piñol and Avila, 1992), which suggests that on average the residence time of groundwater and/or soil water is shorter than the time necessary for the water to reach chemical equilibrium with the weathering source material (Maher, 2011). Where there is little change in  $C_T$  and  $A_T$  concentration with increasing discharge, this implies that the groundwater and/or soil water residence time is long enough to reach equilibrium. Increasing  $C_T$  and  $A_T$  concentrations with discharge appear rarely; permafrost thaw, found to increase both discharge and alkalinity is not a contributing factor in this study (Drake et al., 2018b). Studies are generally riverine, rather than estuarine.

The relationship between river discharge and residual  $C_T$  and  $A_T$  concentrations is shown in Figure 3.13. The estuaries show weak relationships between discharge and  $C_T$  and  $A_T$  concentrations, which may relate to the use of discharge data for the sampling date/time rather than representing discharge at the time of weathering. For four of the five Group 1 estuaries (Avon, Great Ouse, Test and Thames) low-discharge concentrations of  $C_T$  and  $A_T$  are highly variable, but in all four of these estuaries,  $C_T$  and  $A_T$  concentrations at low salinity and where discharge exceeds  $10 \text{ m}^3 \text{ s}^{-1}$  are high. This could suggest either that higher

discharge causes greater physical weathering of carbonates close to the source, or that higher discharge initiates resuspension of particulate carbonate within the sediment which then dissolves in situ, although this would have to occur at low salinity to reflect the low salinity variations in  $C_T$  and  $A_T$  concentrations. That this phenomenon is perhaps occurring in these four estuaries is interesting, given that they are the four catchments with the most chalk bedrock present (Table 3.1), noting that the Trent drains a smaller proportion of carbonate and chalk bedrock than the other estuaries in this group (Table 3.1, Fig. 3.7). Therefore, in catchments with a high proportion of chalk bedrock, rapid chalk weathering can sustain high concentrations of  $C_T$  and  $A_T$  at high discharge.

The Trent, which experiences a substantially greater range of discharge than the other estuaries in this group, also experiences large variability in  $C_T$  and  $A_T$  concentrations at low river discharge, but where river discharge exceeds  $100 \text{ m}^3 \text{ s}^{-1}$ , there is some indication that low salinity  $C_T$  and  $A_T$  may decrease, although this is unclear because sampling generally coincided with low discharge conditions.

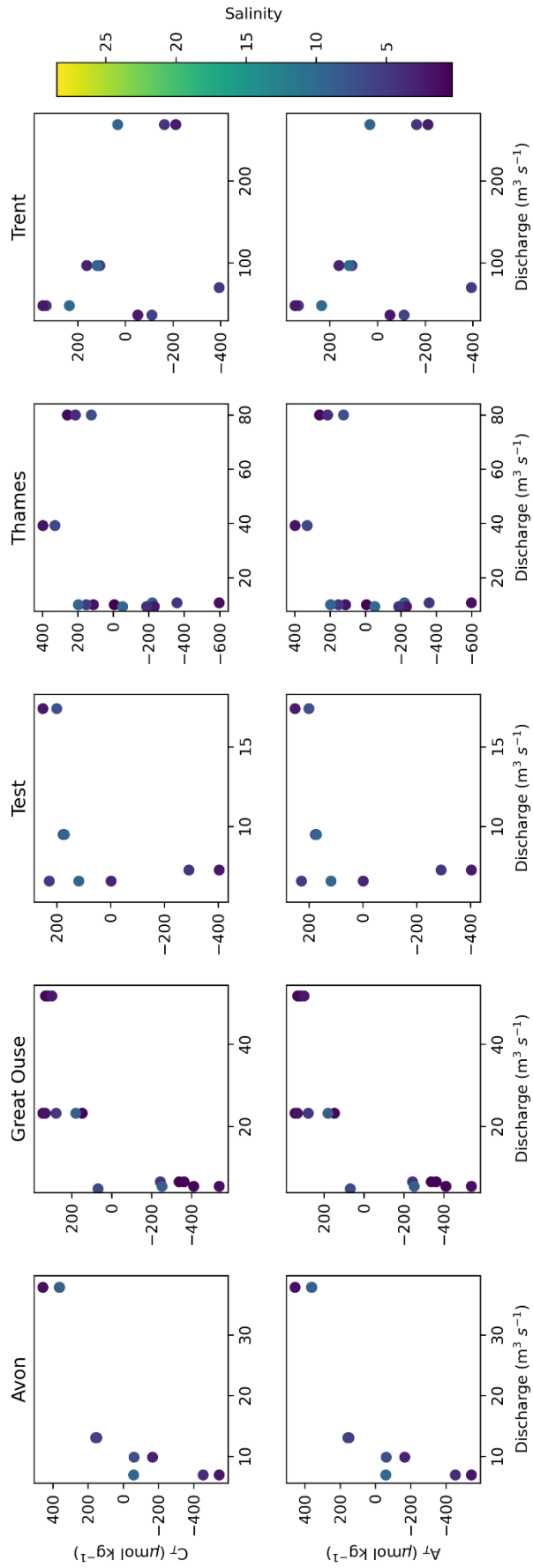


Figure 3.13 - Residual  $C_T$  (upper row) and  $A_T$  (lower row) concentrations as a function of river discharge measured daily at the National River Flow Archive gauging station for each of the Group

1 estuaries. Salinity is represented by colour. N.B. discharge is measured at a single station, so the same value is given to each location along the estuary on a given sampling occasion. Only low salinity data ( $0 < S < 10$ ) are shown for clarity.

### **3.3.2 Group 2: Low freshwater $C_T$ and $A_T$ concentration group**

#### **Estuaries (North to South): Halladale, Tay, Forth, Conwy, Tamar, Dart**

Estuaries where the catchment contains minimal-to-no carbonate bedrock (<2.5% by area, Table 3.1) experience low  $C_T$  and  $A_T$  concentrations at low salinity and increase to typical seawater concentrations at high salinity (Fig. 3.14). The predominantly linear increase in  $C_T$  and  $A_T$  concentrations with salinity, with high coefficients of determination in every estuary and on every sampling occasion (Fig. 3.14) indicates that the carbonate chemistry in these estuaries is also dominated by conservative mixing.

The mean geological age of these estuaries is consistently higher than that of estuaries in Group 1 (Table 3.1, Fig. 3.6). These older lithologies likely include areas where the more easily weathered source materials, such as chalk and carbonate bedrock, have been removed over time, to leave rocks which weather more slowly. The low freshwater concentration group also experiences lower concentrations of  $C_T$  and  $A_T$  across the salinity gradient. The low  $C_T$  and  $A_T$  concentrations at low salinity are more challenging to directly attribute to a given rock type. This group of estuaries exclusively contains rock types other than carbonate rocks, which are not conveniently defined according to chemical composition, though largely are likely to consist of silicate-rich rocks, since the majority of rocks on the planet contain silicate minerals (Wedepohl, 1995).

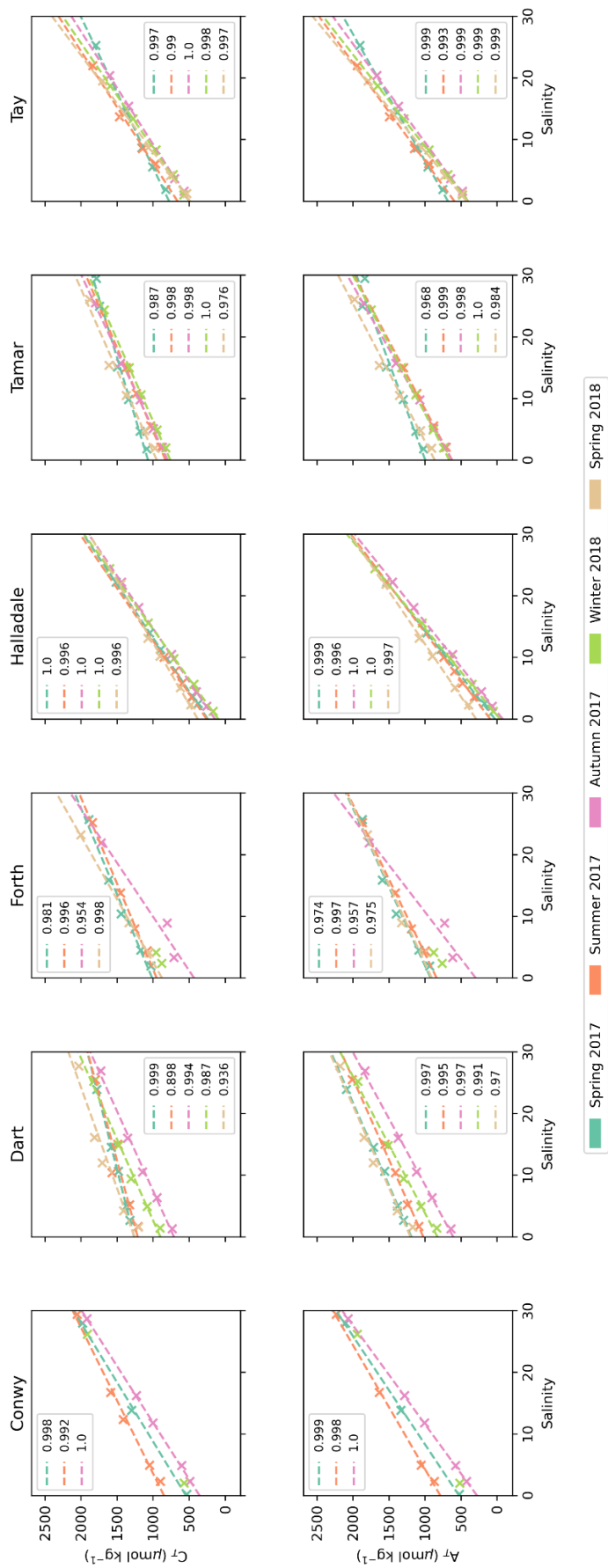


Figure 3.14 - Variations in  $C_T$  and  $A_T$  concentrations with salinity in each of the Group 2 estuaries coloured by season. Dashed lines show the seasonal linear least-squares regressions of the scatter points, and the coefficients of determination,  $r^2$ , are indicated in each subplot.

As was the case for Group 1, the strong, mixing-driven salinity-concentration gradient in these estuaries masks more subtle changes in carbonate chemistry along the salinity gradient (Fig. 3.15), which again are largely reflected in both  $C_T$  and  $A_T$ . The range over which concentrations of  $C_T$  and  $A_T$  vary (the range of the y axis in Fig. 3.15) is much smaller than in Group 1 (Fig. 3.10), which suggests that the biogeochemical factors driving these smaller changes in  $C_T$  and  $A_T$  concentrations affect estuaries quasi-proportionally to their freshwater concentrations.

Looking at the influence of discharge on  $C_T$  and  $A_T$  concentrations, it appears that weathering affects Groups 1 and 2 differently according to discharge, which accounts for the difference in the 'ranking' of seasons with respect to  $C_T$  and  $A_T$  concentration (Figs. 3.13 and 3.16). With the exception of the Dart estuary, increasing discharge corresponds to decreasing concentrations of  $C_T$  and  $A_T$  at low salinity in particular (Fig. 3.16). This suggests that the freshwater residence times in contact with the bedrock/soil in these estuaries are long enough for the water to equilibrate with the bedrock and/or soil it is weathering, and so increases in discharge resulting from precipitation simply act to dilute the pre-existing water composition (Maher, 2011). The Dart estuary does not have a sufficient residence time at source for this to be the case.

Taken together, these findings suggest that in Group 1, increased river discharge, via precipitation, acts to increase chalk and carbonate weathering, which releases  $C_T$  and  $A_T$  (Eq. 3.1, Fig. 3.13), whereas in Group 2 estuaries, increased precipitation and subsequent increased river discharge has little effect on weathering of silicate-dominated bedrock (Fig. 3.16). While silicate weathering also releases  $C_T$  and  $A_T$  in the form of  $HCO_3^-$  (Eq. 3.2), weathering rates of silicate bedrock (here using granite and gneiss) per unit area per unit of time are thought to be approximately twelvefold lower than carbonate weathering rates (Meybeck, 1987). The bedrock in Group 2 catchments is likely to be dominated by silicate minerals (Wedepohl, 1995); slow weathering rates in silicate-dominated catchments explain the consistent provision of  $C_T$  and  $A_T$  into Group 2 estuaries regardless of discharge.

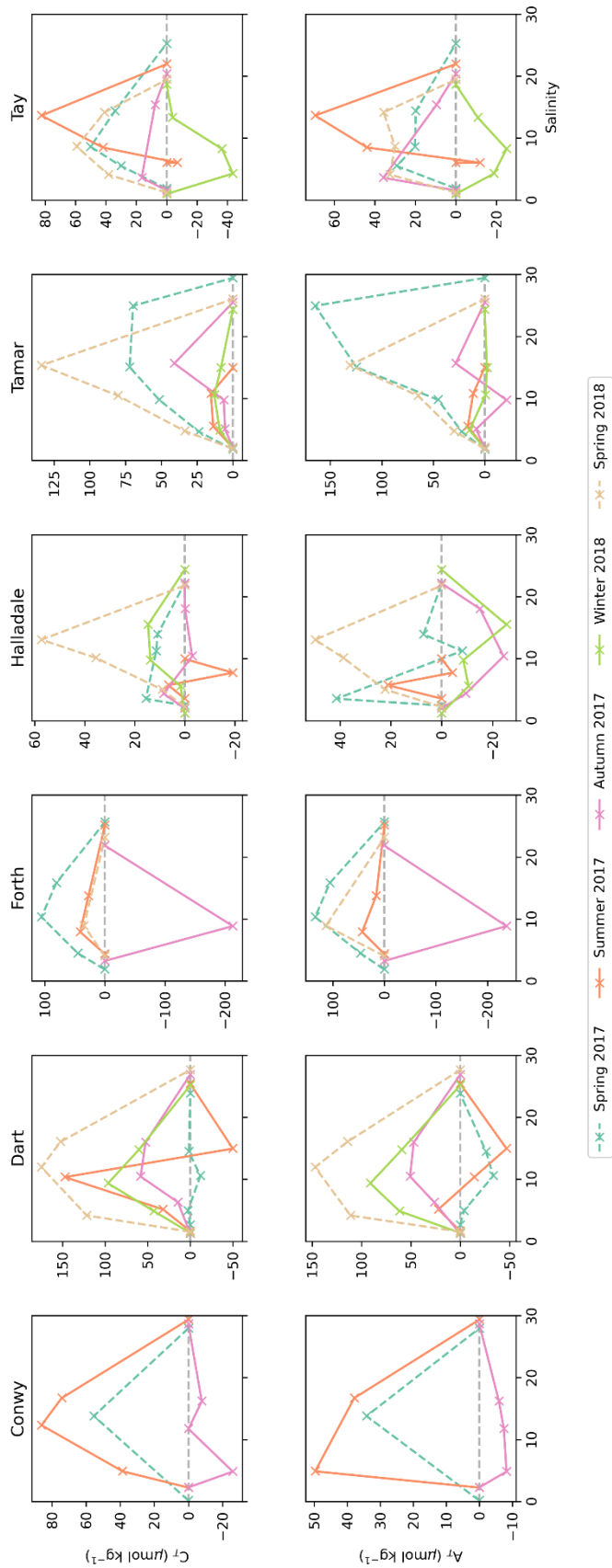


Figure 3.15 - Variations in  $C_T$  and  $A_T$  concentrations relative to the mixing line for each season (calculated as described previously) with salinity in each of the Group 2 estuaries coloured by season.

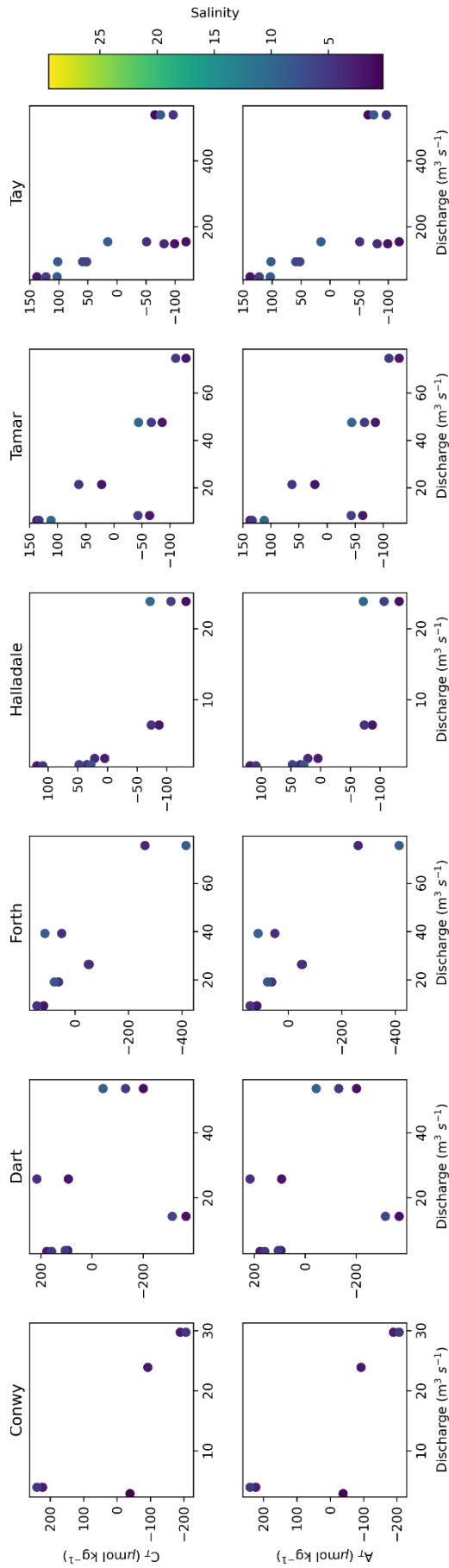


Figure 3.16 - Residual  $C_T$  (upper row) and  $A_T$  (lower row) concentrations as a function of river discharge measured daily at the National River Flow Archive gauging station for each of the Group 74

2 estuaries. Salinity is represented by colour, and only low salinity samples ( $0 < S < 10$ ) are shown for clarity.

### 3.3.3 - Group 3: Estuaries with positive and negative $C_T$ and $A_T$ gradients.

#### Estuaries (North to South): Clyde, Tyne, Clwyd

Thus far, we have seen chalk-rich estuaries with negative  $C_T$  and  $A_T$  concentration-salinity gradients, and estuaries with minimal-to-no carbonate bedrock and positive  $C_T$  and  $A_T$  concentration-salinity gradients. There is a third distinct group of estuaries whose members have non-negligible areas of carbonate bedrock present within the catchment (>10% of catchment area, Table 3.1) but do not contain any chalk (Table 3.1, Fig. 3.6). These estuaries, whose low-salinity  $C_T$  and  $A_T$  concentrations are closest to typical seawater concentration ranges (in comparison to Groups 1 and 2), switch from a positive to a negative salinity-concentration gradient between the sampling occasions (Fig. 3.17).

In Group 3 estuaries, conservative mixing also dominates the signatures of  $C_T$  and  $A_T$  concentrations along the salinity gradient, with generally high  $r^2$  values representing the data. The exceptions here are in the Clyde estuary  $C_T$  data, where in three out of the four seasons with  $r^2$  values calculated, there are low  $r^2$  values ( $r^2 < 0.3$ ; Fig. 3.17), in the Clyde estuary  $A_T$  data in Spring 2017, and in the Clwyd estuary  $A_T$  data in Summer 2017 (Fig. 3.17). This is not because mixing does not dominate in these estuaries; the data points for each of these examples fit their respective regression lines well (Fig. 3.17). Rather, the low values indicate a limitation of using the  $r^2$  metric where regression gradients are close to zero. A zero gradient indicates that there is no relationship between the x and y variables, and an  $r^2$  value quantifies the ability of x to predict y, in this case, for salinity to predict  $C_T$  or  $A_T$ . Here, salinity provides a poor predictor, because the freshwater and seawater  $C_T$  and  $A_T$  concentrations are similar, but the points remain close to the respective regression lines, indicating that conservative mixing remains to be the dominant process.

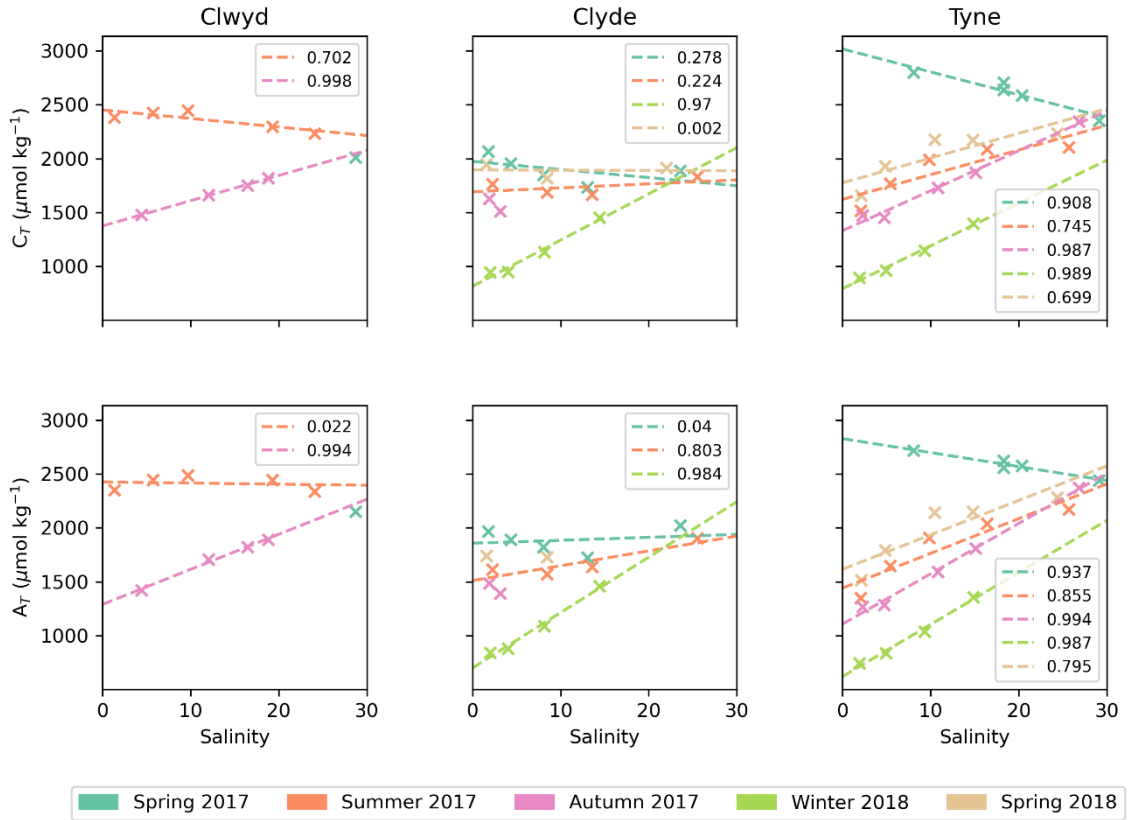


Figure 3.17 – Absolute concentrations of  $C_T$  (upper row) and  $A_T$  (lower row) in the three Group 3 estuaries (Clwyd, Clyde and Tyne) which experience changes in the sign of their salinity gradients of these chemical species between the different sampling occasions. Scatter points are coloured by the season in which samples were collected. Regression lines indicate the seasonal salinity-concentration gradient, and the coefficients of determination,  $r^2$  are given in the legend of each subplot.

All of the 14 sampled estuaries experience variation in their concentration gradient to some extent. For this third group, whether the seasonal switch between positive and negative gradient is a function of that same variability experienced in other estuaries, and the mean  $C_T$  or  $A_T$  concentration at low salinity being similar to seawater is a coincidence, or whether some other process is contributing uniquely to  $C_T$  and  $A_T$  concentrations in these estuaries

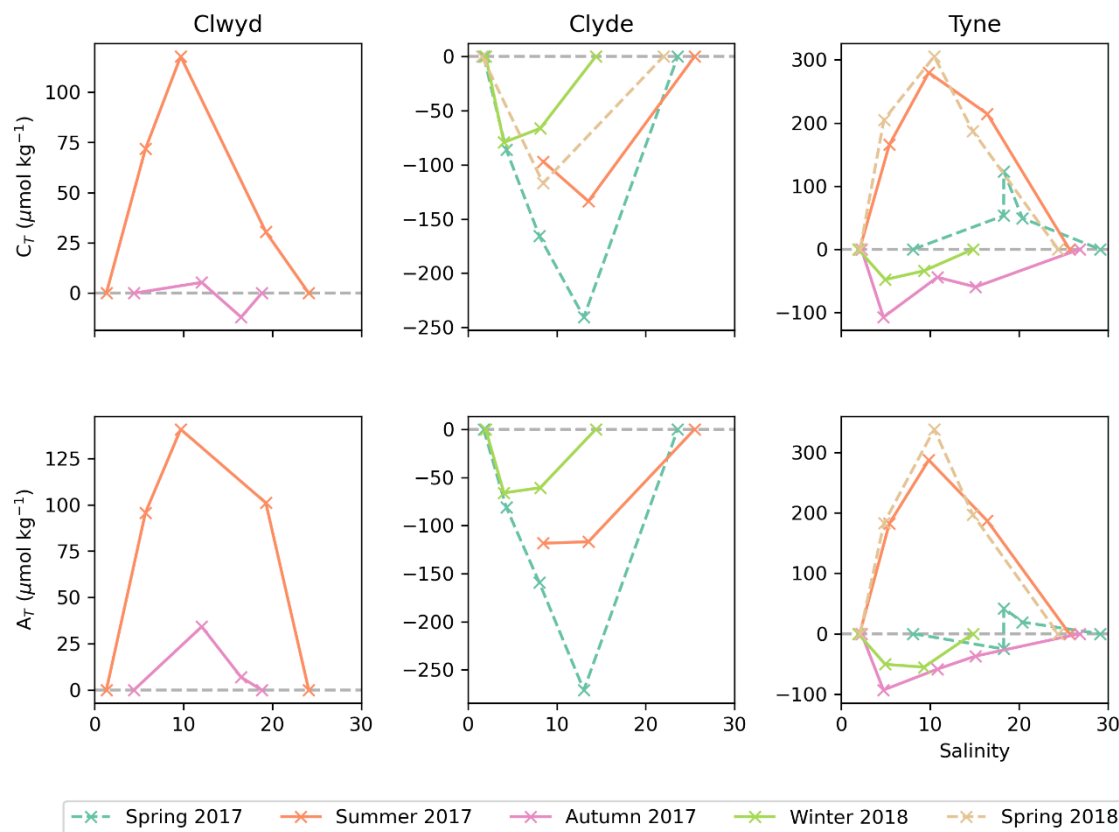


Figure 3.18 - Concentrations of  $C_T$  (upper row) and  $A_T$  (lower row) relative to the mixing line for each season in the three Group 3 estuaries (Clwyd, Clyde and Tyne) which experience changes in the sign of their salinity gradients of these chemical species between the different sampling occasions. Scatter points are coloured by the season in which samples were collected.

The Tyne and Clyde exhibit very different seasonal cycles of  $C_T$  and  $A_T$  concentrations relative to their mixing lines (Fig. 3.17, 3.18). The Clyde only experiences removal of  $C_T$  and  $A_T$  along the salinity gradient, whereas in the Tyne,  $C_T$  and  $A_T$  concentrations are elevated in Summer and Spring 2018, close to conservative in Spring 2017 and reduced in Autumn 2017 and Winter 2018, suggesting that at different times of year, the Tyne is subjected to different biogeochemical controls, whereas the key processes in the Clyde estuary are solely acting to remove  $C_T$  and  $A_T$ .

The Clwyd estuary was more sparsely sampled in time, with a full salinity range of samples collected in the Summer and Autumn of 2017, and only a single sample collected in Spring

2017 (Fig. 3.17). In Summer 2017 the concentrations of  $C_T$  and  $A_T$  in the freshwater and seawater endmembers were similar to one another (end-member linear gradient close to 0, Fig. 3.17), but in the mid-salinity range,  $C_T$  and  $A_T$  increased in concentration relative to the mixing line. The deviations from the mixing line in Autumn 2017 were relatively small.

The switch between positive and negative salinity gradients for both  $C_T$  and  $A_T$  is correlated with river discharge for the estuaries in this group (Fig. 3.19). Low discharge is associated with higher concentrations of  $A_T$  and  $C_T$  across all salinities. This suggests that, like for Group 2, residence times are sufficient in these estuaries to reach equilibrium between the groundwater and the weathering material, and that the changes between seasons are simply due to dilution.

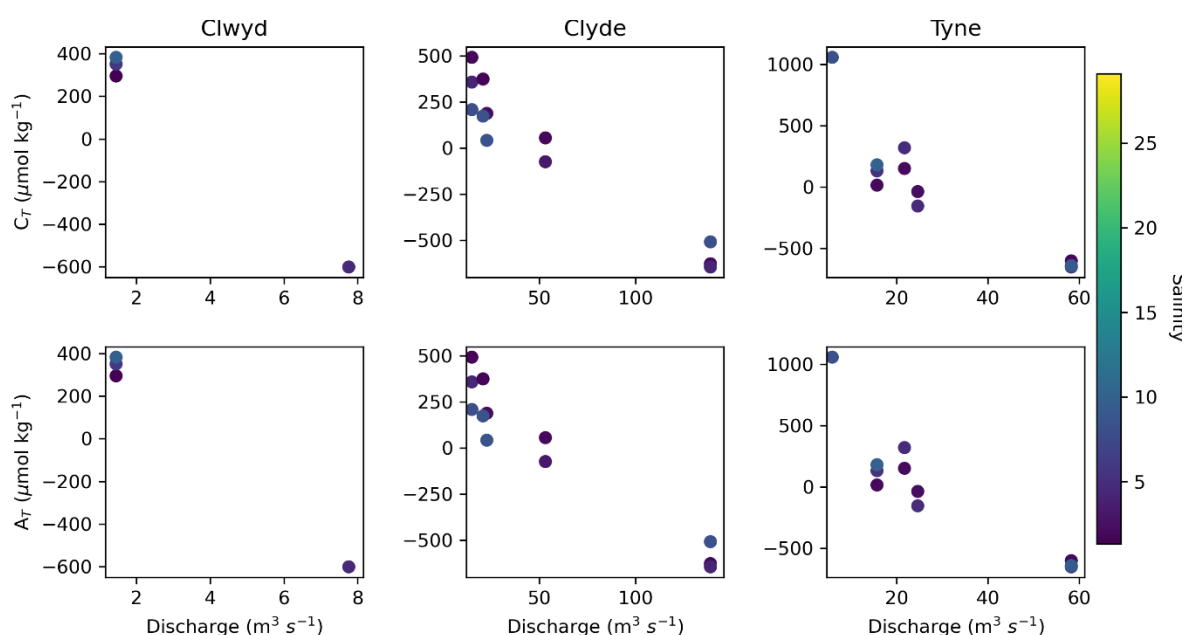


Figure 3.19 - Residual  $C_T$  (upper row) and  $A_T$  (lower row) concentrations as a function of river discharge measured daily at the National River Flow Archive gauging station for each of the Group 3 estuaries. Salinity is represented by colour, with only low salinity samples ( $0 < S < 10$ ) shown for clarity.

Low river discharge is associated with longer residence times, which provide more opportunity for the rocks (including carbonate bedrock) in the Group 3 estuaries to be weathered. Higher-than-average freshwater concentrations of  $C_T$  and  $A_T$  during low discharge conditions suggest that these limestone-containing bedrock types, when in contact with water for longer periods of time, leach alkalinity and dissolved inorganic carbon into the water, providing a source of  $A_T$  and  $C_T$  to the freshwater. Interestingly, of the Group 3 estuaries, the estuary with the biggest  $A_T$  and  $C_T$  concentration difference between salinities at a given discharge (and hence season) is the Tyne, which is also the estuary

with the highest proportion of carbonate bedrock in the catchment within this group (Table 3.1), which suggests that low discharge conditions are preferable for limestone weathering.

Group 3 estuaries experience higher  $A_T$  and  $C_T$  concentrations during low river discharge conditions and vice-versa, with the hypothesis being that long residence times in contact with non-carbonate bedrock increases the potential for bedrock weathering in the carbonate bedrock catchments. It follows that Group 2 estuaries, minimally carbonate-containing bedrock catchments, also decrease in  $A_T$  and  $C_T$  concentrations with increasing discharge, while Group 1 estuaries experience a greater magnitude difference in  $A_T$  and  $C_T$  concentrations between low and high discharge regimes because the chalk-containing bedrock weathers more rapidly than for Group 2 and 3 estuaries.

### 3.4 – Conclusions

The UK experiences a large range of  $C_T$  and  $A_T$  concentrations in estuaries. Differences in the catchment lithology of the riverine input to these estuaries drives differences in  $C_T$  and  $A_T$  concentrations at low salinity from approximately  $0 \mu\text{mol kg}^{-1}$  to in excess of  $5000 \mu\text{mol kg}^{-1}$ . Salinity gradients of these species are approximately linear, which indicates that the dominant driver of their concentrations at a given salinity is mixing. However, large positive and negative quasi-linear salinity gradients mask more subtle changes in estuarine carbonate chemistry. Deviations from linear mixing seasonally suggest that other biogeochemical processes, are having a measurable impact, though much less so than mixing. Whether these changes between the different sampling occasions, used to represent seasons because the samples are sparsely taken in time, are truly seasonal, or other processes acting on a shorter timescale requires further research.

The presence of carbonate, and in particular chalk, bedrock within a catchment has a major influence on low salinity  $C_T$  and  $A_T$  concentrations, which have been shown here to relate to river discharge. Chalk-containing catchments experience highest  $C_T$  and  $A_T$  concentrations at high discharge, whereas non-chalk catchments, including both carbonate and non-carbonate containing catchments experience higher  $C_T$  and  $A_T$  concentrations relative to their annual mean at low discharge. This difference is likely related to a combination of chalk bedrock weathering faster than sedimentary limestone, which in turn weathers faster than silicate bedrock, and differences in groundwater residence times, perhaps due to higher porosity in chalk bedrock. Seasonal changes in estuarine carbonate chemistry are dominated by differences in discharge, rather than temperature.

The influence of non-labelled carbonates in small quantities in igneous extrusions could also have an impact on the imperfect relationship between the percentage of limestone in

a catchment and the freshwater  $C_T$  and  $A_T$  concentrations, but in the absence of data on this, Chapter 4 aims to explore this phenomenon further.

## **Chapter 4**

### **Contribution of catchment lithology to the variation in freshwater $C_T$ and $A_T$ concentrations in UK rivers**

This chapter is based on work completed as a result of a successful grant proposal to the National Environmental Isotope Facility that I wrote and we submitted on 23 March 2020. The original grant proposal is in Appendix A3.

## 4.1 Introduction

Variability in estuarine total alkalinity ( $A_T$ ) and dissolved inorganic carbon ( $C_T$ ) has been observed for as long as estuarine carbonate chemistry variables have been measured. Recent efforts to determine the cause of that variability, which is most notable at low salinity, have highlighted the presence of carbonate bedrock as a potential cause of this phenomenon in a range of estuaries around the British Isles (McGrath et al., 2016, 2019, and Chapter 3). There is a strong theoretical basis to this argument: calcium carbonate dissolution (Eq. 3.1, Chapter 3) consumes  $CO_2$  to release bicarbonate, which contributes to both  $C_T$  and  $A_T$ . Silicate weathering has a similar impact on  $C_T$  and  $A_T$  concentrations (Eq. 3.2, Chapter 3) as carbonate weathering, though at an order of magnitude slower rate.

Measuring conservative variables in tracing experiments may improve our ability to determine precisely how much  $C_T$  and  $A_T$  are sourced from carbonate and silicate weathering, and hence whether the relationship found between carbonate bedrock presence and higher concentrations of  $C_T$  and  $A_T$  is substantiated. Stable and radiogenic isotopes have been used in recent studies to attribute the source material of a solution. Several studies have used the isotopic composition of  $C_T$  ( $\delta^{13}C_{DIC}$ ) in this context. While this variable was measured as part of this study (Appendix A4), insufficient sample numbers were collected for attributing the factors affecting  $\delta^{13}C_{DIC}$  (precipitation, respiration, water-air  $CO_2$  transfer, uptake of anthropogenic  $CO_2$ , formation and remineralisation of organic matter, and carbonate dissolution and precipitation) (Schulte et al., 2011). Specifically, this analysis would have assessed localised elevations or reductions in  $\delta^{13}C_{DIC}$  to be able to quantify these processes. It was not possible to sample a salinity gradient, so the  $\delta^{13}C_{DIC}$  results will not be explored further here.

Recent studies have used strontium (Sr) isotopes as a geochemical tracer of weathering products. Magnone et al. (2019) used  $^{87}Sr/^{86}Sr$  in combination with different conservative chemical tracers (Ca/Na and Mg/Na) to attribute the percentage of groundwater samples that originated from different rock types, which, with some assumptions about the mineralogy of their Cambodian study area, they were able to use to quantify the proportion of  $C_T$  that came from weathering of each individual lithological/compositional classification, in addition to the amount remaining, which they assumed to relate to organic carbon degradation.

Exploring these techniques for use in a riverine context will provide insight into the source material of river flows in the UK and help determine whether the presence of carbonate bedrock indeed drives increased freshwater  $C_T$  and  $A_T$  concentrations.

#### 4.1.1 Summary of relevant findings so far

Chapter 3 suggests that differences in the carbonate system in these estuaries are strongly influenced by the catchment bedrock. Looking at the salinity relationships with  $A_T$  and  $C_T$  respectively, there were three distinct patterns: decreasing  $A_T$  and  $C_T$  with salinity in chalk-containing catchments (Group 1), increasing  $A_T$  and  $C_T$  with salinity in catchments containing less than 2.5% carbonate bedrock (Group 2), and a set of estuaries that switch between these regimes, increasing with salinity in Autumn and Winter, and decreasing in Spring, draining catchments containing more than 10% carbonate bedrock but no chalk (Group 3). Group 3 rivers are of particular interest because their relationships of  $C_T$  and  $A_T$  with salinity could suggest either a change in the carbon source, or a change in the weathering rate and / or efficiency.

I concluded in Chapter 3 that the latter explanation, a change in weathering rate and / or efficiency was more likely, whereby the weathering rate of the bedrock in contact with freshwater flows is slower than increases in discharge. Therefore, increases in discharge, for example in Autumn and Winter when  $C_T$  and  $A_T$  concentrations are lowest, simply act to dilute the dissolved weathering products, including  $\text{HCO}_3^-$  (Eq. 3.1), which contributes to both  $C_T$  and  $A_T$ . Incidentally, this is the same process which causes variability in freshwater  $C_T$  and  $A_T$  concentrations in Group 2 estuaries, whose estuaries contain predominantly non-carbonate bedrock lithologies (Chapter 3).

Figure 4.1 gives examples of these patterns, for four estuaries which would be of particular interest to sample.

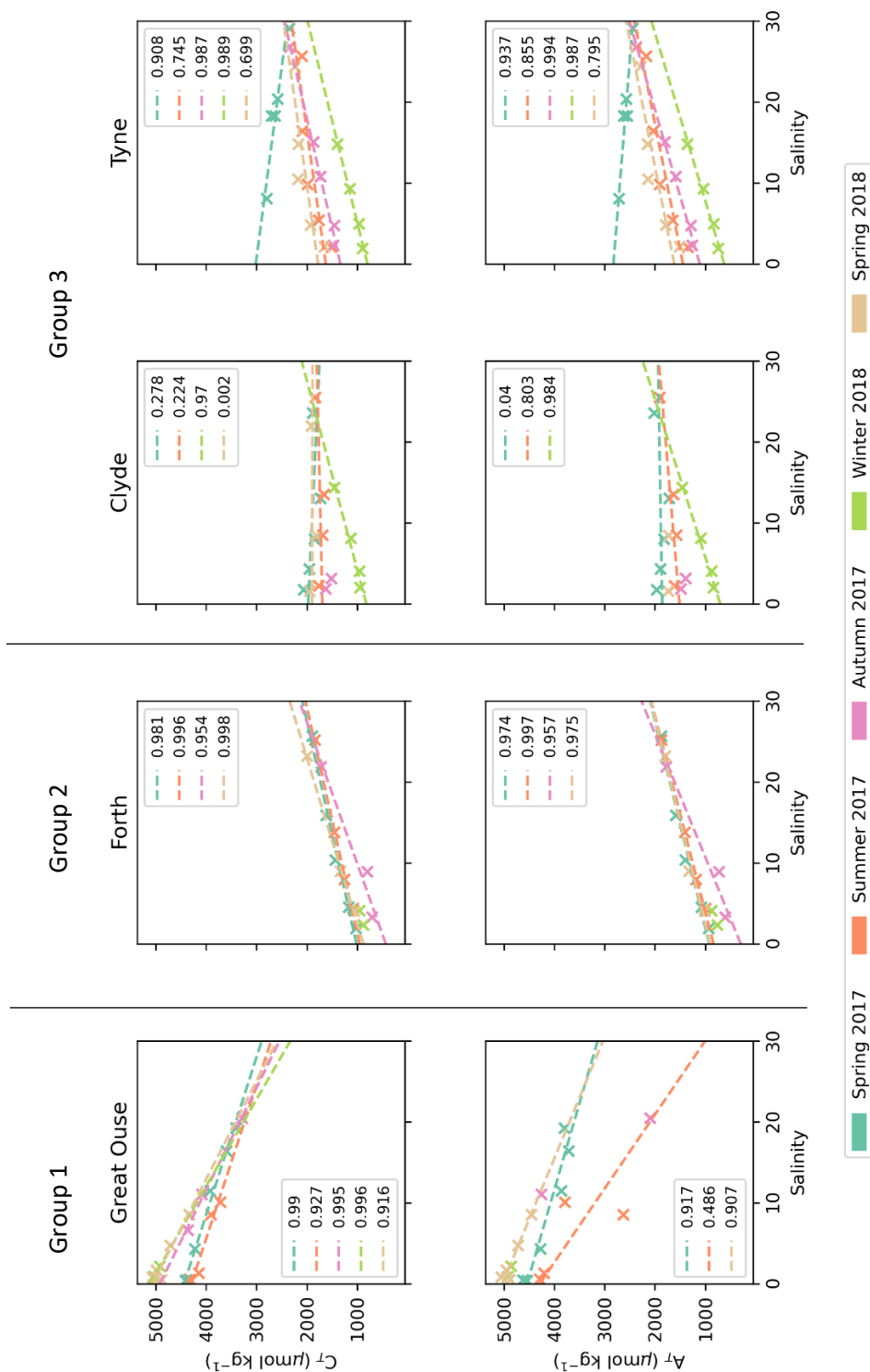


Figure 4.1 – 2017-18  $C_T$  (top row) and  $A_T$  (bottom row) measurements (as presented in Chapter 3) from the four estuaries to be sampled in this study, coloured by season. Lines between subplots delineate the estuaries belonging to Group 1, 2 and 3, respectively. Dashed lines represent per-season least-squares linear regression lines. The coefficients of determination,  $r^2$ , calculated per season, are given in the legend of each subplot.

Differences in carbonate chemistry between estuaries are driven by the  $C_T$  and  $A_T$  concentrations of their freshwater end members, and conservative mixing is the dominant control on  $C_T$  and  $A_T$  concentrations throughout the estuary (Chapter 3). Therefore, understanding the controls on freshwater  $C_T$  and  $A_T$  concentrations will improve understanding of the carbonate chemistry of the entire estuary.

From these factors, the following research question was developed, here broken down into smaller questions:

What proportion of the variation in freshwater  $C_T$  and  $A_T$  concentrations is accounted for by differences in catchment lithology?

- a) Were the  $C_T$  and  $A_T$  behaviours present in 2017-18, the features for which these estuaries were selected for sampling, also present in 2020-21?
- b) Are differences in  $C_T$  and  $A_T$  concentrations between estuaries caused by carbonate bedrock weathering?
- c) Are high  $C_T$  and  $A_T$  concentrations in the Great Ouse directly attributable to  $\text{CaCO}_3$  dissolution from chalk bedrock, as opposed to limestone bedrock weathering in the Tyne and Clyde?
- d) Is the BGS carbonate bedrock classification a good measure of (and so proxy for) the contribution of carbonate weathering to  $C_T$  and  $A_T$  concentrations?

## **4.2 Methods**

### **4.2.1 COVID-19 impacts**

Restrictions during the COVID-19 pandemic had the following effects on the research in this Chapter:

- The planned Level 2 Powerboat Handling course did not take place. As it was not possible for me to attend boat training, only limited sampling from a boat was possible, in the Forth estuary only, and on one sampling occasion only.
- Only essential travel was possible. Scouting out sampling sites in advance was not possible. Sampling sites were determined using Google Street View rather than in person. However, the majority of these planned sampling sites were not appropriate in practice, largely because the bridges were too high above the water to sample.

- Most samples were taken from the shore or bridges because of the boat limitation, and there was a reduced number of accessible sampling sites compared to those planned. This strongly reduced the salinity gradient along which samples were collected in 2020, and in 2021 only one sampling site per estuary was used.
- Without a salinity gradient, it was not possible to put the samples analysed for the isotopic composition of  $C_T$ ,  $\delta^{13}C_{DIC}$ , to use. Changes in  $\delta^{13}C_{DIC}$  along the salinity gradient in conjunction with changes in  $C_T$  and  $A_T$  concentration would have given insight into biogeochemical processing along the salinity gradient, but in the absence of a salinity gradient this attribution was not possible.
- I was supposed to analyse the  $\delta^{13}C_{DIC}$  samples at the Scottish Universities Environmental Research Centre (SUERC) as part of the National Environmental Isotope Facility (NEIF) grant, but SUERC was closed to non-residents. Therefore, the isotope samples were analysed for me, rather than by me.
- There were delays in receiving nutrient data back from the UEA Analytical Facility, which were due to instrument failure and staffing issues due to COVID-19. I analysed samples for nitrate, silicate and phosphate myself in September 2021, but there was an instrument failure during analysis and the nitrate and phosphate results were unreliable. I received these data in March 2022.

#### 4.2.2 Sampling

I sampled each of the Great Ouse, Forth, Clyde and Tyne estuaries on two occasions: in September 2020, and again in April - May 2021. These months were chosen, because the largest differences in freshwater  $C_T$  and  $A_T$  concentrations were found in the Clyde and Tyne estuaries during the same months of the 2017-18 LOCATE sampling programme (Chapter 3; Figure 4.1). It is these estuaries that are of particular interest due to their large variability in salinity-concentration gradients for  $C_T$  and  $A_T$ .

The initial aim was to sample over the salinity gradient in each estuary. Google Maps and its Street View and Satellite modes (Google, 2022) were used to identify sampling locations, which were predominantly public bridges accessible via footpath but where there was no bridge available, sites along the river bank were identified. In practice, some of these sites were not safe or possible to sample from, which would have been identified if an initial site survey had been possible, but the COVID-19 pandemic regulations at the time did not allow it. In September 2020, therefore, three of the four sampled estuaries had a limited number of samples taken, whereas the Forth estuary could be sampled in its entirety as part of a collaboration with CEH Edinburgh. In April / May 2021, boat sampling was not possible, so only the freshwater site was sampled for each estuary (Table 4.1).

Table 4.1 - Salinities of samples collected in 2020 - 2021 in each river / estuary. Samples collected from a bridge are indicated in bold. All other samples were collected from the bank, except for those from the Forth estuary in September 2020, which were collected by boat. Samples from September 2020 are shown in blue, whereas samples from April – May 2021 are shown in white.

River / Estuary	Date	Time (UTC)	Latitude (°N)	Longitude (°E)	Salinity	Temperature (° C)
<b>Great Ouse</b>	21/09/2020	<b>10:38</b>	<b>52.5473</b>	<b>0.3641</b>	<b>0.47</b>	<b>17.34</b>
		<b>12:05</b>	<b>52.6005</b>	<b>0.3567</b>	<b>2.71</b>	<b>16.84</b>
		<b>14:39</b>	<b>52.7008</b>	<b>0.3605</b>	<b>7.02</b>	<b>17.37</b>
	29/04/2021	<b>10:24</b>	<b>52.5473</b>	<b>0.3641</b>	<b>0.41</b>	<b>11.75</b>
<b>Tyne</b>	23/09/2020	07:58	54.9643	-1.8700	0.10	14.12
		08:48	54.9721	-1.8520	0.09	14.17
	30/04/2021	09:26	54.9643	-1.8700	0.16	9.06
<b>Forth</b>	25/09/2020	10:03	56.1224	-3.8784	0.5	11.8
		10:27	56.1130	-3.8558	3.33	12.56
		10:43	56.1129	-3.8335	6.35	12.64
		10:56	56.1018	-3.8263	12.03	12.81
		11:10	56.1035	-3.7932	14.48	12.79
		11:22	56.0846	-3.7751	18.47	12.70
		11:36	56.0711	-3.7391	22.86	13.13
	01/05/2021	07:48	56.1318	-3.9189	0.37	10.16
<b>Clyde</b>	28/09/2020	08:33	55.8286	-4.1517	0.18	9.32
	01/05/2021	09:01	55.8286	-4.1517	0.23	10.11

Bridge samples were collected by a Van Dorn sampling bottle lowered into the water by rope, which was subsequently emptied through a plastic spigot, connected to Tygon tubing, into the various sample bottles. Bankside and boat samples were collected by submerging a bucket into the water. The first bucket of water was used for rinsing sample bottles, and then each sample bottle was submerged into a second bucket of water until filled. During sampling, a Castaway CTD (SonTek) was used to measure water temperature and salinity. Samples for  $C_T$  and  $A_T$  analysis were stored in 250 ml borosilicate bottles, fixed with 50  $\mu$ l saturated mercuric chloride ( $HgCl_2$ ) solution, and sealed shut with Apiezon-L grease. Nutrient (nitrate, phosphate and silicate), dissolved organic carbon (DOC) and  $\delta^{13}C_{DIC}$  samples were filtered through sterile 0.45  $\mu$ m syringe filters into 100 ml Nalgene bottles and fixed with 20  $\mu$ l saturated mercuric chloride solution. Ca, Mg, Na and Sr analysis was conducted using the remaining nutrient sample.  $^{87}Sr/^{86}Sr$  samples were filtered through 0.2  $\mu$ m sterile syringe filters into 60 ml Nalgene bottles. All filtering happened immediately after sampling, with the exception of the samples collected in the Forth estuary in September 2020, which were collected in 1 L Nalgene bottles and stored in a cool box until they were filtered approximately 2 hours later. All bottles were pre-rinsed with the filtered water sample three times. Samples were stored in the dark at room temperature until analysis.  $C_T$  and  $A_T$  analysis was conducted in May – June 2021, DOC and silicate were analysed in September 2021,  $^{87}Sr/^{86}Sr$  was analysed in February 2022, nitrate and phosphate were analysed in March 2022, and Ca, Mg, Na and Sr were analysed in July 2022.

The research questions for this chapter relate to low salinity water only because it was not possible to sample the full salinity gradient except for in the Forth estuary in September 2020. Therefore, only low salinity samples are presented here, where the salinity is below 10. The highest-salinity sample within this category has a salinity of 7.02.

### 4.2.3 Laboratory analysis

I analysed  $C_T$  and  $A_T$  samples using a VINDTA-3C as outlined in Chapter 2.

Dissolved nitrate, phosphate and silicate were measured spectrophotometrically using a discrete analyser (SEAL AQ400) following procedures set out by the manufacturer (AQ methods SEA-527, SEA-156 and SEA-122, respectively). Total organic carbon and non-purgeable organic carbon were measured using a Skalar Formacs CA15-16. Selected ionic concentrations (Ca, Mg, Na, Sr) were measured using Inductively Coupled Plasma Atomic Emission Spectroscopy (ICP-AES). Of these analyses, the silicate analysis was conducted at the UEA Analytical Facilities by the author, and the remainder of these analyses (nitrate,

phosphate, total organic carbon (TOC), non-purgeable organic carbon (NPOC), Ca, Mg, Na, Sr) were completed by the staff of the UEA Analytical Facilities.

$^{87}\text{Sr}/^{86}\text{Sr}$  analysis was conducted at BGS Keyworth using the following procedure. A subsample was acidified and evaporated until dry. The residual solids were mixed with calibrated 2.5 M HCl (hydrochloric acid). Strontium was collected on Eichrom AG50 resin columns and loaded onto a single Re (rhenium) filament following the method of Birck (1986). The isotopic composition of strontium,  $^{87}\text{Sr}/^{86}\text{Sr}$ , was measured by Thermal Ionisation Mass spectroscopy (TIMS) using a Thermo Triton multi-collector mass spectrometer. Measurement of the international calibration standard for  $^{87}\text{Sr}/^{86}\text{Sr}$ , NBS987, gave a value of  $0.710259 \pm .000013$  ( $2 \sigma$ ,  $n = 27$ ) during the analysis of these samples. Sample data were corrected to the accepted value for this standard of 0.710250. Recent laboratory blanks gave  $\sim 85$  pg Sr, which is considered negligible (e.g. Eckardt et al., 2009).

#### **4.2.4 End member mixing model**

End member mixing models of major cations (Ca, Mg, Na and Sr) with the isotopic composition of Sr,  $^{87}\text{Sr}/^{86}\text{Sr}$ , were used to determine the proportion of each river water sample from different end members (Appendix A5, Magnone et al. (2019)). R code containing these equations (Magnone et al., 2019, their supplementary data 3, updated version provided by personal communication, Magnone 2022) was here adapted for use in Python as part of this study.

#### **4.2.5 End member data**

The above end member mixing calculations require as inputs the chemical composition and strontium isotopic composition of three distinct end members, implying that they are the sole three contributors to river flow. Since the hypotheses for this chapter concern carbonate weathering, and in particular its relative importance compared to silicate weathering, monolithological carbonate-influenced stream water was selected, hereon referred to as 'carbonate', and which here includes both limestone and chalk bedrocks, monolithological silicate-influenced stream water, hereon referred to as 'silicate', and rainwater as the three end members initially. These were subsequently found to be an unsuitable combination for the Great Ouse, so for the Great Ouse only, given that bedrock in the Great Ouse catchment is almost entirely composed of chalk and limestone, carbonate, monolithological calcite (chalk)-influenced stream water, hereon referred to as 'calcite' and rainwater were used as end members.

Rainwater end member  $\text{Ca}^{2+}$ ,  $\text{Mg}^{2+}$  and  $\text{Na}^+$  concentrations were sourced from DEFRA's Precip-Net database (DEFRA, 2022), for which the chemical composition of rainwater is measured on either a daily or fortnightly basis at 41 sites around the UK. All  $\text{Ca}^{2+}$ ,  $\text{Mg}^{2+}$  and  $\text{Na}^+$  data were selected from all 41 of these locations for 2020-21, the years over which samples were collected, and calculated the mean concentration and its standard deviation for each variable. Sr isotopic compositions and particularly  $\text{Sr}^{2+}$  concentrations are less commonly measured, so were not available through the Precip-Net database. They are generally less variable in rainwater than the concentrations of other elements. Shand et al. (2007) provide two measurements of rainwater  $\text{Sr}^{2+}$  concentration and  $^{87}\text{Sr}/^{86}\text{Sr}$  in the Plynlimon catchments of Mid-Wales from samples collected in 1995.

Meybeck (1986) provide the concentrations of major ions of pristine (non-polluted) monolithological streams from samples collected around France in 1980-1983. Carbonate  $\text{Ca}^{2+}$ ,  $\text{Mg}^{2+}$  and  $\text{Na}^+$  concentration data were taken from their supplementary table 'Annexe 2', for all rivers classed as 'Calcaires et dolomies' (Meybeck, 1986, pg. 66, n = 33), which includes primarily limestone bedded catchments, with some dolomitic catchments and a single chalk stream.

The Great Ouse is the only river sampled here that contains chalk according to the BGS bedrock classification (British Geological Survey, 2008; Table 3.1; Chapter 3). The non-chalk carbonate rock types are used to describe carbonate rocks in the mixing model for this river basin (n = 32). Calcite ionic concentrations, with 'calcite' used to refer to chalk specifically, were taken from the same data table, for the single stream denoted as 'craie', which translates to 'chalk'.

Silicate solute concentrations were taken from the same data table, for all rivers classed as 'granite', 'granulite' and 'gneiss' and permutations thereof, of the 'Roches plutoniques et metamorphiques' (Meybeck, 1986, pg. 64, n = 55).

All of the data sourced from Meybeck (1986) are used as input to a Temperate Stream Model in later studies from which mean concentrations are summarised, but with no indication of variability (Meybeck, 1994, 1987), so the mean and standard deviations of the original concentrations for monolithological carbonate and silicate stream waters were used. Since only one chalk stream data entry was available, the standard deviation of the ionic concentrations in monolithological calcite stream water was estimated by calculating the ratio of the standard deviation to the mean of each ionic concentration for carbonate streams and assumed a standard deviation in the same ratio to the mean for calcite streams.

Using these data for end member concentrations assumes that the composition of monolithic streams in catchments with carbonate (including chalk) and silicate rocks in France and in the UK is the same. Despite the large sample size of French catchments

provided, the standard deviation around the mean composition of a given ion is close to 100% in most cases (Table 4.2). There is no comparable database for UK monolithological streams; the only information available which corroborates the idea that this range of values could also be representative of the UK is provided by Meybeck (1994). Graphical distributions of certain major ions (see Meybeck, 1994, pg. 67), only one of which (Na<sup>+</sup>) is also selected for use in this Chapter, show that 'monolithologic Miscellaneous Streams' from around the world follow a similar distribution to their Temperate Stream Model as well as to the 'monolithologic French Streams' whose data are used here (Meybeck, 1994). In the absence of specific references for these global monolithologic stream concentration data, which are not given in the original study (Meybeck, 1986), the associated supplementary information, or their later comparative study (Meybeck, 1994), and in the absence of Ca<sup>2+</sup> and Mg<sup>2+</sup> comparisons between studies similar to those provided for other ionic concentrations (Meybeck, 1994), it is difficult to assess the applicability of these data to this Chapter. In the absence of a suitable alternative, these data are used and these potential pitfalls are acknowledged.

Concurrent Sr<sup>2+</sup> concentrations and isotopic compositions were not measured (Meybeck, 1986), so had to be obtained elsewhere. Sr<sup>2+</sup> concentrations can be estimated from the ratio between calcium and magnesium in each end member with respect to rainwater, given that the strontium concentration in rainwater is known:

*Equation 4.1*

$$Sr_{EM} \approx Sr_{rw} \times \frac{Ca_{EM} + Mg_{EM}}{Ca_{rw} + Mg_{rw}}$$

Where 'rw' refers to rainwater and 'EM' refers to the end member in question. Eq. 4.1 (Magnone, 2022, pers. comm.) assumes that the calcium and magnesium content of any given non-rainwater end member is entirely sourced from rock weathering. Since all of the ionic concentrations (Ca<sup>2+</sup>, Mg<sup>2+</sup> and Sr<sup>2+</sup>) in Eq. 4.1 were measured in the river samples taken in this study, it is possible to verify whether this assumption holds true for these river samples, and therefore whether it is a fair assumption for the end member data. Fig. 4.2 suggests that this assumption holds true for the samples in this study, whose deviations from the 1 : 1 line between measured and estimated (Eq. 4.1) Sr concentrations are significantly smaller than the uncertainty in estimated Sr concentration that comes from large variability in Ca and Mg concentrations in each geological category. Mean squared absolute difference of measured Sr concentrations from the 1 : 1 line is 2.46 (μmol l<sup>-1</sup>)<sup>2</sup> (n = 18) over the concentration range shown; the range in estimated Sr concentrations for the end members is much smaller, from 0.0445 to 4.37. Over this range only, the mean squared absolute difference is 0.0269 (μmol l<sup>-1</sup>)<sup>2</sup> (n = 9).

$^{87}\text{Sr}/^{86}\text{Sr}$  data are available for different geological types and ages around the UK using measurements from a variety of media (plant, dentine, water, soil, tooth, bone) (Evans et al., 2009). All of the water-based measurements for silicate were selected, from samples denoted as 'Granite' and 'Gneiss' ( $n = 10$ ), and for carbonate, from samples labelled 'Limestone' or 'Chalk' ( $n = 12$ ) and used to calculate their mean and standard deviation. Similarly, in the Great Ouse mixing model, chalk and non-chalk containing limestone are treated separately;  $^{87}\text{Sr}/^{86}\text{Sr}$  is lower for chalk than for non-chalk limestone (Table 4.2)

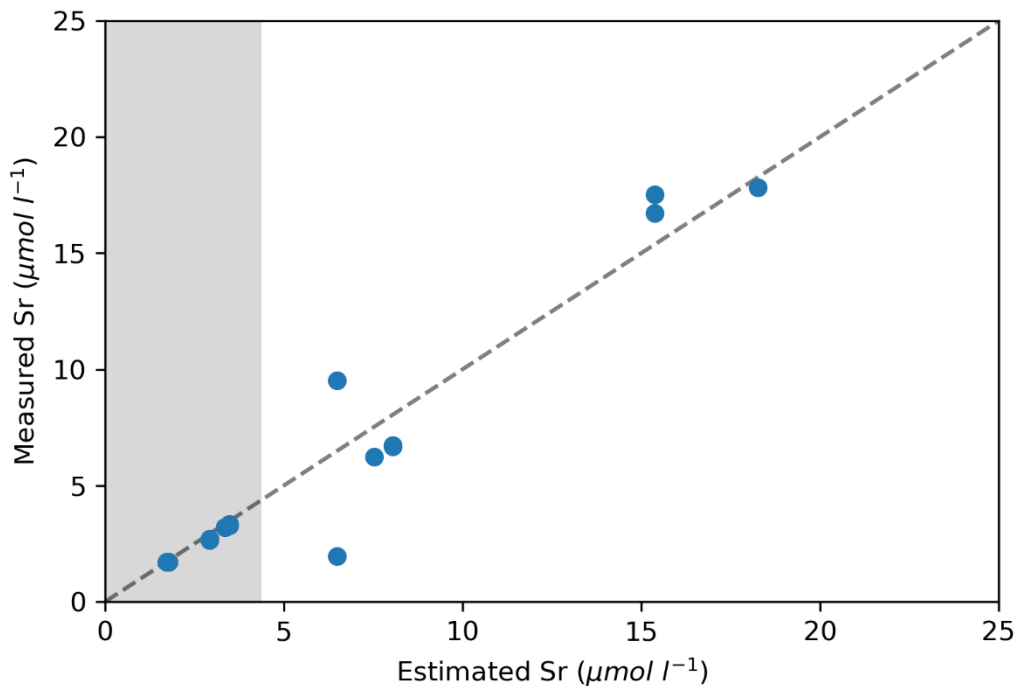


Figure 4.2 - Estimated (Eq. 4.1) and measured Sr concentration. A dashed line indicates values for which measured and estimated Sr concentrations are exactly equal. The area shaded in grey indicates the range of values ( $0.0445 - 4.37 \mu\text{mol l}^{-1}$ ) over which the end member estimated Sr concentrations vary.

All concentrations, both of end members and of sample concentrations, were converted to units of  $\mu\text{mol L}^{-1}$ . This is because all of the end member concentrations are provided per unit of volume, rather than mass:  $\mu\text{eq L}^{-1}$  (Meybeck, 1986) and  $\text{mg L}^{-1}$  (DEFRA, 2022; Shand et al., 2007), but without concurrent salinity and temperature measurements it was not possible to calculate density and subsequently convert to units of mass, whereas these data are available for the samples collected as part of this study, so the conversion to units of volume was possible.

Table 4.2 – End member compositions of rainwater (DEFRA, 2022; Shand et al., 2007), and of pristine stream water influenced by carbonate, silicate and calcite bedrock, respectively (Meybeck, 1986; Evans et al., 2009).  $Sr^{2+}$  concentrations estimated using Eq. 4.1 are indicated in red. Ionic concentrations are expressed to 3 s. f. in  $\mu\text{mol L}^{-1}$  and isotopic ratios are expressed to 6 d. p. and are unitless.

End member	$Ca^{2+}$ ( $\mu\text{M}$ )	$\sigma(Ca^{2+})$ ( $\mu\text{M}$ )	$Mg^{2+}$ ( $\mu\text{M}$ )	$\sigma(Mg^{2+})$ ( $\mu\text{M}$ )	$Na^+$ ( $\mu\text{M}$ )	$\sigma(Na^+)$ ( $\mu\text{M}$ )	$Sr^{2+}$ ( $\mu\text{M}$ )	$^{87}\text{Sr}/^{86}\text{Sr}$	$\sigma(^{87}\text{Sr}/^{86}\text{Sr})$
<b>Rainwater</b>	11.9	32.3	10.4	19.1	99.7	191	0.0445	0.709186	0.000008
<b>Silicate</b>	50.8	45.2	28.9	31.6	156	138	0.159	0.717354	0.002776
<b>Carbonate (all)</b>	1900	550	282	308	142	148	4.36	0.709064	0.001086
<b>Carbonate (excluding chalk)</b>	1900	559	288	312	130	133	4.37	0.709902	0.000436
<b>Calcite (Chalk)</b>	1870	548	99.5	108	526	537	4.25	0.707891	0.000102

### 4.3 Results and Discussion

The Great Ouse, Tyne, Clyde and Forth rivers were selected for sampling in this chapter because they exhibited a range of  $C_T$  and  $A_T$  concentration relationships with salinity in their estuaries. The Great Ouse estuary experienced low-salinity  $C_T$  and  $A_T$  concentrations higher than seawater concentrations year-round. The Forth estuary experienced low-salinity  $C_T$  and  $A_T$  concentrations lower than seawater year-round. The Clyde and Tyne estuaries switched between a positive and negative salinity gradient at different times of year (Fig 4.1). Firstly, therefore, it is important to ascertain whether the samples collected for this chapter follow the same pattern. Figures 4.3 and 4.4 suggest that this is largely true. The Great Ouse and Forth rivers each conformed to the sign and magnitude of the concentration gradient found in 2017-18. The River Tyne samples also fall within the concentration range found in 2017-18, including the change in salinity gradient. The River Clyde samples contained a higher concentration of  $C_T$  and  $A_T$  on both sampling occasions in 2020-21 than at any site or on any sampling occasion than in 2017-18 for the Clyde estuary.

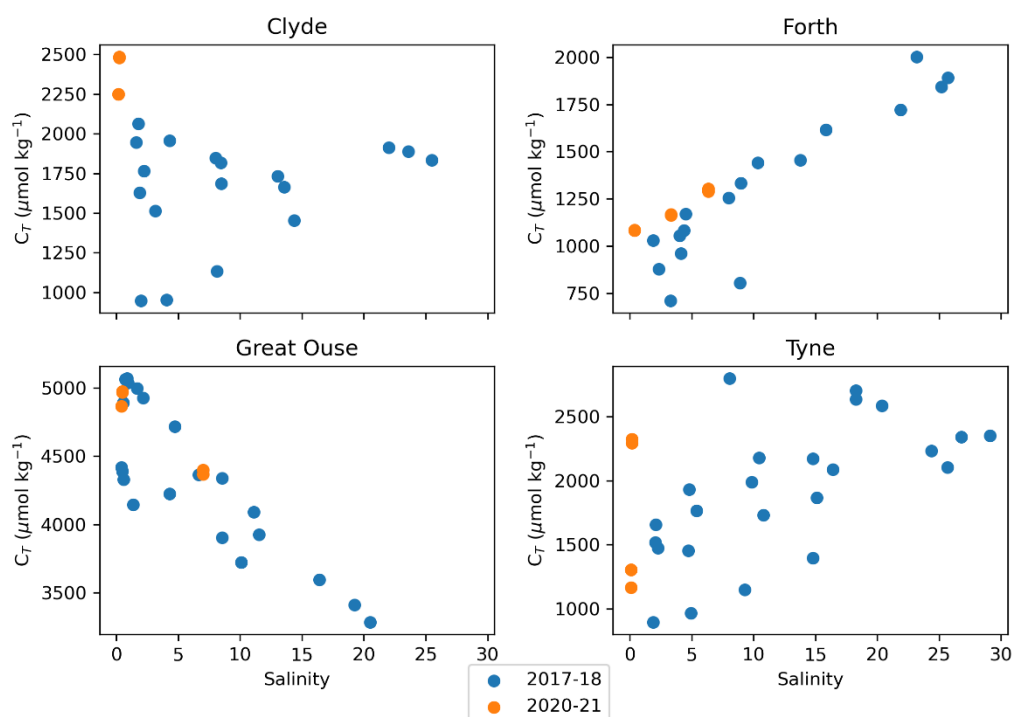


Figure 4.3 -  $C_T$  concentrations in the four estuaries sampled in this chapter with blue indicating samples collected in 2017-18 (Chapter 3) and orange indicating samples collected in 2020-21 for this chapter.

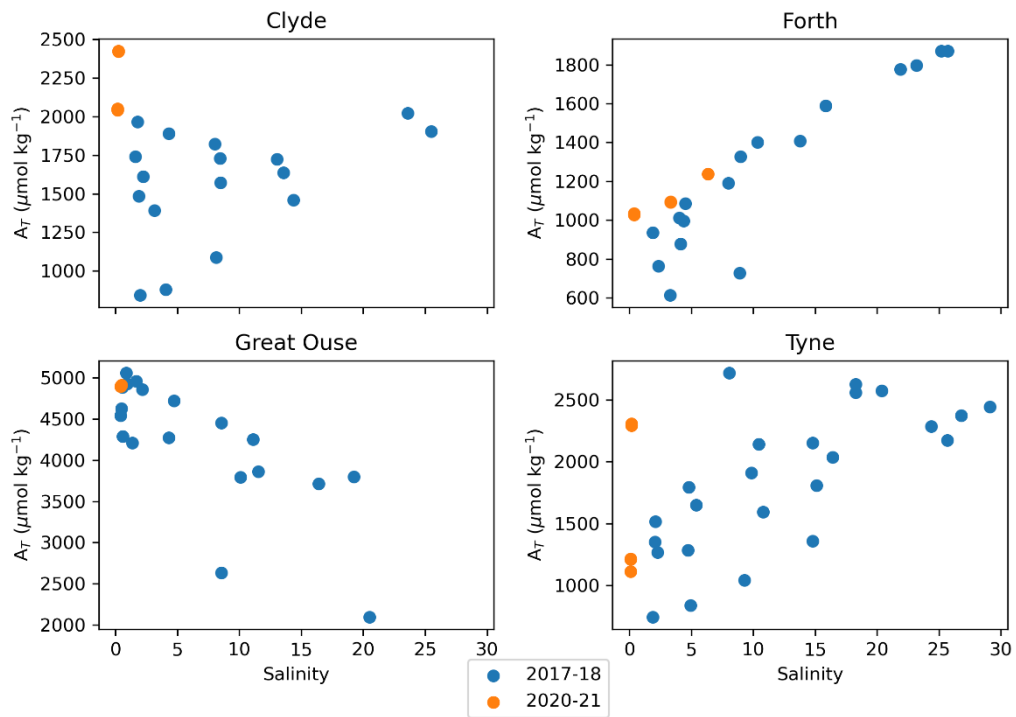


Figure 4.4 –  $A_T$  concentrations in the four estuaries sampled with blue indicating samples collected in 2017-18 (Chapter 3) and orange indicating samples collected in 2020-21 for this chapter.

Chapter 3 concluded that the main factor driving differences in  $C_T$  and  $A_T$  on different sampling occasions within a given estuary was river discharge, with Group 3 estuaries (including the Clyde estuary) experiencing higher low-salinity  $C_T$  and  $A_T$  concentrations at low discharge (Fig. 3.17).

In view of the above, it may be interesting to explore whether this finding is reflected in differences between the Tyne and Clyde in their lithological contribution to flow. With the River Clyde experiencing more consistent and higher concentrations of  $C_T$  and  $A_T$  on the two sampling occasions in 2020-21 than across the sampling occasions and sites in 2017-18, and the Tyne experiencing lower and more variable concentrations in 2020-21 than in 2017-18, this may indicate differences in the source material and/or flow paths between the two rivers.

Mixing diagrams visualise the proportional contribution of each end member to water samples (Fig. 4.5). The three end members (rainwater, carbonate and silicate) can be used to describe the samples collected in three of the four rivers studied here. If a sample falls within the outer mixing lines, then the sample can be formed from a combination of the end members. Given the large standard deviations around the end member tracers, particularly of the Ca/Na ratios for silicate and rainwater, the Mg/Na ratio for all end members, and

$^{87}\text{Sr}/^{86}\text{Sr}$  for carbonate and silicate, it is possible that the end members adequately represent samples from the Forth, Tyne and Clyde rivers, as data points largely fall between the end members (Fig. 4.5)

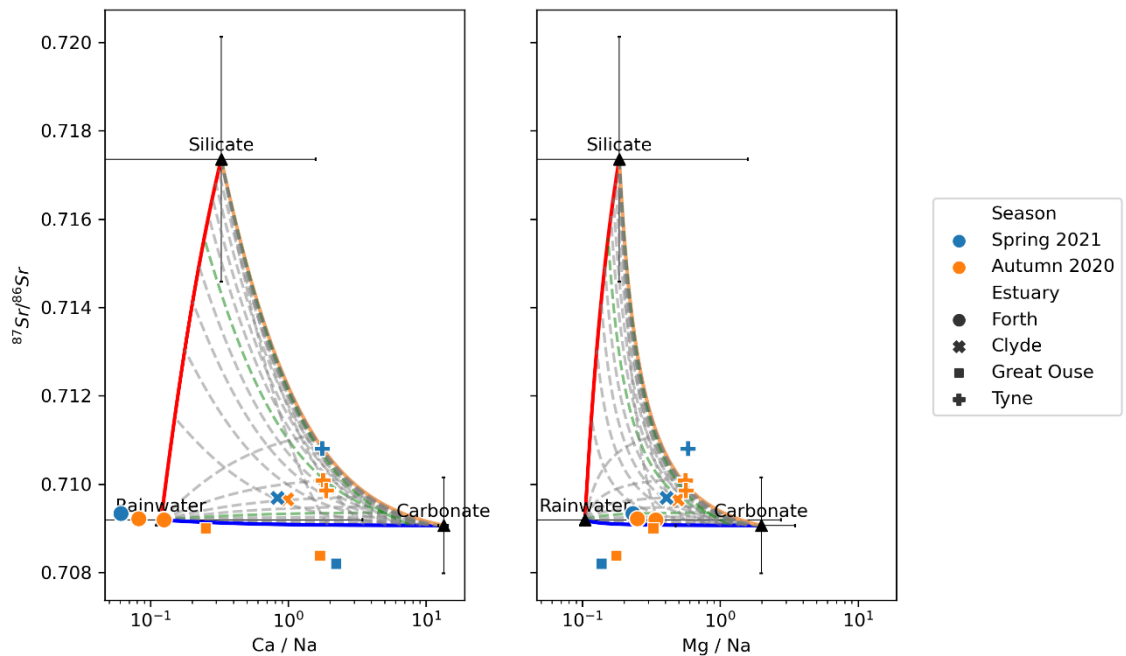


Figure 4.5 - Mixing diagrams using  $\text{Ca}/\text{Na}$  and  $\text{Mg}/\text{Na}$  respectively. Black triangles indicate end member mean concentrations and isotope ratios. Error bars indicate 1 standard deviation around the end member concentration ratios and isotope ratio. Where the error bar extends further than the x axis, this is because it becomes negative, which cannot be computed using a logarithmic x axis. Coloured scatter points represent samples collected in 2020-21, coloured by the sampling occasion and with the shape indicating the estuary. Solid coloured lines represent the direct mixing of two end members (i.e. a zero-contribution from the third end member), with dashed grey lines indicating a 10%, 20% etc. contribution of the third end member, and the dashed green lines indicating where the third end member contributes 50%.

Notably, the River Great Ouse is not well-represented by the end members. With a catchment almost entirely comprised of chalk, a calcium carbonate bedrock, one would expect the Great Ouse to conform closely to the blue line in Fig. 4.5, which represents direct mixing of carbonate-draining water and rainwater. In reality, the River Great Ouse does not.

The key difference between the River Great Ouse and the other carbonate-containing rivers sampled here is that it is the only river of this subset whose catchment specifically contains chalk bedrock (British Geological Survey, 2008) as opposed to limestone more generally.

Limestone bedrock has a more varied composition than chalk alone, particularly in terms of its magnesium content (Fig. 4.6), with limestone being a broader term encompassing, for example, dolomitic rocks which have a higher Mg content than other limestones. Carbonate bedrock in either chalk, or more generically limestone form, comprises 86.2% of the Great Ouse catchment. Including these two rock types (calcite for chalk and carbonate for non-chalk limestone) as separate, distinct end members in a second, similar mixing model shows that the compositional difference between calcite and carbonate could be used to explain the different Ca/Mg ratio found in the River Great Ouse; chalk (calcite) is uniquely low in Mg relative to Ca and has a slightly lower  $^{87}\text{Sr}/^{86}\text{Sr}$  composition than limestone more generally (carbonate) (Fig. 4.6).

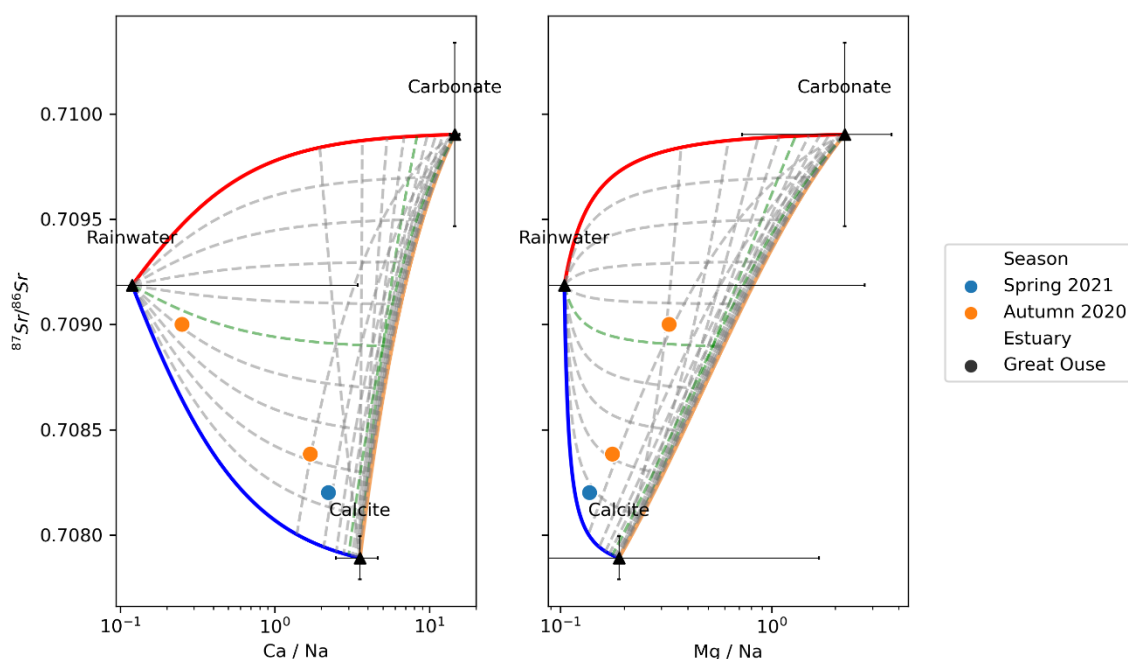


Figure 4.6 - Mixing diagrams using Ca/Na and Mg/Na respectively, as described for Figure 5. Black triangles indicate end member mean concentrations and isotope ratios. Error bars indicate 1 standard deviation around the end member concentration ratios and isotope ratio. Coloured scatter points represent samples collected from the River Great Ouse in 2020-21, coloured by the sampling occasion.

The River Great Ouse, of the four catchments studied here, is the only river to drain a catchment whose bedrock contains a large proportion of, or indeed any, chalk. The Great Ouse also experiences the highest concentrations of  $C_T$  and  $A_T$  year-round, and these two factors may be linked.

The end member mixing models, hereon using two separate models for the River Great Ouse and the other rivers (Tyne, Forth and Clyde), were used to calculate the proportion of each water sample, and thus the proportion of river flow each sample represents, that originated from each end member. The proportion of flow from each end member is calculated twice, once for each geochemical tracer used (Ca/Na vs Mg/Na). Ca- and Mg-calculated percentages of flow from the carbonate end member in the Tyne, Forth and Clyde rivers show agreement in terms of ranking, though not in terms of magnitude (Fig. 4.7a), with the Ca calculation yielding percentages much smaller than those calculated using Mg. Although the absolute percentages are different, the strong relationship between the two, in addition to the ranking of the samples according to each calculation being almost identical, indicates that it may be possible to explore the relationship between the carbonate bedrock end member and  $C_T$  and  $A_T$  concentrations.

For the carbonate and calcite flow percentages calculated for the River Great Ouse model (Fig 4.7b), there is poor correspondence between the Ca and Mg calculations when calculating the contribution of carbonate and calcite to river flow.

In both mixing models (Great Ouse and the three other rivers), the differences between the Ca and Mg calculations arise from differences between the end member concentrations used (taken from the literature as described above) and the real-world end member concentrations. Particularly in the River Great Ouse's case, where the end members are more similar in composition to one other (Fig. 4.6), a small difference in end member composition could have a large effect on the accuracy of the model. The data used to describe each end member comes from several different sources, generally from historic sampling occasions and not always from a similar location, or indeed the UK, all of which acts to introduce uncertainty in the end member composition.

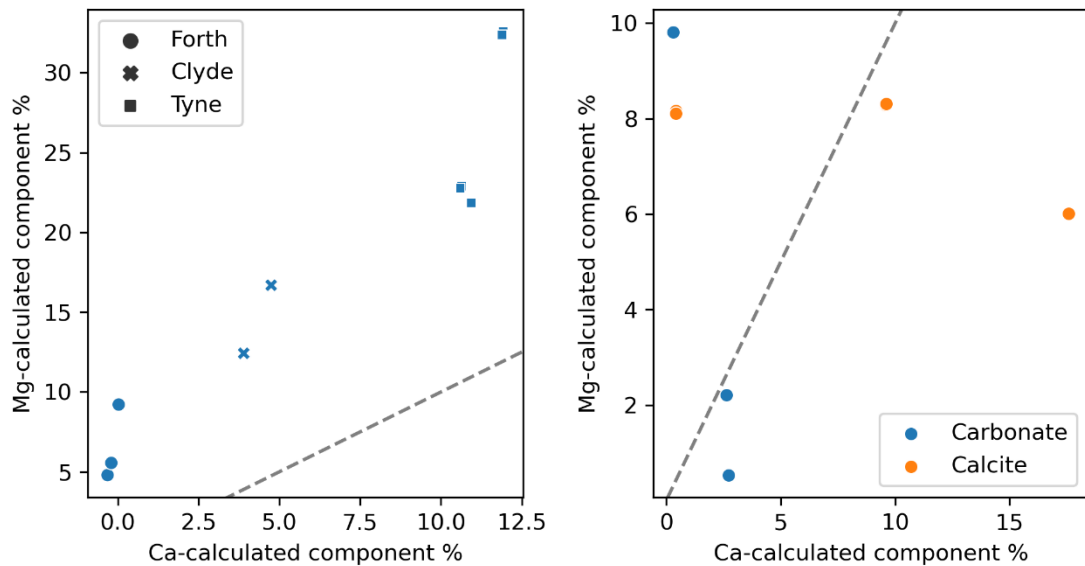


Figure 4.7 – a) A comparison of the percentage of flow for the carbonate endmember calculated using Ca and Mg for the Forth, Clyde and Tyne rivers and with different markers to denote different rivers, and b) the Great Ouse, with the colour here indicating the two different carbonate rock-types (carbonate for limestone and calcite for chalk) used as end members. Grey dashed lines represent 1 : 1, where Ca- and Mg- calculated flow contributions are equal.

Further uncertainty arises from additional  $\text{Na}^+$  input from sea salt aerosols. This may affect the end member Ca/Na and Mg/Na ratios, since atmospheric deposition is the primary source of  $\text{Na}^+$  in streams (Neal and Kirchner, 2000). The analysis presented here implicitly assumes that differences in sodium deposition across the weathering sites pertinent to the rivers measured here are adequately described by the mean and standard deviations of sodium concentrations measured at the times and locations that measurements were taken from the French monolithological streams (Meybeck, 1986). The Ca- and Mg- based calculations for the Forth, Clyde and Tyne are comparable, but the two calculations produce incompatible results for the Great Ouse. The calcite end member was based on a single data entry (Section 4.2.5), whose Na concentration is substantially higher than the means for the other rock types (Table 4.2). It is highly plausible that this single point is not representative of mean sodium concentration for all monolithological chalk streams, either in France or in the UK (Table 4.2).

Data presented in Fig. 4.7a and 4.7b are presented in Tables 4.3 and 4.4, respectively. While it is not possible to say which, if either, of the two measures is closer to the true percentage, the values calculated from Ca are more plausible. Aside from the standard deviation of Ca/Na being much smaller than that of Mg/Na in the end member data, notably

the Ca-calculated contribution of carbonate to river flow in the River Forth samples in all cases is close to 0%. The River Forth catchment contains the lowest percentage surface area contribution of carbonate bedrock (1.12%, Table 3.1; British Geological Survey, 2008), so a near-zero contribution of the carbonate end member to river flow is more plausible than the 5 – 10% estimate yielded by the Mg-based calculation. Future sampling and analysis could improve correspondence between the two calculation types by better constraining the end members, which would implicitly constrain any contribution of sea salt aerosols to their solute concentrations. Specifically, this would involve collecting samples of different bedrock types in addition to a rainwater sample from each catchment being studied and analysing these samples for Ca, Mg, Na, Sr and  $^{87}\text{Sr}/^{86}\text{Sr}$ .

Table 4.3 – Percentages of river flow originating from rainwater and from carbonate and silicate bedrock in the Clyde, Forth and Tyne catchments, from calculations using Ca and Mg. Uncoloured rows are samples collected in 2020, and coloured rows are samples collected in 2021.

Sample Name	Ca			Mg		
	Carbonate (%)	Silicate (%)	Rainwater (%)	Carbonate (%)	Silicate (%)	Rainwater (%)
<b>Clyde 1a</b>	4.75 (±10.3)	11.4 (±36.8)	83.8 (±45.5)	16.7 (±43.2)	35.9 (±192)	47.4 (±190)
<b>Clyde 1b</b>	4.75 (±10.3)	11.5 (±37.1)	83.7 (±45.7)	16.7 (±43.4)	36.2 (±195)	47.1 (±189)
<b>Clyde A</b>	3.90 (±8.66)	10.3 (±38.0)	85.8 (±46.4)	12.4 (±34.0)	28.8 (±157)	58.8 (±229)
<b>Clyde B</b>	3.90 (±8.66)	10.2 (±37.6)	85.9 (±46.2)	12.4 (±33.9)	28.5 (±154)	59.1 (±229)
<b>Forth 2a</b>	-0.196 (±1.88)	0.00275 (±8.16)	100 (±30.1)	5.56 (±19.7)	2.90 (±14.0)	91.5 (±200)
<b>Forth 2b</b>	-0.196 (±1.88)	-0.0386 (±7.46)	100 (±29.7)	5.56 (±19.8)	2.61 (±12.7)	91.8 (±198)
<b>Forth 3a</b>	0.0312 (±2.11)	0.0623 (±7.42)	99.9 (±29.5)	9.21 (±26.9)	4.26 (±14.4)	86.5 (±190)
<b>Forth 3b</b>	0.0319 (±2.12)	0.0237 (±6.83)	99.9 (±29.2)	9.21 (±27.0)	3.88 (±13.1)	86.9 (±1.88)
<b>Forth A</b>	-0.313 (±1.73)	0.226 (±14.6)	100 (±34.6)	4.80 (±17.7)	4.87 (±25.7)	90.3 (±226)
<b>Forth B</b>	-0.312 (±1.73)	0.120 (±14.0)	100 (±34.2)	4.80 (±17.8)	4.66 (±24.5)	90.5 (±223)
<b>Tyne 1a</b>	10.6 (±21.5)	42.4 (±97.1)	47.0 (±73.9)	22.8 (±87.4)	87.2 (±845)	-9.94 (±116)
<b>Tyne 1b</b>	10.6 (±21.6)	43.6 (±101)	45.8 (±75.1)	22.9 (±90.2)	89.8 (±892)	-12.7 (±132)
<b>Tyne 2b</b>	10.9 (±22.1)	33.2 (±69.2)	55.8 (±64.1)	21.9 (±65.9)	63.9 (±472)	14.2 (±94.4)
<b>Tyne A</b>	11.9 (±25.9)	86.8 (±273)	1.29 (±122)	32.4 (±301)	225 (±4980)	-158 (±2170)
<b>Tyne B</b>	11.9 (±26.1)	87.8 (±279)	0.187 (±123)	32.6 (±208)	229 (±5130)	-161 (±2250)

Table 4.4 - Percentages of river flow modified by calcite (for chalk) and carbonate (for limestone in general) bedrock and from rainwater in the Great Ouse catchment, from calculations using Ca and

Sample Name	Ca			Mg		
	Calcite (%)	Carbonate (%)	Rainwater (%)	Calcite (%)	Carbonate (%)	Rainwater (%)
<b>Great Ouse 1a</b>	9.60 (±19.1)	2.64 (±5.79)	87.8 (±55.0)	8.31 (±54.7)	2.21 (±135)	89.5 (±753)
<b>Great Ouse 1b</b>	9.59 (±19.1)	2.64 (±5.80)	87.8 (±54.9)	8.29 (±54.7)	2.21 (±135)	89.5 (±752)
<b>Great Ouse 5a</b>	0.422 (±1.43)	0.305 (±0.357)	99.3 (±31.3)	8.10 (±24.9)	9.81 (±182)	82.1 (±321)
<b>Great Ouse 5b</b>	0.425 (±1.44)	0.303 (±0.355)	99.3 (±31.3)	8.16 (±25.1)	9.82 (±182)	82.0 (±322)
<b>Great Ouse A</b>	17.6 (±36.1)	2.73 (±6.98)	79.7 (±76.1)	6.02 (±56.3)	0.531 (±97.4)	93.5 (±969)

*Mg. Uncoloured rows are samples collected in 2020, and coloured rows are samples collected in 2021.*

Research Question (d) cannot be answered adequately by the data available, because the correspondence between the Ca- and Mg-based calculations is poor and the sample size is small. However, on an order-of-magnitude basis, the calculated percentages for the Great Ouse (Table 4.4) are smaller than one might expect both from the calculated values for the other rivers (Table 4.3) and from the high percentage coverage of carbonate-containing rocks across the catchment (86.2% carbonate bedrock, of which 76.2% is chalk bedrock, Table 3.1; British Geological Survey, 2008). Therefore, while the contribution from chalk to the river flow is low, this suggests that at the point of weathering, chalk-derived concentrations of  $C_T$  and  $A_T$  are much higher than for limestone weathering, which results in higher overall  $C_T$  and  $A_T$  concentrations in the Great Ouse. However, without further sampling and better constraining the end members, it is difficult to have confidence in this result.

This work provided an opportunity to explore the applicability of bedrock classification data as a predictor variable for carbonate chemistry measurements, for example in Chapter 3. Previous authors have had concerns about the use of bedrock classification data as a predictor variable, because this data does not provide sufficient insight into the variability of rock chemical composition, nor their weathering efficiency (Amiotte Suchet et al., 2003; Hagedorn and Cartwright, 2010). For example, Hagedorn and Cartwright (2010) used  $\delta^{13}C$  of  $C_T$  and of both dissolved and particulate organic carbon to calculate that approximately 36% of the riverine  $C_T$  in the Australian Victorian Alps originates from carbonate bedrock, despite less than 5% of the catchment bedrock being defined as carbonate. (Note that the difference between this and values presented in this study are that this refers to a percentage of  $C_T$ , whereas the percentages presented here are of the contributions of specific bedrocks to flow).

Comparing measurements made in this chapter to the bedrock classification presented in Chapter 3, suggests in contrast to this previous work, that the Chapter 3 catchment bedrock classification is in fact a good proxy for the percentage of flow that can be attributed to carbonate bedrock in the three comparable rivers (Clyde, Forth and Tyne) (Fig. 4.8). Both the surface area percentage of carbonate bedrock in the catchment (Fig. 4.8a) and mean catchment bedrock age (Fig. 4.8b) show clear correspondence with the percentage of flow derived from carbonate bedrock. This is interesting on two accounts. Firstly, that, since the two BGS-derived variables (% carbonate bedrock and mean bedrock age) are coincidentally correlated with each other, future studies should avoid using both variables

in statistical models of riverine carbonate chemistry because they are likely to cause autocorrelation. Secondly, that future studies could indeed use spatial geological data similarly to provide insight into the contribution of limestone and chalk to the carbonate chemistry of river and estuarine water, without the additional samples and measurements required to attribute the river water as presented here.

The fact that previous studies found geological data was not adequate as a proxy for the contribution of carbonate bedrock to water chemistry (Amiotte Suchet et al., 2003; Hagedorn and Cartwright, 2010) is not necessarily incompatible with these findings. The UK has a relatively carbonate-rich geology in comparison with many other countries, and the vast differences between catchments' surface area contribution of carbonate bedrock (between 0 – 94.5% of catchment surface area in the 14 estuaries studied in Chapter 3 (Table 3.1)) make differences between catchment carbonate chemistry clear. In other locations, where carbonate bedrock covers relatively small areas of a catchment, these sorts of comparisons may be more problematic. Therefore, the evidence presented here suggests that geological data is a good proxy for the contribution of the carbonate bedrock end member to river flow in the UK. This effectively bypasses the need for analytically complex laboratory measurements of a variety of variables, as presented here, which is particularly beneficial where institutions do not have access to the range of laboratory tools and techniques required.

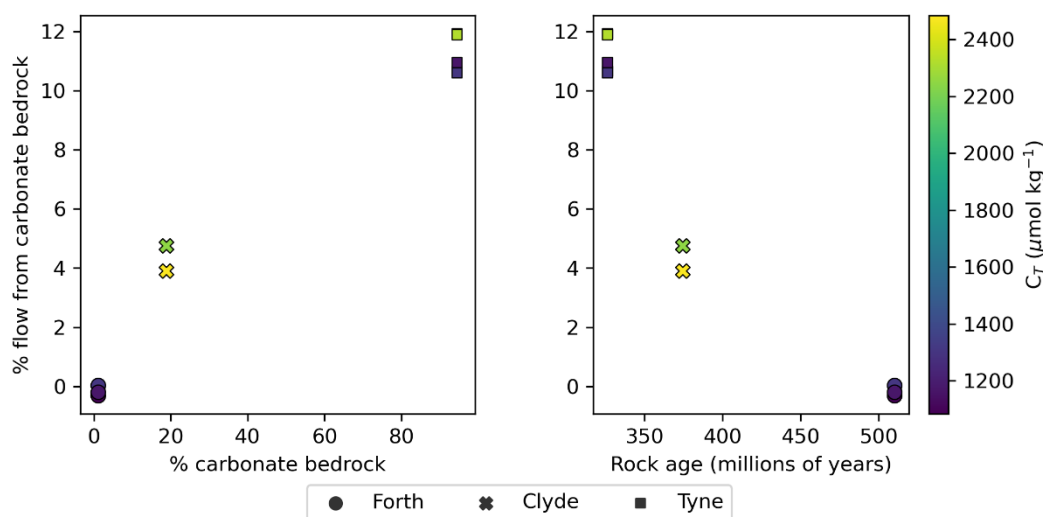


Figure 4.8 - Percentage of river flow from carbonate bedrock (calculated in this chapter using Ca rather than Mg (Fig. 4.7)) as a function of BGS carbonate bedrock data and mean rock age across the catchment. The variables displayed on the x axes were used as predictor variables in Chapter 3. Points are coloured by their  $A_T$  concentration. Mg-calculated contributions are presented in Appendix A6.

Finally, riverine carbonate chemistry (here,  $A_T$  is shown) is not well-defined by the geological variables presented here (Fig. 4.8). Chapter 3 found that estuarine  $C_T$  and  $A_T$  concentrations are generally higher in estuaries with larger surface area contributions of carbonate bedrock, but this was not a perfect correlation and there were exceptions. Here, with a sample size of three rivers represented, it is likely that the weak relationship between carbonate % and  $A_T$  is an example of this imperfect correlation. Differences in seasonal cycle and the representativeness of the sampling occasions relative to the seasonal changes could have a substantial impact, as could a hypothetical input between these sampling sites and the estuarine sampling sites, for example.

#### 4.4 Conclusions

The four rivers studied in this chapter experienced similar  $C_T$  and  $A_T$  concentrations in the 2020-21 sampling period to the freshwater end members in the original 2017-18 sampling period (Fig. 4.3). The similarity in their riverine carbonate chemistry from 2017-18 to three years following that, suggests that controls on  $C_T$  and  $A_T$  concentrations did not substantially change over that period. These rivers were selected for further sampling in this chapter because of their differing carbonate chemistry, so the similarity between the sampling years confirms that choice.

The COVID-19 pandemic substantially hampered the planned sampling effort (Section 4.2.1, Appendix A3). Had the sampling gone ahead to the extent that was originally planned, this would have solved the issue of having a small sample size.

This chapter presents a preliminary study attributing river flow to carbonate and silicate weathering. The study is the first of its kind that applies its findings to the LOAC globally, and the first of its kind to study these phenomena in UK rivers. Attributing river flow to carbonate and silicate weathering proved challenging with the data available, partly due to the small sample size, particularly in the case of the chalk-rich Great Ouse, which required separate end-member model treatment because of the different ionic and isotopic signature of chalk as opposed to limestone more generally. More challenging than the sample size, however, is the constraint of end members. Without more confidence in the correct selection of end member characteristics, it is not possible to reliably quantify the proportion of river flow originating from each end member.

Finally, the proportion of river flow that originates from carbonate bedrock is well-described by the BGS rock classification presented in Chapter 3. With further work to constrain the end members used in the mixing model, as well as a larger sample size, it may be possible to use these spatial geological data as a proxy for carbonate bedrock contribution to flow,

to avoid future studies having to pursue complex analyses, such as those carried out in this Chapter.

The two factors that limit this chapter are the sample size, as previously mentioned, and the use of secondary data for end member chemical compositions. The solute concentrations of end members have large variation within each bedrock category (Meybeck, 1986). There are unanswered questions about their representation of UK bedrock, as opposed to French bedrock, and differences in sodium content resulting from sea salt aerosol deposition between pristine streams. Therefore, in future, prior to further sampling, researchers should focus on better constraining end members to improve confidence in this form of analysis.

## **Chapter 5**

**Propagating inorganic carbon and alkalinity  
measurements in a diverse range of UK estuaries  
through to annual CO<sub>2</sub> outgassing**

## 5.1 Introduction

Atmospheric carbon dioxide (CO<sub>2</sub>) concentrations have seen an unprecedented global increase since pre-industrial times (IPCC, 2021). The increase in anthropogenic CO<sub>2</sub> emissions has been attributed as a major cause of recent and future projected changes to Earth's climate (IPCC, 2021). It is therefore vital that we understand the contributions of the various sources and sinks of atmospheric CO<sub>2</sub>, to enable the prediction and ultimate mitigation of climate change. At a global scale, both the land and the ocean are considered as CO<sub>2</sub> sinks in the present day (Friedlingstein et al., 2022), though in preindustrial times the land and ocean sinks were close to equilibrium with the atmosphere (Gloor et al., 2003; Regnier et al., 2013). Understanding the changing interaction between these, the largest sinks in the Global Carbon Budget (Friedlingstein et al., 2022), would help the international effort to improve carbon cycle budgeting and subsequent climate prediction.

A key uncertainty in carbon dioxide (CO<sub>2</sub>) source and sink attribution lies at the interface between land and ocean (Regnier et al., 2013). Carbon is transported from land, via rivers and estuaries, to the ocean. Riverine inorganic carbon is derived from rock and soil weathering on land, whereas terrestrially derived organic carbon consists of plant matter formed through photosynthesis. Across the land-ocean aquatic continuum, organic carbon is respired, a byproduct of which is CO<sub>2</sub>. This drives supersaturation with respect to atmospheric CO<sub>2</sub> and therefore outgassing of CO<sub>2</sub> to the atmosphere. Budgeting efforts have historically treated rivers and estuaries as passive CO<sub>2</sub> transporters, sometimes described as a 'pipe' through which carbon leaves the land and enters the ocean (Cole et al., 2007). The reality is almost certainly more complex, with rivers and estuaries thought to be sources of CO<sub>2</sub> to the atmosphere in their own right. Of rivers and estuaries, riverine CO<sub>2</sub> fluxes have smaller uncertainties associated with them than estuaries (Bauer et al., 2013), as they have been more comprehensively studied; global riverine carbon flux estimates have existed for nearly 40 years (Meybeck, 1982).

A number of global estuarine outgassing estimates have been proposed so far this century. These estimates vary substantially, from 0.60 to 0.15 Pg C yr<sup>-1</sup>, but the overall trend of the estimates is seemingly a decrease over time (Abril and Borges, 2004; Borges, 2005; Borges et al., 2004; Chen and Borges, 2009; Laruelle et al., 2010, 2013). Perhaps most commonly cited by present literature is the global estuarine outgassing estimate proposed by Regnier et al. (2013), of  $0.25 \pm 0.25$  Pg C yr<sup>-1</sup>. This could represent a substantial contribution to the current carbon budget 'imbalance', the 0.3 Pg C yr<sup>-1</sup> that is currently missing from global CO<sub>2</sub> emissions estimates (Friedlingstein et al., 2022). However, all current estimates of estuarine CO<sub>2</sub> emissions and carbon transport to the coastal ocean are highly uncertain. Current estimates of these terms are commonly reported to be within 50-100% of the true

value (Bauer et al., 2013; Regnier et al., 2013). This issue is further complicated because estuarine CO<sub>2</sub> emissions are likely to be constantly changing in response to climate change and anthropogenic influences.

There are two main causes of uncertainty in present understanding of estuarine CO<sub>2</sub> dynamics. Firstly, measurements of carbonate system variables in estuaries are relatively sparse, in both time and space. Many global and large-scale regional estimates of estuarine outgassing rely on extrapolation from a small number of measurements from few estuaries and from few sampling occasions (Borges, 2005; Cai, 2011; Chen and Borges, 2009; Frankignoulle et al., 1998; Laruelle et al., 2010, 2013). Secondly, there is substantial physical and biogeochemical heterogeneity within and between estuaries (Dürr et al., 2011). This makes it logistically challenging to sample a representative range of estuaries at the necessary resolution. Increasing the number of sampled estuaries, the spatial and temporal coverage of CO<sub>2</sub> flux estimates, will contribute to improved regional and global estuarine CO<sub>2</sub> outgassing estimates in future.

Indeed, an estimate of estuarine CO<sub>2</sub> outgassing in the UK does not exist to date. One European estimate, that estuaries and their plumes emit 30-60 million tons of carbon each day (Frankignoulle et al., 1998) was calculated over 20 years ago now, which data from two UK rivers (Thames and Tamar) contributed to, but the UK is a highly variable environment, as discussed in Chapter 3, so using the available data to determine whether the controls on C<sub>T</sub> and A<sub>T</sub>, are the same as the controls on pCO<sub>2</sub> and CO<sub>2</sub> flux (calculated from C<sub>T</sub> and A<sub>T</sub>) would be a valuable addition to the estuarine CO<sub>2</sub> flux field.

More numerous than CO<sub>2</sub> flux estimates are pCO<sub>2</sub> measurements (direct, and indirect, through C<sub>T</sub> and A<sub>T</sub> measurements, for example). pCO<sub>2</sub> is generally high at low salinity, and decreases towards the seawater endmember (e.g. Abril et al., 2003; Frankignoulle et al., 1998; Gattuso et al., 1998; Jeffrey et al., 2018; Jiang et al., 2008; Raymond and Bauer, 2001). pCO<sub>2</sub> does not share the same controls as C<sub>T</sub> and A<sub>T</sub>, but has been found in previous riverine and estuarine studies to relate to a number of factors: discharge (Liu and Raymond, 2018), temperature (Reum et al., 2014; Wang and Cai, 2004), nutrient concentrations (Abril et al., 2003; Addey et al., 2021; Salisbury et al., 2008) and to organic matter decomposition (Frankignoulle et al., 1998; Salisbury et al., 2008). Net heterotrophy is thought to be the key driving factor of high pCO<sub>2</sub> at low salinity in estuaries, with net respiration of organic matter releasing CO<sub>2</sub> and driving high pCO<sub>2</sub> values, particularly where organic carbon inputs are high and light availability is low at turbid low salinities (Abril and Borges, 2004; Frankignoulle et al., 1998).

The aims of this chapter are to address the following research questions:

### 5.1.1 Research Questions

1. How and why does  $p\text{CO}_2$  change from source to sea in different estuaries and at different times of the year? Are there differences between estuaries and seasons?
2. How does  $\text{CO}_2$  flux vary from source to sea in different estuaries? To what extent is this controlled by the same factors as  $p\text{CO}_2$ ?
3. How much  $\text{CO}_2$  is outgassed by estuaries around the UK?

## 5.2 Methods

### 5.2.1 Sampling + Measurements

This chapter will examine  $p\text{CO}_2$  and  $\text{FCO}_2$  variation between estuaries, seasons and across salinities. These data are calculated from  $C_T$  and  $A_T$  measurements made on samples collected as part of the LOCATE programme in 2017-18. Details of the programme itself as well as the  $C_T$  and  $A_T$  measurement procedures are found in Chapter 3, and the sampling strategy is detailed in Chapter 2. Additionally, this chapter uses variables from the LOCATE dataset to contextualise the variations in  $p\text{CO}_2$ : inorganic nutrient concentrations, temperature, salinity and non-purgeable organic carbon (NPOC) (Tye et al., 2022a).

### 5.2.2 $p\text{CO}_2$ calculation

I calculated  $p\text{CO}_{2 \text{ water}}$  from the  $C_T$  and  $A_T$  measurements presented in Chapter 3 using PyCO2SYS (Version 1.8.1, Humphreys et al., 2022; Lewis and Wallace, 1998) using the carbonic acid dissociation constants of Cai and Wang (1998), the bisulfate dissociation constant of Dickson (1990) and the borate : chlorinity ratio of Uppström (1974). The uncertainty propagation capability inbuilt within PyCO2SYS was used to calculate the uncertainty in  $p\text{CO}_2$  from  $C_T$  and  $A_T$  uncertainty, temperature and salinity measurement uncertainty (Raiteri et al., 2018), and the uncertainties in  $pK$  values from Orr et al. (2018) provided as standard in PyCO2SYS.  $p\text{CO}_2$  uncertainty expressed as the standard deviation was on average 21% of the calculated  $p\text{CO}_2$ , of which  $A_T$  and  $C_T$  measurement uncertainty were the largest contributors (Appendix A1).

### 5.2.3 Statistical Analysis

I ran a linear mixed effects model using the following variables: salinity, temperature ( $^{\circ}\text{C}$ ), river discharge ( $\text{m}^3 \text{s}^{-1}$ ), concentrations of dissolved inorganic nitrogen (DIN,  $\mu\text{mol l}^{-1}$ ), log-scaled soluble reactive phosphorus (SRP) ( $\mu\text{mol kg}^{-1}$ ) and NPOC (ppm), and including interactions between discharge and inorganic nutrients, and temperature and inorganic nutrients, to predict  $\text{pCO}_2$ . The predicted variable,  $\text{pCO}_2$ , was transformed on a log scale to approximately follow a normal distribution. 'Estuary' was included as a random effect to account for multiple measurements in each estuary which could lead to pseudo replication. DIN here represents the sum of nitrate, nitrite and ammonium concentrations. Data for all of the input variables were collected as part of the 2017-18 LOCATE sampling campaign (Tye et al., 2022a), with the exception of river discharge data which are available from the NRFA gauging station network and were formatted as described in Chapter 3.

Variables were checked for multicollinearity using the Variance Inflation Factor (VIF) function. 'Season' was excluded because of its high VIF, likely because it is related to temperature and river discharge, which we can hereon consider to collectively represent in some part the seasonal variations. Non-significant variables were left in the model to avoid other estimates being artificially inflated as they account for the additional variance (Mundry and Nunn, 2009). Non-significant interactions were also left in the model because the a priori reasons for their inclusion still stand, and so it may be interesting to explore the reason for their insignificance. An  $r^2$  value was calculated to indicate the proportion of variance in  $\text{pCO}_2$  accounted for by the variables in the model, according to the method proposed by Nakagawa et al. (2017). The residuals were checked for normality.

This statistical analysis was conducted in RStudio (R Version 4.1.3). Data were cleaned using the packages: 'janitor' (version 2.1.0) (Firke, 2021), 'hablar' (version 0.3.0), 'magrittr' (version 2.0.3) (Bache et al., 2022) and 'tidyverse' (1.3.1) (Wickham, 2019). The linear mixed-effects model was run using the packages: 'lme4' (version 1.1-29) and 'lmerTest' (version 3.1-3) (Kuznetsova et al., 2015). Variance inflation factor was calculated using the 'car' package (version 3.1-0) (Fox et al., 2012). Post-hoc checks used the packages 'performance' ( $r^2$ , version 0.9.1) (Lüdtke et al., 2021) and 'DHARMA' (residual checking, version 0.4.5) (Hartig and Hartig, 2017).

## 5.2.4 Water-to-air CO<sub>2</sub> flux (FCO<sub>2</sub>) calculation

I obtained ERA5 Reanalysis data (Hersbach et al., 2018) at 0.25° x 0.25° spatial and hourly temporal resolution for the following variables: 10 m (above surface) eastward (u) and northward (v) components of wind speed, 2 m (above surface) dewpoint temperature and surface pressure, the pressure exerted by the atmosphere on the surface of land or water, (P in Pa), according to the licence to use Copernicus Products. For each sampling site in this study, the closest ERA5 grid point was selected, and all hourly datapoints for the 5 seasons (Spring 2017 – Spring 2018) over which estuary samples were collected were used. The mean distance between sampling site and ERA5 grid point was 9.4 km (min = 2.1 km, max = 15.9 km). Sampling sites within the same estuary were assigned to between 1 – 6 ERA5 grid points (Table 5.1).

Table 5.1 – Number of ERA5 grid points used per estuary

Avon	Clwyd	Clyde	Conwy	Dart	Forth	Great Ouse	Halladale
1	1	3	2	2	2	2	1
Mersey	Tamar	Tay	Tees	Test	Thames	Trent	Tyne
2	2	3	1	2	4	6	2

I obtained raw atmospheric dry air mole fraction of CO<sub>2</sub> (xCO<sub>2</sub>, μmol mol<sup>-1</sup>) data from the Mace Head Greenhouse Gas Reference Network Site (Dlugokencky et al., 2021, Fig. 5.1). Data are either available in raw or monthly mean format; the raw data were selected here because they provide a more complete timeseries, with mean frequency of approximately 9 days. A piecewise cubic Hermite interpolating polynomial (PCHIP) interpolation function (Fritsch and Butland, 1984) was used to estimate xCO<sub>2</sub> for every hour of the sampling period, to match the frequency of the ERA5 Reanalysis dataset (Fig. 5.2). PCHIP interpolation generates a smooth linear function that does not exceed the minima/maxima of the real data, so performs well with raw data that are not smooth (Fig. 5.2).

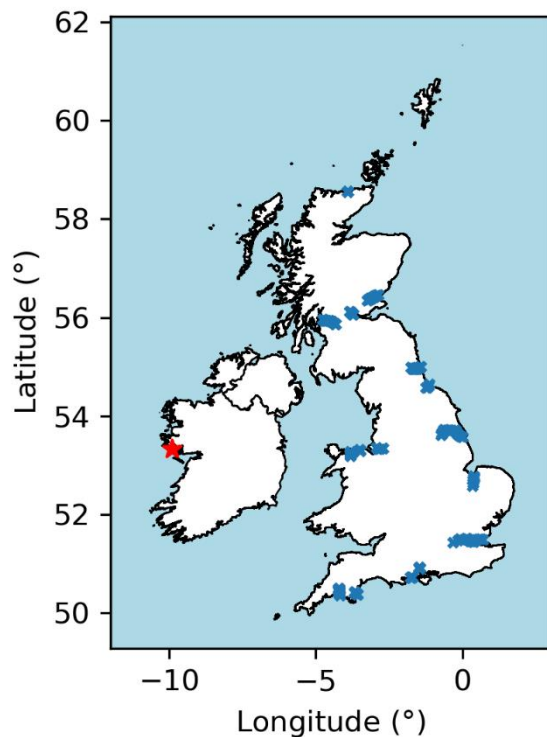


Figure 5.1 - Map showing location of Mace Head atmospheric observatory relative to the estuaries sampled by LOCATE. Blue scatter points correspond to the GPS coordinate of a sampling location (Tye et al., 2022a), displayed with the boundaries of the UK and Ireland (GADM, 2022, (Version 4.1)). The location of Mace Head is shown as a red star.

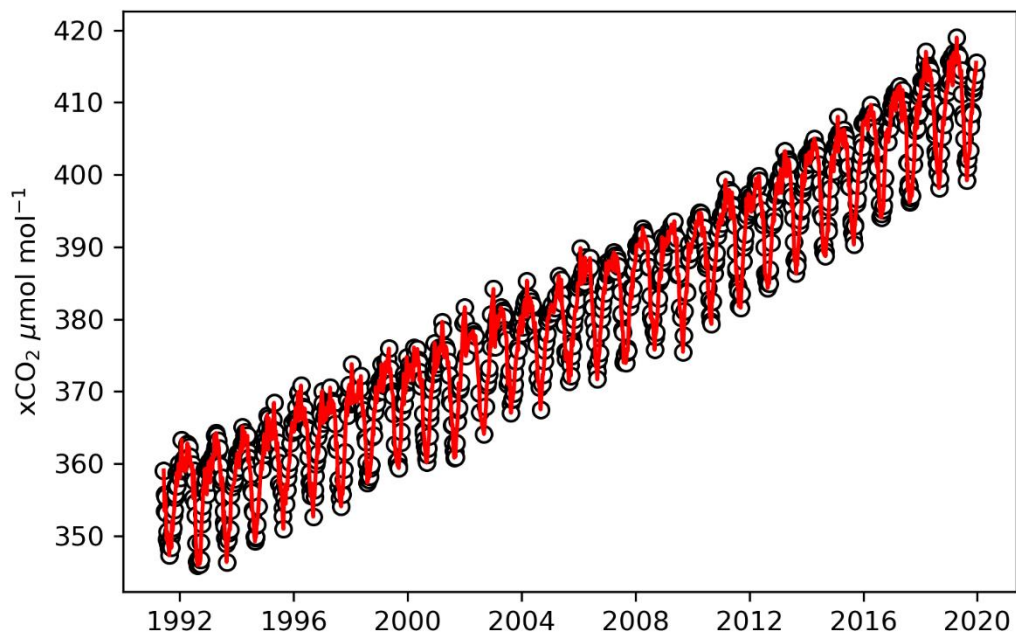


Figure 5.2 – Hourly PCHIP interpolation of discrete  $x\text{CO}_2$  measurements from Mace Head.

Water vapour pressure ( $\varepsilon$ , Pa) was calculated from 2 m dewpoint temperature ( $T_d$ ) (Alduchov and Eskridge, 1996; Lawrence, 2005) (Eq. 5.1):

*Equation 5.6*

$$T_d = \frac{243.04 \ln\left(\frac{\varepsilon}{610.94}\right)}{17.625 - \ln\left(\frac{\varepsilon}{610.94}\right)}$$

This was used to calculate the partial pressure of CO<sub>2</sub> in air ( $pCO_{2 \text{ air}}$ ,  $\mu\text{atm}$ , Eq. 5.2):

*Equation 5.2*

$$pCO_{2 \text{ air}} = \frac{xCO_2(P - \varepsilon)}{1.01325 \times 10^5}$$

where the denominator converts from units of Pa to  $\mu\text{atm}$ .

This  $pCO_{2 \text{ air}}$  calculation was used to provide the partial pressure of CO<sub>2</sub> in the air for each estuary and for every hour during the 5 seasons over which  $A_T$  and  $C_T$  were sampled.  $pCO_{2 \text{ water}}$  on the other hand was calculated from one sample at each location during each season. Interpolation methods to estimate the  $pCO_{2 \text{ water}}$  data at hourly intervals across the sampling period were inappropriate given the temporal sparsity of the input data.

Wind speed was calculated from its eastward and northward components. The relationship between temperature and Schmidt number proposed by Wanninkhof (2014) was used, for which two salinities are given (0 and 35). A linear relationship between Schmidt number and salinity was assumed, following Borges et al. (2004). The gas transfer velocity ( $k$ ,  $\text{m s}^{-1}$ ) was calculated using the parameterisation of Ho et al. (2006); despite its basis on open ocean sampling data, this formulation predicts gas transfer velocity well in a range of estuarine environments (Jiang et al., 2008). The Ho et al. (2006) equation performs particularly well if floating chamber studies are not included. Floating chambers, also often referred to as floating domes, measure  $pCO_2$  directly at the water surface via an infrared gas analyser in an enclosed floating chamber (Frankignoulle, 1988). Floating chamber studies are thought to overestimate gas transfer velocities in riverine and estuarine environments, particularly at low wind speeds (Matthews et al., 2003; Raymond and Cole, 2001; Vachon et al., 2010). For estuarine purposes, deliberate gas tracer studies ( $\text{SF}_6$  and  $^3\text{He}$ ) are most commonly used (Ho et al., 2011, 2014; Raymond et al., 1997).

I calculated the water-air flux of CO<sub>2</sub> ( $\text{mol m}^{-2} \text{ day}^{-1}$ , Eq. 5.3):

$$FCO_2 = k K_0(pCO_{2\ water} - pCO_{2\ air})$$

Where  $K_0$  is the solubility of  $CO_2$  ( $\text{mol m}^{-3} \text{ atm}^{-1}$ ) (Weiss, 1974 (Equation 12)), and where positive values denote outgassing of  $CO_2$  from the water to the air.

### 5.2.5 Temporal interpolation

Care should be taken when applying  $CO_2$  flux data sparsely sampled over time to a larger seasonal context. Carbonate chemistry samples were collected on one occasion during each season, to provide an overview of the seasonal cycle. Therefore, when calculating water-to-air  $CO_2$  flux, steps should be taken to ensure that the calculated flux terms are broadly representative of the real-world conditions during that season. This is not least because an annual estimate of water-to-air  $CO_2$  flux from a given estuary – which, in a similarly temporally sparse dataset as this, can simply be calculated from assuming a single flux term applies to the entire season – will be biased by the specific conditions at the time of sampling, if only the conditions at the sampling time itself are used. Water-to-air  $CO_2$  flux increases quadratically with respect to wind speed (Wanninkhof, 1992), for example, so if the wind speed on the sampling date were atypical for that season, it could bias the annual estimate for water-to-air  $CO_2$  flux in a given estuary.

To this end, flux values were calculated at hourly intervals for each season, with seasons here defined according to Table 2.1, to match the highest-resolution variables used in the calculation: those sourced from ERA5 Reanalysis data. The same hourly resolution was used to interpolate  $xCO_2$  and calculated  $pCO_{2\ water}$  values were held constant throughout each season, because they were calculated once per season, and interpolating between five values to represent an entire annual cycle does not account for the variation within a season, which is not possible to establish from these measurements. Water temperature was also held constant during the season in the absence of mooring data at each individual sampling location. Selecting the wind speed for a given sampling occasion could have a substantial effect on the calculated water-to-air  $CO_2$  flux value (grey line, Fig. 5.3). This is particularly true if the sampling day experienced stronger than average winds for that season, because  $CO_2$  fluxes are calculated using the square of the wind speed (Ho et al., 2006; Wanninkhof, 1992). For the same reason, estimating seasonal fluxes through using the mean input variable conditions for that season is likely to underestimate  $CO_2$  fluxes. To combat this issue, water-to-air  $CO_2$  flux was estimated using all of the variables at hourly

intervals at a given site as described above (Fig. 5.3), and then calculated using the mean flux value for that season.

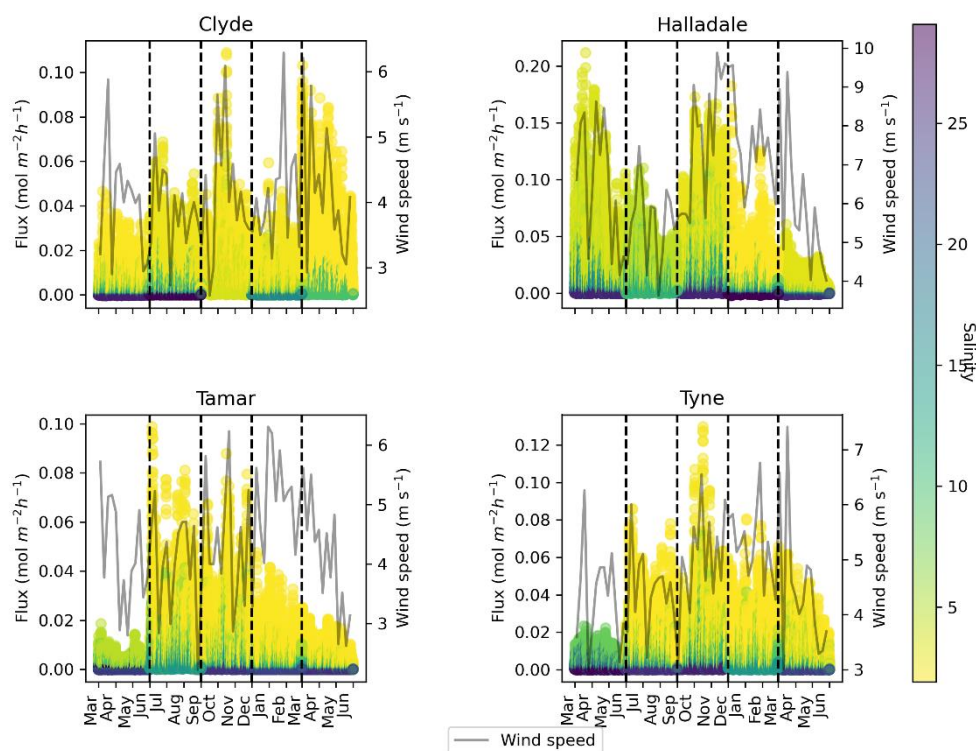


Figure 5.3 - Scatterplot of hourly estimated water-to-air CO<sub>2</sub> flux during the 2017-18 sampling period. The data are separated into the different estuaries and coloured by salinity. Weekly averaged wind speed is represented by an overlain line graph. Dashed vertical lines delineate the five seasons during the sampling period. Data are plotted using an individual scatter point per hourly estimate.

Figure 5.4 illustrates that, particularly at lower salinities, flux values calculated using the ERA5 and (atmospheric) xCO<sub>2</sub> estimates for a specific sampling time can indeed skew the seasonal flux estimate, when compared to a mean flux term calculated for the season. The range of differences between the mean flux term for that season, and all flux terms calculated using the different calculation variables at hourly resolution during the same season, are largely related to the wind speed. Almost exclusively, using input variables for the sampling conditions results in an underestimation of mean seasonal CO<sub>2</sub> flux.

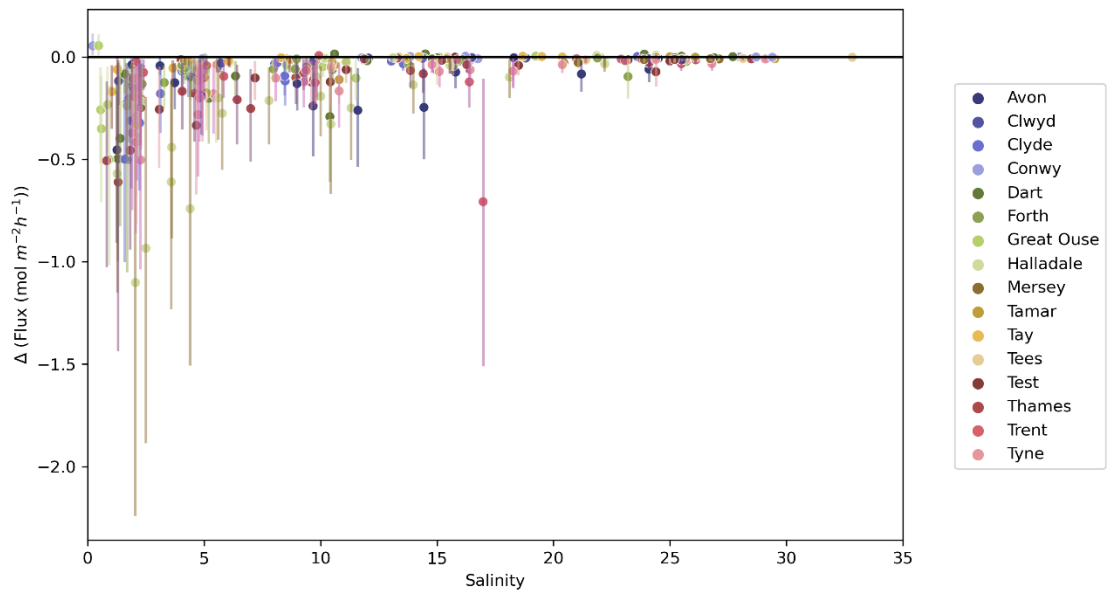


Figure 5.4 - Scatter points represent the difference between  $FCO_2$  at the time of sampling and the mean  $FCO_2$  for an estuary for that season, with a positive value indicating that  $FCO_2$  of the sampling date/time was higher than the mean for the season. Vertical bars show the range of differences one could have achieved by this method depending on which date was sampled during that season.

Calculating seasonal fluxes as a mean of the fluxes from all conditions within that season means that the sub-seasonal variability in those input variable conditions is implicitly represented in the final calculated flux value. However, additional sources of variability is not accounted for. Therefore, there is a systematic need for the identification of variables that may cause significant uncertainty in  $CO_2$  fluxes, and to calculate what the total uncertainty in those fluxes are, both in total and with respect to each identified variable.

## 5.2.7 Uncertainty analysis – CO<sub>2</sub> flux

Uncertainties in CO<sub>2</sub> flux estimates were calculated using a finite-forward-differences approach, as presented by Humphreys et al. (2022) (Eq. 5.4):

Equation 5.4

$$\frac{\delta f(v)}{\partial v} = \frac{f(v + \Delta v) - f(v)}{\Delta v}$$

where  $\Delta v$  is a user-determined change in a given variable,  $v$ , to be used to calculate CO<sub>2</sub> flux,  $f$ . The derivatives of the selected variables are combined to calculate overall uncertainty using Eq. 5.5:

Equation 5.5

$$\sigma = \sqrt{\sum_i \left(\frac{\delta r}{\delta a_i}\right)^2 \sigma^2(a_i)}$$

where  $\sigma$  is one standard deviation.

The variables ( $v$ ) selected for CO<sub>2</sub> flux uncertainty analysis were:

1. pCO<sub>2</sub>: calculated pCO<sub>2</sub> values have their own inherent uncertainty, as discussed above. For the flux calculation, pCO<sub>2</sub> is also held constant across a season, which doesn't reflect real-world variability, but more relevant here, may not reflect the mean pCO<sub>2</sub> across that season, since pCO<sub>2</sub> is affected seasonally by primary production, respiration and temperature. As a rough estimate, the pCO<sub>2</sub> uncertainty as calculated above was multiplied by six to represent  $\Delta v$ . The factor of 6 was selected because the pCO<sub>2</sub> uncertainty is provided as a standard deviation, with 3 standard deviations from the mean approximately equal to the full range of a normal distribution. 3 standard deviations was doubled as an estimation of real-world variability.
2. xCO<sub>2</sub>: Mace Head, where the xCO<sub>2</sub> measurements are taken, is some distance to the west of the sampling locations in this study (Fig. 5.1). Western Europe is subject to prevailing westerlies, as well as easterly events transporting air from mainland Europe, which occurred 35% of the time during a two year period (Biraud et al., 2000). Mace Head will be more representative during westerlies, as air is advected towards the UK sampling sites from the Atlantic. Mace Head will be less representative during the winter months as fossil fuel usage increases across Europe.  $\Delta v = 6 \mu\text{mol mol}^{-1}$  was used in line with Borges and Frankignoulle (2003)

who found  $x\text{CO}_2$  in the English Channel to be  $6 \mu\text{mol mol}^{-1}$  higher on average than at Mace Head. It is reasonable to use a single figure for all locations, since  $x\text{CO}_2$  at Mace Head was found to be comparable to distant urban measurements (Bozec et al., 2012).

3. Wind speed: while the temporal variability in wind speed is accounted for in the mean seasonal flux approach, the accuracy of using reanalysis data for a given location is not. Gualtieri (2022) provides a root mean squared error (RMSE) estimate each for 'inland' and 'coastal' areas, between observed wind speed and ERA5 wind speed data. The mean of the 'inland' and 'coastal' estimates was applied to the entire dataset:  $\Delta v = 1.56 \text{ m s}^{-1}$ . N.B. The other ERA5 variables (dewpoint temperature and pressure) are comparatively minor contributors to the flux equation, so were not included in this analysis.
4. Wind speed parameterisation: This is likely to be a major source of uncertainty. The parameterisation of gas exchange velocity from wind speed is a much-debated phenomenon in the open ocean, the focus of the majority of studies, let alone for riverine, estuarine or coastal ocean environments. Ho et al. (2011) calculated the RMSE of their earlier parameterisation also used in this study (Ho et al., 2006) against three different dual tracer experimental results, so the mean of the three RMSE estimates was calculated and used as  $\Delta v = 18.0\%$ . In this case, with  $\Delta v$  as a percentage,  $k$  is calculated using the Ho et al. (2006) parameterisation as usual, and then multiplied by 1.18 (18%).

### 5.2.8 Spatial Interpolation & overall outgassing estimate

$\text{CO}_2$  outgassing can be estimated by interpolating/extrapolating  $\text{CO}_2$  flux data over the surface area of an estuary. Flux data were interpolated using their relationship with latitude/longitude over a 2D grid covering the maximum coordinates of each estuary for each season. The intersection of each 2D grid with the corresponding estuary boundary geometry, where available, using the JNCC estuary boundary shapefile (JNCC, 2013) was summed to calculate  $\text{CO}_2$  flux over the surface area of the estuary. This value was then multiplied by the length of time in each season. The seasonal flux estimates for the two 'Spring' sampling occasions in 2017 and 2018 respectively were averaged to form a generic 'Spring' flux estimate, and the flux estimates for the four seasons of the year were summed to estimate total annual  $\text{CO}_2$  flux from each estuary. Where an estuary boundary was not included in the JNCC estuary boundary shapefile (Avon, Dart and Tees) it was not possible to calculate total estuarine flux. The JNCC estuary definition is entirely shape-derived, with the freshwater end where the river 'widens' and with the seawater end where a straight line

can be drawn at the land boundary. The seaward end is in agreement with the definition presented here, although it is not possible to determine the effect of the difference in definition at the freshwater end.

The JNCC estuary boundary shapefile (JNCC, 2013) contains estuary boundary geometries across the UK. A UK estimate for total estuarine CO<sub>2</sub> outgassing was calculated by applying the mean seasonal flux for all the sampled estuaries in this study to the total surface area of estuaries in the JNCC shapefile. It is important to note the difference in definition between UK estuary boundary location data (JNCC, 2013) and the definition chosen for this thesis (Chapter 1.3). At the seaward end, the definitions are identical, where a straight line is drawn between the banks at the estuarine mouth. At the freshwater end, however, JNCC defines an estuary as the 'Downstream part of a river where it widens to enter the sea' (JNCC, 2013), whereas for this thesis the freshwater inflow location is governed by the limit of salt intrusion (Chapter 1.3). The JNCC boundary data are essentially cartographical; in the absence of high-resolution salinity data it is not possible to determine the impact of these differences on the total surface area, and subsequently on the results presented here.

## 5.3 Results and Discussion

### 5.3.1 pCO<sub>2</sub> water

pCO<sub>2</sub> is highly variable at low salinity and converges to lower values at higher salinity (Fig. 5.5). Low salinity pCO<sub>2</sub> values range from approximately 0 – 7000 µatm at the zero-salinity end member and converge to between 400 – 1000 µatm towards seawater salinities ( $S > 30$ ). Notably, pCO<sub>2</sub> values at high salinity are higher than atmospheric pCO<sub>2</sub> at this scale, which implies that inner estuaries at high salinity remain to be a weak source to the atmosphere.

Variation in pCO<sub>2</sub> at the estuary scale at any given salinity exceeds variation between estuaries, such that estuaries appear to be indistinguishable in pCO<sub>2</sub> magnitudes. For example, at low salinities ( $S < 5$ ), while the Halladale estuary experiences the highest individual pCO<sub>2</sub> value (6875 µatm, salinity = 1.31), it also experiences relatively low pCO<sub>2</sub> values (463.7 µatm, salinity = 4.01). Furthermore, symbols indicate the different estuary groupings used in Chapter 3 (Fig. 5.5), where circles denote the estuaries only sampled on one occasion which therefore did not satisfy the conditions of any group. The groups do not behave differently in terms of pCO<sub>2</sub> variation with salinity, despite their differences in C<sub>T</sub> and A<sub>T</sub> behaviour. This implies that the drivers of C<sub>T</sub> and A<sub>T</sub> differences are not the same as the drivers of pCO<sub>2</sub> behaviour in estuaries (Fig. 5.5).

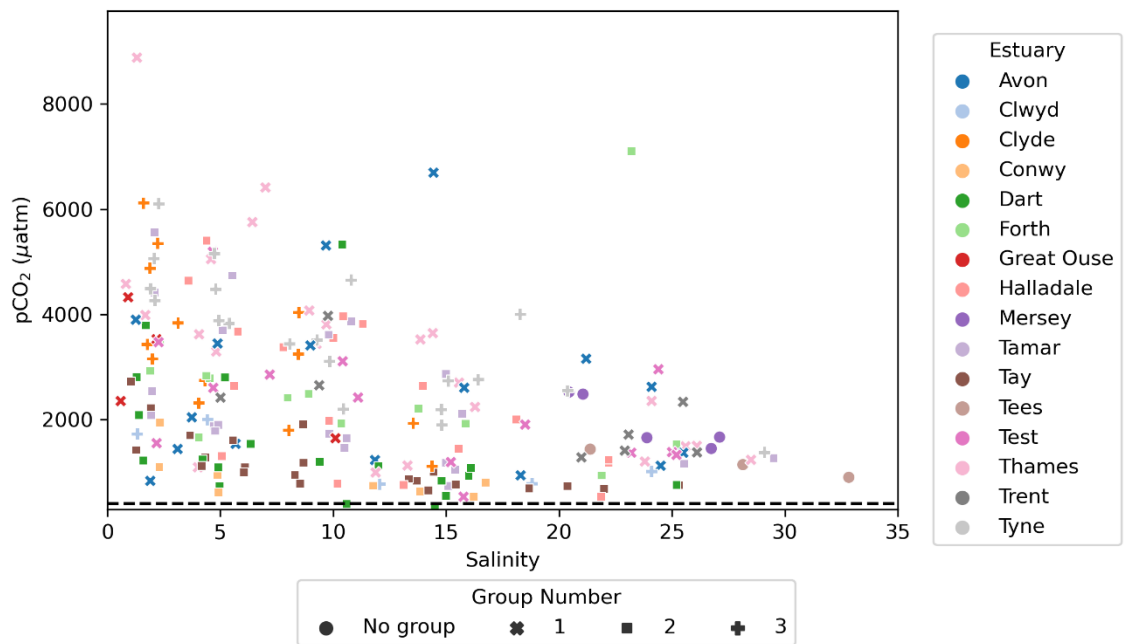


Figure 5.5 - calculated  $p\text{CO}_2$  values across the salinity gradient. Different colours represent the different estuaries, and symbols denote which 'Group' of estuaries that estuary belongs in, as described in Chapter 3. A horizontal dashed line indicates a  $p\text{CO}_2$  of  $400 \mu\text{atm}$ .

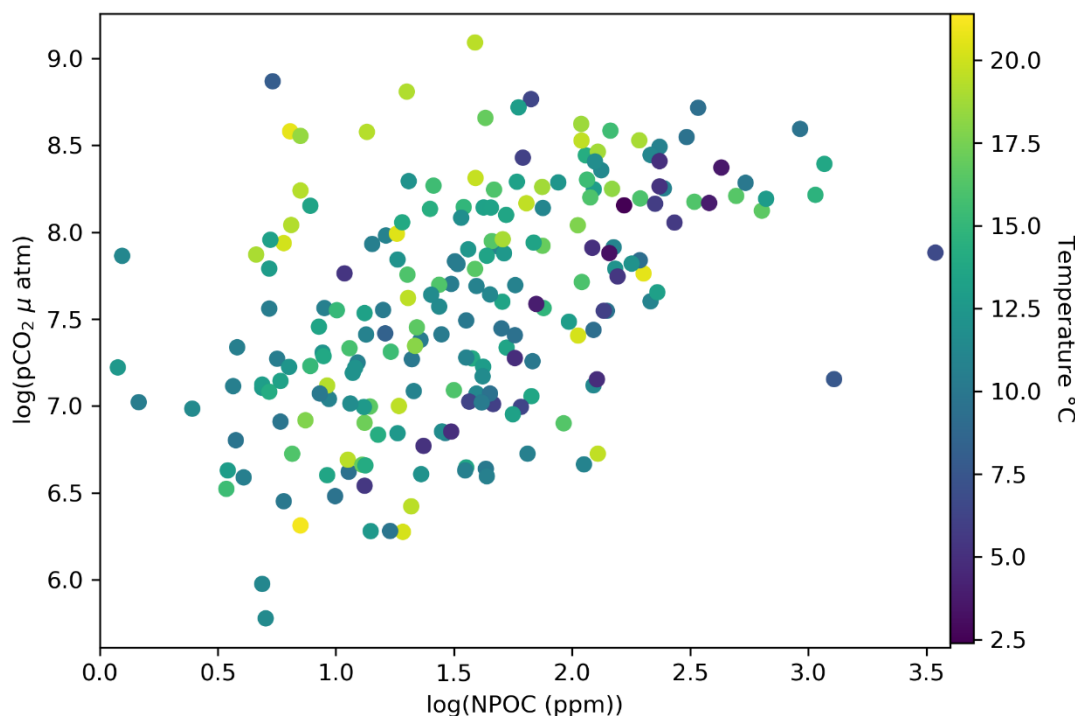
Salinity clearly has an effect on  $p\text{CO}_2$  in estuaries (Fig. 5.5): high  $p\text{CO}_2$  water enters the estuary at low salinity, and by the mouth, the water is close to atmospheric  $p\text{CO}_2$  equilibrium, whether by mixing with low- $p\text{CO}_2$  seawater or  $\text{CO}_2$  outgassing sustained by other factors.  $p\text{CO}_2$  becomes less soluble with increases in salinity (Weiss et al., 1982), which promotes  $\text{CO}_2$  outgassing along the salinity gradient and subsequently reduces  $p\text{CO}_2$ . Simultaneously, pH increases along the salinity gradient (Appendix A7) act to reduce  $\text{CO}_2(\text{aq})$  concentrations in favour of  $\text{CO}_3^{2-}$  concentrations, which acts to reduce  $p\text{CO}_2$  with increasing salinity. Linear mixed effects model results show that salinity does indeed have a significant impact on  $p\text{CO}_2$ , with increasing salinity acting to reduce  $p\text{CO}_2$ , as Figure 5.6 also suggests (Table 5.2). The estimated effect size of salinity on  $\log(p\text{CO}_2)$  is interpreted as the effect on  $\log(p\text{CO}_2)$  of a unit increase in salinity if all other variables in the model are held constant. In practice, this is a first-order estimate of the importance of conservative mixing of high- $p\text{CO}_2$  freshwater and low- $p\text{CO}_2$  seawater to  $p\text{CO}_2$  changes.

Table 5.2 – model results from linear mixed effects model predicting  $\log(p\text{CO}_2)$ . Data are emboldened where  $p$ -values are significant at the 0.05 level.

Predictors	Estimates	95% Confidence intervals	p values
(Intercept)	8.48	6.22 – 10.75	<0.001
Salinity	-0.03	-0.04 – -0.02	<0.001
Water temperature (°C)	0.12	0.06 – 0.18	<0.001
DIN ( $\mu\text{mol l}^{-1}$ )	0	-0.00 – 0.00	0.912
$\log(\text{SRP } (\mu\text{mol kg}^{-1}))$	0.1	-0.09 – 0.30	0.297
NPOC (ppm)	0.03	0.01 – 0.05	0.004
River discharge ( $\text{m}^3 \text{s}^{-1}$ )	0	-0.00 – 0.00	0.222
$\log(\text{temperature}) * \log(\text{DIN})$	-0.05	-0.10 – -0.00	0.043
$\log(\text{temperature}) * \log(\text{SRP})$	0.03	-0.02 – 0.08	0.186
$\log(\text{river discharge}) * \log(\text{DIN})$	0.02	-0.02 – 0.05	0.331
$\log(\text{river discharge}) * \log(\text{SRP})$	0	-0.01 – 0.01	0.754
Number of observations	270		
Marginal $R^2$ / Conditional $R^2$	0.374 / 0.550		

Two other main effects are significant. Firstly, the predictor variable with the largest effect is water temperature. It is important to note that temperature was included in the model, while season was excluded because of high multicollinearity, so temperature to some extent provides a proxy for seasonality. A unit increase in temperature causes an increase in  $\log(p\text{CO}_2)$  of 0.12 (Table 5.2, Fig. 5.6).  $\text{CO}_2$  is less soluble in warmer water, so at a higher temperature the pressure of that  $\text{CO}_2$  ( $p\text{CO}_2$ ) within surface waters is greater, making conditions more favourable for degassing. This is consistent with Wang and Cai (2004) who found strong seasonal gradients in  $p\text{CO}_2$  that correlated with temperature changes in one estuary, whereas Reum et al. (2014) found the temperature- $p\text{CO}_2$  relationship to differ from

season to season, with  $p\text{CO}_2$  increasing with temperature only during the February sampling occasion. These examples show that there is variability in the temperature- $p\text{CO}_2$  relation between estuaries, with both studies sampling a single estuary (though the latter study from two inlets). The present study, using samples from a range of different estuaries, may better represent the variability in different temperature- $p\text{CO}_2$  relationships between estuaries. The effect of temperature on  $p\text{CO}_2$  suggests that in future, estuaries will be greater sources of  $\text{CO}_2$  to the atmosphere, since  $p\text{CO}_2$  is directly related to outgassing fluxes.



*Figure 5.6 - relationship between  $\log(\text{NPOC})$  concentration and  $\log(p\text{CO}_2)$  concentration. Scatter points are coloured by water temperature. NPOC is on a log scale here, but not in the model to aid visualisation only: one particularly high NPOC value obscures the relationship when plotted.*

Secondly, NPOC also had a significant impact on changes in  $\log(p\text{CO}_2)$  in the sampled estuaries (Table 5.2, Fig. 5.6), such that for a unit increase in NPOC, there is an increase in  $\log(p\text{CO}_2)$  of 0.03. Higher  $p\text{CO}_2$  and NPOC concentrations generally coincide with lower salinity (Fig. 5.6), which suggests that to some extent, greater than atmospheric  $p\text{CO}_2$  values and subsequent outgassing fluxes are driven by high riverine organic matter inputs. This supports previous findings that high  $p\text{CO}_2$  values and  $\text{CO}_2$  outgassing fluxes are explained by decomposition of organic carbon from allochthonous sources during estuarine transit, although the source itself, whether riverine or land-derived, varies between estuaries (Abril and Borges, 2004; Cai, 2011; Cai and Wang, 1998; Frankignoulle et al., 1998;

Raymond and Bauer, 2001; Salisbury et al., 2008; Wang and Cai, 2004). It is also possible that the effect of NPOC on  $p\text{CO}_2$  is influenced by organic alkalinity. Elevated  $p\text{CO}_2$  is associated with a decrease in  $A_T$  for a given  $C_T$ , salinity, temperature and pressure. Therefore, negative organic alkalinity could contribute to this phenomenon, but in the absence of organic alkalinity measurements this is not possible to establish.

Dissolved inorganic nutrient fluxes were hypothesised to contribute to  $p\text{CO}_2$ , as riverine-sourced nutrient enrichment enhances productivity, given sufficient light availability, which in turn reduces  $p\text{CO}_2$  because primary production utilises  $\text{CO}_2$ . This feedback is inherently seasonal, and so DIN and SRP were included in the model with interactions with temperature (Cloern, 1996; Pomeroy et al., 2000) and river discharge (Addey et al., 2021). Interestingly, nutrient concentrations alone did not significantly affect  $p\text{CO}_2$  (Table 5.2). However, one of the nutrient interactions was significant. The interaction between DIN and temperature is significant (Table 5.2). In practice, this means that elevated DIN concentrations alone do not alter  $p\text{CO}_2$  concentrations, but when elevated DIN concentrations coincide with elevated temperatures, for example seasonally,  $p\text{CO}_2$  decreases.

That  $p\text{CO}_2$  is unrelated to SRP, including via seasonal interactions, is unsurprising, and confirms previous findings that estuarine primary production is regulated more by DIN than SRP, whereas freshwater primary productivity is limited by SRP inputs (Paerl, 2009; Statham, 2012). The significance of the interaction between temperature and DIN concentrations suggests that primary production is taking place seasonally within inner estuaries. This is consistent with Salisbury et al. (2008) who found extremely low estuarine  $p\text{CO}_2$  values associated with high chlorophyll-a and DIN concentrations, inferring that DIN-driven primary production reduces  $p\text{CO}_2$ , and with Addey et al. (2021) who found  $p\text{CO}_2$  undersaturation where riverine nutrient provision and light availability promoted higher chlorophyll-a concentrations. Other previous studies have highlighted the reduction in  $p\text{CO}_2$  due to seasonal primary productivity as a phenomenon in estuarine plumes and coastal waters, limited by nutrient concentrations and light availability (e.g. Addey et al., 2021; Cloern, 1996), which is in turn related to suspended particulate matter, particularly in our, inner estuarine case.

Finally, discharge did not have a significant influence on  $p\text{CO}_2$ , as a standalone variable or in combination with nutrient concentrations (Table 5.2). Previous riverine work suggests that discharge is an important factor on a stream-by-stream basis (Liu and Raymond, 2018), so the contradiction here may be an artefact of the general approach used in this study, given that there are not sufficient data to fit varying slopes based on discharge relationships in individual estuaries. Discharge also did not significantly interact with nutrient concentrations.

The conditional  $R^2$  of 0.550 means that 55% of the variation in  $\log(p\text{CO}_2)$  is explained by the fixed and random effects in the model. 45% therefore remains to be explained.

### 5.3.2 CO<sub>2</sub> flux

Water-to-air CO<sub>2</sub> flux is generally highest in freshwater and decreases as salinity increases (Fig. 5.7). At approximately zero salinity, water-air flux is almost exclusively positive, though with variable magnitude. As with pCO<sub>2</sub>, the estuary a sample is taken from does not appear to dictate the magnitude of CO<sub>2</sub> flux. Indeed, CO<sub>2</sub> flux variation with salinity is similar to pCO<sub>2</sub> (Fig. 5.7 vs Fig. 5.5), as would be expected since pCO<sub>2</sub> is used to calculate flux. Differences between the two are due to seasonal deviations from mean annual wind speed.

The pattern of generally higher flux estimates decreasing towards zero flux at the seawater endmember is consistent with previous observations that riverine CO<sub>2</sub> fluxes are generally positive, and coastal waters usually take up CO<sub>2</sub> (Cai, 2011; Chen et al., 2012; Laruelle et al., 2010); given that our observations remain solely within the inner estuary and our flux estimates decrease towards 0 at high salinity, it is highly plausible that the estuarine plumes of the estuaries here studied are net sinks of CO<sub>2</sub>. However, whilst CO<sub>2</sub> flux generally decreases along the salinity gradient of estuaries, it tends towards near-zero, but positive, flux values (Fig. 5.7. Insert). This suggests that the transition from CO<sub>2</sub> source to sink is more likely to occur in the estuarine plume rather than within the estuary, here defined as the salinity gradient prior to the estuary mouth.

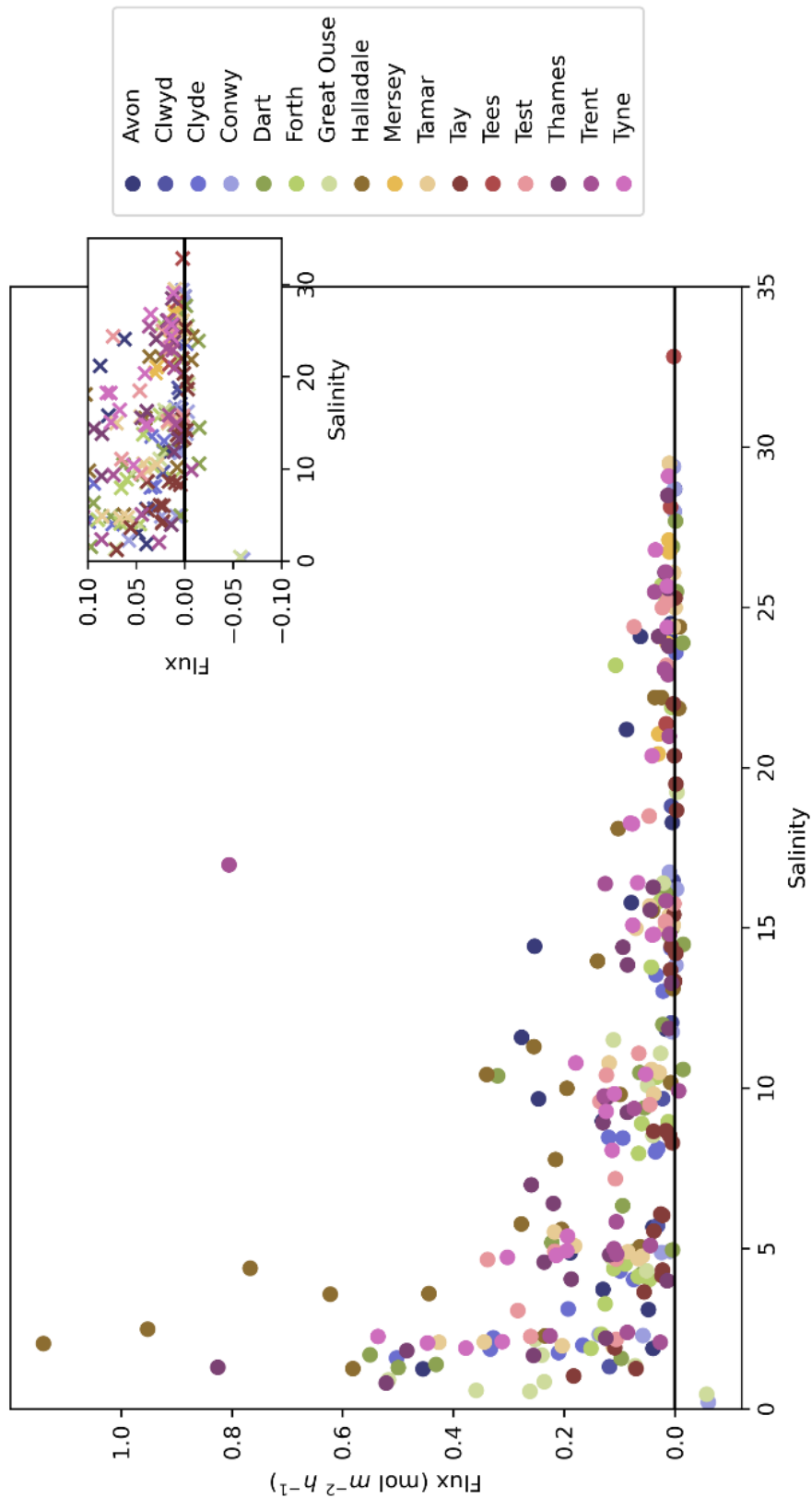


Figure 5.7 - Water-to-air CO<sub>2</sub> flux across the salinity range in each estuary sampled in the 2017-18 sampling campaign. Each scatter point reflects the mean calculated CO<sub>2</sub> flux across the season using the available input variables. Insert: a zoom window to near-zero fluxes across the salinity range showing that most small fluxes are positive. Positive values indicate net flux from water to air.

Table 5.3 – mean water-to-air CO<sub>2</sub> flux terms (mol m<sup>-2</sup> day<sup>-1</sup>) averaged across 3 major salinity brackets. Blank cells indicate that no data was collected in that salinity bracket. Numbers in brackets indicate the number of FCO<sub>2</sub> measurements within each bracket, and hence how many datapoints were used to calculate each mean. Estuaries are ordered by highest mean flux in the low salinity bracket, with the exception of the Mersey and Tees which did not have low salinity samples collected.

Estuary	0 ≤ S < 10	10 ≤ S < 20	20 ≤ S < 30
Halladale	0.47 (n=12)	0.14 (n=8)	0.011 (n=4)
Tyne	0.27 (n=11)	0.076 (n=8)	0.023 (n=5)
Thames	0.26 (n=14)	0.046 (n=6)	0.017 (n=5)
Dart	0.21 (n=10)	0.047 (n=9)	-0.0020 (n=5)
Great Ouse	0.19 (n=11)	0.040 (n=5)	
Clyde	0.18 (n=12)	0.021 (n=3)	0.0021 (n=2)
Test	0.18 (n=9)	0.051 (n=5)	0.031 (n=4)
Tamar	0.17 (n=11)	0.042 (n=8)	0.0049 (n=5)
Avon	0.16 (n=8)	0.13 (n=5)	0.043 (n=4)
Trent	0.090 (n=10)	0.24 (n=4)	0.022 (n=5)
Forth	0.086 (n=10)	0.034 (n=3)	0.038 (n=4)
Clwyd	0.068 (n=4)	0.0051 (n=3)	0.0049 (n=4)
Tay	0.047 (n=13)	0.0013 (n=7)	0.00089 (n=3)
Conwy	0.033 (n=5)	0.0023 (n=4)	0.0013 (n=3)
Mersey			0.019 (n=5)
Tees			0.012 (n=2)

Water-to-air CO<sub>2</sub> flux is highly variable in some estuaries, and less variable in others. For example, the Halladale, Tyne and Thames estuaries experience the largest ranges of water-to-air CO<sub>2</sub> fluxes, and indeed the highest-magnitude individual seasonal flux estimates at low salinity (Fig. 5.7, Table 5.3), but are very different estuarine environments. The balance between seasonal variations in wind speed and pCO<sub>2</sub>, rather than catchment features is likely the driving factor between differences in flux between different estuaries and seasons. Given that the places which experience similar variability in fluxes are geographically, geologically and industrially distinct, as are the places that experience different variability in fluxes (e.g. Halladale, G. Ouse, Thames vs Tay and Conwy), wind speed is unlikely to be the major differentiator here, particularly since the effect of individual high wind events on flux values is reduced because of the mean seasonal flux treatment. Rather, pCO<sub>2</sub> differences are the key drivers of water-air CO<sub>2</sub> flux differences between estuaries, so temperature and riverine organic matter inputs also influence CO<sub>2</sub> flux.

In general, water-air CO<sub>2</sub> fluxes calculated using only the data for the sampling date and time are similar to, or slightly higher than, those calculated as seasonal averages, across the different estuaries and seasons measured (Fig. 5.8), which suggests that for the most part, the impact of using seasonal flux estimates rather than only using the sampling date does not have a large effect in this case. The exception here is in the Tamar estuary in Summer 2017, where low salinity fluxes were approximately 0.5 mol m<sup>2</sup> day<sup>-1</sup> higher on the sampling occasion than the mean seasonal estimate, which suggests that elevated wind speeds on the sampling occasion resulted in higher outgassing fluxes. It is important to note, however, that these observed small differences between the sampling occasion and the seasonal mean in most cases, and larger differences in the Tamar in Summer 2017, are simply dependent on the sampling day. There are large variations in the flux estimate for individual dates/times during each season (Fig. 5.8, vertical bars), and it is by chance that the conditions present on the sampling date were not more, or less, extreme, relative to the seasonal estimate. Therefore, using the seasonal estimate is more appropriate, because it is more robust to the substantial changes in CO<sub>2</sub> flux values that can be calculated by using wind speed data from across the season.

Looking at water-to-air CO<sub>2</sub> flux in this context – the mean seasonal flux estimate for each sampling point – suggests that differences between estuaries are not related to the estuarine characteristics, notwithstanding the difficulty in disentangling the signal of a particular estuary (Fig. 5.7). If this is the case, that there is no tangible difference between estuaries, extrapolating to an estimate for the UK is easier, because one can assume the entire dataset provides insight into a hypothetical, generic estuary. The same can also be said of seasons, since the uncertainty in estimated fluxes is sufficiently large that there are no significant differences between seasons (Fig. 5.8).

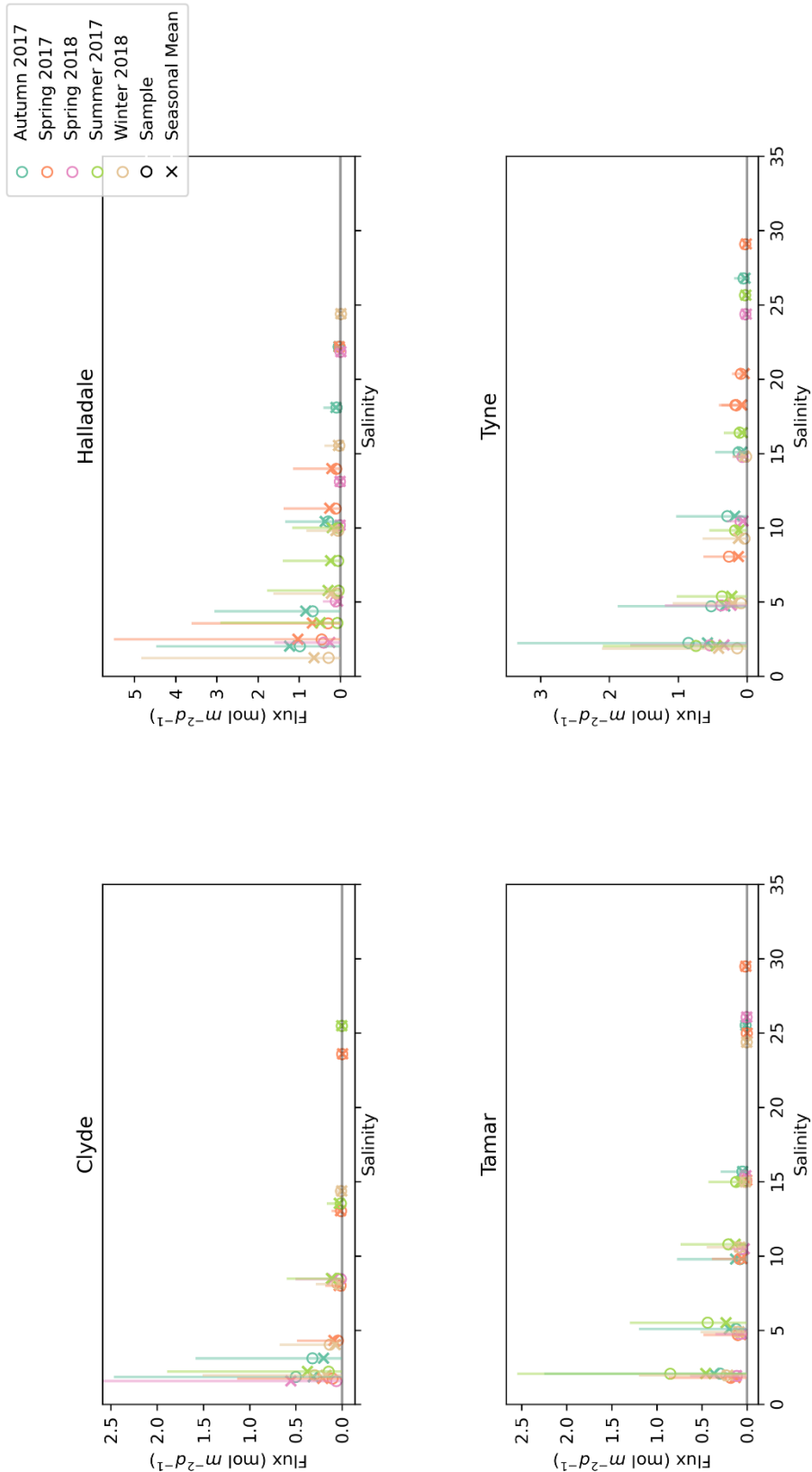


Figure 5.8 – Water-air  $\text{CO}_2$  flux data by salinity for four example estuaries (Clyde, Halladale, Tamar, Tyne), coloured by season. Vertical bars indicate the range in flux estimates across a season. These example estuaries were chosen due to their relatively large sample sizes, with all seasons represented in these estuaries. Open circles indicate fluxes calculated using data from the sampling date only, whereas crosses indicate seasonal flux estimates.

The large uncertainties around seasonal flux estimates are due primarily to uncertainties in  $p\text{CO}_2$  and gas transfer parameterisation, with the former accounting in general for a higher proportion of the uncertainty (Fig. 5.9). Wind speed and  $x\text{CO}_2$  by contrast have very little influence on  $\text{CO}_2$  flux uncertainty.

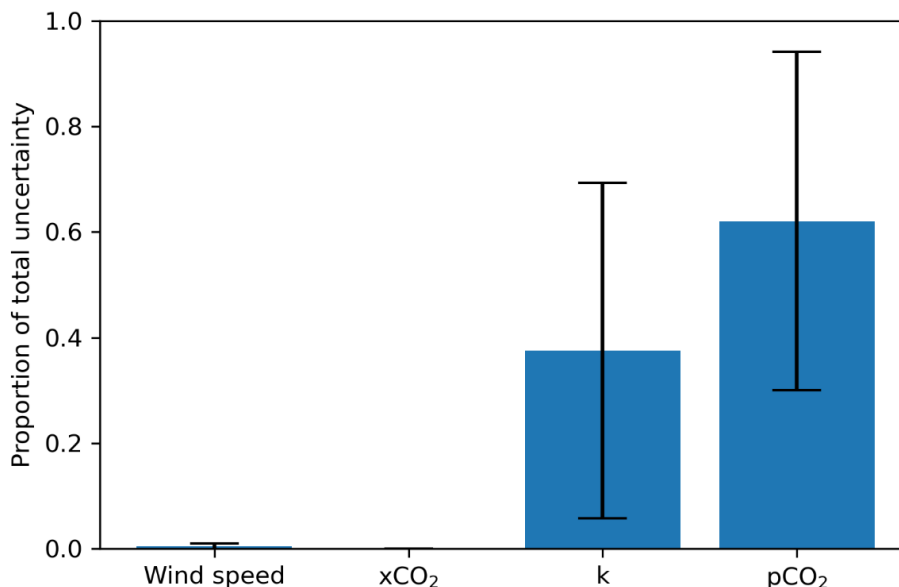


Figure 5.9 - Constituents of uncertainty in  $\text{CO}_2$  flux estimates and their significance as a proportion of overall uncertainty. Error bars indicate the standard deviation, since each individual seasonal mean flux estimate had a different uncertainty associated with it.

The general consensus in recent research into estuarine gas transfer parameterisation is that it is very difficult to achieve a parameterisation that can accurately apply across different estuarine environments (e.g. Borges et al., 2004; Orton et al., 2010; Raymond and Cole, 2001; Zappa et al., 2003). Estimates of water-air  $\text{CO}_2$  flux in similar future work would therefore be easiest to, and most substantially, improved by increasing the temporal coverage of  $p\text{CO}_2$  measurements (either direct or indirect, via  $C_T$  and  $A_T$  as was used here), as well as systematically taking replicate measurements.  $p\text{CO}_2$  uncertainty is both the easier of the two major contributors to decrease, but also on average the larger problem for this study, so this should be a focus of future work.

Interestingly, studies in different temperate regions around the world have yielded comparable results to both  $p\text{CO}_2$  and  $\text{CO}_2$  flux values calculated here (summarised in Abril and Borges, 2005 - Table 7.1, excluding the Mandovi-Zuavi River which is not temperate).  $p\text{CO}_2$  values of the UK-wide dataset presented here are comparable to the full range of other studies, regardless of location, though the full complement of these previous studies

is needed to represent the full range of pCO<sub>2</sub> values found here. Similarly, the full range of CO<sub>2</sub> flux values from previous studies is required to represent the variability in this study, though in general the fluxes in the estuaries in this study are higher overall than previous studies.

An overarching aim of this chapter is to estimate annual estuarine CO<sub>2</sub> flux. An example of the spatial interpolation to generate a total annual estimate is shown in Figure 5.10 (all other interpolations are found in Appendix A2). Multiplying the flux by the surface area that experiences that flux gives a total estimate of estuarine CO<sub>2</sub> flux for that estuary/season. Figure 5.10 indicates that the low salinity high flux water only occupies a very small percentage of the total estuarine surface area, which is advantageous from an uncertainty perspective, because the highest uncertainties in CO<sub>2</sub> flux estimates are around the highest flux magnitudes (Fig. 5.8). Fig. 5.10 (and Appendix A2) suggests that this higher-uncertainty, high flux area occupies a much smaller surface area than the better-constrained low fluxes found at low salinities.

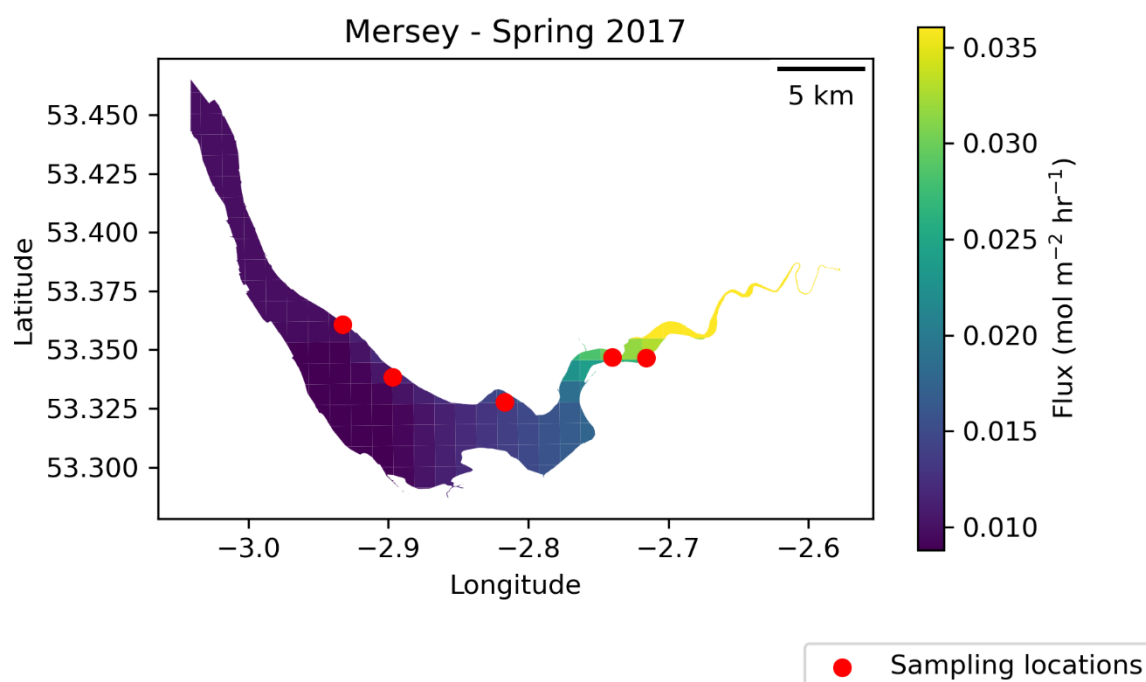


Figure 5.10 - Example water-to-air CO<sub>2</sub> flux interpolation for the Mersey Estuary, Spring 2017

All of the interpolated flux data were combined, as described in the methods section of this chapter, to create a UK-wide estimate of the estuarine CO<sub>2</sub> emission totalling  $8.5 \times 10^{10}$  g C d<sup>-1</sup>. The only comparable recent estimate to my knowledge is that of Frankignoulle et al. (1998) who calculated the European estuarine outgassing term to be between  $3 \times 10^{13}$  and  $6 \times 10^{13}$  g C d<sup>-1</sup>, based on a total estuarine surface area estimate (including inner estuaries

and estuarine plumes) of 111,200 km<sup>2</sup>. According to the JNCC estuary definition, identical to that used in this study, whereby an estuary 'ends' at its mouth, the UK accounts for approximately ¼ of the European estuarine surface area. In the context of my estimate, this would suggest a European inner estuarine outgassing term of approximately 3.3 x 10<sup>11</sup> g C d<sup>-1</sup>, with an approximate inner estuarine surface area of 12,593 km<sup>2</sup> (JNCC, 2018). To estimate the European inner estuarine surface area they use a European total (inner and outer) estuarine surface area estimate (Woodwell et al., 1973) of which they crudely approximate that inner estuaries cover 25 – 50% (Frankignoulle et al., 1998).

Using this larger European inner estuarine surface area estimate of 27,800 – 55,600 km<sup>2</sup>, my estimate would be revised to approximately 7.3 x 10<sup>11</sup> – 1.5 x 10<sup>12</sup> g C d<sup>-1</sup>. It is not possible to calculate a comparable inner estuary-only estimate for the literature study (Frankignoulle et al., 1998) because the precise calculation they use is not distinguishable from the paper. Their total (inner and outer) estuarine estimate, however, is over an order of magnitude higher than this iteration of my European estimate. Indeed, their outer estuarine CO<sub>2</sub> flux estimate is small, but positive (0.01 mol m<sup>-2</sup> d<sup>-1</sup>, Frankignoulle et al., 1998), and they find outer estuarine CO<sub>2</sub> fluxes to be almost exclusively positive, indicating year-round outgassing to the atmosphere. This outer estuarine outgassing flux would not be large enough to make up the difference between the estimate presented by Frankignoulle et al. (1998) and that presented here.

Two possible explanations exist for the difference between the estimates. Firstly, that the differences in methodology caused an overestimation in one case, or an underestimation in another. This is unlikely to be the cause of this difference, because Frankignoulle et al. (1998) use direct floating chamber measurements, which are broadly thought to underestimate CO<sub>2</sub> flux because they disrupt the turbulence at the aqueous boundary layer (Ho et al., 2011; Raymond and Cole, 2001; Vachon et al., 2010), and they made measurements at low wind speeds. Their inner estuarine pCO<sub>2</sub> values also cover a similar range to those presented here.

The second, more likely explanation, is that outgassing fluxes have changed in the 20 years between the measurements. This would require time series data to establish with certainty, but much has changed in the last 20 years. The atmospheric CO<sub>2</sub> mole fraction has increased, which itself impacts CO<sub>2</sub> flux. CO<sub>2</sub> efflux is driven by the partial pressure difference of CO<sub>2</sub> in the surface water and the overlying air. With increasing atmospheric CO<sub>2</sub> mole fraction over time, if high aqueous CO<sub>2</sub> partial pressures are held constant, outgassing fluxes reduce because the difference in air and water pCO<sub>2</sub> becomes smaller. In reality, organic carbon inputs that sustain high pCO<sub>2</sub> in estuarine waters are also increasing due to anthropogenic pressures (Regnier et al., 2022), but the net decrease in

outgassing fluxes implies that this may be at a slower rate relative to the anthropogenic increase in atmospheric CO<sub>2</sub>.

#### 5.4 Conclusions

C<sub>T</sub> and A<sub>T</sub> measurements for a diverse range of estuaries around the UK were used to calculate pCO<sub>2</sub> and CO<sub>2</sub> flux. The factors that affect C<sub>T</sub> and A<sub>T</sub> concentrations (Chapter 3) do not have a significant effect on pCO<sub>2</sub>, and subsequently CO<sub>2</sub> flux. Rather, pCO<sub>2</sub> variation is partly explained by salinity, with pCO<sub>2</sub> decreasing from river to sea, as well as by temperature, organic carbon and by seasonal nutrient cycling, although 45% of the variation in pCO<sub>2</sub> is yet to be explained by the available variables. This supports the findings of previous studies, which suggest that net heterotrophy and seasonal bursts of primary production have a strong influence on estuarine pCO<sub>2</sub>. Additionally, the effect of temperature on pCO<sub>2</sub> in its own right suggests that temperature increases with climate change may drive an increase in estuarine pCO<sub>2</sub>, and hence outgassing. Outgassing also generally decreases from river to sea, although estimates are subject to large errors, particularly at low salinity. Though rivers are sources of CO<sub>2</sub>, and coastal oceans are generally sinks of CO<sub>2</sub> to the atmosphere, inner estuarine data presented here suggests that the switch between source and sink occurs beyond the estuarine mouth. A UK-wide estuarine emission estimate of  $8.5 \times 10^{10}$  g C d<sup>-1</sup> was reached – the first of its kind to the author's knowledge.

## **Chapter 6**

### **Synthesis and Future Work**

## 6.1 Thesis overview

The aims of this thesis, as laid out in Section 1.4, were to address the following outstanding questions about riverine and estuarine carbonate chemistry in the context of land ocean aquatic continuum (LOAC) carbon cycling:

### 6.1.1 What factors define the carbonate chemistry of rivers and estuaries, and what are their relative importance?

The relatively small surface areas of rivers and estuaries have meant that until relatively recently, they were considered to be minor components of the global carbon cycle. Over the last 25 years, a range of observational studies have measured the carbonate chemistry dynamics in rivers (Barnes and Raymond, 2009; Cai et al., 2008, 2021; Cai and Wang, 1998; Drake et al., 2018b; Hill and Neal, 1997; Jarvie et al., 1997, 2017; Piñol and Avila, 1992; Raymond and Cole, 2003; Tye et al., 2022b) and estuaries (Abril et al., 2003, 2004; Cai, 2003; Cai et al., 2004; Ghosh et al., 2021; Howland et al., 2000; McGrath et al., 2019; Oliveira et al., 2017), finding that these aquatic environments are important sites for organic carbon processing and CO<sub>2</sub> evasion.

Riverine and estuarine C<sub>T</sub> and A<sub>T</sub> concentrations have been related to a range of factors including chemical bedrock weathering (e.g. Cai et al., 2008; McGrath et al., 2019; Raymond and Cole, 2003), differences in river discharge resulting from precipitation variability (e.g. Cai et al., 2008; Drake et al., 2018b; Raymond and Cole, 2003), land use (e.g. Barnes and Raymond, 2009), but some studies have produced conflicting results. For example, Hill and Neal (1997) found geology and land use to have no effect on riverine carbonate chemistry in contrast to other studies (Cai et al., 2008; McGrath et al., 2019). Abril et al. (2004) found changes in C<sub>T</sub> and A<sub>T</sub> concentrations to be driven by sediment resuspension in the Loire estuary whereas in other studies mixing appears to dominate estuarine carbonate chemistry (Cai et al., 2004; McGrath et al., 2019; Oliveira et al., 2017). Contrasting findings between studies as to the key factors influencing riverine and estuarine carbonate chemistry dynamics are due in part to the limitations of studying a small number of catchments, generally biased towards large and easily accessible catchments. This may not adequately represent LOAC carbonate processing in general, as the contribution of small rivers and estuaries to the global inorganic carbon cycle is potentially important but highly uncertain (Cai and Wang, 1998).

This thesis presents a comprehensive analysis of estuarine carbonate chemistry in 16 estuaries spanning the breadth of the UK, specifically selected as representative of the land

use composition of the UK (Chapter 3). This range of estuaries, which only includes two catchments that have been sampled in previous carbonate chemistry studies (Thames (Borges et al., 2004; Frankignoulle et al., 1998) and Trent (Jarvie et al., 1997)) is variable in size, discharge and geology, thus encompassing a broad range of factors which may alter their carbonate chemistry. This provides the first opportunity of its kind to determine the relative importance of key factors (e.g. chemical weathering, temperature, river discharge, primary production / organic matter remineralisation balance) in determining carbonate chemistry along the course of an estuary. Measurements of  $C_T$  and  $A_T$  concentrations across the salinity gradient are used to explore the differences in carbonate chemistry between and within estuaries as a function of a number of different factors, primarily using freely available secondary geological and hydrological datasets.

Carbonate dissolution contributes to high  $C_T$  and  $A_T$  concentrations (Eq. 3.1). Recent LOAC carbonate chemistry studies found that differences in  $C_T$  and  $A_T$  in low salinity estuarine waters between two limestone-containing catchments and two non-limestone bedded catchments related to this lithological difference (McGrath et al., 2016, 2019). Bedrock weathering contributes directly to freshwater  $C_T$  and  $A_T$  concentrations, due to their proximity to the weathering source. Substantial differences in bedrock composition are thought to influence carbonate chemistry even through estuarine environments and into the coastal ocean (McGrath et al., 2016, 2019). No study to date has directly quantified different bedrock contributions to  $C_T$  and  $A_T$  delivery into freshwaters.

I identified four catchments with different catchment bedrock compositions, and with differing estuarine  $C_T$  and  $A_T$  signatures along the salinity gradient (Chapter 3). The Great Ouse catchment is dominated by carbonate bedrock (76% chalk bedrock, 10% limestone bedrock). The Tyne catchment is almost entirely formed from carbonate bedrock (95% limestone). The Clyde catchment contains 19% limestone, and the Forth catchment contains a negligible proportion of carbonate bedrock (1% limestone). Measurements of their riverine carbonate chemistry, solute concentrations and strontium isotopic composition were made (Chapter 4). Three end member mixing models were formulated following the method proposed by Magnone et al. (2019) for groundwaters, here in a riverine context, to estimate the quantitative contribution of each bedrock type to river flow (Chapter 4). These results were compared with secondary geological data used in Chapter 3 to comment on the application of these dataset types as predictor variables in riverine and estuarine carbonate chemistry studies.

### 6.1.2 How much CO<sub>2</sub> is emitted from estuaries into the atmosphere, and what drives that emission?

Rivers and inner estuaries experience large CO<sub>2</sub> outgassing flux densities, which means that despite their small surface areas relative to other constituent elements of the carbon cycle, they remain important sources of CO<sub>2</sub> to the atmosphere. A number of observational studies have measured CO<sub>2</sub> fluxes from rivers (Alin et al., 2011; Attermeyer et al., 2021; Hagedorn and Cartwright, 2010; Lauerwald et al., 2015; Liu and Raymond, 2018; Raymond et al., 2013) and estuaries (Borges et al., 2004; Bozec et al., 2012; Cai and Wang, 1998; Chen et al., 2012; Frankignoulle et al., 1998; Ho et al., 2014; Jeffrey et al., 2018; Laruelle et al., 2017; Maher and Eyre, 2012; Oliveira et al., 2017; Raymond et al., 2000; Wang and Cai, 2004; Yao and Hu, 2017). Again, the logistical challenges of sampling a variety of estuaries have resulted in the majority of study areas covering temperate large watersheds. The major rivers of the northern hemisphere are therefore well-studied, but scaling approaches use these data to represent a variety of riverine and estuarine environments, ranging in physical and biogeochemical contexts. Perhaps this is an appropriate approach, but without confirmation from studying a range of systems, it is not possible to have confidence in this approach.

Here, CO<sub>2</sub> fluxes (FCO<sub>2</sub>) are calculated from 16 estuaries across the UK which in itself acts as a step forward in data coverage of estuaries of a range of sizes (Chapter 5). C<sub>T</sub> and A<sub>T</sub> measurements, as presented in Chapter 3, are used to calculate pCO<sub>2</sub>, which in turn is used to calculate FCO<sub>2</sub>. Changes in pCO<sub>2</sub> are explored in relation to a range of predictor variables, including those that were important in determining C<sub>T</sub> and A<sub>T</sub> concentrations (Chapter 3) and with particular emphasis on indicators of organic matter decomposition (e.g. non-purgeable organic carbon, temperature, inorganic nutrients), since the breakdown of organic matter is thought to sustain outgassing fluxes in estuaries.

FCO<sub>2</sub> data are spatially interpolated over the surface area of the estuaries where both FCO<sub>2</sub> data are calculated and estuary boundary shapefile data are available, to determine the total flux of CO<sub>2</sub> outgassed from each estuary seasonally (Chapter 5). The mean annual outgassing flux for all estuaries is also applied to the surface area of all UK estuaries where estuary boundary data are available to estimate the total estuarine CO<sub>2</sub> emission for the UK (Chapter 5).

## 6.2 Key findings

### 6.2.1 Chapter 3: Drivers of dissolved inorganic carbon and alkalinity in the inner estuaries of the UK.

Chapter 3 aimed to answer two key research questions. Here, the findings of the chapter are used to answer each question:

*How do  $C_T$  and  $A_T$  vary from river to sea, and why?*

The main driver of  $C_T$  and  $A_T$  dynamics along the salinity gradient of the UK estuaries studied here is conservative mixing. Changes in  $C_T$  and  $A_T$  concentrations along the salinity gradient in all of the sampled estuaries are strongly linear, so the  $C_T$  and  $A_T$  concentration at any given salinity is largely a function of direct mixing of the freshwater and seawater end members. When the effects of mixing are removed, by looking at deviations from the mixing line, it is clear that a combination of primary production / organic matter remineralisation and  $\text{CaCO}_3$  precipitation / dissolution also affect in-estuary  $C_T$  and  $A_T$  conditions, though to a much lesser extent. Outgassing fluxes of  $\text{CO}_2$ , as presented in Chapter 5 of this thesis, which would be visible as a decrease in  $C_T$  concentration without an accompanying change in  $A_T$  concentration, are not big enough to be seen in this data.

*How different are freshwater end member  $C_T$  and  $A_T$  concentrations in a range of estuaries, why do those differences exist, and how do these differences affect  $C_T$  and  $A_T$  concentrations downstream?*

UK estuarine dissolved inorganic carbon and total alkalinity concentrations are driven by their freshwater end member, which can vary from approximately  $0 \mu\text{mol kg}^{-1}$  to approximately  $5000 \mu\text{mol kg}^{-1}$ . These differences in mean freshwater  $C_T$  and  $A_T$  concentrations between estuaries are caused by differences in catchment lithology. Estuaries which drain catchments containing chalk bedrock have freshwater  $C_T$  and  $A_T$  concentrations higher than their seawater end member year-round. Estuaries draining limestone-bedded catchments experience freshwater  $C_T$  and  $A_T$  concentrations similar to seawater, and catchments with no or negligible carbonate bedrock have estuaries with freshwater  $C_T$  and  $A_T$  concentrations lower than seawater. This supports previous findings that the presence of carbonate bedrock exerts a strong influence on low salinity  $C_T$  and  $A_T$  concentrations (McGrath et al., 2019). The large variety of catchment lithologies presented in Chapter 3 enables the further differentiation between the behaviour of chalk and limestone bedrocks more specifically.

Within a specific estuary, differences in the freshwater  $C_T$  and  $A_T$  concentration across the year are related to variability in river discharge. Estuaries with chalk bedrock experience higher freshwater  $C_T$  and  $A_T$  concentrations in high discharge conditions, which implies that chalk weathers at a faster rate in high discharge conditions. Estuaries with non-chalk (either limestone or non-limestone) bedrock experience freshwater  $C_T$  and  $A_T$  concentrations higher than their annual mean in low discharge conditions, which implies that increased discharge acts to dilute the weathering products.

Strong gradients between freshwater and seawater  $C_T$  and  $A_T$  concentrations are the main drivers of their in-estuarine concentrations. Strongly linear salinity-concentration relationships indicate that conservative mixing is the most important process in determining  $C_T$  and  $A_T$  concentrations along the estuary. Therefore, catchment lithology is the key defining factor of estuarine  $C_T$  and  $A_T$  concentrations along the salinity gradient, and subsequently the flux of inorganic carbon across the LOAC.

#### **6.2.2 Chapter 4: Contribution of catchment lithology to the variation in freshwater $C_T$ and $A_T$ concentrations in UK rivers.**

*Were the  $C_T$  and  $A_T$  behaviours present in 2017-18, the features for which these estuaries were selected for sampling, also present in 2020-21?*

I selected four estuaries for sampling for Chapter 4 because their catchments spanned the range of lithological makeups experienced across all 16 of the estuaries studied in Chapter 3, and therefore spanned the range of freshwater  $C_T$  and  $A_T$  concentrations in Chapter 3. The rivers experienced similar magnitude  $C_T$  and  $A_T$  concentrations in 2020 – 2021 (Chapter 4) to their freshwater estuarine concentrations in 2017 – 2018 (Chapter 3), which gives support to their selection as appropriate study catchments. Additionally, this corroborates the findings of Chapter 3, because the catchment geology is not variable interannually, so the similar  $C_T$  and  $A_T$  concentrations three years later support an unchanging variable being the key influence on freshwater  $C_T$  and  $A_T$  concentrations.

*Are differences in  $C_T$  and  $A_T$  concentrations between estuaries caused by carbonate bedrock weathering?*

$A_T$  measurements were not well-defined by geological variables calculated from the end member mixing model in Chapter 4 (% of flow from carbonate bedrock) and from secondary catchment data in Chapter 3 (% carbonate bedrock as a percentage of total catchment surface area; mean bedrock age) (Fig. 4.8). This is likely to be a function of the imperfect

relationship between geology and  $C_T$  and  $A_T$  concentrations found in Chapter 3, but with a small sample size, this is difficult to establish with certainty. The findings of Chapter 4 are limited by sample size and by large uncertainty in the secondary data used to describe end member concentrations. In this case, these limitations are manifested particularly in the uncertainty in the mixing model results, which affects the % flow from carbonate bedrock variable.

*Are high  $C_T$  and  $A_T$  concentrations in the Great Ouse directly attributable to  $\text{CaCO}_3$  dissolution from chalk bedrock, as opposed to limestone bedrock weathering in the Tyne and Clyde?*

While there are large uncertainties in the end member mixing model results, the same mixing model as was used for the Tyne, Clyde and Forth estuaries, which uses silicate and carbonate (which here includes both limestone and chalk) bedrock with rainwater, was unsuitable for the Great Ouse. The Ca / Mg ratio of chalk bedrock is very different from the Ca / Mg ratio of either silicate or carbonate bedrock; chalk contains less magnesium with respect to calcium than the other bedrock types. Chalk and limestone were separated into distinct end members for the Great Ouse and were a better fit to the measurement data. The Great Ouse Ca / Mg relationship could only be described using chalk, which implies that the key difference between the  $C_T$  and  $A_T$  concentrations in the Great Ouse relates to chalk weathering specifically.

*Is the BGS carbonate bedrock classification a good measure of, and therefore a proxy for, the contribution of carbonate weathering to  $C_T$  and  $A_T$  concentrations?*

The bedrock classification presented in Chapter 3 and using BGS UK bedrock data (British Geological Survey, 2008) shows good linear correspondence with the percentage of flow that originated from carbonate bedrock for the three comparable rivers (Tyne, Clyde and Forth) used in Chapter 4. This is in contrast to a previous study which found poor correspondence between bedrock classification data and carbonate chemistry measurements (Hagedorn and Cartwright, 2010). The UK contains highly variable catchment lithologies, including large differences in the contribution of carbonate bedrock to a catchment (e.g. Table 3.1) and including large areas of chalk bedrock (Fig. 3.2). This variation in catchment bedrock is reflected in the  $C_T$  and  $A_T$  concentration data, as well as in the different contributions of carbonate bedrock to flow (Chapter 4). In other countries, less variable catchment bedrock compositions may be less well represented in bedrock classification data, such as that provided by the BGS. Smaller differences in the real-world

catchment compositions mean that any errors in the bedrock classification data have a larger impact.

### **6.2.3 Chapter 5: Propagating inorganic carbon and alkalinity measurements in a diverse range of UK estuaries through to annual estimated CO<sub>2</sub> outgassing.**

*How and why does pCO<sub>2</sub> change from source to sea in different estuaries and at different times of the year? Are there differences between estuaries and seasons?*

Estuarine pCO<sub>2</sub> is not controlled by the same factors as C<sub>T</sub> and A<sub>T</sub>, from which it was calculated, with the exception of salinity. pCO<sub>2</sub> experiences a large range at low salinity, but converges towards (but never to, and never below) the atmospheric mole fraction at high salinity. This general decrease in pCO<sub>2</sub> with salinity results from a combination of mixing and outgassing. Temperature exerts a positive influence on pCO<sub>2</sub>. CO<sub>2</sub> is less soluble in warm water (e.g. Weiss, 1974) so it follows that pCO<sub>2</sub> increases in warmer waters for the same concentration of CO<sub>2</sub>. Non-purgeable organic carbon (NPOC) also exerts a positive influence on pCO<sub>2</sub>. In the context of LOAC carbon cycling, this suggests that as land-derived dissolved organic carbon imports to estuarine environments increased, so too does pCO<sub>2</sub>, which supports previous studies' findings that high estuarine pCO<sub>2</sub> is driven by land-derived organic matter decomposition *in situ* (Borges et al., 2006). Finally, where elevated temperatures coincide with increased dissolved inorganic nitrogen (DIN) concentrations, pCO<sub>2</sub> decreases. This suggests that seasonal photosynthesis is sustained by DIN inputs, and this process acts to decrease pCO<sub>2</sub>, as CO<sub>2</sub> is converted into organic matter and oxygen during photosynthesis.

The 'season' variable was excluded from the model because it was multicollinear with other variables that are used to explain pCO<sub>2</sub>. Temperature and river discharge, the two variables which 'season' relates to are used to describe seasonal changes. Of these, temperature is the only factor that exerts an influence on pCO<sub>2</sub>, as described above. River discharge is not related to pCO<sub>2</sub> variation in this dataset. Differences between estuaries are visibly indistinguishable (Fig. 5.5). The 'estuary' variable is included in the model as a random effect and does absorb some of the variation in pCO<sub>2</sub> (difference between marginal and conditional mean, Table 5.2). This implies that differences in some factor between the estuaries affects pCO<sub>2</sub>, that is not accounted for by the variables in the model.

*How does CO<sub>2</sub> flux vary from source to sea in different estuaries? To what extent is this controlled by the same factors as pCO<sub>2</sub>?*

Water-to-air CO<sub>2</sub> fluxes are calculated directly from pCO<sub>2</sub> values, so the variability in FCO<sub>2</sub> is similar to, and is accounted for, by the same factors as for pCO<sub>2</sub>. Similarly to pCO<sub>2</sub>, FCO<sub>2</sub> values are generally higher but more variable in freshwaters and decrease and converge towards zero at the seawater end member (Fig. 5.7). The majority of flux estimates remain positive, even at the seawater end member, suggesting that the switch between the estuarine source of CO<sub>2</sub> to the atmosphere, and the coastal ocean atmospheric CO<sub>2</sub> sink occurs in the estuarine plume, or outer estuary, rather than within the confines of the estuarine mouth.

*How much CO<sub>2</sub> is outgassed by estuaries around the UK?*

CO<sub>2</sub> flux data are interpolated across the surface area of the studied estuaries, from which a mean flux for the entire estuarine area is calculated and scaled to the UK estuarine surface area (Chapter 5; JNCC, 2013). This gives a total estimate of UK inner estuarine outgassing of  $8.5 \times 10^{10}$  g C d<sup>-1</sup>. This value, which as a point of comparison, is equivalent to approximately ¼ of the UK's provisional fossil fuel emissions estimate for 2021 (27%, compared to O'Sullivan, 2022), is the first of its kind. It is likely to be larger than the total emission from inner and outer estuaries, given that outer estuaries, which likely have a larger surface area than inner estuaries (Frankignoulle et al., 1998), are the likely location of the switch between CO<sub>2</sub> source and CO<sub>2</sub> sink in estuaries. Strong outgassing fluxes from inner estuaries therefore constitute an important term in the UK carbon budget.

### **6.3 General discussion and future directions**

This work was made possible because of a large number of samples collected prior to its commencement by the LOCATE sampling programme. It therefore seems important, and indeed fitting, to consider the findings presented here in the context of the findings from the wider LOCATE community.

Two of the three key objectives of the LOCATE programme are particularly relevant to this thesis:

- “1. To quantify the fate of terrigenous organic matter from soils to the ocean, with particular focus on estuaries and coastal waters.
2. To quantify and understand the loss processes in estuarine environments.”  
(LOCATE, 2022)

As such, the findings presented here are directly related to three other studies, whose focuses pertain to riverine organic carbon (Williamson et al., 2021), riverine inorganic carbon (Tye et al., 2022b) and estuarine organic carbon (García-Martín et al., 2021). This thesis therefore fills in the estuarine inorganic carbon piece of the jigsaw. Therefore, here the findings of these three LOCATE studies are linked to the results presented in this thesis, to see whether the findings are similar to those for the inorganic carbon study, and to see how the inorganic and organic components link together in this estuarine context.

### 6.3.1 Riverine inorganic carbon

Riverine  $C_T$  and  $HCO_3^-$  concentrations were related to catchment geology, including carbonate and sandstone bedrock, annual precipitation and heather grassland coverage according to a stepwise regression model (Tye et al., 2022b). The results of this thesis indicate that the contribution of carbonate bedrock strongly affects  $C_T$  concentrations, but that there is a tangible difference between chalk and limestone bedrock contributions (Chapters 3 and 4), which was beyond the scope of the riverine study to identify. Furthermore, the riverine study found annual precipitation to have a negative effect on  $C_T$  concentrations (Tye et al., 2022b). Similarly, Chapter 3 concluded that daily precipitation had a negative effect on  $C_T$  concentrations in limestone and non-carbonate bedded catchments, but a positive influence on  $C_T$  concentrations in chalk bedded catchments.

These similar, but subtly different findings arise for two reasons. Firstly, examining chalk, limestone, and non-carbonate bedrocks separately enabled the identification of more subtle differences between catchments (Chapters 3 and 4). Secondly, stepwise regression modelling can be problematic (Smith, 2018; Whittingham et al., 2006). Stepwise regressions are conducted by including all possible predictor variables initially and removing non-significant variables one by one, until all the remaining predictor variables are significant. For example, here 22 predictor variables initially are reduced to 4 for  $C_T$  and 5 for  $HCO_3^-$ , respectively (Tye et al., 2022b including their Supplementary Information 7). This can lead to biased estimates of the effect sizes of the predictor variables left in the model, because they are absorbing variation in the response that would have been absorbed by variables that have now been removed (Smith, 2018; Whittingham et al., 2006). Therefore the riverine  $C_T$  findings (Tye et al., 2022b) are not directly comparable to Chapters 3 and 4 of this thesis, because the estimated effect sizes may be biased. Furthermore, it is not problematic that Chapter 5 did not use heather grassland as an explanatory variable, because it was not a variable identified as likely to effect  $C_T$ . Its significance in a riverine stepwise regression (Tye et al., 2022b) is either a correlation by chance, or a correlation for some reason as yet unidentified in the literature.

Finally, with the pitfalls of stepwise regression still in mind (Smith, 2018; Whittingham et al., 2006), free CO<sub>2</sub> concentrations were found to positively correlate with DIN, SRP and NPOC concentrations (Tye et al., 2022b). Free CO<sub>2</sub> is a term here used to describe C<sub>T</sub> present as CO<sub>2</sub> in water (as opposed to H<sub>2</sub>CO<sub>3</sub>, HCO<sub>3</sub><sup>-</sup>, CO<sub>3</sub><sup>2-</sup>; Eq. 1.2 – 1.3), which is used to represent CO<sub>2</sub> that has the potential to exchange with the atmosphere (Tye et al., 2022b). pCO<sub>2</sub> variability was modelled in Chapter 5 in a similar context and this analysis showed that NPOC has a significant positive effect on pCO<sub>2</sub>, the effect of SRP was positive but not statistically significant, and DIN had a negative interaction effect with temperature, meaning that in the presence of increasing temperature, pCO<sub>2</sub> increases when DIN decreases, and pCO<sub>2</sub> decreases when DIN increases (Chapter 5). Both studies agree on the key finding that some variable relating to potential atmospheric CO<sub>2</sub> exchange is elevated in the presence of increased NPOC concentrations. This supports previous findings that decomposition of riverine-derived DOC in estuarine environments help sustain CO<sub>2</sub> outgassing (Borges et al., 2006).

### **6.3.2 Riverine organic carbon**

The riverine organic carbon study is less directly applicable to my thesis, because of the differing environment, the different key variable being studied, and here too because of the limitations of stepwise regression modelling (Smith, 2018; Whittingham et al., 2006; Williamson et al., 2021), so here direct comparison with the model results is avoided.

The measurements themselves yield an interesting point of comparison, however. Measured DOC concentrations were used with daily and annual discharge data to calculate total DOC export and yield (export per unit area) (Williamson et al., 2021). DOC yield is highest in small, peaty catchments, which means that the mean DOC yield for the UK is higher than previous estimates, both for the UK, and for many of the world's major countries and rivers (Williamson et al., 2021). They suggest that poor representation of smaller, particularly peat-rich, rivers, may lead to underestimation of DOC yields globally (Williamson et al., 2021). Poor representation of smaller estuaries was also one of the key motivators for this thesis. Given that outgassing fluxes are thought to be sustained by degradation of riverine DOC inputs in part (Borges et al., 2006), this further cements the importance of studying a broad range of channel sizes when forming representative estimates of regional and global scale fluxes (Chapters 3 – 5).

### 6.3.3 Estuarine organic carbon

Estuarine DOC composition varies depending on land use (García-Martín et al., 2021). While peaty catchments experience higher yields of DOC (Williamson et al., 2021), their dissolved organic matter (DOM) composition is predominantly refractory, and is transported conservatively downstream (García-Martín et al., 2021). In estuaries with more human activity (labelled arable and (sub)urban), a larger proportion of DOM is more labile (García-Martín et al., 2021). In these estuaries, this bioavailable organic matter is variable, but non-conservative, and indicates that a combination of processes are at play, including biological production and / or decomposition of the labile DOM fraction (Asmala et al., 2013; García-Martín et al., 2021).

There is a complex relationship between DOM composition and land use, in particular with DOC concentration not necessarily reflecting the bioavailability of that organic component (García-Martín et al., 2021). This may account for the variation in the pCO<sub>2</sub> model presented in Chapter 5 that was absorbed by the inclusion of 'estuary' as a random effect despite there being no visible relationship between 'estuary' and pCO<sub>2</sub>. Different estuaries experiencing different land use conditions, which in turn influence the bioavailability of organic matter for decomposition, which releases CO<sub>2</sub> and increases pCO<sub>2</sub> may form the missing link in explaining pCO<sub>2</sub> variation between estuaries.

### 6.3.4 Future directions

This work provides insight into the primary drivers of riverine and inner estuarine C<sub>T</sub> and A<sub>T</sub> concentrations and provides valuable data on these variables to the small, yet ever-growing pool of estuarine carbonate chemistry measurements.

Outer estuarine, or estuarine plume, carbonate chemistry data are much scarcer. Outer estuaries cover a potentially large surface area (e.g. Frankignoulle et al., 1998; Woodwell et al., 1973), and can experience very different FCO<sub>2</sub> conditions. Estuarine plumes can vary from strong sources (Borges and Frankignoulle, 2002; de la Paz et al., 2010) to strong sinks of CO<sub>2</sub> to the atmosphere (Zhai and Dai, 2009). The status of an outer estuary as a net emitter or sink of atmospheric CO<sub>2</sub> is thought to be caused by the presence or absence of haline stratification, with stratified plumes acting as sources and well-mixed waters acting as sinks of CO<sub>2</sub> (Borges, 2005). An original aim of this project was to contribute to understanding on this subject, by improving the representation of a range of estuaries in the data available in this field, but nutrient data for samples collected around the North Sea estuarine outflows in 2019 – 2021 were unavailable at the time of writing, so calculating North Sea A<sub>T</sub> and therefore pCO<sub>2</sub> and FCO<sub>2</sub> has not been possible to date. When these

data are available, calculating outer estuarine  $\text{FCO}_2$  and placing those results in the context of those presented here would be a valuable exercise.

Increases in  $\text{pCO}_2$  are driven by increases in temperature and organic carbon concentrations (Chapter 5), both of which are in turn affected by anthropogenic changes to our climate (IPCC, 2021; Regnier et al., 2022). This suggests that as further projected changes to our climate unfold,  $\text{pCO}_2$  will continue to increase. A comparison between European estuarine outgassing estimates (Frankignoulle et al., 1998, Chapter 5) provides convincing evidence that inner estuarine outgassing fluxes have changed over time, but in fact that they have reduced, because the rate of change of atmospheric  $\text{CO}_2$  mole fraction is faster than the rate of change of estuarine  $\text{pCO}_2$ . Atmospheric  $\text{CO}_2$  mole fractions are well-documented, but there is no equivalent long-term time series data for  $\text{pCO}_2$  or  $\text{FCO}_2$  in an estuarine setting. This would provide valuable insight into the sensitivity of estuarine carbon fluxes to climatic changes.

Estuarine carbonate chemistry studies in the Southern Hemisphere and particularly within the tropics are scarce. Estuaries exhibit highly variable morphology depending on their climatic regime and physical controls (Potter et al., 2010). Understanding the impact this may have on estuarine carbonate chemistry is vital for representing estuarine contributions to carbon cycling at a global scale.

Estuarine biogeochemical models simulate a variety of biogeochemical conditions and processes, including carbonate chemistry dynamics, at the individual estuarine scale (e.g. Jarvie et al., 2017; Volta et al., 2016). These have been recently developed and are limited by inadequate input data, for example estimating  $C_T$  concentrations from  $A_T$  concentrations (Volta et al., 2016), and would benefit from validation datasets. As measurement data availability, in addition to our understanding of the driving processes, continue to improve, from studies like this, our ability to model estuarine carbonate chemistry dynamics.

The contribution of organic alkalinity can be determined by measuring  $A_T$  alongside two other carbonate system variables, such as pH,  $\text{pCO}_2$  or  $C_T$ , from which inorganic alkalinity can be quantified, with the difference between measured and calculated alkalinity values accounted for by organic alkalinity (Kerr et al., 2021). In this study it was not possible to calculate organic alkalinity concentrations because replicate pH measurements were inconsistent. Future studies should aim to constrain this potentially important term, by sampling for three carbonate parameters, to include  $A_T$ . High organic alkalinity loads have been associated with high organic matter (Tishchenko et al., 2006) so sampling from estuaries which cover a range of different organic matter concentrations would provide information on the dynamics of organic alkalinity as organic matter concentration scales.

There is an imperfect relationship between the proportion of carbonate and chalk bedrock in a catchment and  $C_T$  and  $A_T$  concentrations at low salinities (Chapter 3). One possible

explanation for this is that only the bedrock and / or superficial deposits that intersect with the riverine flow path contribute to  $C_T$  and  $A_T$  delivery into the river, and subsequently into the estuary. Rather than looking at catchment geology as a whole, future work could intersect the BGS UK Geology map with shapefiles denoting the linear location of the river itself, rather than a whole catchment. This analysis would result in two variables: the geological makeup and the superficial deposits along the line of the river. The BGS also provide modelled superficial thickness data, which could be intersected with the latter variable to give an understanding of both sediment type and sediment thickness. Relationships between these variables and  $C_T$  and  $A_T$  concentrations in low salinity water should be compared to the analysis presented here to examine the impact of the two different methodologies.

Geochemical isotope analysis (Chapter 4) was limited by large uncertainties in the end member chemical and isotopic compositions. Several different secondary data sources were used for this purpose which were taken in different locations from the measurements presented here; in the case of the geological end members, from mainland Europe rather than the UK sampling locations. Large variability within these datasets caused large uncertainties in the results presented here. Future studies should focus on constraining these end members by taking bedrock samples of each contributing bedrock within a catchment and analysing their strontium isotopic composition and Ca, Mg, Na and Sr concentrations of water in contact with these samples. This, in conjunction with the sample sizes that were originally planned for this chapter, would enable the same end member models to be run but with more robust results.

In this study, sampling for  $C_T$  and  $A_T$  concentrations in estuaries was conducted on 5 occasions over the course of one year, and these measurements were used to characterise the carbonate chemistry across that year (Chapters 3 and 5). To account for variation in carbonate chemistry during an annual cycle, more frequent sampling is needed. A sampling effort such as that conducted by LOCATE is a logistical challenge but the use of autonomous sampling could greatly reduce this challenge. Furthermore, at the riverine end member in particular, existing monitoring programmes, for example by the Environment Agency and as part of the gauging station network, collect samples routinely for nutrients and in some cases alkalinity, so extending this to include other carbonate variables may be possible. Nevertheless, limited availability of equipment and the costs of extra sample analysis bring a need to be selective on sampling sites and timescales studied. To aid sampling site and frequency selection, a future study could use data from the LOCATE riverine sample collection in conjunction with the data presented here. Alkalinity measurements were taken in both studies, though using different methods. The use of machine learning approaches such as Kriging would enable the riverine alkalinity data to be projected down the salinity gradient, with the algorithm learning the salinity /

concentration behaviour from the estuarine alkalinity dataset. The riverine concentrations were collected monthly across a 12 month period, so this analysis would determine whether this temporal resolution was more appropriate, as well as giving more insight into the estuarine systems that may experience the most interesting biogeochemical changes across space and time.

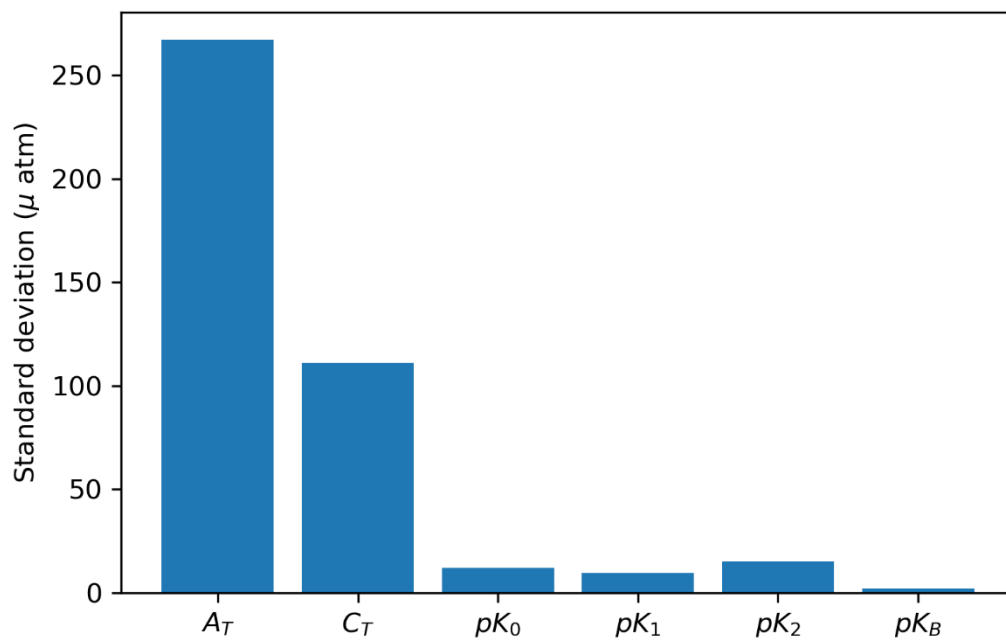
#### **6.4 Concluding Remarks**

This thesis provides a comprehensive assessment of the carbonate chemistry of the UK estuaries sampled. Direct measurements of  $C_T$  and  $A_T$  concentrations were made in 16 estuaries around the UK, whose catchments varied substantially in their geological makeup (Chapter 3). Estuarine  $C_T$  and  $A_T$  concentrations are driven primarily by differences in their freshwater end member concentrations and reflect the contribution of carbonate bedrock types to their catchment lithology. Chalk bedded catchments experience the highest freshwater  $C_T$  and  $A_T$  concentrations, followed by limestone bedded catchments, and with non-carbonate catchments experiencing the lowest freshwater  $C_T$  and  $A_T$  concentrations (Chapter 3). A first attempt at using an end member mixing model tracing chalk and limestone weathering products in river waters was made (Chapter 4), to assess the suitability of using secondary data to represent the contribution of different bedrock types.  $C_T$  and  $A_T$  measurements (Chapter 3) were used to calculate  $pCO_2$  and subsequently water-to-air  $CO_2$  fluxes in a subset of UK estuaries (Chapter 5).  $pCO_2$ , and hence  $FCO_2$ , was significantly related to organic carbon, water temperature and the interaction between temperature and dissolved inorganic nitrogen concentrations, supporting previous findings that river-derived organic carbon degradation sustains estuarine outgassing. Water-to-air  $CO_2$  flux was interpolated over the surface area of estuaries, and upscaled to estimate UK-wide inner estuarine outgassing of  $3.3 \times 10^{10} \text{ g C d}^{-1}$ , which is approximately equivalent to  $\frac{1}{4}$  of the current UK fossil fuel emission. This is the first study of its kind, both in terms of the number of estuaries studied and the representation of different estuarine sizes and geologies in particular, and it forms the first UK estimate of estuarine outgassing.

## **Appendix**

## Appendix

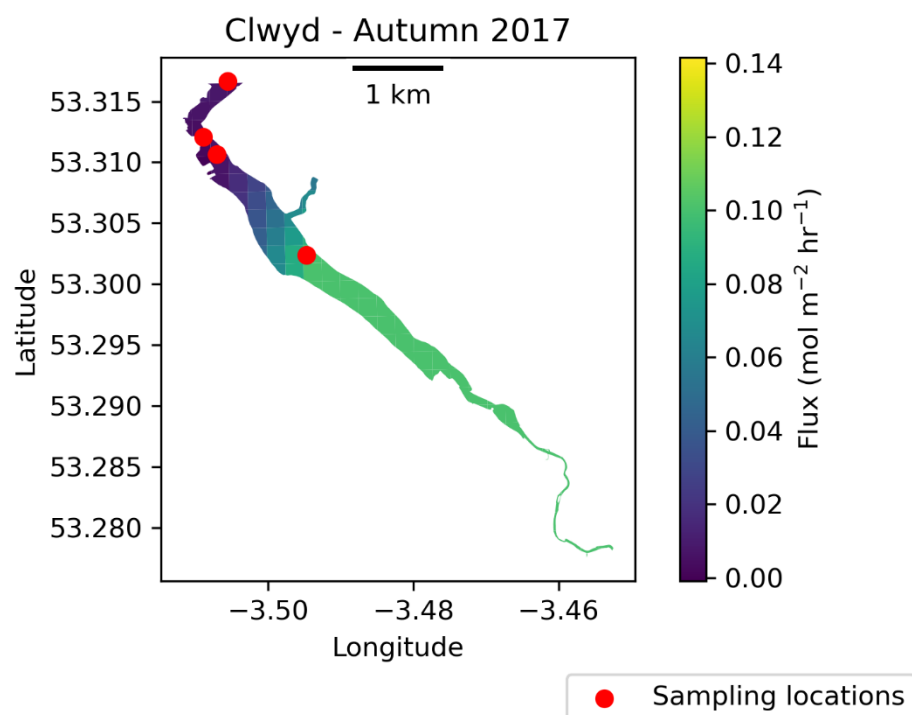
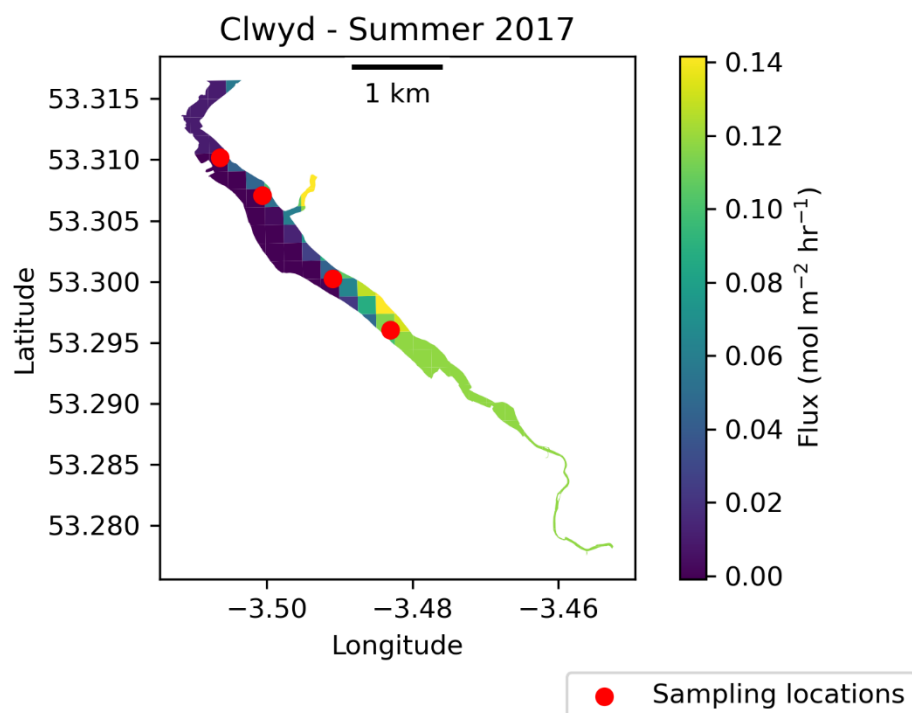
### A1 – pCO<sub>2</sub> uncertainty contributions



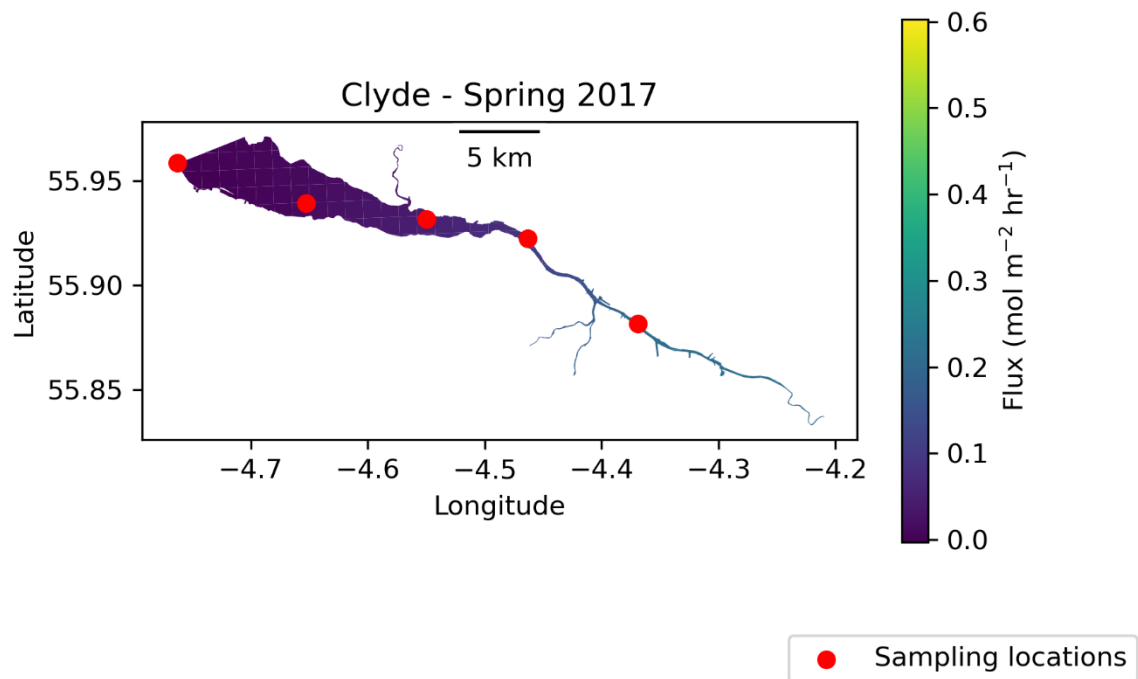
*Absolute contribution of each term to the total 1 standard deviation uncertainty in pCO<sub>2</sub>. Only variables where the contribution was greater than 0.5 μatm are shown.*

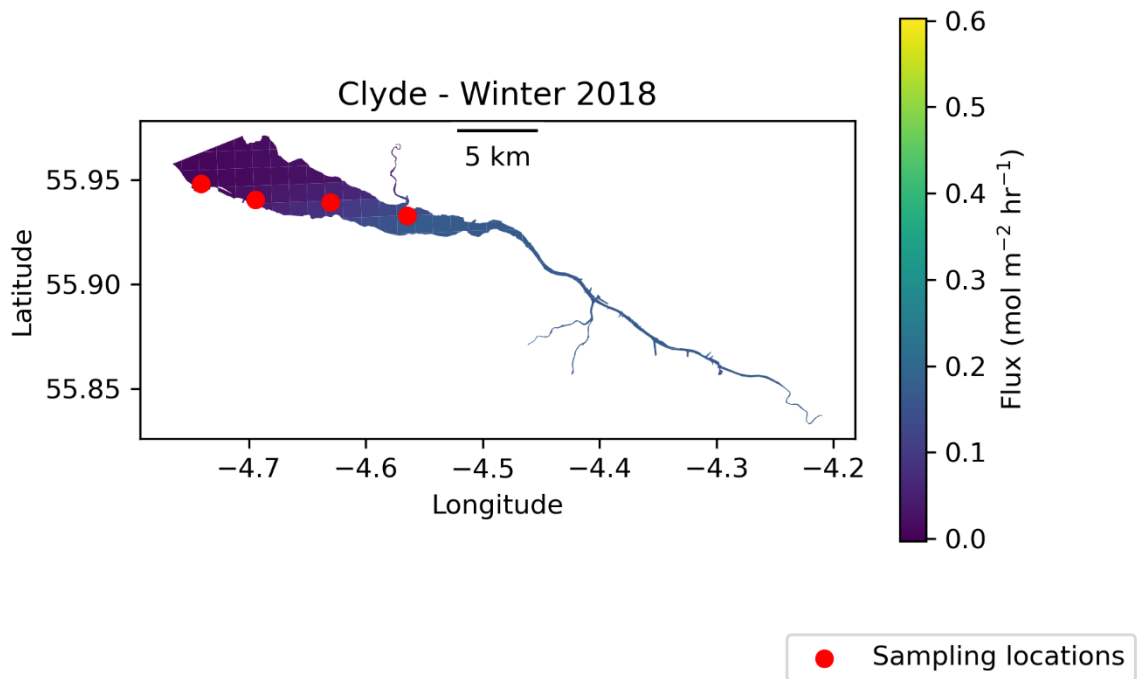
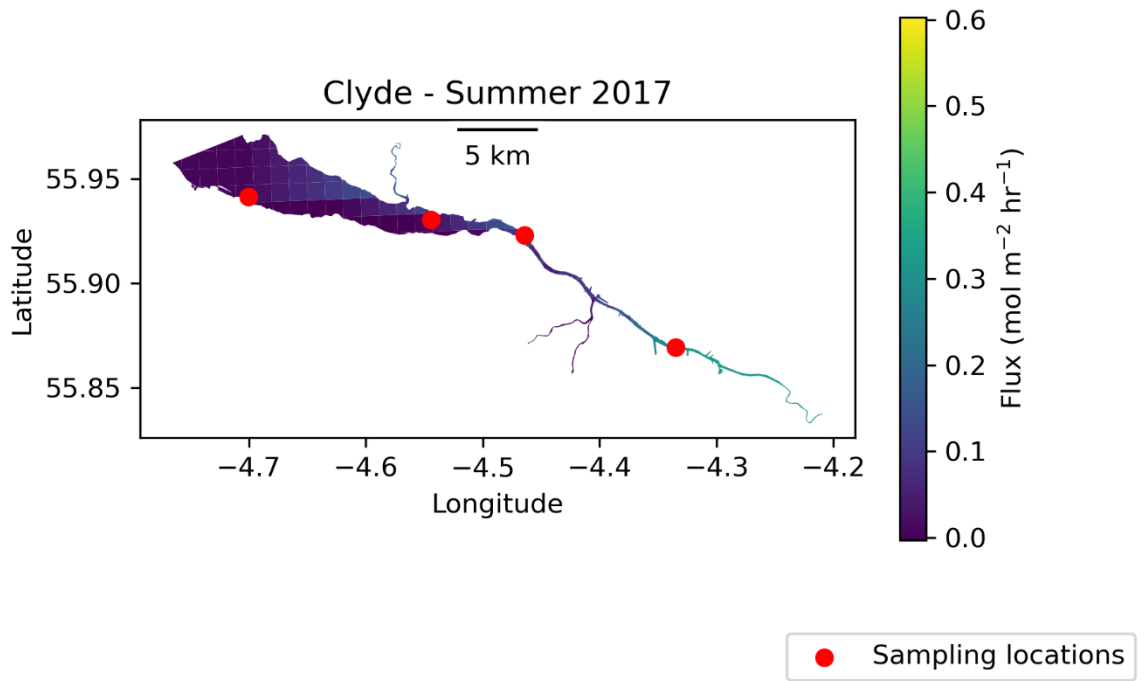
## A2 – Interpolation of flux data across estuary surface areas

### A2.1 – Clwyd



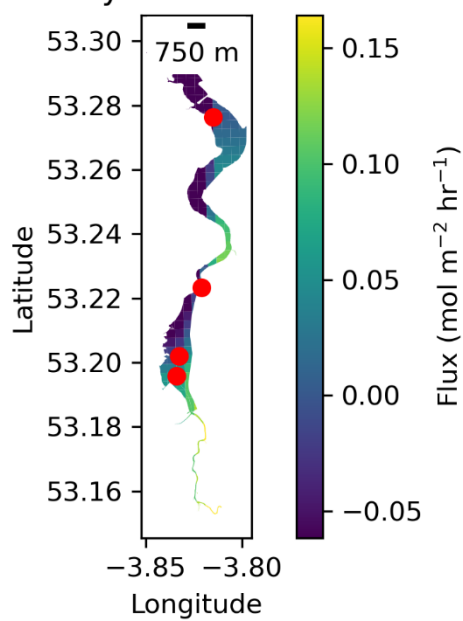
## A2.2 Clyde





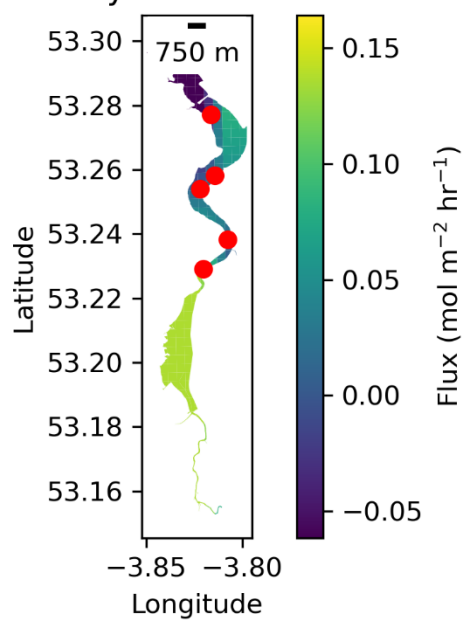
### A2.3 – Conwy

Conwy - Summer 2017



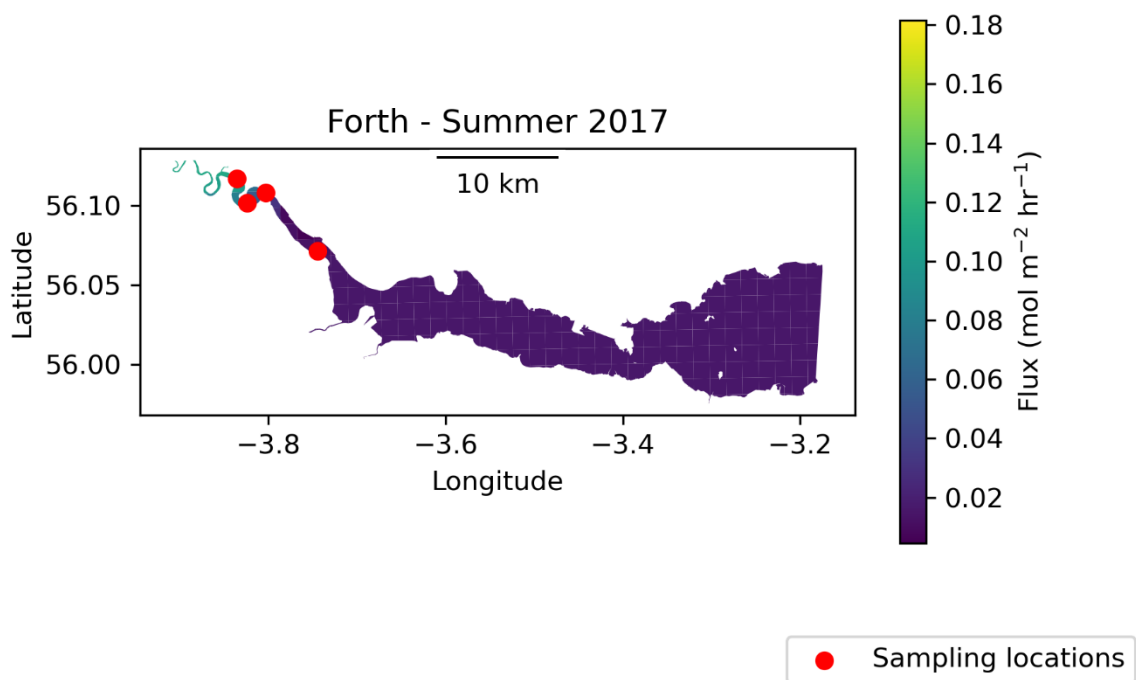
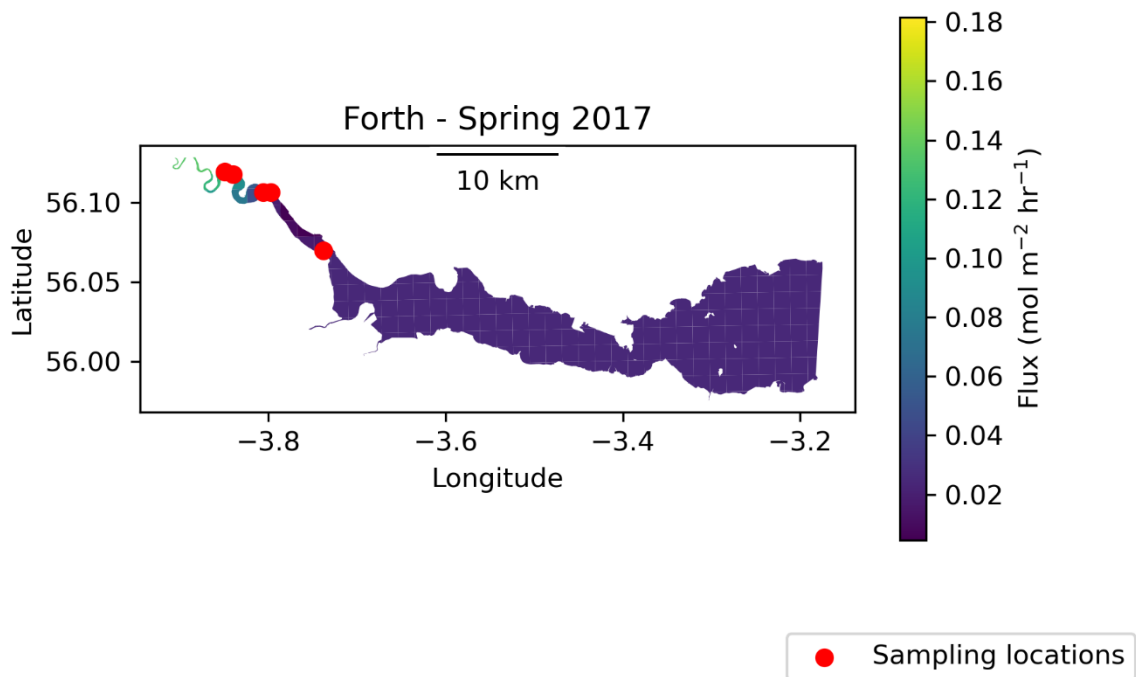
● Sampling locations

Conwy - Autumn 2017

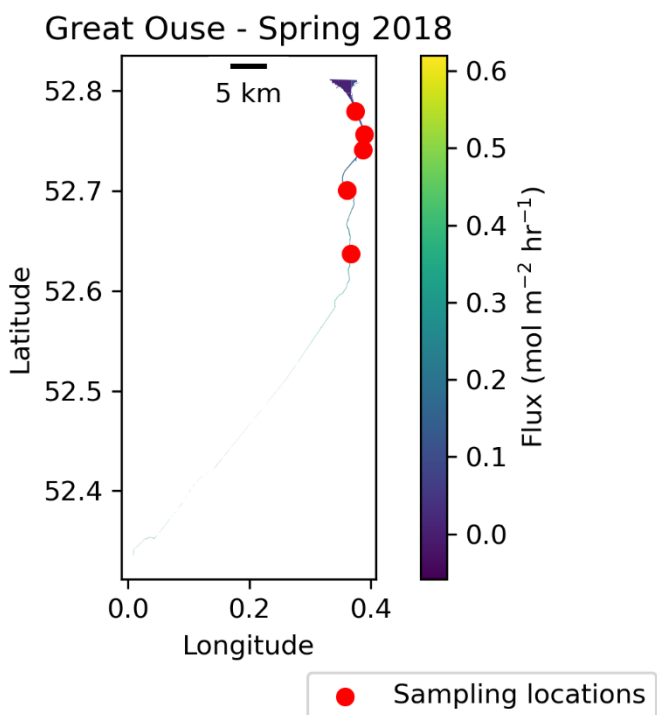
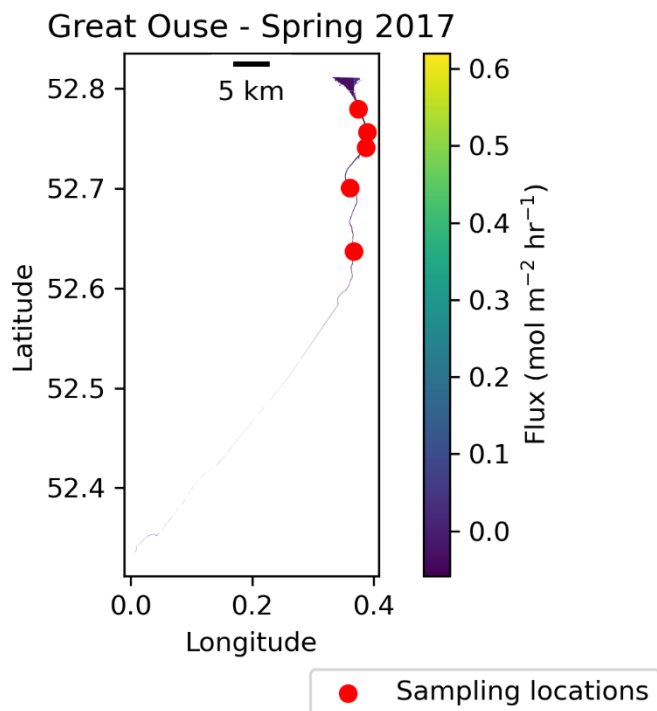


● Sampling locations

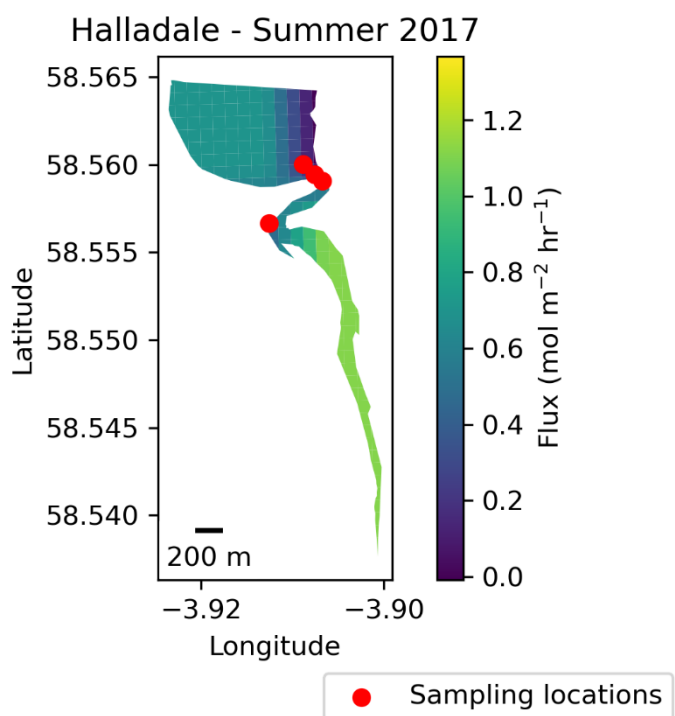
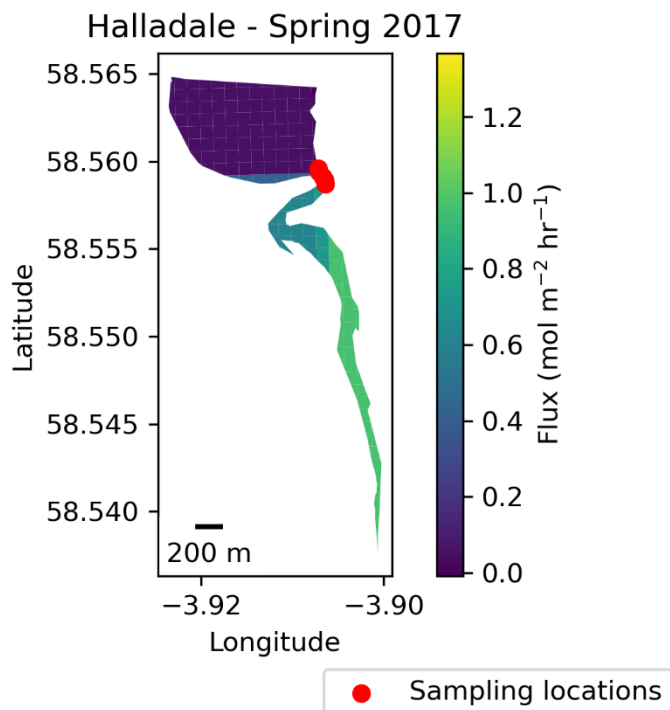
## A2.4 - Forth



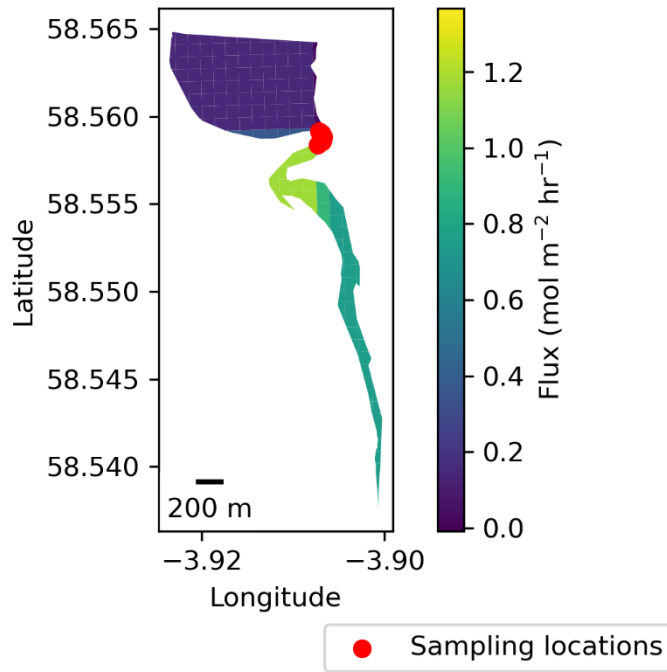
## A2.5 – Great Ouse



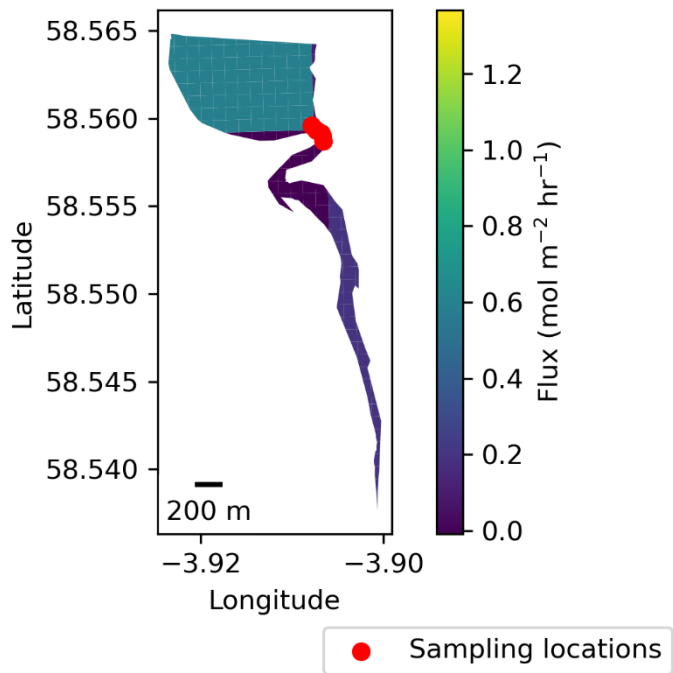
## A2.6 – Halladale

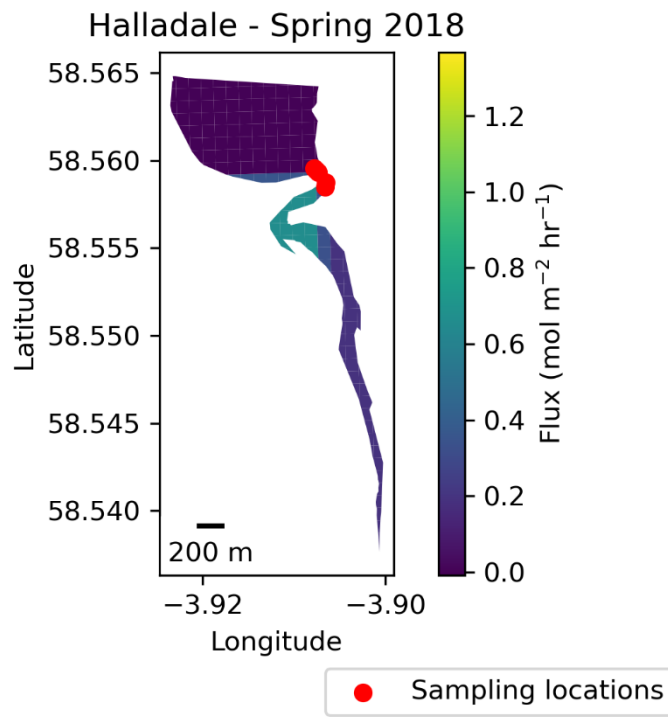


Halladale - Autumn 2017

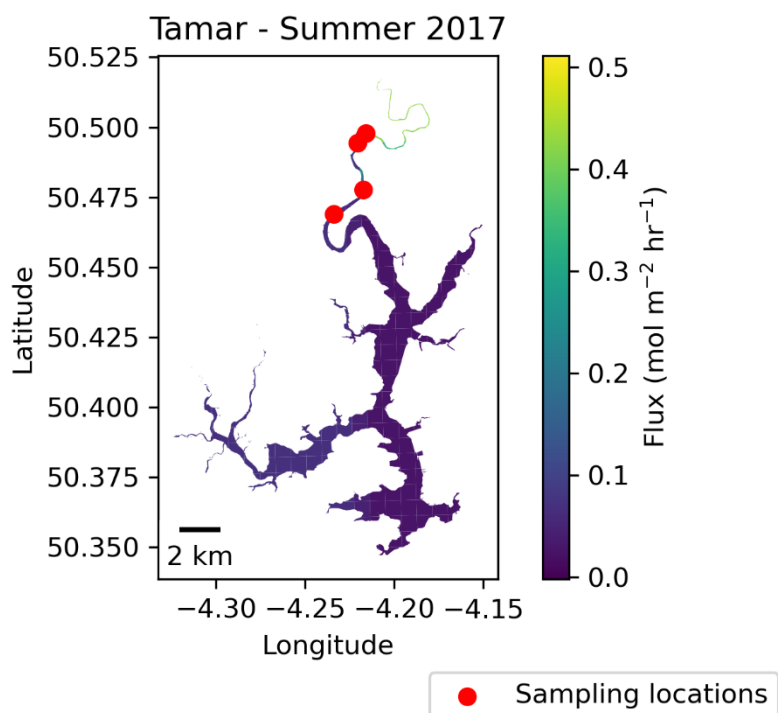
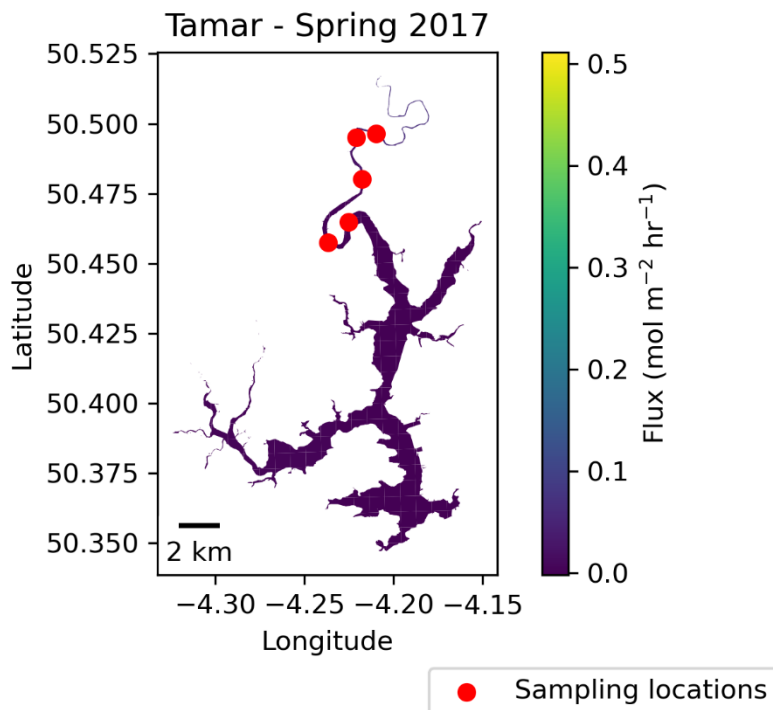


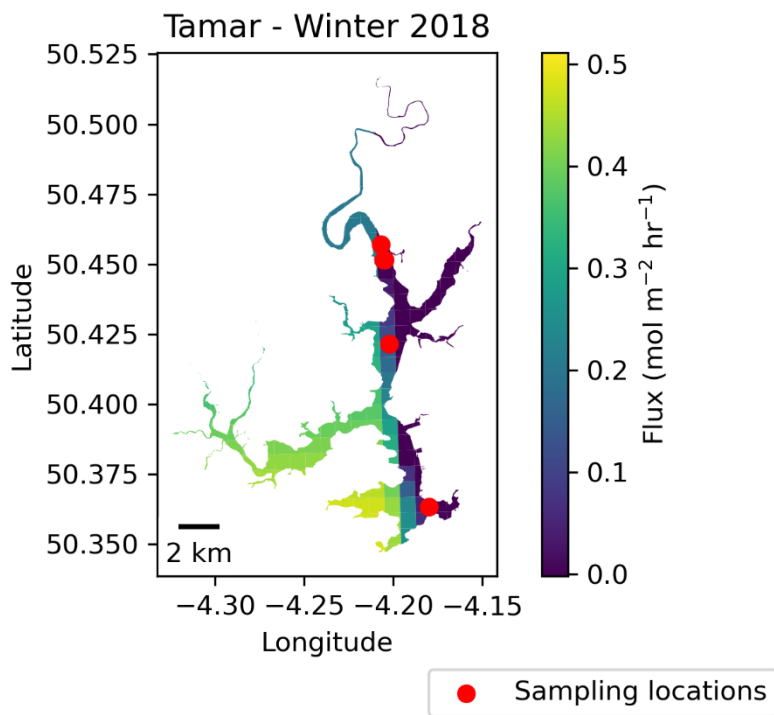
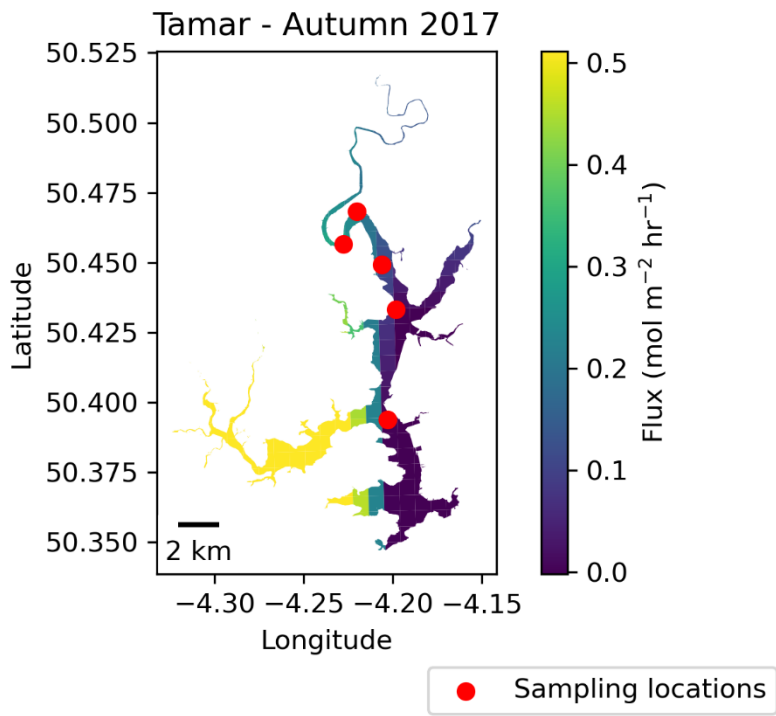
Halladale - Winter 2018

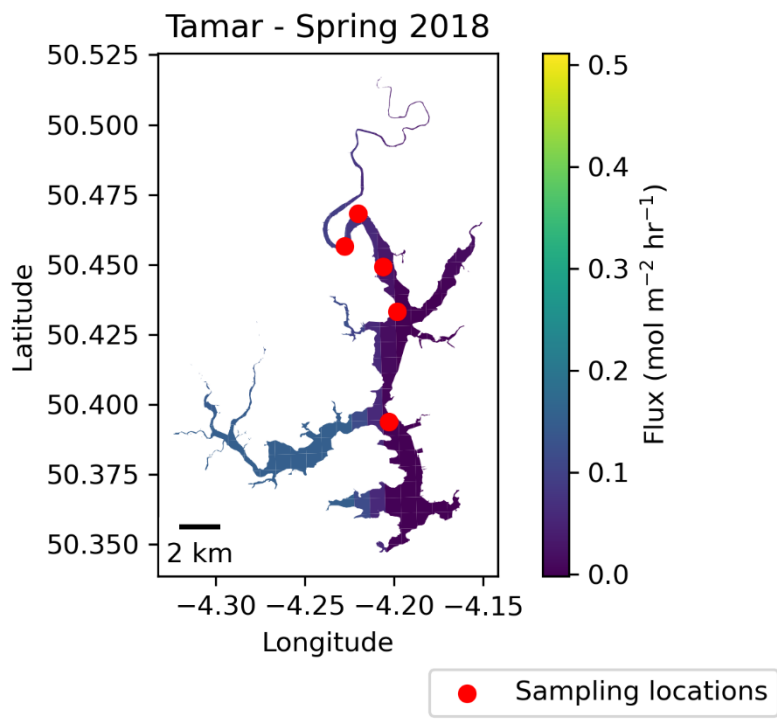




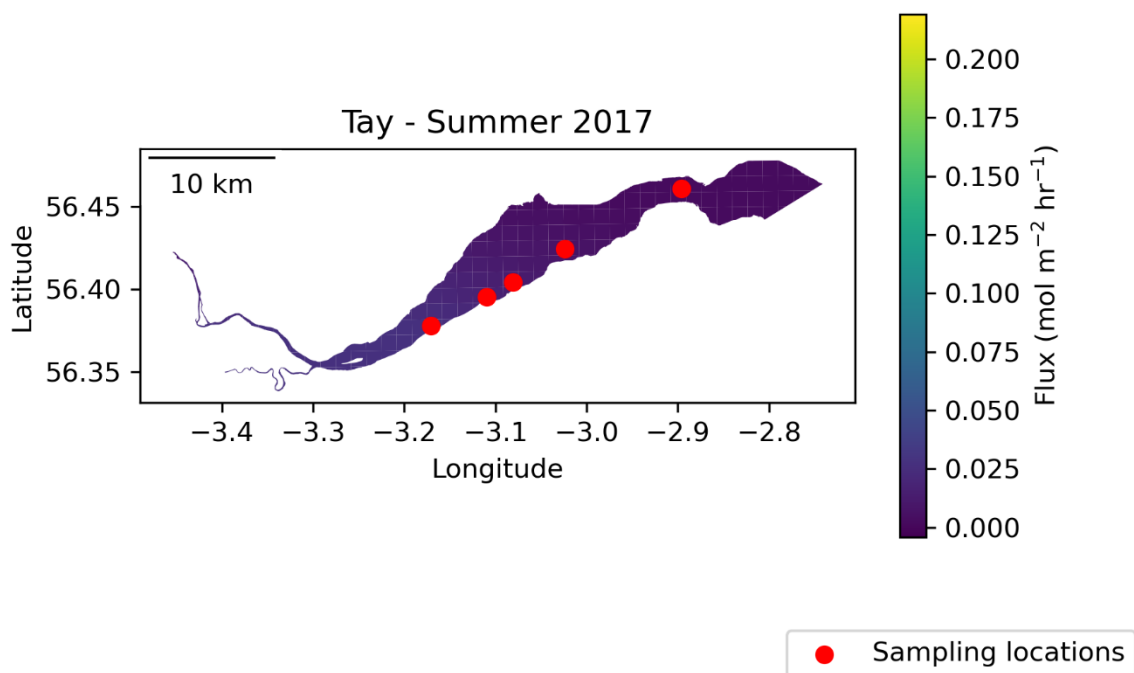
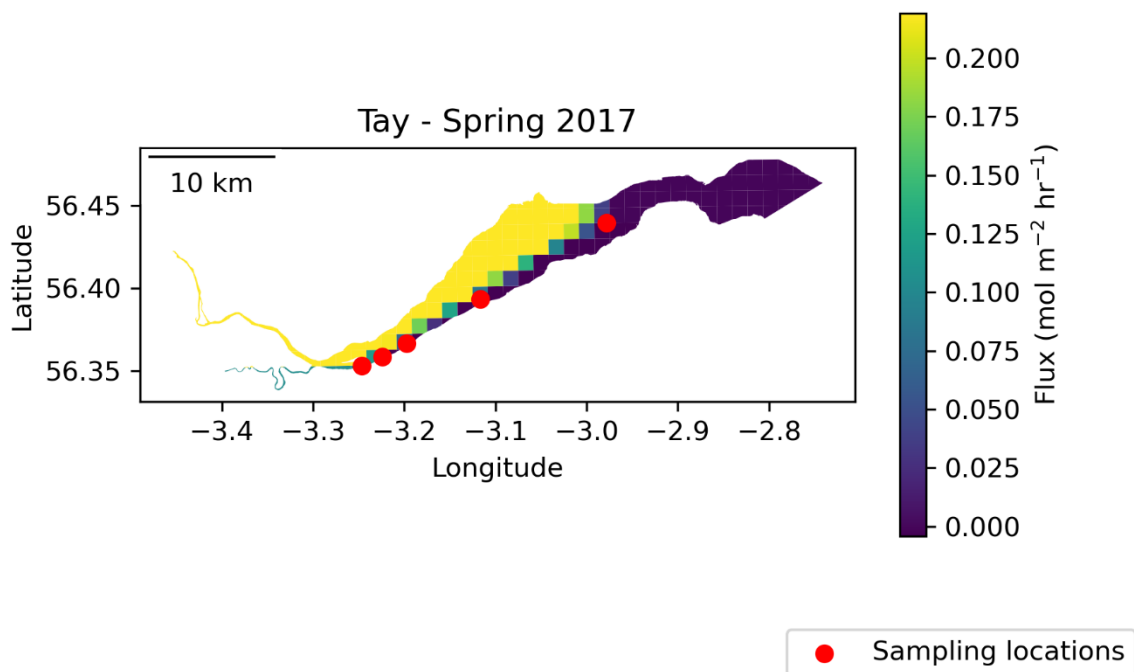
## A2.7 – Tamar

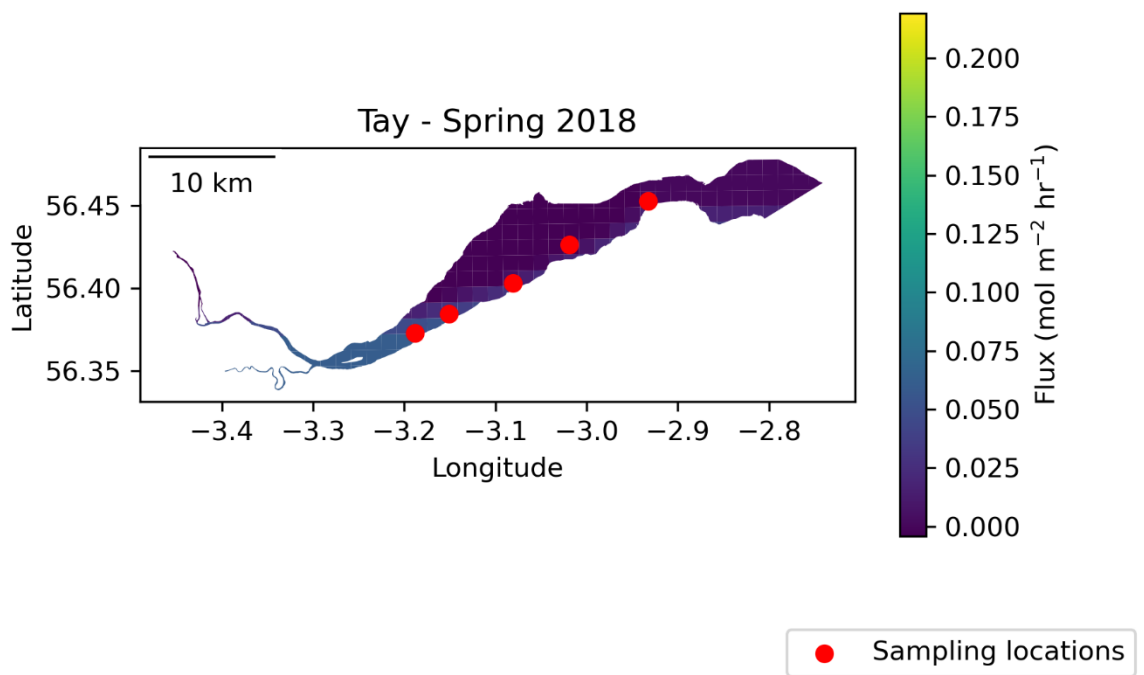
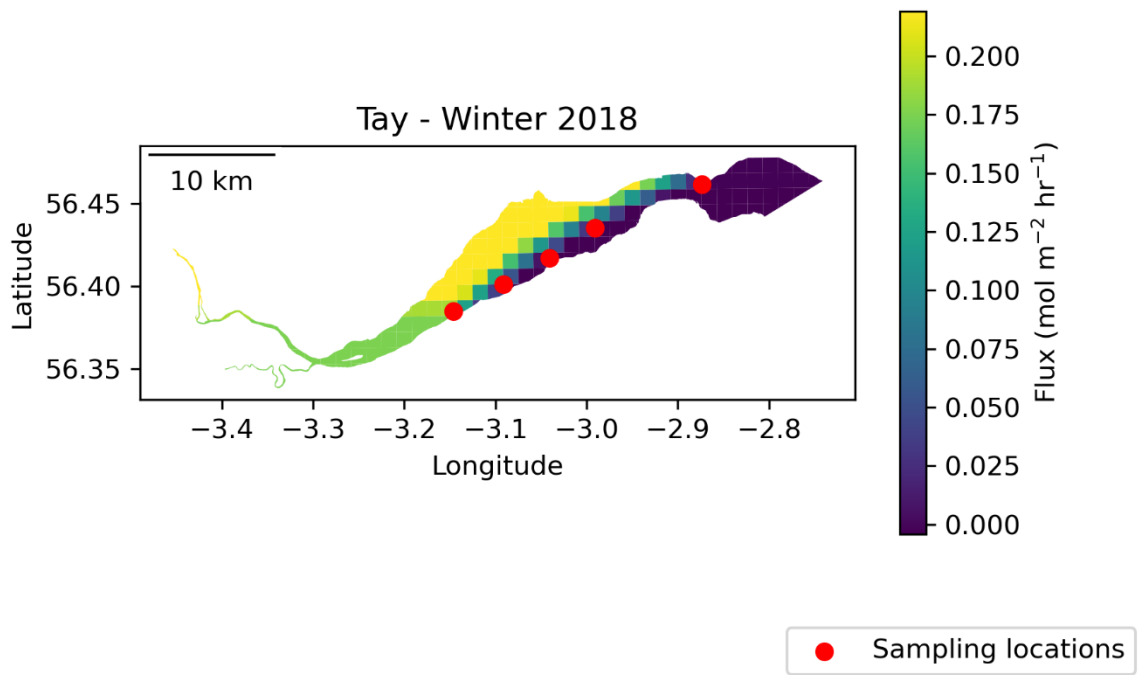




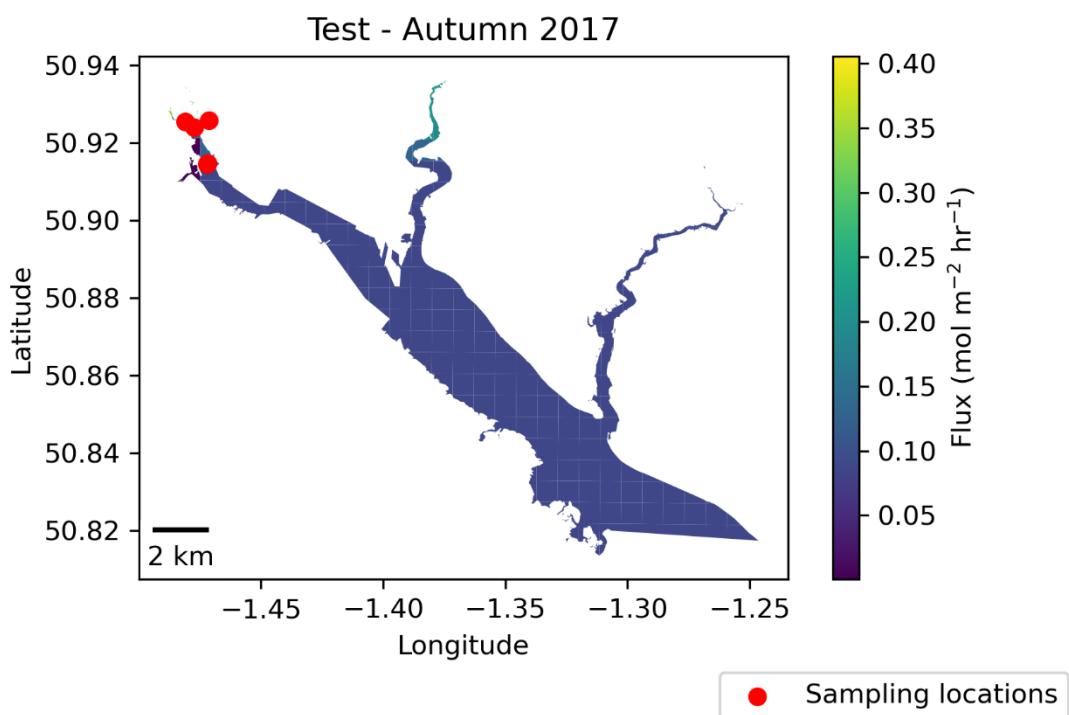
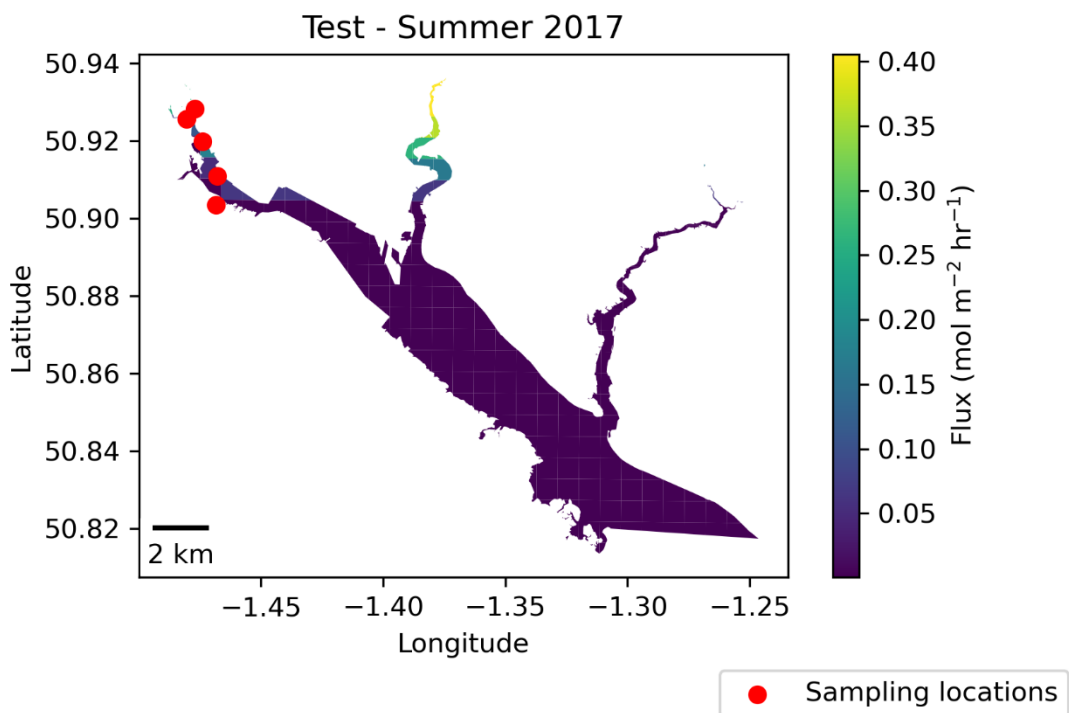


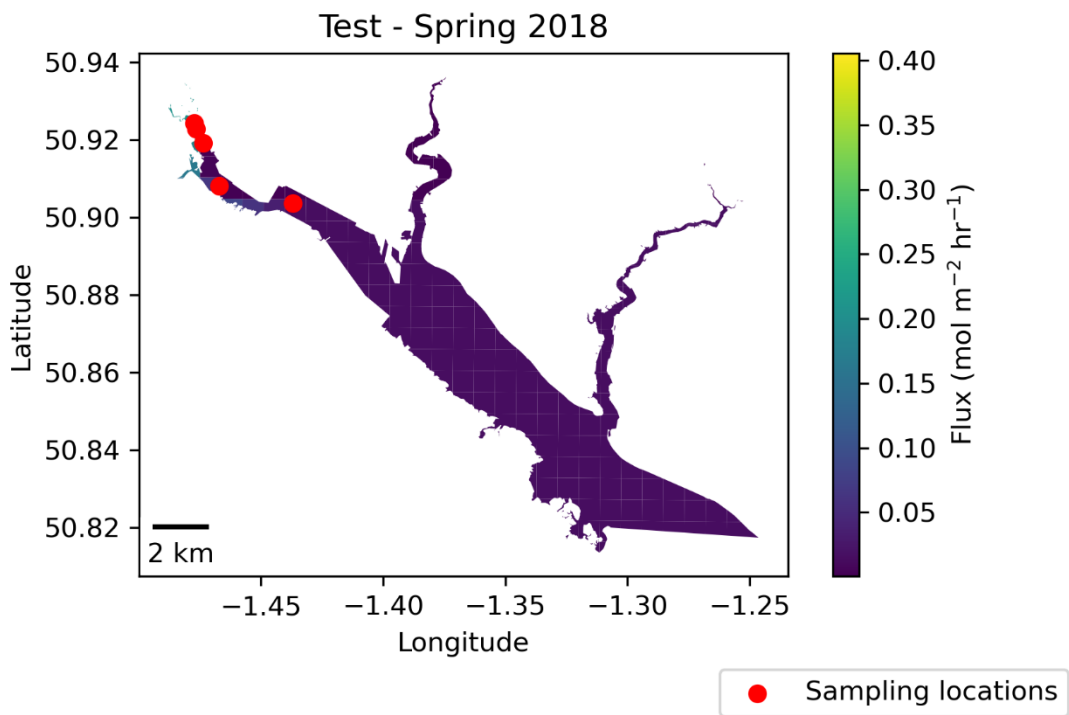
## A2.8 – Tay



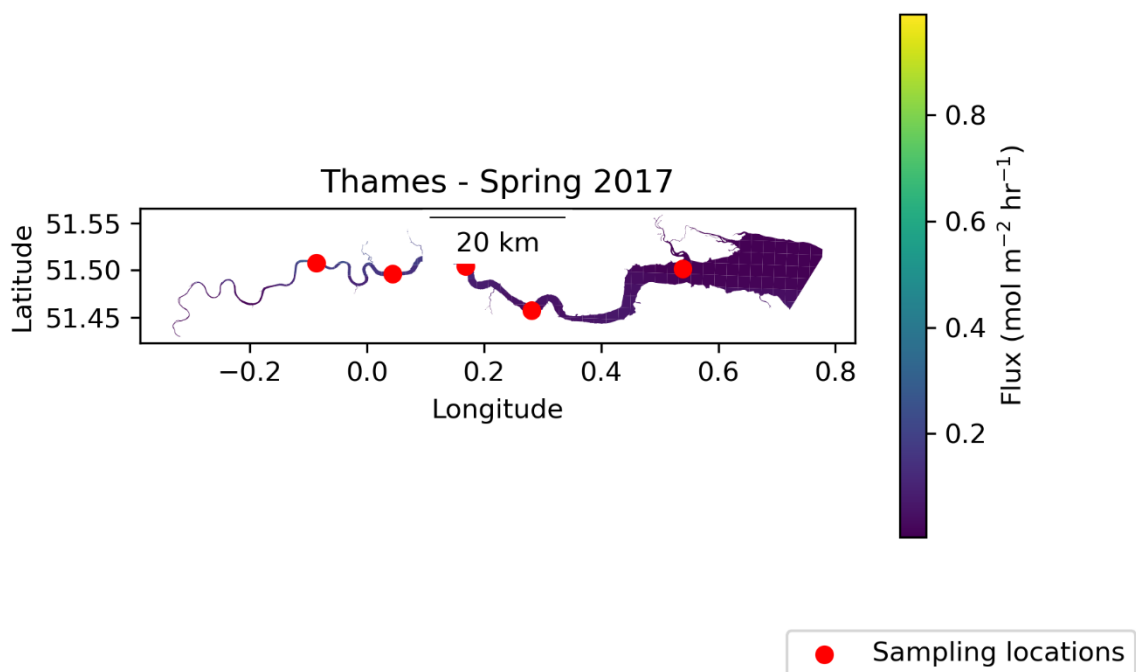


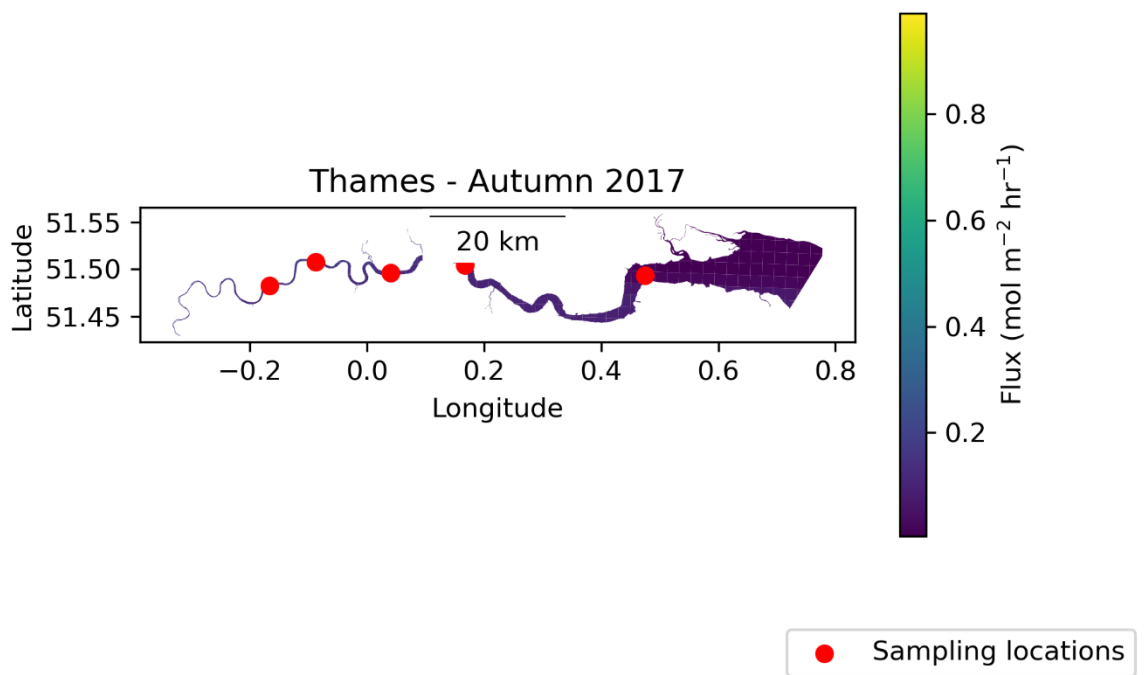
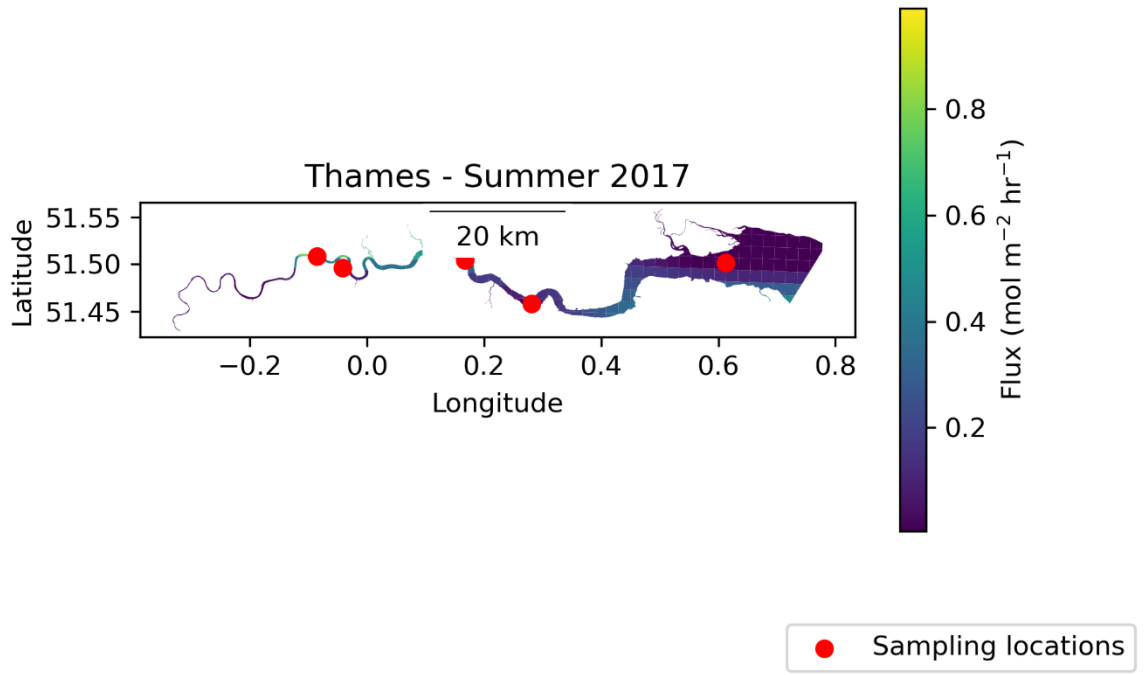
## A 2.9 – Test

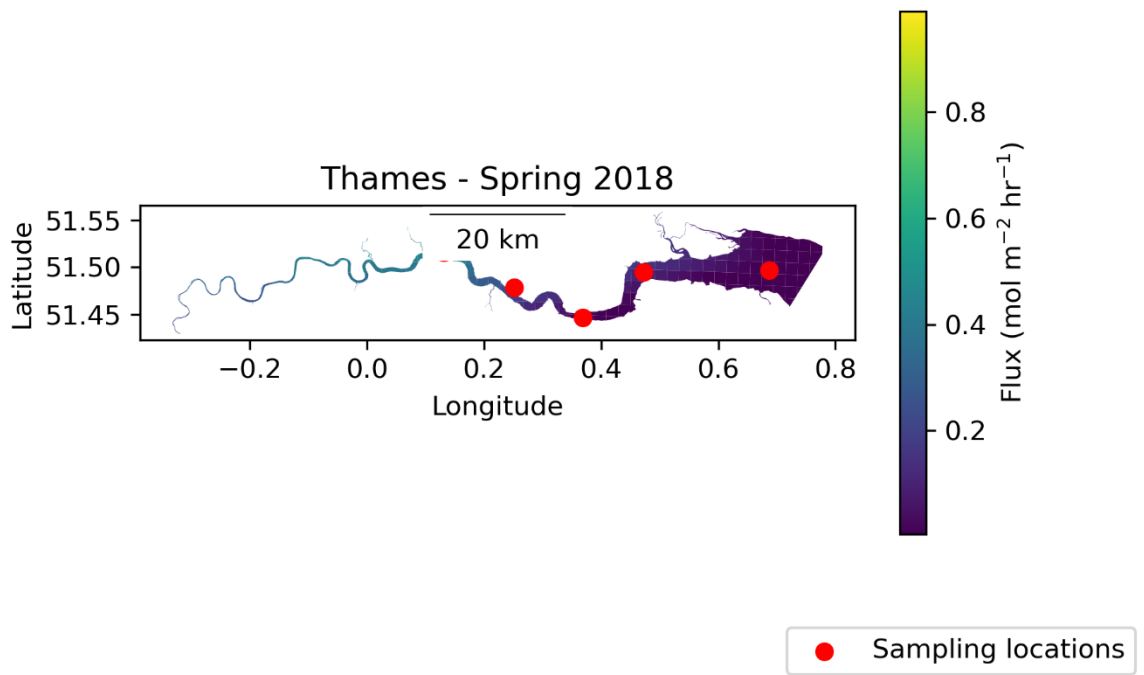
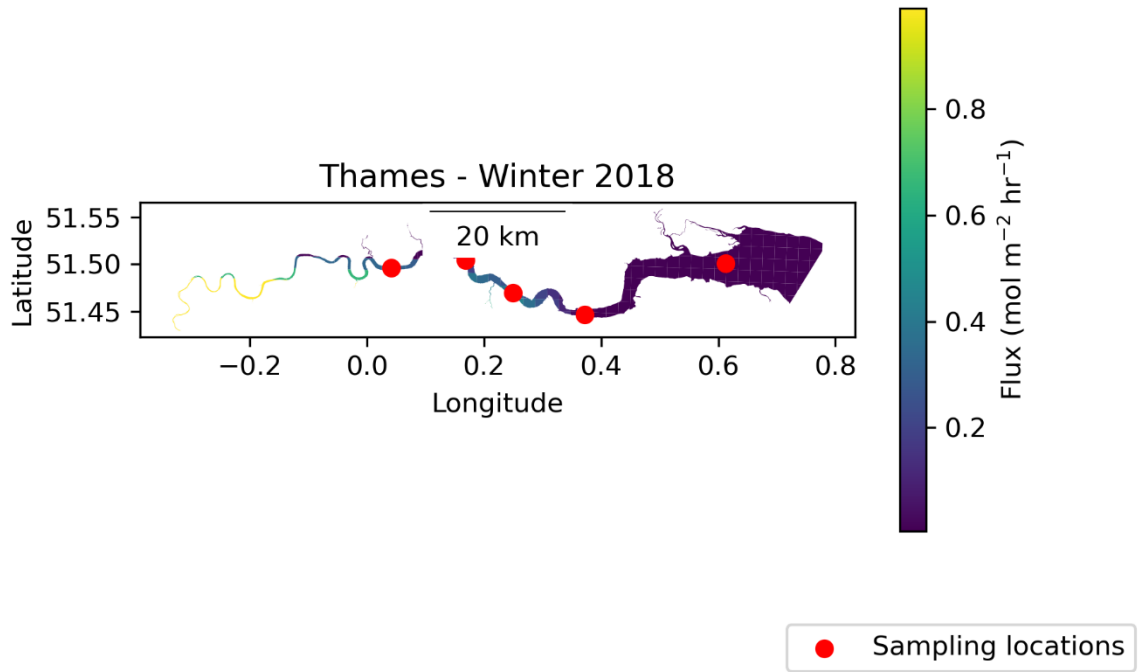




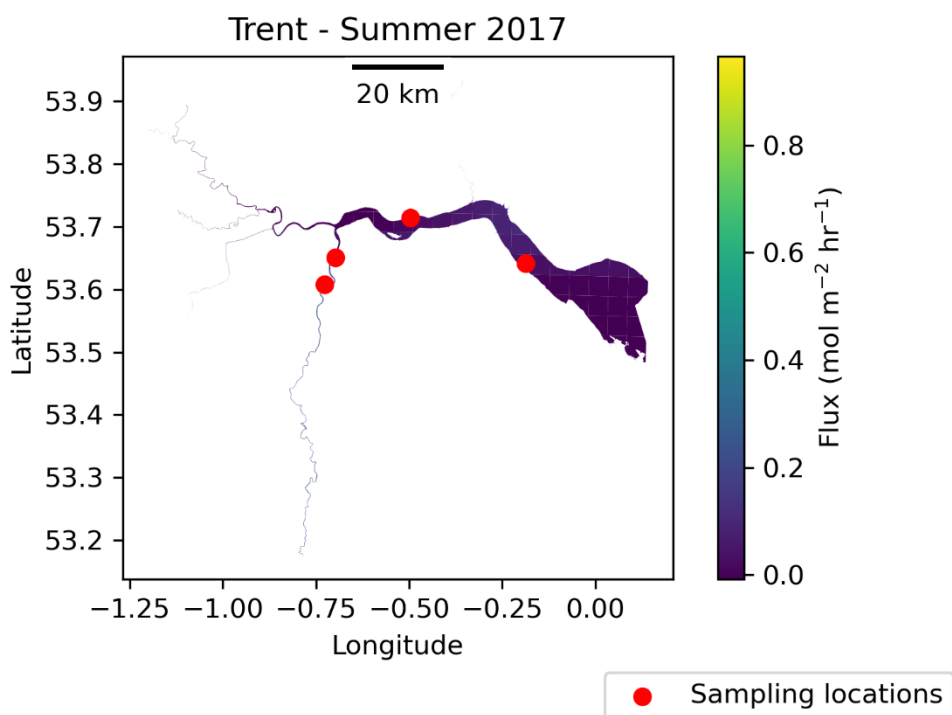
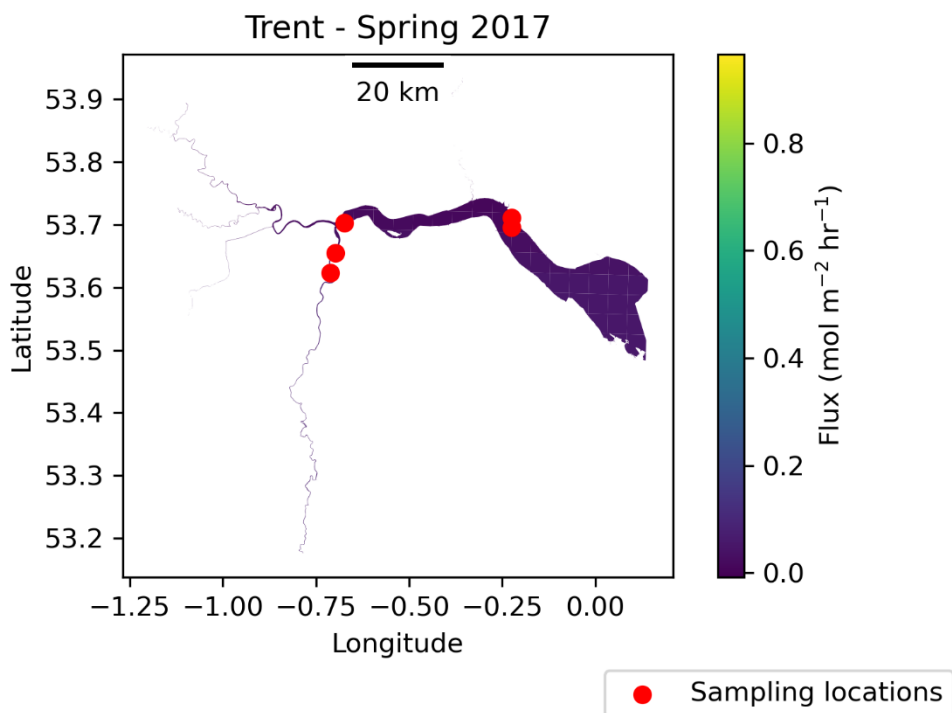
## A2.10 – Thames

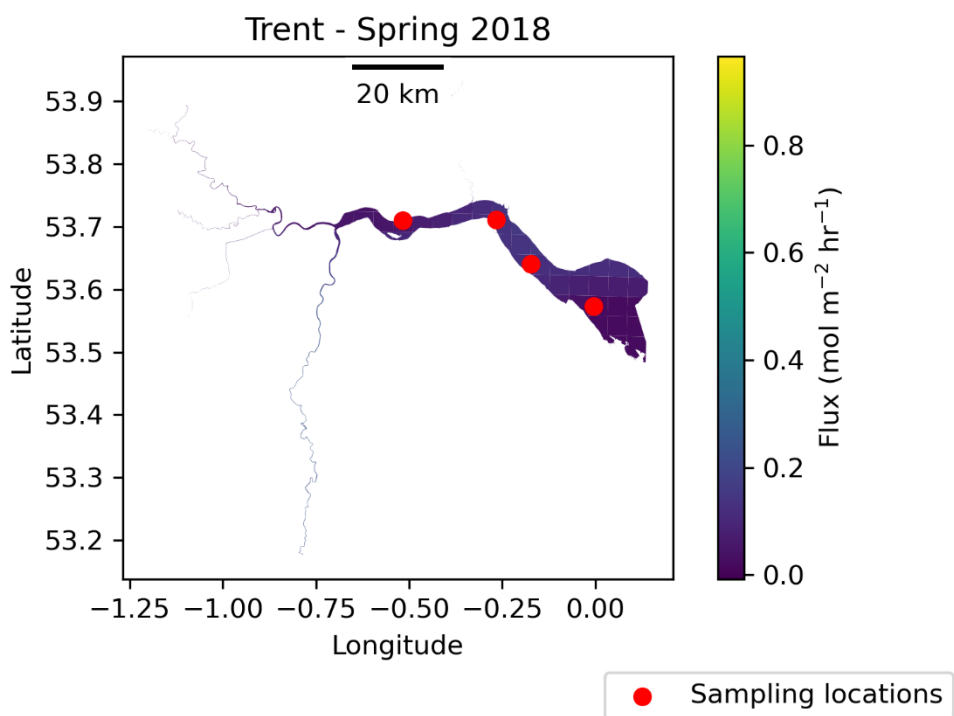
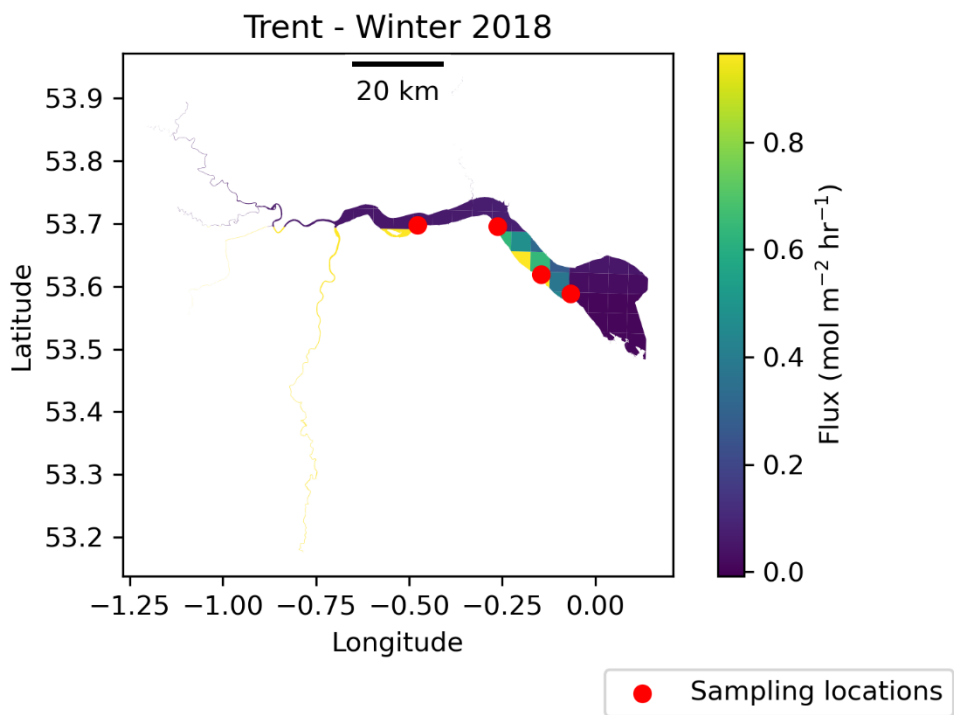




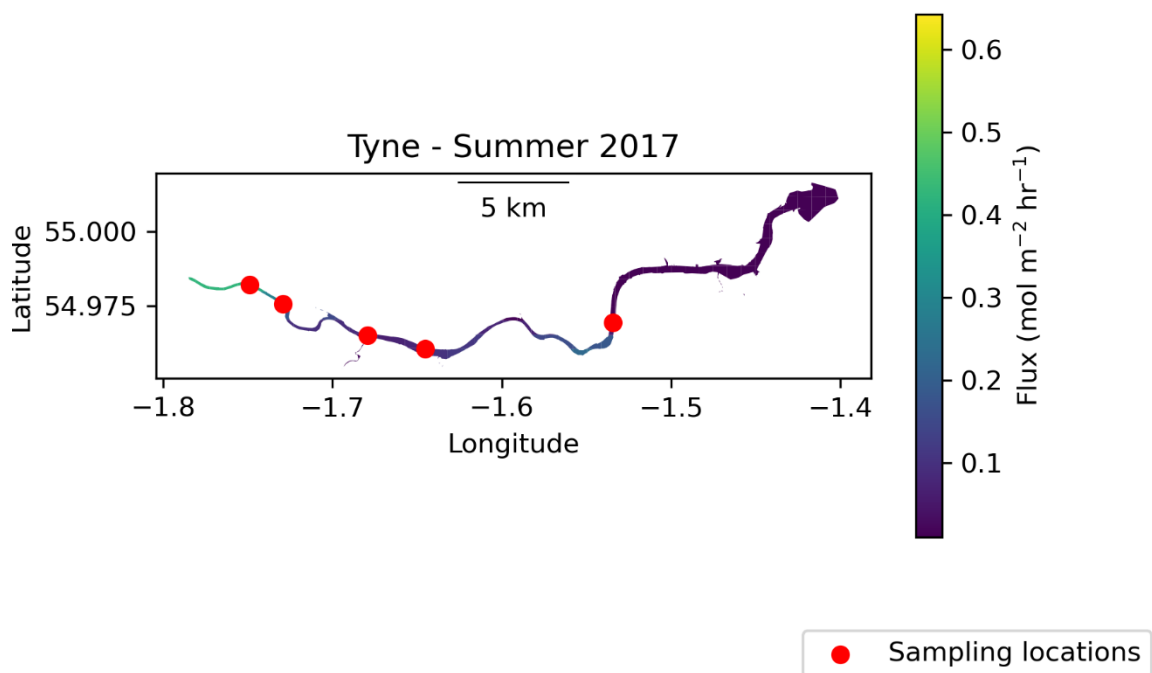
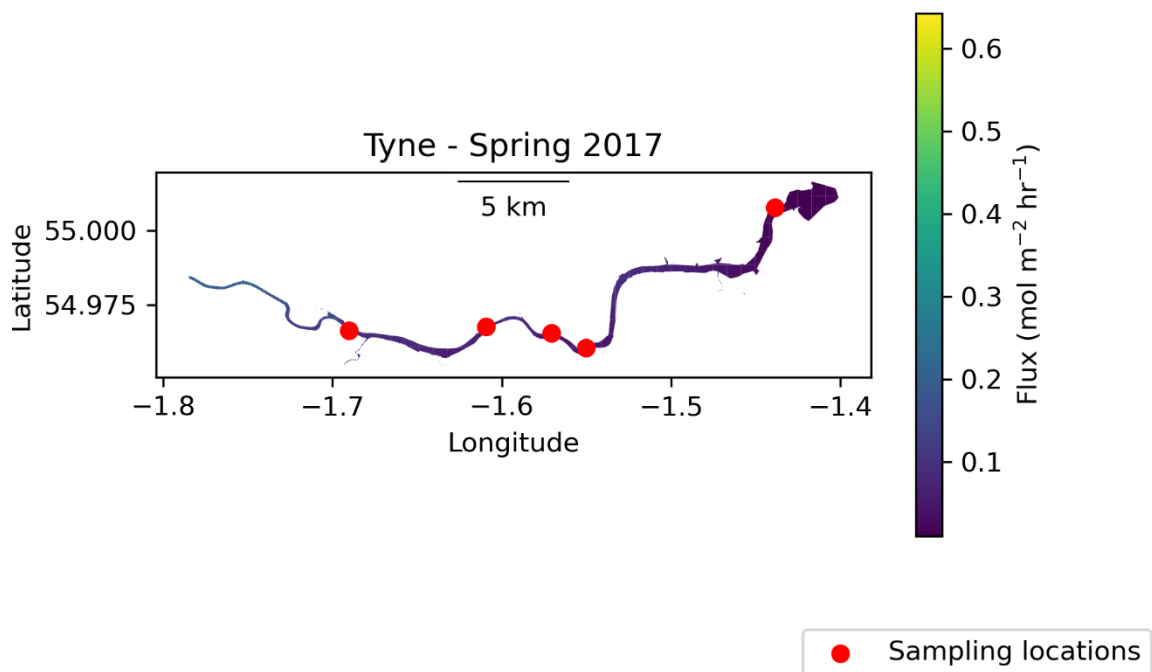


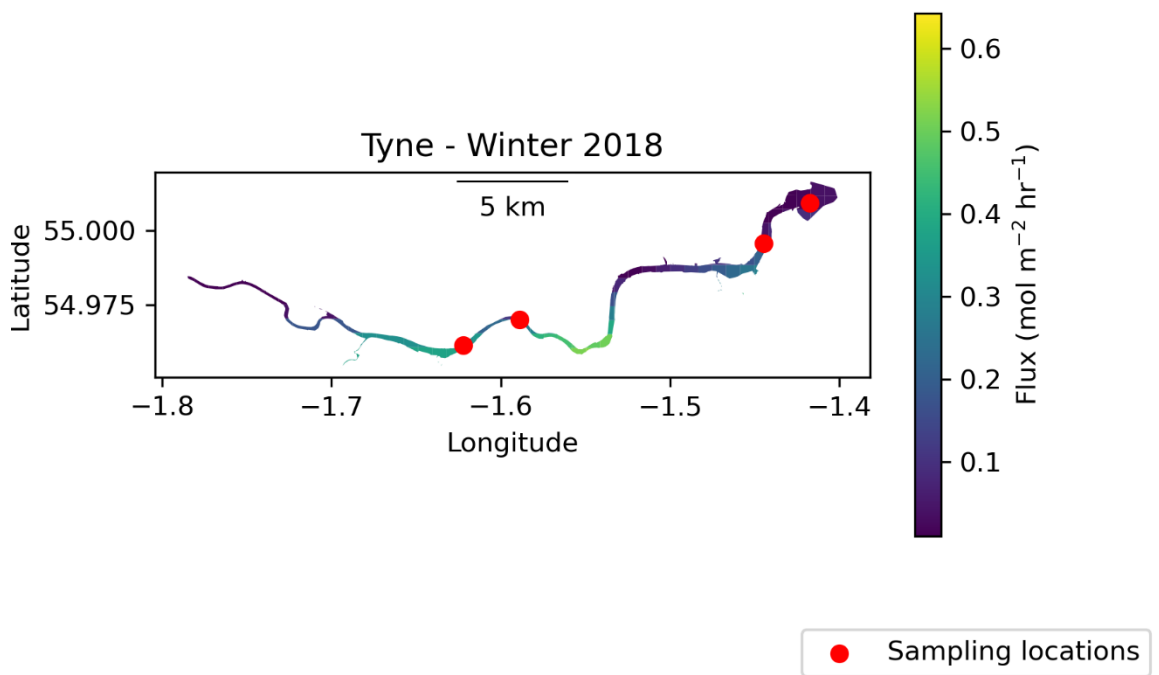
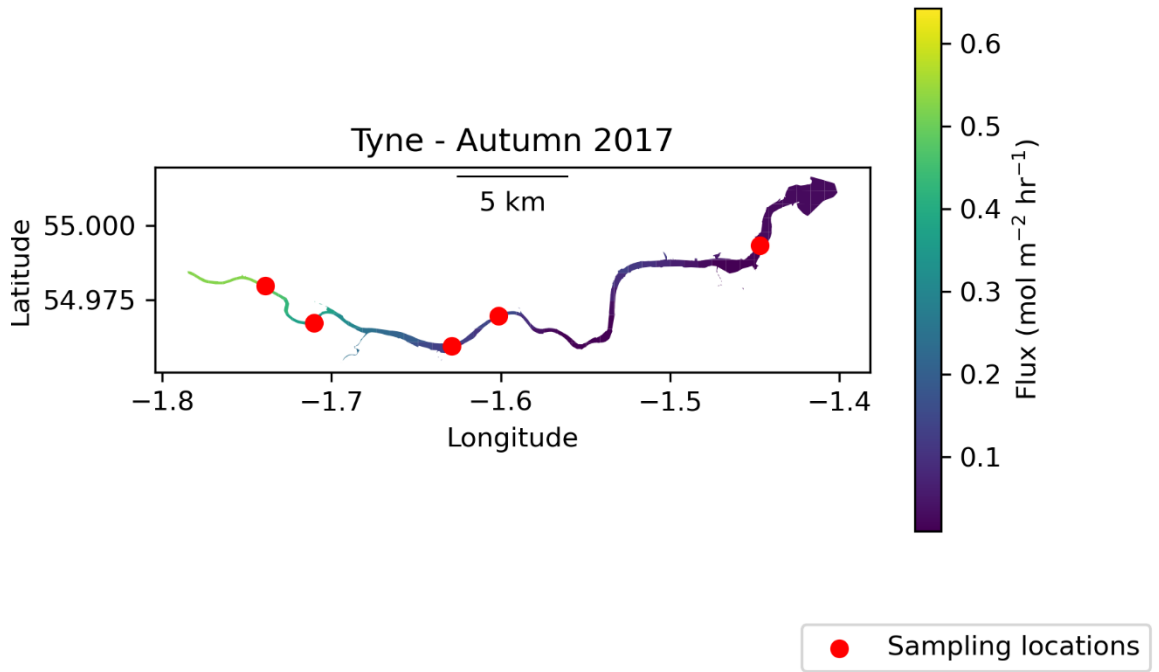
## A2.11 – Trent

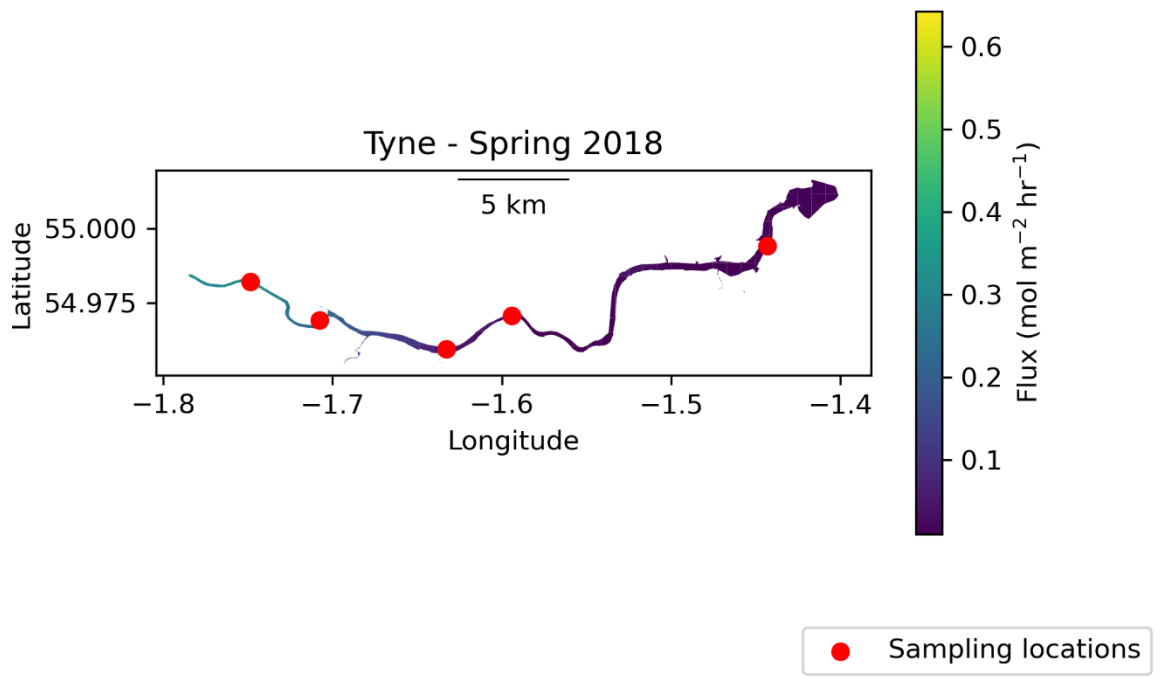




## A2.12 – Tyne







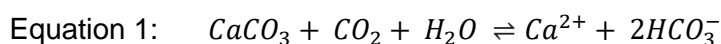
### A3 – Successful NEIF Grant application (2020) relating to Chapter 4

#### Attributing inorganic carbon and alkalinity sources in UK estuaries

##### Introduction

Carbon dioxide (CO<sub>2</sub>) is an important radiatively-active ‘greenhouse’ gas, whose anthropogenic increase in atmospheric concentration since preindustrial times has substantially contributed to changes in the earth’s climate. Accurate quantification and understanding of the sinks and sources of atmospheric CO<sub>2</sub> is fundamental to our ability to understand the current climate, to model future changes, and to understand the potential impact of mitigation strategies. Estuaries are supersaturated with CO<sub>2</sub> and outgas 0.25 ± 0.25 Pg C yr<sup>-1</sup> to the atmosphere (Regnier et al., 2013), potentially negating the coastal ocean CO<sub>2</sub> sink (Borges et al., 2006). Clearly, this estuarine outgassing term is highly uncertain. This uncertainty results both from the heterogeneity of coastal systems, and from the small number of estuaries that have been sampled. Furthermore, there is an “absence of independent evidence” concerning any changes in estuarine-atmosphere CO<sub>2</sub> flux since the preindustrial (Regnier et al., 2013), so globally-important budgets, such as the Global Carbon Budget 2019, assume there has been no anthropogenic perturbation to estuarine CO<sub>2</sub> emissions (Friedlingstein et al., 2019; Regnier et al., 2013). It is therefore a priority to determine the magnitude of the estuarine CO<sub>2</sub> source, and to attribute that inorganic carbon to natural and anthropogenic sources.

A number of studies have reported heterogeneity between estuaries, particularly in terms of their loads of alkalinity (A<sub>T</sub>) and dissolved inorganic carbon (DIC): two commonly measured variables that enable the full characterisation of the carbonate system (Zeebe and Wolf-Gladrow, 2001). In particular, (McGrath et al., 2016, 2019) qualitatively observed that the gradient of the relationships between salinity and both A<sub>T</sub> and DIC in different estuaries is related to the presence of limestone in the catchment bedrock. They theorised that high DIC and A<sub>T</sub> concentrations at low salinities result from the weathering of carbonate bedrock (McGrath et al., 2019). This is highly plausible, given that calcium carbonate formation and dissolution can be described by:



Carbonate weathering is therefore likely to impact upon the carbonate chemistry of natural waters because each mole of CaCO<sub>3</sub> dissolved releases 1 mole of DIC and 2 moles of A<sub>T</sub> (Wolf-Gladrow et al., 2007), which decreases the partial pressure of CO<sub>2</sub> (pCO<sub>2</sub>) in the water, which in turn promotes the uptake of atmospheric CO<sub>2</sub> (Humphreys et al., 2018). However, as noted by (Schulte et al., 2011) and references therein, variability in within-catchment lithology, and the challenges associated with its measurement, hinder the use of concentrations of aqueous species to quantitatively attribute the DIC and alkalinity sources.

Sampling for stable/radiogenic isotopes has improved our ability to determine the source of a given constituent in solution. DIC and  $A_T$  are directly affected by carbonate weathering (Eq. 1), so analysis for  $\delta^{13}\text{C}$  DIC is a logical candidate. (Brunet et al., 2005) measured  $\delta^{13}\text{C}$  DIC in Patagonian rivers, but they were unable to quantitatively attribute the source of DIC because biogeochemical processes affect the isotopic signature of DIC, and it is not possible to distinguish between these processes and the geological source material by  $\delta^{13}\text{C}$  DIC alone. In particular,  $\delta^{13}\text{C}$  DIC is affected by precipitation, respiration,  $\text{CO}_2$  degassing, uptake of both natural and anthropogenic  $\text{CO}_2$ , and formation/remineralisation of organic matter, in addition to carbonate dissolution/precipitation (Schulte et al., 2011). Clearly, it is necessary to measure an additional signature to fully attribute the source.

A variety of additional geochemical parameters have been used in this context. (Hagedorn and Cartwright, 2010) used  $\delta^{13}\text{C}$  of DIC and of both dissolved and particulate organic carbon to determine that approximately 36% of the riverine DIC in the Australian Victorian Alps comes from carbonate weathering, despite less than 5% of the catchment bedrock being defined as carbonate. This result affirms the concerns of (Amiotte Suchet et al., 2003) of using only concentration relationships with bedrock classification schemes, as this does not necessarily reflect the chemical composition of rocks, nor their weathering efficiency.

A number of studies have recognised the value of strontium (Sr) isotopes as a geochemical tracer. Sr is a soluble trace element present in a wide range of rock types (McNutt, 2000). Sr is found at higher concentrations, but with a lower  $^{87}\text{Sr}/^{86}\text{Sr}$  signature in areas with carbonate bedrock (Blum and Erel, 2003). The  $^{87}\text{Sr}/^{86}\text{Sr}$  ratio has been used only a few times in combination with  $\delta^{13}\text{C}$  DIC, but these studies have been successful in attributing solutes to their sources in freshwater systems (Pawellekl et al., 2002; Wei et al., 2013). However, to our knowledge, no studies to date have attributed estuarine DIC and  $A_T$  to their sources.

### **Current work**

The NERC-funded LOCATE (Land-Ocean Carbon Transfer) programme (NE/N018087/1) sampled 16 UK estuaries seasonally for a range of variables during 2017-18 (Fig. 1). Ruth Matthews, a NERC-funded iCASE PhD student (NE/R007632/1), developed and conducted the  $A_T$  and DIC analysis, and provisional results suggest that differences in the carbonate system in these estuaries are strongly influenced by the catchment bedrock.

Looking at the salinity relationships with  $A_T$  and DIC respectively, there are three distinct patterns: decreasing  $A_T$  and DIC with salinity (A), increasing  $A_T$  and DIC with salinity (B), and a set of estuaries that switch between these regimes, increasing with salinity in Autumn/Winter, and decreasing in Spring (C). Subset C are of particular interest because their relationships of DIC and  $A_T$  with salinity suggest either a change in the carbon source, or, more likely, a change in the weathering rate and/or efficiency. Figure 2 gives examples of these patterns, for 4 estuaries which would be of particular interest to sample.



Figure 1 - Map of LOCATE sampling locations

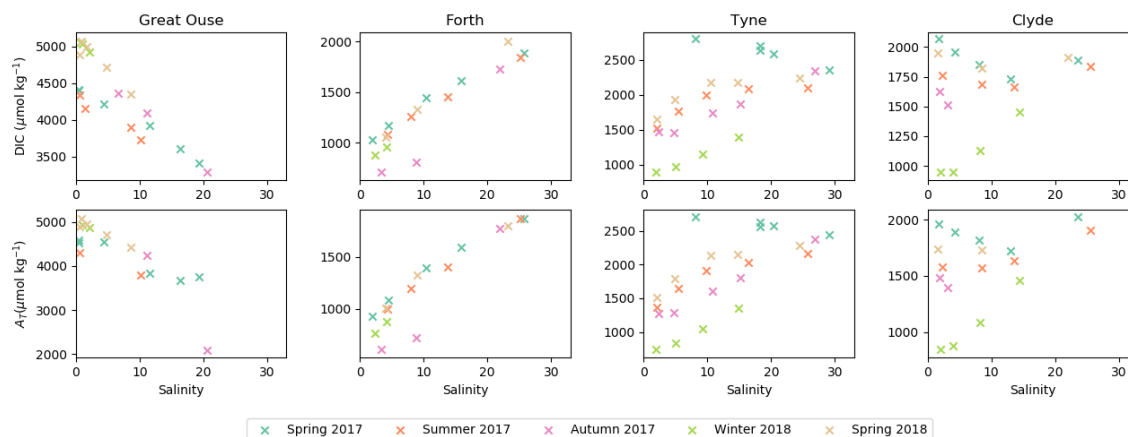


Figure 2 – DIC- and  $A_T$ -Salinity relationships for each of the 4 estuaries we propose to sample (Matthews et al., unpublished results).

### Proposed work

We propose to sample at 5 sites along the salinity gradient of each of four estuaries as part of Ruth Matthews' iCASE PhD research. Additionally, we plan to take a freshwater end-member and a sediment sample for both the main channel and any tributaries which feed into the main channel across the salinity gradient. We will sample on two occasions: in October 2020 and in April 2021, because it was during these months in 2017-18 that the

biggest differences in DIC and  $A_T$  were seen in subset C. We hypothesize that this may relate to changes in weathering efficiency under different seasonal rainfall regimes (Wei et al., 2013).

Three East coast estuaries (Great Ouse (A), Tyne (C) and Forth (B)) will be sampled because we are currently sampling along sections of the East coast of the UK for DIC and  $A_T$  seasonally, with further cruises planned in May, August and November 2020, and in February 2021 as part of both the Cefas Eutrophication Monitoring Programme and the International Beam Trawl Survey. Sampling will occur close to the mouths of each of these three estuaries on at least two occasions during the year. Coastal isotope samples from these cruises will place estuary samples in a wider context and enable us to propagate the impact of the carbon source into the coastal ocean. The Clyde (C) will also be sampled because of the striking gradient change seasonally (Fig. 2), in addition to its proximity to SUERC.

Figure 3 indicates the direction of expected changes in  $\delta^{13}\text{C}$  DIC and  $^{87}\text{Sr}/^{86}\text{Sr}$  in a water parcel for given processes: degassing/uptake of  $\text{CO}_2$ , net ecosystem production, and dissolution of carbonate bedrock.

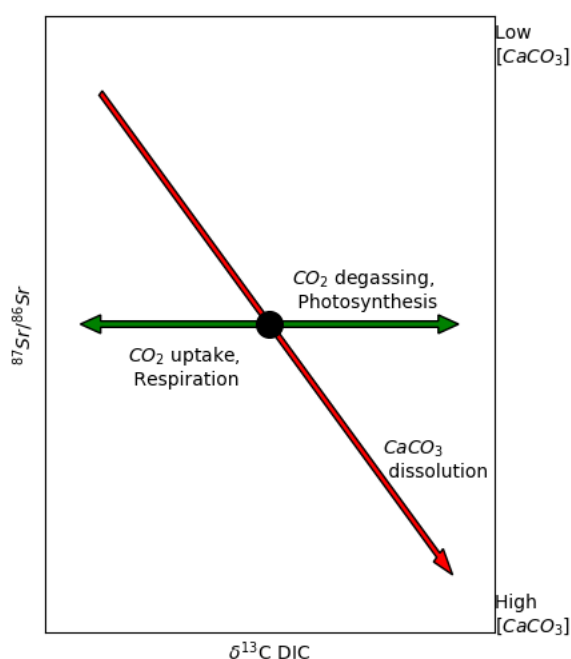


Figure 3 - Hypothesis schematic representing the direction of change in  $\delta^{13}\text{C}$  DIC and  $^{87}\text{Sr}/^{86}\text{Sr}$  resulting from carbonate dissolution (red arrow) and biological and gas exchange processes (green arrows) (Blum and Erel, 2003; Schulte et al., 2011) .

From this, we have developed the following hypotheses:

1. The Great Ouse (A) will have the lowest  $^{87}\text{Sr}/^{86}\text{Sr}$ , the highest  $\delta^{13}\text{C}$  DIC and the highest [Sr], followed by the Clyde and Tyne (C), and then the Forth (B); the high DIC and alkalinity at low salinity in the Great Ouse will be attributable to  $\text{CaCO}_3$  dissolution.
2. In April  $^{87}\text{Sr}/^{86}\text{Sr}$  will be lower and  $\delta^{13}\text{C}$  DIC will be higher to reflect greater weathering rate during prolonged rainfall. The weathering efficiency will see the greatest seasonal difference in the Clyde/Tyne.
3. [Sr] will decrease with salinity, but  $^{87}\text{Sr}/^{86}\text{Sr}$  will remain constant, as the Sr source remains the same, but its concentration is diluted by seawater.
4.  $\delta^{13}\text{C}$  DIC will decrease with salinity because of  $\text{CO}_2$  outgassing.

We will analyse samples for  $^{87}\text{Sr}/^{86}\text{Sr}$ , [Sr] and  $\delta^{13}\text{C}$  DIC as part of this proposal, and the concentrations of DIC,  $A_T$ ,  $\text{SO}_4^{2-}$  and inorganic nutrients at UEA. Including replicates, we aim to collect approximately 100 samples for each variable, with all samples collected by the end of April 2021.

#### A4 – $\delta^{13}\text{C}_{\text{DIC}}$ sampling, analysis and data

$\delta^{13}\text{C}_{\text{DIC}}$  samples were taken in duplicate following the procedure for DIC and Total Alkalinity sampling laid out in the Methods chapter. Each sample was analysed for  $^{13}\text{C} / ^{12}\text{C}$  using a VG Optima isotope ratio mass spectrometer at the Scottish Universities Environmental Research Centre (SUERC). SUERC uses their own standards (known as MAB3, NA and CA) to calibrate the results to the Vienna Pee Dee Belemnite international calibration standard (Table A5.1). The majority of samples were analysed in duplicate, in addition to having been sampled in duplicate, so many sampling sites/occasions have four values associated with them, providing the user with information about both the sampling quality and the analytical replicability. Measured sample data are provided in Table A5.2

Table A4.1 – SUERC calibration standards' certified values and measurement data

	$d^{13}\text{C}_{\text{DIC}}$ (‰)	Standard Deviation (‰)	No. points	Certified $d^{13}\text{C}_{\text{DIC}}$ (‰)
NA	-4.67	0.04	17	-4.67
CA	-24.29	0.07	8	-24.23
MAB3	2.50	0.05	8	2.48

Table A4.2 – Measured  $\delta^{13}\text{C}_{\text{DIC}}$  data for the estuaries sampled in this study. GO is the shortened form of Great Ouse. DUP indicates duplicated analysis.

Sample name	$d^{13}\text{C}_{\text{DIC}}$ (‰)
Great Ouse 1A 21.9.20	-12.6
GO 1A 21.9.20 DUP.	-12.8
GO 1B 21.9.20	-12.6
GO 1B 21.9.20 DUP.	-12.6
Great Ouse 2A 21.9.20	-11.6
GO 2A 21.9.20 DUP.	-11.6
GO 2B 21.9.20	-11.5
GO 2B 21.9.20 DUP	-11.6
Great Ouse 5A 21.9.20	-11.3
GO 5B 21.9.20	-11.4
GO 5B 21.9.20 DUP	-11.4
A Great Ouse 29.4.21	-11.2
B GO 29.4.21	-11.2

B GO 29.4.21 DUP	-11.3
CLYDE 1A 28.9.20	-10.6
CLYDE 1A 28.9.20DUP	-10.4
CLYDE 1B 28.9.20	-10.6
CLYDE 1B 28.9.20 DUP.	-10.6
A CLYDE 01.05.21	-9.3
A CLYDE 01.05.21 DUP.	-9.2
B CLYDE 01.05.21	-9.0
TYNE 1A 23.9.20	-9.8
TYNE 1A 23.9.20 DUP.	-9.6
TYNE 1B 23.9.20	-8.8
TYNE 2A 23.9.20	-10.1
TYNE 2A 23.9.20 DUP.	-10.1
TYNE 2B 23.9.20	-10.0
TYNE 2B 23.9.20 DUP.	-10.0
TYNE 5A 23.9.20	-3.8
TYNE 5A 23.9.20 DUP	-3.8
TYNE 5B 23.9.20	-3.8
A TYNE 30.4.21	-6.8
A TYNE 30.4.21 DUP.	-6.6
B TYNE 30.04.21	-6.5
B TYNE 30.04.21 DUP.	-6.6
FORTH 1A 25.9.20	-12.5
FORTH 1B 25.9.20	-11.7
FORTH 2A 25.9.20	-10.5
FORTH 2B 25.9.20	-10.7
FORTH 2B 25.9.20 DUP.	-10.7

FORTH 3A 25.9.20	-9.0
FORTH 3B 25.9.20	-9.2
FORTH 4A 25.9.20	-6.9
FORTH 4B 25.9.20	-6.9
FORTH 5A 25.9.20	-5.7
FORTH 5B 25.9.20	-5.7
FORTH 6A 25.9.20	-4.7
FORTH 6A 25.9.20 DUP.	-4.9
FORTH 6B 25.9.20	-4.7
A FORTH 01.5.21	-11.1
A FORTH 01.5.21 DUP.	-11.0
B FORTH 01.5.21	-11.3

**A5 – Equations for calculating proportion of sample from different end members  
(Magnone et al., 2019, Supplementary Information 2)**

In a three end-member system, the proportional contribution of each end member to the volume of a given water sample is represented by:

$$X_a + X_b + X_c = 1$$

where a, b and c denote the end members.

These proportional contributions are calculated using the following equations:

$$X_a = \frac{\alpha_{a.3}\beta_{a.1} - \alpha_{a.1}\beta_{a.3}}{\alpha_{a.1}\beta_{a.2} - \alpha_{a.2}\beta_{a.1}}$$

$$X_b = \frac{\alpha_{b.3}\beta_{b.1} - \alpha_{b.1}\beta_{b.3}}{\alpha_{b.1}\beta_{b.2} - \alpha_{b.2}\beta_{b.1}}$$

$$X_c = \frac{\alpha_{c.3}\beta_{c.1} - \alpha_{c.1}\beta_{c.3}}{\alpha_{c.1}\beta_{c.2} - \alpha_{c.2}\beta_{c.1}}$$

With  $\alpha$  and  $\beta$  defined as follows:

$$\alpha_{a.1} = ([^{86}\text{Sr}_b] - [^{86}\text{Sr}_c]) \left( \frac{^{87}\text{Sr}}{^{86}\text{Sr}} \right)_{\text{samp}} + ([^{87}\text{Sr}_b] - [^{87}\text{Sr}_c])$$

$$\alpha_{a.2} = ([^{86}\text{Sr}_a] - [^{86}\text{Sr}_c]) \left( \frac{^{87}\text{Sr}}{^{86}\text{Sr}} \right)_{\text{samp}} + ([^{87}\text{Sr}_a] - [^{87}\text{Sr}_c])$$

$$\alpha_{a.3} = [^{86}\text{Sr}_c] \left( \frac{^{87}\text{Sr}}{^{86}\text{Sr}} \right)_{\text{samp}} - [^{87}\text{Sr}_c]$$

$$\beta_{a.1} = ([\text{Na}_b] - [\text{Na}_c]) \left( \frac{[\text{Y}]}{[\text{Na}]} \right)_{\text{samp}} + ([\text{Y}_b] - [\text{Y}_c])$$

$$\beta_{a.2} = ([\text{Na}_a] - [\text{Na}_c]) \left( \frac{[\text{Y}]}{[\text{Na}]} \right)_{\text{samp}} + ([\text{Y}_a] - [\text{Y}_c])$$

$$\beta_{a.3} = [\text{Na}_c] \left( \frac{[\text{Y}]}{[\text{Na}]} \right)_{\text{samp}} - [\text{Y}_c]$$

$$\alpha_{b.1} = ([^{86}\text{Sr}_c] - [^{86}\text{Sr}_a]) \left( \frac{^{87}\text{Sr}}{^{86}\text{Sr}} \right)_{\text{samp}} + ([^{87}\text{Sr}_c] - [^{87}\text{Sr}_a])$$

$$\alpha_{b.2} = ([^{86}\text{Sr}_b] - [^{86}\text{Sr}_a]) \left( \frac{^{87}\text{Sr}}{^{86}\text{Sr}} \right)_{\text{samp}} + ([^{87}\text{Sr}_b] - [^{87}\text{Sr}_a])$$

$$\alpha_{b.3} = [^{86}\text{Sr}_a] \left( \frac{^{87}\text{Sr}}{^{86}\text{Sr}} \right)_{\text{samp}} - [^{87}\text{Sr}_a]$$

$$\beta_{b.1} = ([\text{Na}_c] - [\text{Na}_a]) \left( \frac{[\text{Y}]}{[\text{Na}]} \right)_{\text{samp}} + ([\text{Y}_c] - [\text{Y}_a])$$

$$\beta_{b.2} = ([\text{Na}_b] - [\text{Na}_a]) \left( \frac{[\text{Y}]}{[\text{Na}]} \right)_{\text{samp}} + ([\text{Y}_b] - [\text{Y}_a])$$

$$\beta_{b.3} = [\text{Na}_a] \left( \frac{[\text{Y}]}{[\text{Na}]} \right)_{\text{samp}} - [\text{Y}_a]$$

$$\alpha_{c.1} = ([^{86}\text{Sr}_a] - [^{86}\text{Sr}_b]) \left( \frac{^{87}\text{Sr}}{^{86}\text{Sr}} \right)_{\text{samp}} + ([^{87}\text{Sr}_a] - [^{87}\text{Sr}_b])$$

$$\alpha_{c.2} = ([^{86}\text{Sr}_c] - [^{86}\text{Sr}_b]) \left( \frac{^{87}\text{Sr}}{^{86}\text{Sr}} \right)_{\text{samp}} + ([^{87}\text{Sr}_c] - [^{87}\text{Sr}_b])$$

$$\alpha_{c.3} = [^{86}\text{Sr}_b] \left( \frac{^{87}\text{Sr}}{^{86}\text{Sr}} \right)_{\text{samp}} - [^{87}\text{Sr}_b]$$

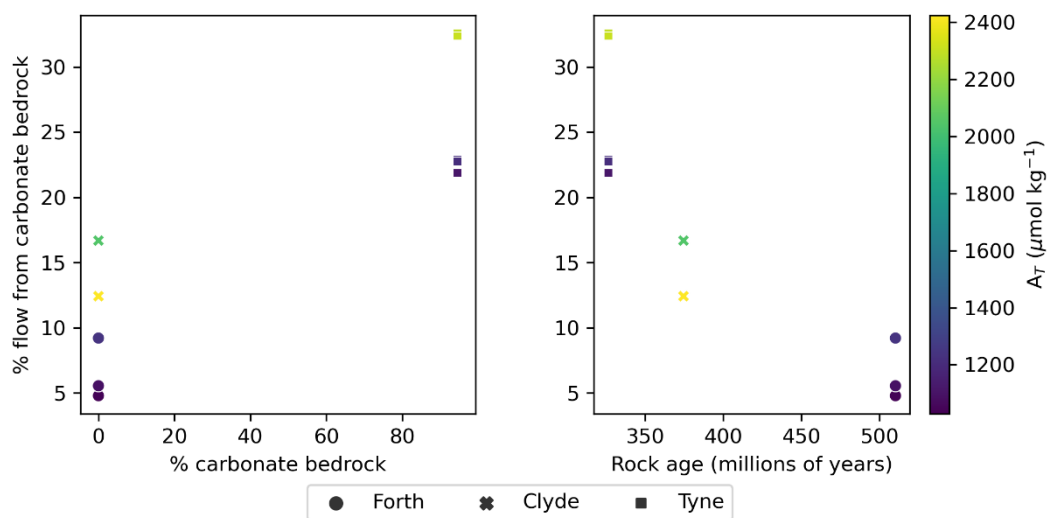
$$\beta_{c.1} = ([\text{Na}_a] - [\text{Na}_b]) \left( \frac{[\text{Y}]}{[\text{Na}]} \right)_{\text{samp}} + ([\text{Y}_a] - [\text{Y}_b])$$

$$\beta_{c.2} = ([\text{Na}_c] - [\text{Na}_b]) \left( \frac{[\text{Y}]}{[\text{Na}]} \right)_{\text{samp}} + ([\text{Y}_c] - [\text{Y}_b])$$

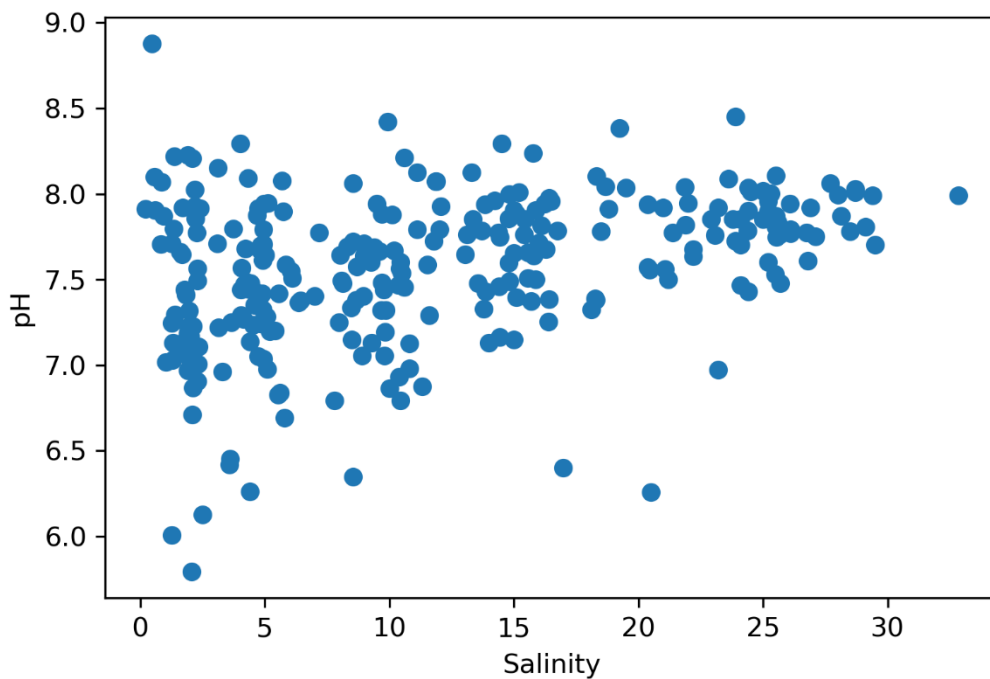
$$\beta_{c.3} = [\text{Na}_b] \left( \frac{[\text{Y}]}{[\text{Na}]} \right)_{\text{samp}} - [\text{Y}_b]$$

Where the subscript 'samp' denotes a given sample, and 'Y' denotes the concentration of cation Y, which in this case is either Ca or Mg.  $^{86}\text{Sr}$  is assumed to comprise 9.86% of total Sr concentration (De Laeter et al., 2003), and the isotope ratio  $^{87}\text{Sr}/^{86}\text{Sr}$  is used to calculate the concentration of  $^{87}\text{Sr}$  from  $^{86}\text{Sr}$ .

**A6 – Chapter 3 Figure 8 graph using Mg calculations rather than Ca calculations presented in the main body of the text**



**A7 – Variation in pH along the salinity gradient in all LOCATE estuaries 2017-18**



## List of Abbreviations/Terms

(IPCC) AR6	(Intergovernmental Panel on Climate Change) 6 <sup>th</sup> Assessment Report
A <sub>T</sub>	Total alkalinity
B	Volume of acid
B <sub>(tot)</sub>	Coulometer background measurement in total counts measured in the minute following the measurement
BGS	British Geological Survey
C	Carbon
C <sub>a</sub>	Concentration of acid
CaCO <sub>3</sub>	Calcium carbonate
CEH	Centre for Ecology and Hydrology
CO <sub>2</sub>	Carbon dioxide
CO <sub>3</sub> <sup>2-</sup>	Carbonate
CRM	Certified Reference Material
C <sub>T</sub>	Dissolved inorganic carbon
C <sub>T (tot)</sub>	C <sub>T</sub> measurement in total counts
C <sub>T crm</sub>	Certified CRM C <sub>T</sub> concentration
DEFRA	Department for Environment, Food and Rural Affairs
DIN	Dissolved inorganic nitrogen
DOC	Dissolved organic carbon
EM	End member
EMF	Electromotive force
FCO <sub>2</sub>	Water-to-air CO <sub>2</sub> flux
Free-CO <sub>2</sub>	C <sub>T</sub> in solution as CO <sub>2 (aq)</sub>
GIS	Geographical Information Systems
GPS	Global Positioning System
H <sub>2</sub> CO <sub>3</sub>	Carbonic acid
HCO <sub>3</sub> <sup>-</sup>	Bicarbonate
IPCC	Intergovernmental Panel on Climate Change
JNCC	Joint Nature Conservation Committee
k	Gas transfer velocity
K	Dissociation constant
K <sub>0</sub>	Solubility of CO <sub>2</sub>
LOAC	Land-Ocean Aquatic Continuum
LOCATE	Land Ocean CARbon TransfER
n	Proportionality constant between wind speed and k

NEIF	National Environmental Isotope Facility
NERC	Natural Environment Research Council
NPOC	Non-purgeable organic carbon
NRFA	National River Flow Archive
OC	Organic Carbon
PCHIP	Piecewise cubic hermite interpolating polynomial
pCO <sub>2</sub>	Partial pressure of carbon dioxide
pH	$-\log_{10}([H^+])$
PI	Principal Investigator
PIC	Particulate Inorganic Carbon
pK	Equilibrium constants, $K_0$ , $K_1$ , $K_2$ , $K_B$ , etc. for carbonate chemistry calculations are often denoted as 'pK', where $pK = -\log_{10}K$
pSal	Salinity
r <sup>2</sup>	Coefficient of determination
rw	Rainwater
Sc	Schmidt number
SRP	Soluble reactive phosphorus
t	Time
Td	Dewpoint temperature at 2 m
TIMS	Thermal Ionisation Mass Spectrometry
TOC	Total organic carbon
U <sub>10</sub>	Wind speed at 10 m
UEA	University of East Anglia
UK	United Kingdom
VIF	Variance inflation factor
VINDTA	Versatile INstrument for the Determination of Total inorganic carbon and titration Alkalinity
V <sub>sample</sub>	Volume of sample
δ <sup>13</sup> C <sub>DIC</sub>	Isotopic composition of dissolved inorganic carbon
Δv	User-determined change in a variable for finite-forward-differences uncertainty analysis
ε	Water vapour pressure
ρ	Density
σ	Standard deviation

## Reference list

- Abril, G., Borges, A.V., 2004. Carbon Dioxide and Methane Emissions from Estuaries, in: Tremblay, A., Varfalvy, L., Roehm, C., Garneau, M. (Eds.), *Greenhouse Gas Emissions — Fluxes and Processes*, Environmental Science. Springer, Berlin, Heidelberg, pp. 187–207. [https://doi.org/10.1007/978-3-540-26643-3\\_8](https://doi.org/10.1007/978-3-540-26643-3_8)
- Abril, G., Bouillon, S., Darchambeau, F., Teodoru, C.R., Marwick, T.R., Tamooh, F., Ochieng Omengo, F., Geeraert, N., Deirmendjian, L., Polsenaere, P., Borges, A.V., 2015. Technical Note: Large overestimation of  $p\text{CO}_2$  calculated from pH and alkalinity in acidic, organic-rich freshwaters. *Biogeosciences* 12, 67–78. <https://doi.org/10.5194/bg-12-67-2015>
- Abril, G., Commarieu, M.-V., Maro, D., Fontugne, M., Guérin, F., Etcheber, H., 2004. A massive dissolved inorganic carbon release at spring tide in a highly turbid estuary. *Geophysical Research Letters* 31. <https://doi.org/10.1029/2004GL019714>
- Abril, G., Etcheber, H., Delille, B., Frankignoulle, M., Borges, A., 2003. Carbonate dissolution in the turbid and eutrophic Loire estuary. *Mar. Ecol. Prog. Ser.* 259, 129–138. <https://doi.org/10.3354/meps259129>
- Addey, C.I., Jiang, Z.-P., Chen, J., Afelumo, A.J., Adesina, B.R., Osanyintuyi, A.J., 2021. The Variability of Partial Pressure of Carbon Dioxide ( $p\text{CO}_2$ ) in a River-Influenced Coastal Upwelling System: A Case of the Northeast Pacific Coast. *Journal of Geoscience and Environment Protection* 9, 133–148. <https://doi.org/10.4236/gep.2021.97009>
- Alduchov, O.A., Eskridge, R.E., 1996. Improved Magnus form approximation of saturation vapor pressure. *Journal of Applied Meteorology and Climatology* 35, 601–609.
- Alin, S.R., de Fátima F. L. Rasesa, M., Salimon, C.I., Richey, J.E., Holtgrieve, G.W., Krusche, A.V., Snidvongs, A., 2011. Physical controls on carbon dioxide transfer velocity and flux in low-gradient river systems and implications for regional carbon budgets. *Journal of Geophysical Research: Biogeosciences* 116. <https://doi.org/10.1029/2010JG001398>
- Amiotte Suchet, P., Probst, J.-L., Ludwig, W., 2003. Worldwide distribution of continental rock lithology: Implications for the atmospheric/soil  $\text{CO}_2$  uptake by continental weathering and alkalinity river transport to the oceans. *Global Biogeochemical Cycles* 17, 1038. <https://doi.org/10.1029/2002GB001891>
- Asmala, E., Autio, R., Kaartokallio, H., Pitkänen, L., Stedmon, C.A., Thomas, D.N., 2013. Bioavailability of riverine dissolved organic matter in three Baltic Sea estuaries and the effect of catchment land use. *Biogeosciences* 10, 6969–6986. <https://doi.org/10.5194/bg-10-6969-2013>
- Attenborough, D., 2021. Statement given at official COP26 opening ceremony.

- Attermeyer, K., Casas-Ruiz, J.P., Fuss, T., Pastor, A., Cauvy-Fraunié, S., Sheath, D., Nydahl, A.C., Doretto, A., Portela, A.P., Doyle, B.C., Simov, N., Gutmann Roberts, C., Niedrist, G.H., Timoner, X., Evtimova, V., Barral-Fraga, L., Bašić, T., Audet, J., Deininger, A., Busst, G., Fenoglio, S., Catalán, N., de Eyto, E., Pilotto, F., Mor, J.-R., Monteiro, J., Fletcher, D., Noss, C., Colls, M., Nagler, M., Liu, L., Romero González-Quijano, C., Romero, F., Pansch, N., Ledesma, J.L.J., Pegg, J., Klaus, M., Freixa, A., Herrero Ortega, S., Mendoza-Lera, C., Bednařík, A., Fonvielle, J.A., Gilbert, P.J., Kenderov, L.A., Rulík, M., Bodmer, P., 2021. Carbon dioxide fluxes increase from day to night across European streams. *Commun Earth Environ* 2, 1–8. <https://doi.org/10.1038/s43247-021-00192-w>
- Bache, S.M., Wickham, H., Henry, L., Henry, M.L., 2022. Package ‘magrittr.’
- Bakker, D.C., Bange, H.W., Gruber, N., Johannessen, T., Upstill-Goddard, R.C., Borges, A.V., Delille, B., Loscher, C.R., Naqvi, S.W.A., Omar, A.M., 2014. Air-Sea Interactions of Natural Long-Lived Greenhouse in a Changing Gases Climate (CO<sub>2</sub>, N<sub>2</sub>O, CH<sub>4</sub>). Springer, Berlin, Heidelberg.
- Barnes, R.T., Raymond, P.A., 2009. The contribution of agricultural and urban activities to inorganic carbon fluxes within temperate watersheds. *Chemical Geology* 266, 318–327. <https://doi.org/10.1016/j.chemgeo.2009.06.018>
- Battin, T.J., Kaplan, L.A., Findlay, S., Hopkinson, C.S., Marti, E., Packman, A.I., Newbold, J.D., Sabater, F., 2008. Biophysical controls on organic carbon fluxes in fluvial networks. *Nature Geosci* 1, 95–100. <https://doi.org/10.1038/ngeo101>
- Battin, T.J., Luysaert, S., Kaplan, L.A., Aufdenkampe, A.K., Richter, A., Tranvik, L.J., 2009. The boundless carbon cycle. *Nature Geosci* 2, 598–600. <https://doi.org/10.1038/ngeo618>
- Bauer, J.E., Cai, W.-J., Raymond, P.A., Bianchi, T.S., Hopkinson, C.S., Regnier, P.A.G., 2013. The changing carbon cycle of the coastal ocean. *Nature* 504, 61–70. <https://doi.org/10.1038/nature12857>
- Berner, R.A., Lasaga, A.C., Garrels, R.M., 1983. Carbonate-silicate geochemical cycle and its effect on atmospheric carbon dioxide over the past 100 million years. *American Journal of Science* 283, 641–683. <https://doi.org/10.2475/ajs.283.7.641>
- Biraud, S., Ciais, P., Ramonet, M., Simmonds, P., Kazan, V., Monfray, P., O’Doherty, S., Spain, T.G., Jennings, S.G., 2000. European greenhouse gas emissions estimated from continuous atmospheric measurements and radon 222 at Mace Head, Ireland. *Journal of Geophysical Research: Atmospheres* 105, 1351–1366. <https://doi.org/10.1029/1999JD900821>
- Birck, J.L., 1986. Precision K-Rb-Sr isotopic analysis: application to Rb-Sr chronology. *Chemical geology* 56, 73–83.
- Blum, J.D., Erel, Y., 2003. Radiogenic Isotopes in Weathering and Hydrology, in: *Treatise on Geochemistry*. <https://doi.org/10.1016/B0-08-043751-6/05082-9>

- Borges, A., Abril, G., 2012. Carbon Dioxide and Methane Dynamics in Estuaries, in: Wolanski, E., McLusky, D. (Eds.), *Treatise on Estuarine and Coastal Science, Biogeochemistry*. Academic Press, Waltham, United States, pp. 119–161. <https://doi.org/10.1016/B978-0-12-374711-2.00504-0>
- Borges, A.V., 2005. Do we have enough pieces of the jigsaw to integrate CO<sub>2</sub> fluxes in the coastal ocean? *Estuaries* 28, 3–27. <https://doi.org/10.1007/BF02732750>
- Borges, A.V., Delille, B., Frankignoulle, M., 2005. Budgeting sinks and sources of CO<sub>2</sub> in the coastal ocean: Diversity of ecosystems counts. *Geophysical Research Letters* 32, 1–4. <https://doi.org/10.1029/2005GL023053>
- Borges, A.V., Delille, B., Schiettecatte, L.-S., Gazeau, F., Abril, G., Frankignoulle, M., 2004. Gas transfer velocities of CO<sub>2</sub> in three European estuaries (Randers Fjord, Scheldt, and Thames). *Limnology and Oceanography* 49, 1630–1641. <https://doi.org/10.4319/lo.2004.49.5.1630>
- Borges, A.V., Frankignoulle, M., 2003. Distribution of surface carbon dioxide and air-sea exchange in the English Channel and adjacent areas. *Journal of Geophysical Research: Oceans* 108, 1–14. <https://doi.org/10.1029/2000JC000571>
- Borges, A.V., Frankignoulle, M., 2002. Distribution and air-water exchange of carbon dioxide in the Scheldt plume off the Belgian coast. *Biogeochemistry* 59, 41–67.
- Borges, A.V., Schiettecatte, L.-S., Abril, G., Delille, B., Gazeau, F., 2006. Carbon dioxide in European coastal waters. *Estuarine, Coastal and Shelf Science, Trace gases in the European coastal zone* 70, 375–387. <https://doi.org/10.1016/j.ecss.2006.05.046>
- Bozec, Y., Cariou, T., Macé, E., Morin, P., Thuillier, D., Vernet, M., 2012. Seasonal dynamics of air-sea CO<sub>2</sub> fluxes in the inner and outer Loire estuary (NW Europe). *Estuarine, Coastal and Shelf Science, Recent advances in biogeochemistry of coastal seas and continental shelves* 100, 58–71. <https://doi.org/10.1016/j.ecss.2011.05.015>
- British Geological Survey, 2008. BGS Geology 625K.
- Brunet, F., Gaiero, D., Probst, J.L., Depetris, P.J., Lafaye, F.G., Stille, P., 2005.  $\delta^{13}\text{C}$  tracing of dissolved inorganic carbon sources in patagonian rivers (Argentina). *Hydrological Processes*. <https://doi.org/10.1002/hyp.5973>
- Cai, W.-J., 2011. Estuarine and Coastal Ocean Carbon Paradox: CO<sub>2</sub> Sinks or Sites of Terrestrial Carbon Incineration? *Annual Review of Marine Science* 3, 123–145. <https://doi.org/10.1146/annurev-marine-120709-142723>
- Cai, W.-J., 2003. Riverine inorganic carbon flux and rate of biological uptake in the Mississippi River plume. *Geophysical Research Letters* 30, 1–4. <https://doi.org/10.1029/2002GL016312>
- Cai, W.-J., Dai, M., Wang, Y., Zhai, W., Huang, T., Chen, S., Zhang, F., Chen, Z., Wang, Z., 2004. The biogeochemistry of inorganic carbon and nutrients in the Pearl River

- estuary and the adjacent Northern South China Sea. *Continental Shelf Research* 24, 1301–1319. <https://doi.org/10.1016/j.csr.2004.04.005>
- Cai, W.-J., Feely, R.A., Testa, J.M., Li, M., Evans, W., Alin, S.R., Xu, Y.-Y., Pelletier, G., Ahmed, A., Greeley, D.J., Newton, J.A., Bednaršek, N., 2021. Natural and Anthropogenic Drivers of Acidification in Large Estuaries. *Annual Review of Marine Science* 13, 23–55. <https://doi.org/10.1146/annurev-marine-010419-011004>
- Cai, W.-J., Guo, X., Chen, C.-T.A., Dai, M., Zhang, L., Zhai, W., Lohrenz, S.E., Yin, K., Harrison, P.J., Wang, Y., 2008. A comparative overview of weathering intensity and  $\text{HCO}_3^-$  flux in the world's major rivers with emphasis on the Changjiang, Huanghe, Zhujiang (Pearl) and Mississippi Rivers. *Continental Shelf Research, Coastal Ecosystem Responses to Changing Nutrient Inputs from Large Temperate and Subtropical Rivers* 28, 1538–1549. <https://doi.org/10.1016/j.csr.2007.10.014>
- Cai, W.-J., Wang, Y., 1998. The chemistry, fluxes, and sources of carbon dioxide in the estuarine waters of the Satilla and Altamaha Rivers, Georgia. *Limnology and Oceanography* 43, 657–668. <https://doi.org/10.4319/lo.1998.43.4.0657>
- Cai, W.-J., Wang, Y., Hodson, R.E., 1998. Acid-base properties of dissolved organic matter in the estuarine waters of Georgia, USA. *Geochimica et Cosmochimica Acta* 62, 473–483.
- Canadell, J.G., Monteiro, P.M.S., Costa, M.H., Cotrim da Cunha, L., Cox, P.M., Eliseev, A.V., Henson, S., Ishii, M., Jaccard, S., Koven, C., Lohila, A., Patra, P.K., Piao, S., Rogelj, J., Syampungani, S., Zaehle, S., Zickfeld, K., 2021. Global Carbon and Other Biogeochemical Cycles and Feedbacks, in: Masson-Delmotte, V., Zhai, P., Pirani, A., Connors, S.L., Péan, C., Berger, S., Caud, N., Chen, Y., Goldfarb, L., Gomis, M.I., Huang, M., Leitzell, K., Lonnoy, E., Matthews, J.B.R., Maycock, T.K., Waterfield, T., Yelekçi, O., Yu, R., Zhou, B. (Eds.), *Climate Change 2021: The Physical Science Basis, Contribution of Working Group I to the Sixth Assessment Report of the Intergovernmental Panel on Climate Change*. Cambridge University Press, Cambridge, United Kingdom and New York, NY, USA, pp. 673–816.
- Carstensen, J., Chierici, M., Gustafsson, B.G., Gustafsson, E., 2018. Long-Term and Seasonal Trends in Estuarine and Coastal Carbonate Systems. *Global Biogeochemical Cycles* 32, 497–513. <https://doi.org/10.1002/2017GB005781>
- Cerco, C.F., 1989. Estimating estuarine reaeration rates. *Journal of Environmental Engineering* 115, 1066–1070.
- Chen, C.-T.A., Borges, A.V., 2009. Reconciling opposing views on carbon cycling in the coastal ocean: Continental shelves as sinks and near-shore ecosystems as sources of atmospheric  $\text{CO}_2$ . *Deep Sea Research Part II: Topical Studies in Oceanography* 56, 578–590. <https://doi.org/10.1016/j.dsr2.2009.01.001>

- Chen, C.-T.A., Huang, T.-H., Chen, Y.-C., Bai, Y., He, X., Kang, Y., 2013. Air–sea exchanges of CO<sub>2</sub> in the world’s coastal seas. *Biogeosciences* 10, 6509–6544. <https://doi.org/10.5194/bg-10-6509-2013>
- Chen, C.-T.A., Huang, T.-H., Fu, Y.-H., Bai, Y., He, X., 2012. Strong sources of CO<sub>2</sub> in upper estuaries become sinks of CO<sub>2</sub> in large river plumes. *Current Opinion in Environmental Sustainability, Carbon and nitrogen cycles* 4, 179–185. <https://doi.org/10.1016/j.cosust.2012.02.003>
- Chen, C.-T.A., Wang, S.-L., 1999. Carbon, alkalinity and nutrient budgets on the East China Sea continental shelf. *Journal of Geophysical Research: Oceans* 104, 20675–20686. <https://doi.org/10.1029/1999JC900055>
- Ciais, P., Yao, Y., Gasser, T., Baccini, A., Wang, Y., Lauerwald, R., Peng, S., Bastos, A., Li, W., Raymond, P.A., Canadell, J.G., Peters, G.P., Andres, R.J., Chang, J., Yue, C., Dolman, A.J., Haverd, V., Hartmann, J., Laruelle, G., Konings, A.G., King, A.W., Liu, Y., Luyssaert, S., Maignan, F., Patra, P.K., Peregon, A., Regnier, P., Pongratz, J., Poulter, B., Shvidenko, A., Valentini, R., Wang, R., Broquet, G., Yin, Y., Zscheischler, J., Guenet, B., Goll, D.S., Ballantyne, A.-P., Yang, H., Qiu, C., Zhu, D., 2021. Empirical estimates of regional carbon budgets imply reduced global soil heterotrophic respiration. *National Science Review* 8, 1–14. <https://doi.org/10.1093/nsr/nwaa145>
- Cloern, J.E., 1996. Phytoplankton bloom dynamics in coastal ecosystems: A review with some general lessons from sustained investigation of San Francisco Bay, California. *Reviews of Geophysics* 34, 127–168. <https://doi.org/10.1029/96RG00986>
- Cole, J.J., Prairie, Y.T., Caraco, N.F., McDowell, W.H., Tranvik, L.J., Striegl, R.G., Duarte, C.M., Kortelainen, P., Downing, J.A., Middelburg, J.J., Melack, J., 2007. Plumbing the global carbon cycle: Integrating inland waters into the terrestrial carbon budget. *Ecosystems* 10, 171–184. <https://doi.org/10.1007/s10021-006-9013-8>
- de la Paz, M., Padín, X.A., Ríos, A.F., Pérez, F.F., 2010. Surface fCO<sub>2</sub> variability in the Loire plume and adjacent shelf waters: High spatio-temporal resolution study using ships of opportunity. *Marine Chemistry* 118, 108–118. <https://doi.org/10.1016/j.marchem.2009.11.004>
- De Laeter, J.R., Böhlke, J.K., De Bièvre, P., Hidaka, H., Peiser, H.S., Rosman, K.J.R., Taylor, P.D.P., 2003. Atomic weights of the elements. Review 2000 (IUPAC Technical Report). *Pure and applied chemistry* 75, 683–800.
- Defense Mapping Agency, 1992. Digital chart of the world.
- DEFRA, 2022. UKEAP: Precip-Net [WWW Document]. URL [https://uk-air.defra.gov.uk/data/data\\_selector](https://uk-air.defra.gov.uk/data/data_selector) (accessed 10.21.22).

- Delaigue, L., Thomas, H., Mucci, A., 2020. Spatial variations in CO<sub>2</sub> fluxes in the Saguenay Fjord (Quebec, Canada) and results of a water mixing model. *Biogeosciences* 17, 547–566.
- Dickson, A.G., 1990. Standard potential of the reaction: AgCl(s) + 12H<sub>2</sub>(g) = Ag(s) + HCl(aq), and the standard acidity constant of the ion HSO<sub>4</sub><sup>-</sup> in synthetic sea water from 273.15 to 318.15 K. *The Journal of Chemical Thermodynamics* 22, 113–127. [https://doi.org/10.1016/0021-9614\(90\)90074-Z](https://doi.org/10.1016/0021-9614(90)90074-Z)
- Dickson, A.G., 1981. An exact definition of total alkalinity and a procedure for the estimation of alkalinity and total inorganic carbon from titration data. *Deep Sea Research Part A. Oceanographic Research Papers* 28, 609–623. [https://doi.org/10.1016/0198-0149\(81\)90121-7](https://doi.org/10.1016/0198-0149(81)90121-7)
- Dickson, A. G., Sabine, C.L., Christian, J.R., 2007. Guide to best practices for ocean CO<sub>2</sub> measurements, PICES Special Publication. North Pacific Marine Science Organization.
- Dlugokencky, E.J., Mund, J.W., Crotwell, A.M., Crotwell, M.J., Thoning, K.W., 2021. Atmospheric Carbon Dioxide Dry Air Mole Fractions from the NOAA GML Carbon Cycle Cooperative Global Air Sampling Network, 1968-2019, Version: 2021-02.
- Drake, T.W., Raymond, P.A., Spencer, R.G.M., 2018a. Terrestrial carbon inputs to inland waters: A current synthesis of estimates and uncertainty. *Limnology and Oceanography Letters* 3, 132–142. <https://doi.org/10.1002/lol2.10055>
- Drake, T.W., Tank, S.E., Zhulidov, A.V., Holmes, R.M., Gurtovaya, T., Spencer, R.G.M., 2018b. Increasing Alkalinity Export from Large Russian Arctic Rivers. *Environ. Sci. Technol.* 52, 8302–8308. <https://doi.org/10.1021/acs.est.8b01051>
- Dürr, H.H., Laruelle, G.G., van Kempen, C.M., Slomp, C.P., Meybeck, M., Middelkoop, H., 2011. Worldwide Typology of Nearshore Coastal Systems: Defining the Estuarine Filter of River Inputs to the Oceans. *Estuaries and Coasts* 34, 441–458. <https://doi.org/10.1007/s12237-011-9381-y>
- Eckardt, H., Chenery, C., Booth, P., Evans, J.A., Lamb, A., Müldner, G., 2009. Oxygen and strontium isotope evidence for mobility in Roman Winchester. *Journal of Archaeological Science* 36, 2816–2825. <https://doi.org/10.1016/j.jas.2009.09.010>
- Environment Agency, 2018. Water Quality Archive 2017-18.
- Evans, J., Montgomery, J., Wildman, G., 2009. Isotope domain mapping of <sup>87</sup>Sr/<sup>86</sup>Sr biosphere variation, UK. Scotland. *Journal of The Geological Society, London* 166, 617–631.
- Firke, S., 2021. Simple tools for examining and cleaning dirty data [R package janitor version 2.1. 0].
- Fofonoff, N.P., Millard Jr, R., C, 1983. Algorithms for computation of fundamental properties of seawater, UNESCO Technical Papers in Marine Sciences. UNESCO, Paris, France.

- Fox, J., Weisberg, S., Adler, D., Bates, D., Baud-Bovy, G., Ellison, S., Firth, D., Friendly, M., Gorjanc, G., Graves, S., 2012. Package 'car.' Vienna: R Foundation for Statistical Computing 16.
- Frankignoulle, M., 1988. Field measurements of air-sea CO<sub>2</sub> exchange. *Limnology and Oceanography* 33, 313–322. <https://doi.org/10.4319/lo.1988.33.3.0313>
- Frankignoulle, M., Abril, G., Borges, A.V., Bourge, I., Canon, C., Delille, B., Libert, E., Theate, J.-M., 1998. Carbon Dioxide Emission from European Estuaries. *Science* 282, 434–436. <https://doi.org/10.1126/science.282.5388.434>
- Friedlingstein, P., O'Sullivan, M., Jones, M.W., Andrew, R.M., Gregor, L., Hauck, J., Le Quéré, C., Lujikx, I.T., Olsen, A., Peters, G.P., Peters, W., Pongratz, J., Schwingshackl, C., Sitch, S., Canadell, J.G., Ciais, P., Jackson, R.B., Alin, S.R., Alkama, R., Arneeth, A., Arora, V.K., Bates, N.R., Becker, M., Bellouin, N., Bittig, H.C., Bopp, L., Chevallier, F., Chini, L.P., Cronin, M., Evans, W., Falk, S., Feely, R.A., Gasser, T., Gehlen, M., Gkritzalis, T., Gloege, L., Grassi, G., Gruber, N., Gürses, Ö., Harris, I., Hefner, M., Houghton, R.A., Hurtt, G.C., Iida, Y., Ilyina, T., Jain, A.K., Jersild, A., Kadono, K., Kato, E., Kennedy, D., Klein Goldewijk, K., Knauer, J., Korsbakken, J.I., Landschützer, P., Lefèvre, N., Lindsay, K., Liu, J., Liu, Z., Marland, G., Mayot, N., McGrath, M.J., Metz, N., Monacci, N.M., Munro, D.R., Nakaoka, S.-I., Niwa, Y., O'Brien, K., Ono, T., Palmer, P.I., Pan, N., Pierrot, D., Pockock, K., Poulter, B., Resplandy, L., Robertson, E., Rödenbeck, C., Rodriguez, C., Rosan, T.M., Schwinger, J., Séférian, R., Shutler, J.D., Skjelvan, I., Steinhoff, T., Sun, Q., Sutton, A.J., Sweeney, C., Takao, S., Tanhua, T., Tans, P.P., Tian, X., Tian, H., Tilbrook, B., Tsujino, H., Tubiello, F., van der Werf, G.R., Walker, A.P., Wanninkhof, R., Whitehead, C., Willstrand Wranne, A., Wright, R., Yuan, W., Yue, C., Yue, X., Zaehle, S., Zeng, J., Zheng, B., 2022. Global Carbon Budget 2022. *Earth Syst. Sci. Data* 14, 4811–4900. <https://doi.org/10.5194/essd-14-4811-2022>
- Fritsch, F.N., Butland, J., 1984. A Method for Constructing Local Monotone Piecewise Cubic Interpolants. *SIAM J. Sci. and Stat. Comput.* 5, 300–304. <https://doi.org/10.1137/0905021>
- GADM, 2022. United Kingdom shapefile (Version 4.1).
- Gaillardet, J., Calmels, D., Romero-Mujalli, G., Zakharova, E., Hartmann, J., 2019. Global climate control on carbonate weathering intensity. *Chemical Geology, Evolution of Carbonate and Karst Critical Zones* 527, 1–11. <https://doi.org/10.1016/j.chemgeo.2018.05.009>
- García-Martín, E.E., Sanders, R., Evans, C.D., Kitidis, V., Lapworth, D.J., Rees, A.P., Spears, B.M., Tye, A., Williamson, J.L., Balfour, C., Best, M., Bowes, M., Breimann, S., Brown, I.J., Burden, A., Callaghan, N., Felgate, S.L., Fishwick, J., Fraser, M., Gibb, S.W., Gilbert, P.J., Godsell, N., Gomez-Castillo, A.P.,

- Hargreaves, G., Jones, O., Kennedy, P., Lichtschlag, A., Martin, A., May, R., Mawji, E., Mounteney, I., Nightingale, P.D., Olszewska, J.P., Painter, S.C., Pearce, C.R., Pereira, M.G., Peel, K., Pickard, A., Stephens, J.A., Stinchcombe, M., Williams, P., Woodward, E.M.S., Yarrow, D., Mayor, D.J., 2021. Contrasting Estuarine Processing of Dissolved Organic Matter Derived From Natural and Human-Impacted Landscapes. *Global Biogeochemical Cycles* 35, e2021GB007023. <https://doi.org/10.1029/2021GB007023>
- Garrels, R.M., Berner, R.A., 1983. The Global Carbonate-Silicate Sedimentary System — Some Feedback Relations, in: Westbroek, P., de Jong, E.W. (Eds.), *Biom mineralization and Biological Metal Accumulation: Biological and Geological Perspectives Papers Presented at the Fourth International Symposium on Biom mineralization*, Renesse, The Netherlands, June 2–5, 1982. Springer, Dordrecht, pp. 73–87. [https://doi.org/10.1007/978-94-009-7944-4\\_6](https://doi.org/10.1007/978-94-009-7944-4_6)
- Gattuso, J.-P., Frankignoulle, M., Wollast, R., 1998. Carbon and Carbonate Metabolism in Coastal Aquatic Ecosystems. *Annual Review of Ecology and Systematics* 29, 405–434.
- GCP, 2021. Global Carbon Project (GCP) [WWW Document]. URL <https://www.globalcarbonproject.org/> (accessed 4.17.23).
- Geyer, W.R., 1993. The Importance of Suppression of Turbulence by Stratification on the Estuarine Turbidity Maximum. *Estuaries* 16, 113. <https://doi.org/10.2307/1352769>
- Ghosh, J., Chakraborty, K., Chanda, A., Akhand, A., Bhattacharya, T., Das, S., Das, I., Hazra, S., Choudhury, S.B., Wells, M., 2021. Outwelling of total alkalinity and dissolved inorganic carbon from the Hooghly River to the adjacent coastal Bay of Bengal. *Environ Monit Assess* 193, 1–14. <https://doi.org/10.1007/s10661-021-09191-y>
- Gloor, M., Gruber, N., Sarmiento, J., Sabine, C.L., Feely, R.A., Rödenbeck, C., 2003. A first estimate of present and preindustrial air-sea CO<sub>2</sub> flux patterns based on ocean interior carbon measurements and models. *Geophysical Research Letters* 30, 1–4. <https://doi.org/10.1029/2002GL015594>
- Godsey, S.E., Kirchner, J.W., Clow, D.W., 2009. Concentration–discharge relationships reflect chemostatic characteristics of US catchments. *Hydrological Processes* 23, 1844–1864. <https://doi.org/10.1002/hyp.7315>
- Google, 2022. Google Maps [WWW Document]. URL <https://www.google.co.uk/maps>
- Gualtieri, G., 2022. Analysing the uncertainties of reanalysis data used for wind resource assessment: A critical review. *Renewable and Sustainable Energy Reviews* 167, 1–20. <https://doi.org/10.1016/j.rser.2022.112741>
- Hagedorn, B., Cartwright, I., 2010. The CO<sub>2</sub> system in rivers of the Australian Victorian Alps: CO<sub>2</sub> evasion in relation to system metabolism and rock weathering on multi-

- annual time scales. *Applied Geochemistry*.  
<https://doi.org/10.1016/j.apgeochem.2010.03.006>
- Hagedorn, B., Cartwright, I., 2009. Climatic and lithologic controls on the temporal and spatial variability of CO<sub>2</sub> consumption via chemical weathering: an example from the Australian Victorian Alps. *Chemical Geology* 260, 234–253.
- Harris, C.R., Millman, K.J., van der Walt, S.J., Gommers, R., Virtanen, P., Cournapeau, D., Wieser, E., Taylor, J., Berg, S., Smith, N.J., Kern, R., Picus, M., Hoyer, S., van Kerkwijk, M.H., Brett, M., Haldane, A., del Río, J.F., Wiebe, M., Peterson, P., Gérard-Marchant, P., Sheppard, K., Reddy, T., Weckesser, W., Abbasi, H., Gohlke, C., Oliphant, T.E., 2020. Array programming with NumPy. *Nature* 585, 357–362. <https://doi.org/10.1038/s41586-020-2649-2>
- Hartig, F., Hartig, M.F., 2017. Package 'DHARMA.' Vienna, Austria: R Development Core Team.
- Hartman, S.E., Humphreys, M.P., Kivimäe, C., Woodward, E.M.S., Kitidis, V., McGrath, T., Hydes, D.J., Greenwood, N., Hull, T., Ostle, C., Pearce, D.J., Sivyer, D., Stewart, B.M., Walsham, P., Painter, S.C., McGovern, E., Harris, C., Griffiths, A., Smilenova, A., Clarke, J., Davis, C., Sanders, R., Nightingale, P., 2019. Seasonality and spatial heterogeneity of the surface ocean carbonate system in the northwest European continental shelf. *Progress in Oceanography, Shelf Sea Biogeochemistry: Pelagic Processes*. 177, 101909.  
<https://doi.org/10.1016/j.pocean.2018.02.005>
- Hartmann, J., Moosdorf, N., Lauerwald, R., Hinderer, M., West, A.J., 2014. Global chemical weathering and associated P-release — The role of lithology, temperature and soil properties. *Chemical Geology* 363, 145–163.  
<https://doi.org/10.1016/j.chemgeo.2013.10.025>
- Herrmann, M., Najjar, R.G., Kemp, W.M., Alexander, R.B., Boyer, E.W., Cai, W.-J., Griffith, P.C., Kroeger, K.D., McCallister, S.L., Smith, R.A., 2015. Net ecosystem production and organic carbon balance of U.S. East Coast estuaries: A synthesis approach. *Global Biogeochemical Cycles* 29, 96–111.  
<https://doi.org/10.1002/2013GB004736>
- Hersbach, H., Bell, B., Berrisford, P., Biavati, G., Horanyi, A., Muñoz Sabater, J., Nicolas, J., Peubey, C., Radu, R., Rozum, I., Schepers, D., Simmons, A., Soci, C., Dee, D., Thepaut, J.-N., 2018. ERA5 hourly data on single levels from 1979 to present.
- Hill, T., Neal, C., 1997. Spatial and temporal variation in pH, alkalinity and conductivity in surface runoff and groundwater for the Upper River Severn catchment. *Hydrology and Earth System Sciences* 1, 697–715. <https://doi.org/10.5194/hess-1-697-1997>
- Ho, D.T., Coffineau, N., Hickman, B., Chow, N., Koffman, T., Schlosser, P., 2016. Influence of current velocity and wind speed on air-water gas exchange in a

- mangrove estuary. *Geophysical Research Letters* 43, 3813–3821.  
<https://doi.org/10.1002/2016GL068727>
- Ho, D.T., Ferrón, S., Engel, V.C., Larsen, L.G., Barr, J.G., 2014. Air-water gas exchange and CO<sub>2</sub> flux in a mangrove-dominated estuary. *Geophysical Research Letters* 41, 108–113. <https://doi.org/10.1002/2013GL058785>
- Ho, D.T., Law, C.S., Smith, M.J., Schlosser, P., Harvey, M., Hill, P., 2006. Measurements of air-sea gas exchange at high wind speeds in the Southern Ocean: Implications for global parameterizations. *Geophysical Research Letters* 33, 1–6.  
<https://doi.org/10.1029/2006GL026817>
- Ho, D.T., Schlosser, P., Orton, P.M., 2011. On Factors Controlling Air–Water Gas Exchange in a Large Tidal River. *Estuaries and Coasts* 34, 1103–1116.  
<https://doi.org/10.1007/s12237-011-9396-4>
- Hofmann, A.F., Soetaert, K., Middelburg, J.J., 2008. Present nitrogen and carbon dynamics in the Scheldt estuary using a novel 1-D model. *Biogeosciences* 5, 981–1006. <https://doi.org/10.5194/bg-5-981-2008>
- Howland, R.J.M., Tappin, A.D., Uncles, R.J., Plummer, D.H., Bloomer, N.J., 2000. Distributions and seasonal variability of pH and alkalinity in the Tweed Estuary, UK. *Science of The Total Environment* 251/252, 125–138.  
[https://doi.org/10.1016/S0048-9697\(00\)00406-X](https://doi.org/10.1016/S0048-9697(00)00406-X)
- Humphreys, M.P., Daniels, C.J., Wolf-Gladrow, D.A., Tyrrell, T., Achterberg, E.P., 2018. On the influence of marine biogeochemical processes over CO<sub>2</sub> exchange between the atmosphere and ocean. *Marine Chemistry* 199, 1–11.  
<https://doi.org/10.1016/j.marchem.2017.12.006>
- Humphreys, M.P., Lewis, E.R., Sharp, J.D., Pierrot, D., 2022. PyCO2SYS v1.8: marine carbonate system calculations in Python. *Geoscientific Model Development* 15, 15–43. <https://doi.org/10.5194/gmd-15-15-2022>
- Humphreys, M.P., Matthews, R.S., 2022. Calculate: total alkalinity from titration data in Python.
- Hunter, J.D., 2007. Matplotlib: A 2D Graphics Environment. *Computing in Science & Engineering* 9, 90–95. <https://doi.org/10.1109/MCSE.2007.55>
- Hydes, D.J., Hartman, S.E., 2012. Seasonal and inter-annual variability in alkalinity in Liverpool Bay (53.5° N, 3.5° W) and in major river inputs to the North Sea. *Ocean Dynamics* 62, 321–333. <https://doi.org/10.1007/s10236-011-0503-7>
- IPCC, 2021. *Climate Change 2021: The Physical Science Basis. Contribution of Working Group I to the Sixth Assessment Report of the Intergovernmental Panel on Climate Change*. Cambridge University Press, Cambridge, United Kingdom and New York.
- IPCC, 2014. *Climate Change 2013: The Physical Science Basis: Working Group I Contribution to the Fifth Assessment Report of the Intergovernmental Panel on Climate Change*. Cambridge University Press.

- Jacobson, A.R., Mikaloff Fletcher, S.E., Gruber, N., Sarmiento, J.L., Gloor, M., 2007. A joint atmosphere-ocean inversion for surface fluxes of carbon dioxide: 1. Methods and global-scale fluxes. *Global Biogeochemical Cycles* 21, 1–13. <https://doi.org/10.1029/2005GB002556>
- Jaeger, L., Uning, R., Mohd Hanif, N., Latif, M.T., 2019. Distribution of Surfactants in the Sea Surface Microlayer and Sub-surface Water in the Melaka River Estuary. *Bull Environ Contam Toxicol* 103, 374–379. <https://doi.org/10.1007/s00128-019-02662-6>
- Jähne, B., Heinz, G., Dietrich, W., 1987. Measurement of the diffusion coefficients of sparingly soluble gases in water. *Journal of Geophysical Research: Oceans* 92, 10767–10776. <https://doi.org/10.1029/JC092iC10p10767>
- Jarvie, H.P., King, S.M., Neal, C., 2017. Inorganic carbon dominates total dissolved carbon concentrations and fluxes in British rivers: Application of the THINCARB model – Thermodynamic modelling of inorganic carbon in freshwaters. *Science of The Total Environment* 575, 496–512. <https://doi.org/10.1016/j.scitotenv.2016.08.201>
- Jarvie, H.P., Neal, C., Leach, D.V., Ryland, G.P., House, W.A., Robson, A.J., 1997. Major ion concentrations and the inorganic carbon chemistry of the Humber rivers. *Science of The Total Environment, U.K. Fluxes to the North Sea, Land Ocean Interaction Study (LOIS) Rivers Basins Research, the First Two Years* 194–195, 285–302. [https://doi.org/10.1016/S0048-9697\(96\)05371-5](https://doi.org/10.1016/S0048-9697(96)05371-5)
- Jeffrey, L.C., Maher, D.T., Santos, I.R., Call, M., Reading, M.J., Holloway, C., Tait, D.R., 2018. The spatial and temporal drivers of pCO<sub>2</sub>, pCH<sub>4</sub> and gas transfer velocity within a subtropical estuary. *Estuarine, Coastal and Shelf Science* 208, 83–95. <https://doi.org/10.1016/j.ecss.2018.04.022>
- Jiang, L.-Q., Cai, W.-J., Wang, Y., 2008. A comparative study of carbon dioxide degassing in river- and marine-dominated estuaries. *Limnology and Oceanography* 53, 2603–2615. <https://doi.org/10.4319/lo.2008.53.6.2603>
- JNCC, 2013. Coastal Physiographic Features - Estuaries.
- Joesoef, A., Kirchman, D.L., Sommerfield, C.K., Cai, W.-J., 2017. Seasonal variability of the inorganic carbon system in a large coastal plain estuary. *Biogeosciences* 14, 4949–4963. <https://doi.org/10.5194/bg-14-4949-2017>
- Johnson, K.M., Wills, K.D., Butler, D.B., Johnson, W.K., Wong, C.S., 1993. Coulometric total carbon dioxide analysis for marine studies: maximizing the performance of an automated gas extraction system and coulometric detector. *Marine Chemistry* 44, 167–187.
- Kempe, S., 1979. Carbon in the freshwater cycle., in: Bolin, B., Degens, E.T., Kempe, S., Ketner, P. (Eds.), *The Global Carbon Cycle*, SCOPE Report. SCOPE, United States, pp. 343–377.

- Kerr, D.E., Brown, P.J., Grey, A., Kelleher, B.P., 2021. The influence of organic alkalinity on the carbonate system in coastal waters. *Marine Chemistry* 237, 104050. <https://doi.org/10.1016/j.marchem.2021.104050>
- Ketchum, B.H., 1983. Estuarine characteristics, in: Ketchum, B.H. (Ed.), *Estuaries and Enclosed Seas*. Elsevier, Amsterdam, The Netherlands, p. 13.
- Kim, H.-C., Lee, K., 2009. Significant contribution of dissolved organic matter to seawater alkalinity. *Geophysical Research Letters* 36. <https://doi.org/10.1029/2009GL040271>
- Kuliński, K., Schneider, B., Hammer, K., Machulik, U., Schulz-Bull, D., 2014. The influence of dissolved organic matter on the acid–base system of the Baltic Sea. *Journal of Marine Systems* 132, 106–115.
- Kuznetsova, A., Brockhoff, P.B., Christensen, R.H.B., 2015. Package 'lmerTest.' R package version 2, 734.
- Lacroix, F., Ilyina, T., Hartmann, J., 2020. Oceanic CO<sub>2</sub> outgassing and biological production hotspots induced by pre-industrial river loads of nutrients and carbon in a global modeling approach. *Biogeosciences* 17, 55–88. <https://doi.org/10.5194/bg-17-55-2020>
- Laruelle, G.G., Dürr, H.H., Lauerwald, R., Hartmann, J., Slomp, C.P., Goossens, N., Regnier, P.A.G., 2013. Global multi-scale segmentation of continental and coastal waters from the watersheds to the continental margins. *Hydrol. Earth Syst. Sci.* 17, 2029–2051. <https://doi.org/10.5194/hess-17-2029-2013>
- Laruelle, G.G., Dürr, H.H., Slomp, C.P., Borges, A.V., 2010. Evaluation of sinks and sources of CO<sub>2</sub> in the global coastal ocean using a spatially-explicit typology of estuaries and continental shelves. *Geophysical Research Letters* 37, 1–6. <https://doi.org/10.1029/2010GL043691>
- Laruelle, G.G., Goossens, N., Arndt, S., Cai, W.-J., Regnier, P., 2017. Air–water CO<sub>2</sub> evasion from US East Coast estuaries. *Biogeosciences* 14, 2441–2468. <https://doi.org/10.5194/bg-14-2441-2017>
- Lauerwald, R., Laruelle, G.G., Hartmann, J., Ciais, P., Regnier, P.A.G., 2015. Spatial patterns in CO<sub>2</sub> evasion from the global river network. *Global Biogeochemical Cycles* 29, 534–554. <https://doi.org/10.1002/2014GB004941>
- Lawrence, M.G., 2005. The relationship between relative humidity and the dewpoint temperature in moist air: A simple conversion and applications. *Bulletin of the American Meteorological Society* 86, 225–234.
- Lehmann, J., Kleber, M., 2015. The contentious nature of soil organic matter. *Nature* 528, 60–68. <https://doi.org/10.1038/nature16069>
- Lewis, E.R., Wallace, D.W.R., 1998. Program developed for CO<sub>2</sub> system calculations. Carbon Dioxide Information Analysis Center, Tennessee, United States.

- Li, M., Peng, C., Wang, M., Xue, W., Zhang, K., Wang, K., Shi, G., Zhu, Q., 2017. The carbon flux of global rivers: A re-evaluation of amount and spatial patterns. *Ecological Indicators* 80, 40–51. <https://doi.org/10.1016/j.ecolind.2017.04.049>
- Liu, S., Raymond, P.A., 2018. Hydrologic controls on pCO<sub>2</sub> and CO<sub>2</sub> efflux in US streams and rivers. *Limnology and Oceanography Letters* 3, 428–435. <https://doi.org/10.1002/lol2.10095>
- LOCATE, 2022. About | LOCATE – Land Ocean Carbon Transfer [WWW Document]. LOCATE. URL <https://locate.ac.uk/about> (accessed 12.29.22).
- Lüdecke, D., Ben-Shachar, M.S., Patil, I., Waggoner, P., Makowski, D., 2021. performance: An R package for assessment, comparison and testing of statistical models. *Journal of Open Source Software* 6.
- Magnone, D., Richards, L.A., van Dongen, B.E., Bryant, C., Evans, J.A., Polya, D.A., 2019. Calculating <sup>14</sup>C mean residence times of inorganic carbon derived from oxidation of organic carbon in groundwater using the principles of <sup>87</sup>Sr/<sup>86</sup>Sr and cation ratio mixing. *Geochimica et Cosmochimica Acta* 267, 322–340. <https://doi.org/10.1016/j.gca.2019.09.019>
- Maher, D.T., Eyre, B.D., 2012. Carbon budgets for three autotrophic Australian estuaries: Implications for global estimates of the coastal air-water CO<sub>2</sub> flux. *Global Biogeochemical Cycles* 26, 1–18. <https://doi.org/10.1029/2011GB004075>
- Maher, K., 2011. The role of fluid residence time and topographic scales in determining chemical fluxes from landscapes. *Earth and Planetary Science Letters* 312, 48–58. <https://doi.org/10.1016/j.epsl.2011.09.040>
- Matthews, C.J.D., St.Louis, V.L., Hesslein, R.H., 2003. Comparison of Three Techniques Used To Measure Diffusive Gas Exchange from Sheltered Aquatic Surfaces. *Environ. Sci. Technol.* 37, 772–780. <https://doi.org/10.1021/es0205838>
- McGrath, T., McGovern, E., Cave, R.R., Kivimäe, C., 2016. The Inorganic Carbon Chemistry in Coastal and Shelf Waters Around Ireland. *Estuaries and Coasts* 39, 27–39.
- McGrath, T., McGovern, E., Gregory, C., Cave, R.R., 2019. Local drivers of the seasonal carbonate cycle across four contrasting coastal systems. *Regional Studies in Marine Science* 30, 1–12. <https://doi.org/10.1016/j.rsma.2019.100733>
- McNutt, R.H., 2000. Strontium Isotopes, in: *Environmental Tracers in Subsurface Hydrology*. <https://doi.org/10.1007/978-1-4615-4557-6>
- Meybeck, M., 1994. Origin and variable composition of present day riverborne material, in: National Research Council (Ed.), *Material Fluxes on the Surface of the Earth*. National Academies Press, Washington DC, United States, pp. 61–73.
- Meybeck, M., 1987. Global chemical weathering of surficial rocks estimated from river dissolved loads. *American Journal of Science* 287, 401–428. <https://doi.org/10.2475/ajs.287.5.401>

- Meybeck, M., 1986. Composition chimique des ruisseaux non pollués en France. Chemical composition of headwater streams in France. *Sciences Géologiques, bulletins et mémoires* 39, 3–77. <https://doi.org/10.3406/sgeol.1986.1719>
- Meybeck, M., 1982. Carbon, nitrogen, and phosphorus transport by world rivers. *American Journal of Science*. <https://doi.org/10.2475/ajs.282.4.401>
- Middelburg, J.J., Soetaert, K., Hagens, M., 2020. Ocean Alkalinity, Buffering and Biogeochemical Processes. *Reviews of Geophysics* 58, 1–28. <https://doi.org/10.1029/2019RG000681>
- Millero, F.J., 1995. Thermodynamics of the carbon dioxide system in the oceans. *Geochimica et Cosmochimica Acta* 59, 661–677. [https://doi.org/10.1016/0016-7037\(94\)00354-O](https://doi.org/10.1016/0016-7037(94)00354-O)
- Mintrop, L., 2004. VINDTA, Versatile instrument for the Determination of Titration Alkalinity.
- Mintrop, L., Pérez, F., González-Dávila, M., Santana-Casiano, J., Körtzinger, A., 2000. Alkalinity determination by potentiometry: intercalibration using three different methods. *Cienc. Mar.* 26, 23–27. <https://doi.org/10.7773/cm.v26i1.573>
- Mundry, R., Nunn, C.L., 2009. Stepwise Model Fitting and Statistical Inference: Turning Noise into Signal Pollution. *The American Naturalist* 173, 119–123. <https://doi.org/10.1086/593303>
- Nakagawa, S., Johnson, P.C.D., Schielzeth, H., 2017. The coefficient of determination R<sup>2</sup> and intra-class correlation coefficient from generalized linear mixed-effects models revisited and expanded. *Journal of The Royal Society Interface* 14, 20170213. <https://doi.org/10.1098/rsif.2017.0213>
- Neal, C., Kirchner, J.W., 2000. Sodium and chloride levels in rainfall, mist, streamwater and groundwater at the Plynlimon catchments, mid-Wales: inferences on hydrological and chemical controls. *Hydrology and Earth System Sciences* 4, 295–310.
- NRFA, 2020. Gauged Daily Flow Archive.
- NRFA, 2017. Catchment Boundary and Areas.
- Oliveira, A.P., Cabeçadas, G., Mateus, M.D., 2017. Inorganic carbon distribution and CO<sub>2</sub> fluxes in a large European estuary (Tagus, Portugal). *Sci Rep* 7, 1–14. <https://doi.org/10.1038/s41598-017-06758-z>
- Ordnance Survey, 2015. OS Open Rivers.
- Orr, J.C., Epitalon, J.-M., Dickson, A.G., Gattuso, J.-P., 2018. Routine uncertainty propagation for the marine carbon dioxide system. *Marine Chemistry* 207, 84–107. <https://doi.org/10.1016/j.marchem.2018.10.006>
- Orton, P.M., Zappa, C.J., McGillis, W.R., 2010. Tidal and atmospheric influences on near-surface turbulence in an estuary. *Journal of Geophysical Research: Oceans* 115, 1–17. <https://doi.org/10.1029/2010JC006312>

- O'Sullivan, C., 2022. 2021 UK Provisional Greenhouse Gas Emissions.
- Paerl, H.W., 2009. Controlling Eutrophication along the Freshwater–Marine Continuum: Dual Nutrient (N and P) Reductions are Essential. *Estuaries and Coasts* 32, 593–601. <https://doi.org/10.1007/s12237-009-9158-8>
- Pawellekl, F., Frauenstein, F., Veizer, J., 2002. Hydrochemistry and isotope geochemistry of the upper Danube River. *Geochimica et Cosmochimica Acta*. [https://doi.org/10.1016/S0016-7037\(01\)00880-8](https://doi.org/10.1016/S0016-7037(01)00880-8)
- Penman, D.E., Caves Rügenstein, J.K., Ibarra, D.E., Winnick, M.J., 2020. Silicate weathering as a feedback and forcing in Earth's climate and carbon cycle. *Earth-Science Reviews* 209, 1–16. <https://doi.org/10.1016/j.earscirev.2020.103298>
- Piñol, J., Avila, A., 1992. Streamwater pH, alkalinity, pCO<sub>2</sub> and discharge relationships in some forested Mediterranean catchments. *Journal of Hydrology* 131, 205–225. [https://doi.org/10.1016/0022-1694\(92\)90218-K](https://doi.org/10.1016/0022-1694(92)90218-K)
- Pio, C.A., Alves, C.A., Duarte, A.C., 2001. Identification, abundance and origin of atmospheric organic particulate matter in a Portuguese rural area. *Atmospheric Environment* 35, 1365–1375. [https://doi.org/10.1016/S1352-2310\(00\)00391-5](https://doi.org/10.1016/S1352-2310(00)00391-5)
- Pomeroy, L.R., Sheldon, J.E., Sheldon, W.M., Blanton, J.O., Amft, J., Peters, F., 2000. Seasonal Changes in Microbial Processes in Estuarine and Continental Shelf Waters of the South-eastern U.S.A. *Estuarine, Coastal and Shelf Science* 51, 415–428. <https://doi.org/10.1006/ecss.2000.0690>
- Potter, I.C., Chuwen, B.M., Hoeksema, S.D., Elliott, M., 2010. The concept of an estuary: A definition that incorporates systems which can become closed to the ocean and hypersaline. *Estuarine, Coastal and Shelf Science* 87, 497–500. <https://doi.org/10.1016/j.ecss.2010.01.021>
- Prentice, I.C., Farquhar, G.D., Fasham, M.J.R., Goulden, M.L., Heimann, M., Jaramillo, V.J., Kheshgi, H.S., Quéré, C.L., Scholes, R.J., Wallace, D.W.R., Archer, D., Ashmore, M.R., Aumont, O., Baker, D., Battle, M., Bender, M., Bopp, L.P., Bousquet, P., Caldeira, K., Ciais, P., Cox, P.M., Cramer, W., Dentener, F., Enting, I.G., Field, C.B., Friedlingstein, P., Holland, E.A., Houghton, R.A., House, J.I., Ishida, A., Jain, A.K., Janssens, I.A., Joos, F., Kaminski, T., Keeling, C.D., Keeling, R.F., Kicklighter, D.W., Kohfeld, K.E., Knorr, W., Law, R., Lenton, T., Lindsay, K., Maier-Reimer, E., Manning, A.C., Matear, R.J., Mcguire, A.D., Melillo, J.M., Meyer, R., Mund, M., Orr, J.C., Piper, S., Plattner, K., Rayner, P.J., Sitch, S., Slater, R., Taguchi, S., Tans, P.P., Tian, H.Q., Weirig, M.F., Whorf, T., Yool, A., 2001. The carbon cycle and atmospheric carbon dioxide, in: *Climate Change 2001: The Scientific Basis*, Intergovernmental Panel on Climate Change. Cambridge University Press, Cambridge, United Kingdom and New York.

- Pritchard, D.W., 1967. What is an estuary: physical viewpoint, in: Lauff, G.H. (Ed.), . American Association for the Advancement of Science, Washington DC, United States, pp. 149–1176.
- Radtke, D.B., Wilde, F.D., Davis, J.V., Popowski, T.J., 1998. Alkalinity and acid neutralizing capacity, in: Wilde, F.D., Radtke, D.B. (Eds.), National Field Manual for the Collection of Water Quality Data, Handbooks for Water-Resources Investigations. US Geological Survey.
- Raiteri, G., Bordone, A., Ciuffardi, T., Pennechi, F., 2018. Uncertainty evaluation of CTD measurements: a metrological approach to water-column coastal parameters in the Gulf of La Spezia area. *Measurement* 126, 156–163.  
<https://doi.org/10.1016/j.measurement.2018.05.058>
- Raymond, P., Cole, J., 2001. Technical notes and comments: Gas exchange in rivers and estuaries: Choosing a gas transfer velocity. *Estuaries* 24, 312–317.
- Raymond, P.A., Bauer, J.E., 2001. DOC cycling in a temperate estuary: A mass balance approach using natural <sup>14</sup>C and <sup>13</sup>C isotopes. *Limnology and Oceanography* 46, 655–667. <https://doi.org/10.4319/lo.2001.46.3.0655>
- Raymond, P.A., Bauer, J.E., Cole, J.J., 2000. Atmospheric CO<sub>2</sub> evasion, dissolved inorganic carbon production, and net heterotrophy in the York River estuary. *Limnology and Oceanography* 45, 1707–1717.  
<https://doi.org/10.4319/lo.2000.45.8.1707>
- Raymond, P.A., Caraco, N.F., Cole, J.J., 1997. Carbon Dioxide Concentration and Atmospheric Flux in the Hudson River. *Estuaries* 20, 381–390.  
<https://doi.org/10.2307/1352351>
- Raymond, P.A., Cole, J.J., 2003. Increase in the Export of Alkalinity from North America's Largest River. *Science* 301, 88–91. <https://doi.org/10.1126/science.1083788>
- Raymond, P.A., Hartmann, J., Lauerwald, R., Sobek, S., McDonald, C., Hoover, M., Butman, D., Striegl, R., Mayorga, E., Humborg, C., Kortelainen, P., Dürr, H., Meybeck, M., Ciais, P., Guth, P., 2013. Global carbon dioxide emissions from inland waters. *Nature* 503, 355–359. <https://doi.org/10.1038/nature12760>
- Regnier, P., Friedlingstein, P., Ciais, P., Mackenzie, F.T., Gruber, N., Janssens, I.A., Laruelle, G.G., Lauerwald, R., Luysaert, S., Andersson, A.J., Arndt, S., Arnosti, C., Borges, A.V., Dale, A.W., Gallego-Sala, A., Godd ris, Y., Goossens, N., Hartmann, J., Heinze, C., Ilyina, T., Joos, F., LaRowe, D.E., Leifeld, J., Meysman, F.J.R., Munhoven, G., Raymond, P.A., Spahni, R., Suntharalingam, P., Thullner, M., 2013. Anthropogenic perturbation of the carbon fluxes from land to ocean. *Nature Geosci* 6, 597–607. <https://doi.org/10.1038/ngeo1830>
- Regnier, P., Resplandy, L., Najjar, R.G., Ciais, P., 2022. The land-to-ocean loops of the global carbon cycle. *Nature* 603, 401–410. <https://doi.org/10.1038/s41586-021-04339-9>

- Resplandy, L., Keeling, R.F., Rödenbeck, C., Stephens, B.B., Khatiwala, S., Rodgers, K.B., Long, M.C., Bopp, L., Tans, P.P., 2018. Revision of global carbon fluxes based on a reassessment of oceanic and riverine carbon transport. *Nature Geosci* 11, 504–509. <https://doi.org/10.1038/s41561-018-0151-3>
- Reum, J.C.P., Alin, S.R., Feely, R.A., Newton, J., Warner, M., McElhany, P., 2014. Seasonal Carbonate Chemistry Covariation with Temperature, Oxygen, and Salinity in a Fjord Estuary: Implications for the Design of Ocean Acidification Experiments. *PLOS ONE* 9, 1–12. <https://doi.org/10.1371/journal.pone.0089619>
- Riipinen, I., Pierce, J.R., Yli-Juuti, T., Nieminen, T., Hakkinen, S., Ehn, M., Junninen, H., Lehtipalo, K., Petaja, T., Slowik, J., Chang, R., Shantz, N.C., Abbatt, J., Leaitch, W.R., Pandis, S.N., Donahue, N.M., Kulmala, M., 2011. Organic condensation: a vital link connecting aerosol formation to cloud condensation nuclei (CCN) concentrations. *Atmos. Chem. Phys.* 11, 3865–3878.
- Salisbury, J.E., Vandemark, D., Hunt, C.W., Campbell, J.W., McGillis, W.R., McDowell, W.H., 2008. Seasonal observations of surface waters in two Gulf of Maine estuary-plume systems: Relationships between watershed attributes, optical measurements and surface pCO<sub>2</sub> - ScienceDirect. *Estuarine, Coastal and Shelf Science* 77, 245–252.
- Sarmiento, J.L., Sundquist, E.T., 1992. Revised budget for the oceanic uptake of anthropogenic carbon dioxide. *Nature* 356, 589–593. <https://doi.org/10.1038/356589a0>
- Schiettecatte, L.-S., Gazeau, F., Zee, C. van der, Brion, N., Borges, A.V., 2006. Time series of the partial pressure of carbon dioxide (2001–2004) and preliminary inorganic carbon budget in the Scheldt plume (Belgian coastal waters). *Geochemistry, Geophysics, Geosystems* 7, 1–16. <https://doi.org/10.1029/2005GC001161>
- Schmidt, M.W.I., Torn, M.S., Abiven, S., Dittmar, T., Guggenberger, G., Janssens, I.A., Kleber, M., Kögel-Knabner, I., Lehmann, J., Manning, D.A.C., Nannipieri, P., Rasse, D.P., Weiner, S., Trumbore, S.E., 2011. Persistence of soil organic matter as an ecosystem property. *Nature* 478, 49–56. <https://doi.org/10.1038/nature10386>
- Schulte, P., van Geldern, R., Freitag, H., Karim, A., Négrel, P., Petelet-Giraud, E., Probst, A., Probst, J.L., Telmer, K., Veizer, J., Barth, J.A.C., 2011. Applications of stable water and carbon isotopes in watershed research: Weathering, carbon cycling, and water balances. *Earth-Science Reviews*. <https://doi.org/10.1016/j.earscirev.2011.07.003>
- Shand, P., Darbyshire, D.P.F., Goody, D., H. Haria, A., 2007. <sup>87</sup>Sr/<sup>86</sup>Sr as an indicator of flowpaths and weathering rates in the Plynlimon experimental catchments, Wales,

- U.K. *Chemical Geology* 236, 247–265.  
<https://doi.org/10.1016/j.chemgeo.2006.09.012>
- Sharp, J.D., Byrne, R.H., 2020. Interpreting measurements of total alkalinity in marine and estuarine waters in the presence of proton-binding organic matter. *Deep Sea Research Part I: Oceanographic Research Papers* 165, 103338.  
<https://doi.org/10.1016/j.dsr.2020.103338>
- Shen, C., Testa, J.M., Li, M., Cai, W.-J., Waldbusser, G.G., Ni, W., Kemp, W.M., Cornwell, J., Chen, B., Brodeur, J., Su, J., 2019. Controls on Carbonate System Dynamics in a Coastal Plain Estuary: A Modeling Study. *Journal of Geophysical Research: Biogeosciences* 124, 61–78. <https://doi.org/10.1029/2018JG004802>
- Simoneit, B.R.T., Elias, V.O., 2000. Organic tracers from biomass burning in atmospheric particulate matter over the ocean. *Marine Chemistry* 69, 301–312.  
[https://doi.org/10.1016/S0304-4203\(00\)00008-6](https://doi.org/10.1016/S0304-4203(00)00008-6)
- Simpson, E., Ianson, D., Kohfeld, K.E., 2022. Using End-Member Models to Estimate Seasonal Carbonate Chemistry and Acidification Sensitivity in Temperate Estuaries. *Geophysical Research Letters* 49, e2021GL095579.  
<https://doi.org/10.1029/2021GL095579>
- Sims, R.P., Bedington, M., Schuster, U., Watson, A.J., Kitidis, V., Torres, R., Findlay, H.S., Fishwick, J.R., Brown, I., Bell, T.G., 2022. Tidal mixing of estuarine and coastal waters in the western English Channel is a control on spatial and temporal variability in seawater CO<sub>2</sub>. *Biogeosciences* 19, 1657–1674.  
<https://doi.org/10.5194/bg-19-1657-2022>
- Smith, G., 2018. Step away from stepwise. *J Big Data* 5, 32.  
<https://doi.org/10.1186/s40537-018-0143-6>
- Smith, S.V., Hollibaugh, J.T., 1993. Coastal metabolism and the oceanic organic carbon balance. *Reviews of Geophysics* 31, 75–89. <https://doi.org/10.1029/92RG02584>
- Snyder, D.C., Rutter, A.P., Collins, R., Worley, C., Schauer, J.J., 2009. Insights into the Origin of Water Soluble Organic Carbon in Atmospheric Fine Particulate Matter. *Aerosol Science and Technology* 43, 1099–1107.
- Sontek, 2012. *CastAway CTD User Manual* 1.5.
- Statham, P.J., 2012. Nutrients in estuaries — An overview and the potential impacts of climate change. *Science of The Total Environment, Climate Change and Macronutrient Cycling along the Atmospheric, Terrestrial, Freshwater and Estuarine Continuum - A Special Issue dedicated to Professor Colin Neal* 434, 213–227. <https://doi.org/10.1016/j.scitotenv.2011.09.088>
- Thomas, H., Friederike Prowe, A.E., van Heuven, S., Bozec, Y., de Baar, H.J.W., Schiettecatte, L.-S., Suykens, K., Koné, M., Borges, A.V., Lima, I.D., Doney, S.C., 2007. Rapid decline of the CO<sub>2</sub> buffering capacity in the North Sea and

- implications for the North Atlantic Ocean. *Global Biogeochemical Cycles* 21.  
<https://doi.org/10.1029/2006GB002825>
- Thomas, H., Schiettecatte, L.-S., Suykens, K.O.N.E., Koné, Y.J.M., Shadwick, E.H., Prowe, A.W.F., Bozec, Y., de Baar, H.J.W., Borges, A.V., 2009. Enhanced ocean carbon storage from anaerobic alkalinity generation in coastal sediments. *Biogeosciences* 6, 267–274.
- Thorp, J.H., DeLong, M.D., 2002. Dominance of autochthonous autotrophic carbon in food webs of heterotrophic rivers. *Oikos* 96, 543–550. <https://doi.org/10.1034/j.1600-0706.2002.960315.x>
- Tishchenko, P.Ya., Wallmann, K., Vasilevskaya, N.A., Volkova, T.I., Zvalinskii, V.I., Khodorenko, N.D., Shkirnikova, E.M., 2006. The contribution of organic matter to the alkaline reserve of natural waters. *Oceanology* 46, 192–199.  
<https://doi.org/10.1134/S0001437006020068>
- Tranvik, L.J., Downing, J.A., Cotner, J.B., Loiselle, S.A., Striegl, R.G., Ballatore, T.J., Dillon, P., Finlay, K., Fortino, K., Knoll, L.B., Kortelainen, P.L., Kutser, T., Larsen, Soren., Laurion, I., Leech, D.M., McCallister, S.L., McKnight, D.M., Melack, J.M., Overholt, E., Porter, J.A., Prairie, Y., Renwick, W.H., Roland, F., Sherman, B.S., Schindler, D.W., Sobek, S., Tremblay, A., Vanni, M.J., Verschoor, A.M., von Wachenfeldt, E., Weyhenmeyer, G.A., 2009. Lakes and reservoirs as regulators of carbon cycling and climate. *Limnology and Oceanography* 54, 2298–2314.  
[https://doi.org/10.4319/lo.2009.54.6\\_part\\_2.2298](https://doi.org/10.4319/lo.2009.54.6_part_2.2298)
- Tye, A.M., Balfour, C.A., Bowes, M., Brown, I., Evans, C.D., Felgate, S.L., Fishwick, J., Hargreaves, G., Harris, C., Kitidis, V., Lapworth, D.J., Martin, A.P., Matthews, R., Mayor, D.J., Mounteney, I., Nightingale, P.D., Pickard, A., Rees, A., Sanders, R., Spears, B.M., Stephens, J., Stinchcombe, M.C., Williams, P., Williamson, J., Woodward, E.M.S., Boothroyd, I.M., Bowes, M.J., Breimann, S.A., Burden, A., Callaghan, N., Gillbert, P.J., Ives, S., Juergens, M.D., Hughes, L., Lichtschlag, A., Mack, S., Mallin Martin, D., Mawji, E., McDonald, R., Olszewska, J.P., Parkes, D., Pearce, C.R., Peel, K.E., dos Santos Pereira, M.G., Pugh, J.P., Worrall, F., Yarrow, D.M., 2022a. Sampling of estuarine chemistry and organic matter for 16 estuaries in Great Britain in 2017/8 as part of the LOCATE project.  
<https://doi.org/10.5285/d111d44e-0794-28dc-e053-6c86abc0fc99>
- Tye, A.M., Williamson, J.L., Jarvie, H.P., Dise, N.B., Lapworth, D.J., Monteith, D., Sanders, R., Mayor, D.J., Bowes, M.J., Bowes, M., Burden, A., Callaghan, N., Farr, G., Felgate, S.L., Gibb, S., Gilbert, P.J., Hargreaves, G., Keenan, P., Kitidis, V., Jürgens, M.D., Martin, A., Mounteney, I., Nightingale, P.D., Gloria Pereira, M., Olszewska, J., Pickard, A., Rees, A.P., Spears, B., Stinchcombe, M., White, D., Williams, P., Worrall, F., Evans, C.D., 2022b. Dissolved inorganic carbon export from rivers of Great Britain: Spatial distribution and potential catchment-scale

- controls. *Journal of Hydrology* 615, 1–13.  
<https://doi.org/10.1016/j.jhydrol.2022.128677>
- Uncles, R.J., Stephens, J.A., Harris, C., 2006. Runoff and tidal influences on the estuarine turbidity maximum of a highly turbid system: The upper Humber and Ouse Estuary, UK. *Marine Geology, Proceedings of the 6th International Congress on Tidal Sedimentology (Tidalites 2004)* 235, 213–228.  
<https://doi.org/10.1016/j.margeo.2006.10.015>
- Uppström, L.R., 1974. The boron/chlorinity ratio of deep-sea water from the Pacific Ocean. *Deep Sea Research and Oceanographic Abstracts* 21, 161–162.  
[https://doi.org/10.1016/0011-7471\(74\)90074-6](https://doi.org/10.1016/0011-7471(74)90074-6)
- Vachon, D., Prairie, Y.T., Cole, J.J., 2010. The relationship between near-surface turbulence and gas transfer velocity in freshwater systems and its implications for floating chamber measurements of gas exchange. *Limnology and Oceanography* 55, 1723–1732. <https://doi.org/10.4319/lo.2010.55.4.1723>
- Van Dam, B.R., Crosswell, J.R., Anderson, I.C., Paerl, H.W., 2018. Watershed-Scale Drivers of Air-Water CO<sub>2</sub> Exchanges in Two Lagoonal North Carolina (USA) Estuaries. *Journal of Geophysical Research: Biogeosciences* 123, 271–287.  
<https://doi.org/10.1002/2017JG004243>
- Van Dam, B.R., Wang, H., 2019. Decadal-Scale Acidification Trends in Adjacent North Carolina Estuaries: Competing Role of Anthropogenic CO<sub>2</sub> and Riverine Alkalinity Loads. *Frontiers in Marine Science* 6, 1–11.
- Vanderborght, J.P., Wollast, R., Loijens, M., Regnier, P., 2002. Application of a transport-reaction model to the estimation of biogas fluxes in the Scheldt Estuary. *Biogeochemistry* 59, 207–237. <https://doi.org/10.1023/A:1015573131561>
- Virtanen, P., Gommers, R., Oliphant, T.E., Haberland, M., Reddy, T., Cournapeau, D., Burovski, E., Peterson, P., Weckesser, W., Bright, J., van der Walt, S.J., Brett, M., Wilson, J., Millman, K.J., Mayorov, N., Nelson, A.R.J., Jones, E., Kern, R., Larson, E., Carey, C.J., Polat, İ., Feng, Y., Moore, E.W., VanderPlas, J., Laxalde, D., Perktold, J., Cimrman, R., Henriksen, I., Quintero, E.A., Harris, C.R., Archibald, A.M., Ribeiro, A.H., Pedregosa, F., van Mulbregt, P., 2020. SciPy 1.0: fundamental algorithms for scientific computing in Python. *Nat Methods* 17, 261–272.  
<https://doi.org/10.1038/s41592-019-0686-2>
- Volta, C., Laruelle, G.G., Regnier, P., 2016. Regional carbon and CO<sub>2</sub> budgets of North Sea tidal estuaries. *Estuarine, Coastal and Shelf Science* 176, 76–90.  
<https://doi.org/10.1016/j.ecss.2016.04.007>
- Wang, Z.A., Cai, W.-J., 2004. Carbon dioxide degassing and inorganic carbon export from a marsh-dominated estuary (the Duplin River): A marsh CO<sub>2</sub> pump. *Limnology and Oceanography* 49, 341–354. <https://doi.org/10.4319/lo.2004.49.2.0341>

- Wanninkhof, R., 2014. Relationship between wind speed and gas exchange over the ocean revisited. *Limnology and Oceanography: Methods* 12, 351–362. <https://doi.org/10.4319/lom.2014.12.351>
- Wanninkhof, R., 1992. Relationship between wind speed and gas exchange over the ocean. *Journal of Geophysical Research: Oceans* 97, 7373–7382. <https://doi.org/10.1029/92JC00188>
- Ward, N.D., Bianchi, T.S., Medeiros, P.M., Seidel, M., Richey, J.E., Keil, R.G., Sawakuchi, H.O., 2017. Where Carbon Goes When Water Flows: Carbon Cycling across the Aquatic Continuum. *Frontiers in Marine Science* 4, 1–27.
- Waskom, M.L., 2021. Seaborn: statistical data visualization. *Journal of Open Source Software* 6, 1–4. <https://doi.org/10.21105/joss.03021>
- Wedepohl, K.H., 1995. The composition of the continental crust. *Geochimica et Cosmochimica Acta* 59, 1217–1232.
- Wei, G., Ma, J., Liu, Y., Xie, L., Lu, W., Deng, W., Ren, Z., Zeng, T., Yang, Y., 2013. Seasonal changes in the radiogenic and stable strontium isotopic composition of Xijiang River water: Implications for chemical weathering. *Chemical Geology*. <https://doi.org/10.1016/j.chemgeo.2013.02.004>
- Weiss, R.F., 1974. Carbon dioxide in water and seawater: the solubility of a non-ideal gas. *Marine Chemistry* 2, 203–215.
- Weiss, R.F., Jahnke, R.A., Keeling, C.D., 1982. Seasonal effects of temperature and salinity on the partial pressure of CO<sub>2</sub> in seawater. *Nature* 300, 511–513. <https://doi.org/10.1038/300511a0>
- Wetzel, R.G., 2001. *Limnology: lake and river ecosystems*, 3rd Edition. ed. Academic Press, Cambridge, Massachusetts.
- White, A.F., Blum, A.E., 1995. Effects of climate on chemical weathering in watersheds. *Geochimica et Cosmochimica Acta* 59, 1729–1747.
- White, A.F., Blum, A.E., Bullen, T.D., Vivit, D.V., Schulz, M., Fitzpatrick, J., 1999. The effect of temperature on experimental and natural chemical weathering rates of granitoid rocks. *Geochimica et Cosmochimica Acta* 63, 3277–3291. [https://doi.org/10.1016/S0016-7037\(99\)00250-1](https://doi.org/10.1016/S0016-7037(99)00250-1)
- Whittingham, M.J., Stephens, P.A., Bradbury, R.B., Freckleton, R.P., 2006. Why do we still use stepwise modelling in ecology and behaviour? *Journal of Animal Ecology* 75, 1182–1189. <https://doi.org/10.1111/j.1365-2656.2006.01141.x>
- Wickham, H., 2019. Package ‘tidyverse.’ See <http://tidyverse.org> 1–5.
- Williamson, J.L., Tye, A., Lapworth, D.J., Monteith, D., Sanders, R., Mayor, D.J., Barry, C., Bowes, Mike, Bowes, Michael, Burden, A., Callaghan, N., Farr, G., Felgate, S., Fitch, A., Gibb, S., Gilbert, P., Hargreaves, G., Keenan, P., Kitidis, V., Juergens, M., Martin, A., Mounteney, I., Nightingale, P.D., Pereira, M.G., Olszewska, J., Pickard, A., Rees, A.P., Spears, B., Stinchcombe, M., White, D., Williams, P.,

- Worrall, F., Evans, C., 2021. Landscape controls on riverine export of dissolved organic carbon from Great Britain. *Biogeochemistry* 160, 1–22.  
<https://doi.org/10.1007/s10533-021-00762-2>
- Wolf-Gladrow, D.A., Zeebe, R.E., Klaas, C., Körtzinger, A., Dickson, A.G., 2007. Total alkalinity: The explicit conservative expression and its application to biogeochemical processes. *Marine Chemistry*.  
<https://doi.org/10.1016/j.marchem.2007.01.006>
- Woodwell, G.M., Rich, P.H., Hall, C.A.S., 1973. Carbon in estuaries, in: *Brookhaven Symposia in Biology*. Associates Universities, California, United States, pp. 221–240.
- Yao, H., Hu, X., 2017. Responses of carbonate system and CO<sub>2</sub> flux to extended drought and intense flooding in a semiarid subtropical estuary: Carbonate chemistry and CO<sub>2</sub> flux in an estuary. *Limnol. Oceanogr.* 62, S112–S130.  
<https://doi.org/10.1002/lno.10646>
- Zappa, C.J., Raymond, P.A., Terray, E.A., McGillis, W.R., 2003. Variation in surface turbulence and the gas transfer velocity over a tidal cycle in a macro-tidal estuary. *Estuaries* 26, 1401–1415. <https://doi.org/10.1007/BF02803649>
- Zeebe, R.E., Wolf-Gladrow, D., 2001. CO<sub>2</sub> in seawater: equilibrium, kinetics, isotopes, 1st Edition. ed. Elsevier Science, Amsterdam, The Netherlands.
- Zhai, W., Dai, M., 2009. On the seasonal variation of air – sea CO<sub>2</sub> fluxes in the outer Changjiang (Yangtze River) Estuary, East China Sea. *Marine Chemistry*, 10th International Estuarine Biogeochemistry Symposium - “Estuaries in a Changing World” 117, 2–10. <https://doi.org/10.1016/j.marchem.2009.02.008>
- Zscheischler, J., Mahecha, M.D., Avitabile, V., Calle, L., Carvalhais, N., Ciais, P., Gans, F., Gruber, N., Hartmann, J., Herold, M., Ichii, K., Jung, M., Landschützer, P., Laruelle, G.G., Lauerwald, R., Papale, D., Peylin, P., Poulter, B., Ray, D., Regnier, P., Rödenbeck, C., Roman-Cuesta, R.M., Schwalm, C., Tramontana, G., Tyukavina, A., Valentini, R., van der Werf, G., West, T.O., Wolf, J.E., Reichstein, M., 2017. Reviews and syntheses: An empirical spatiotemporal description of the global surface–atmosphere carbon fluxes: opportunities and data limitations. *Biogeosciences* 14, 3685–3703. <https://doi.org/10.5194/bg-14-3685-2017>